INFORMATION TO USERS

This manuscript has been reproduced from the microfilm master. UMI films the text directly from the original or copy submitted. Thus, some thesis and dissertation copies are in typewriter face, while others may be from any type of computer printer.

The quality of this reproduction is dependent upon the quality of the copy submitted. Broken or indistinct print, colored or poor quality illustrations and photographs, print bleedthrough, substandard margins, and improper alignment can adversely affect reproduction.

In the unlikely event that the author did not send UMI a complete manuscript and there are missing pages, these will be noted. Also, if unauthorized copyright material had to be removed, a note will indicate the deletion.

Oversize materials (e.g., maps, drawings, charts) are reproduced by sectioning the original, beginning at the upper left-hand corner and continuing from left to right in equal sections with small overlaps. Each original is also photographed in one exposure and is included in reduced form at the back of the book.

Photographs included in the original manuscript have been reproduced xerographically in this copy. Higher quality 6" x 9" black and white photographic prints are available for any photographs or illustrations appearing in this copy for an additional charge. Contact UMI directly to order.

UMI®

Bell & Howell Information and Learning
300 North Zeeb Road, Ann Arbor, MI 48106-1346 USA
800-521-0600

SELECTED GEOCHEMICAL REACTIONS IN HEAVY METAL - CHLOROPHENOL SYSTEMS.

Christopher J. Daughney

June, 1997

A thesis submitted to the Faculty of Graduate Studies and Research in partial fulfillment of the requirements of the degree of Doctor of Philosophy

Department of Earth and Planetary Sciences
McGill University
3450 University St.
Montréal, PQ H3A 2A7 Canada

ABSTRACT

The subsurface mobility of metals and chlorophenols occurring together in contaminated groundwaters is controlled by the extent of aqueous complexation between them and by their adsorption onto aquifer materials. However, no previous experimental studies have quantified these interactions within a thermodynamic framework. This study has investigated the aqueous complexation of Cd, Pb and Cu by 2,4,6-trichlorophenolate (TCP^-) and pentachlorophenolate (PCP^-) at 25°C, using ion selective electrode potentiometry and ultraviolet spectrophotometry. A single 1:1 aqueous complex forms in each system, with log stability constants and 1*s* errors calculated to be: $Cd(TCP)^+$, 2.5 ± 0.2; $Pb(TCP)^+$, 3.0 ± 0.3; $Cu(TCP)^+$, 4.9 ± 0.2; $Cd(PCP)^+$, 2.9 ± 0.2; $Pb(PCP)^+$, 2.8 ± 0.3; and $Cu(PCP)^+$, 4.2 ± 0.2. The adsorption of Cd, Pb, Cu and Al by the common soil bacterium *Bacillus licheniformis* has been examined at 25°C in electrolytes of varying ionic strength. The cell walls display carboxyl, phosphate and hydroxyl surface functional groups, with pK_a values and 1*s* errors of 5.2 ± 0.3, 7.5 ± 0.4 and 10.2 ± 0.5, respectively. The average log K values for Cd, Pb, Cu and Al adsorption onto the *B. licheniformis* surface carboxyl sites, with 1*s* errors, are 3.9 ± 0.5, 4.6 ± 0.3, 4.9 ± 0.4 and 5.8 ± 0.3, respectively. The Constant Capacitance double layer model provides the best description of ionic strength-dependent adsorption behaviour, although the model parameters vary between independently grown bacterial cultures, possibly due to cell wall variation arising from genetic variation during reproduction. There is insignificant adsorption of

TCP to α-Al_2O_3, but a strong affinity between TCP and *B. subtilis*. The TCP-*B. subtilis* adsorption data are best described by a site-specific model in which the negative form of TCP forms a 1:1 surface complex with the neutral hydroxyl functional groups of the bacteria ($\log K = 2.3 \pm 0.3$) and the neutral form of TCP forms a 1:1 surface complex with the neutral hydroxyl surface functional groups ($\log K = 3.7 \pm 0.3$). A simple correlation technique can be used to estimate stability constants describing complexation or adsorption in systems containing other metals, chlorophenols or bacterial surfaces. The stability constants reported here may be readily incorporated into thermodynamic models to predict the mobility of heavy metals co-occurring with chlorophenols in natural groundwater systems.

RÉSUMÉ

La mobilité des métaux et des chlorophénols qui se retrouvent ensembles dans une nappe souterraine contaminée est contrôlée par le degré de complexation entre les deux éléments et par leur adsorption sur le substrat geologique de l'aquifère. Cependant, jusqu'à présent, les études experimentales n'ont jamais fait une évaluation quantitative de ces intéractions dans un cadre thermodynamique. Dans la présente étude nous avons examiné la complexation aqueuse du Cd, Pb et Cu par le 2,4,6-trichlorophénolate (TCP) et le pentachlorophénolate (PCP) à 25°C en utilisant la potentiométrie d'électrodes d'ion sélectives et la spectrophotométrie ultraviolete. Un seul complexe aqueux 1:1 se forme dans chaque système. Les constantes de stabilité logarithmique et les erreurs 1*s* sont: $Cd(TCP)^+$, 2.5 ± 0.2; $Pb(TCP)^+$, 3.0 ± 0.3; $Cu(TCP)^+$, 4.9 ± 0.2; $Cd(PCP)^+$, 2.9 ± 0.2; $Pb(PCP)^+$, 2.8 ± 0.3; et $Cu(PCP)^+$, 4.2 ± 0.2. L'adsorption du Cd, Pb, Cu et Al par le bactérium commun du sol, *Bacillus licheniformis*, a été étudié à une température de 25°C dans des électrolytes de force ionique variable. Des groupes fonctionnels carboxyle, phosphate et hydroxyle sont présent sur les surfaces cellulaires, et sont caractérisés respectivement par les valeurs pK_a et erreurs 1*s* suivants: 5.2 ± 0.3, 7.5 ± 0.4 et 10.2 ± 0.5. Les valeurs moyennes du log K de l'adsorption du Cd, Pb, Cu et Al sur les carboxyles superficiels du *B. licheniformis*, et leurs erreurs 1*s*, sont respectivement 3.9 ± 0.5, 4.6 ± 0.3, 4.9 ± 0.4 et 5.8 ± 0.3. Le modèle à double couche de Capacitance Constante permet la meilleure description de l'adsorption en fonction de la force ionique. Cependant, les paramètres du modèle

varient entre les différentes cultures bactériennes, peut-être à cause de variations chez les surfaces cellulaires naissant de l'alteration génétique durant la reproduction. L'adsorption du TCP sur α-Al_2O_3 est négligeable, mais l'affinité du TCP pour *B. subtilis* est très forte. La meilleure description des données d'adsorption du TCP-*B. subtilis* est donné par un modèle à site-spécifique où la forme négative du TCP forme un complexe superficiel 1:1 avec les groupes fonctionnels hydroxyles neutres des bactéries (log K = 2.3 $\pm$ 0.3) et la forme neutre du TCP forme un complexe superficiel 1:1 avec les groupes fonctionnels hydroxyles neutres (log K = 3.7 $\pm$ 0.3). Nous pouvons nous servir d'une simple technique d'analyse de corrélation pour estimer les constantes de stabilité décrivant la complexation ou l'adsorption dans des systèmes où l'on trouve d'autres métaux, chlorophénols ou des surfaces bactériennes. Les constantes de stabilité que nous présentons ici peuvent être utilisées dans un cadre thermodynamique pour prédire la mobilité de métaux qui se présentent ensembles avec des chlorophénols dans des systèmes naturels de nappes souterraines.

ACKNOWLEDGEMENTS

I wish to express my deepest and most respectful thanks to my supervisor, Prof. J Fein, for his encouragement and enthusiasm, and for his patient reviews of my work. In addition to providing invaluable advice on topics related to research, I am indebted to him for providing advice on life in general. The student-advisor relationship is the most pivotal factor affecting quality of education, and I could not have had a better advisor.

Thanks are extended to Prof. P. Linder and Prof. M. Fey at the University of Cape Town, South Africa, for accepting me as a visiting scientist in 1995 and for assisting me in my work there, and to Prof. A. Hynes at McGill University, who helped me arrange the temporary position at UCT. I thank Prof A. Mucci and Prof. J. Paquette of McGill University, who, as members of my advisory committee, provided important insights and valuable comments on this research. Additional thanks are due to Prof. Mucci for the use of his auto-titrator and his ultraviolet spectrophotometer. I also thank Prof. A. E. Williams-Jones for the opportunities that he provided me during my time at McGill.

Many others have also provided stimulating discussions on my research, most notably J-F Boily, but also P. Wightman, L. Yane, C. Gammons and M. Temmam and W. Halter. Assistance in the laboratory was provided by Nathan Yee, Tom Davis, Dave Yiptong, Krystyne Blaikie, Lydia Scratch, Christian Gravel, and Pascal Benalil. Lastly, I extend my thanks to my friends and family,

who supported me during my studies and helped me to lead a balanced life away from school. Thanks to all of you.

This thesis was funded by an NSERC Operating Grant and a FCAR Nouveaux Chercheurs Grant to Prof. J. Fein, and an NSERC 1967 Scholarship to the author.

PREFACE

The research presented in this thesis represents original research by the author in collaboration with his advisor, Prof. J. Fein. The thesis is divided into six chapters, four of which are manuscripts, with the remaining two being a general introduction and a conclusion. Chapter 2 was published in *Geochimica et Cosmochimica Acta*, 1997, v. 61, p. 719 - 729. Chapters 3, 4 and 5 have been submitted to *Chemical Geology*, *The Journal of Colloid and Interface Science*, and *Environmental Science and Technology*, respectively. Each manuscipt is co-authored by Prof. J. Fein, who proposed topics of research, provided advice on experimental methodology, assisted in the interpretation of data, and critically reviewed the text. Nathan Yee performed roughly one third of the laboratory work for Chapters 3 and 4, and is listed as third author. The majority of experimental work was completed by the author, including experimental design, bacterial growth and culture maintenance, acid-base and ion-selective electrode titrimetry, ultraviolet spectroscopy, optical microscopy, high performance liquid chromatography, and flame atomic absorption spectroscopy. Interpretation of the data was carried out by the author, using the computer speciation program FITEQL. The students David Yiptong, Krystyne Blaikie, Lydia Scratch, Christian Gravel, and Pascal Benalil provided laboratory assistance during short stages of this work.

The following is an excerpt from the "Guidelines Concerning Thesis Preparation", as required by the Faculty of Graduate Studies and Research at McGill University:

> Candidates have the option of including, as part of the thesis, the text of one or more papers submitted or to be submitted for publications, or the clearly duplicated text of one or more published papers. These texts must be bound as an integral part of the thesis.
>
> If this option is chosen, **connecting texts that provide logical bridges between the different papers are mandatory**. The thesis must be written in such a way that it is more than a mere collection of manuscripts; in other words, results of a series of papers must be integrated.
>
> The thesis must still conform to all other requirements of the "Guidelines for Thesis Preparation". **The thesis must include**: A Table of Contents, an abstract in English and French, an introduction which clearly states the rationale and objectives of the study, a review of the literature, a final conclusion and summary, and a thorough bibliography or reference list.
>
> Additional material must be provided where appropriate (e.g. in appendices) and in sufficient detail to allow a clear and precise judgement to be made of the importance and originality of the research reported in the thesis.
>
> In the case of manuscripts co-authored by the candidate and others, **the candidate is required to make an explicit statement in the thesis as to who contributed to such work and to what extent**. Supervisors must attest to the accuracy of such statements at the doctoral oral defense. Since the task of the examiners is made more difficult in these cases, it is in the candidate's interest to make perfectly clear the responsibilities of all authors of the co-authored papers.

TABLE OF CONTENTS

CHAPTER 1:

INTRODUCTION

A great proportion of the water removed from the subsurface is extracted from near-surface sedimentary aquifers. Such aquifers are highly susceptible to anthropogenic contamination. The increasing frequency and complexity of subsurface contamination has necessitated the development of techniques for the prediction of pollutant migration and environmental fate. These techniques allow the environmental hazard posed to be quantified should aquifer contamination occur, and they assist in the development of effective strategies for remediation.

The migration of any pollutant in the subsurface is controlled by both physical and chemical processes. The physical processes involve diffusion, dispersion, and the transport of the pollutant by flowing groundwater, and can be modelled by various forms of Darcy's Law (Freeze and Cherry, 1979; Domenico and Schwartz, 1990). In addition to transport by flowing groundwater, the mobility of any subsurface contaminant is controlled by chemical interactions with other dissolved species and with the aquifer materials. These chemical reactions include, for example, aqueous complexation and adsorption. These reactions can lead the pollutant to migrate at a rate which differs from the average groundwater velocity (Domenico and Schwartz, 1990). Many of these chemical reactions can be modelled successfully within the framework of equilibrium thermodynamics, with a unique stability constant describing the extent to which each reaction will proceed, under a given set of chemical conditions (Stumm and Morgan, 1981; Nordstrom and Munoz, 1986; Langmuir, 1997). The stability constant for each important reaction is determined experimentally in a system containing only the reactants of interest. The stability constants for all relevant

reactions can then be combined in a single chemical model which predicts the speciation of the contaminant in groundwater. Subsequently, the chemical model predicting speciation can be coupled with a physical model for fluid flow to ultimately predict the fate of the contaminant in a natural, chemically complex groundwater system.

This thesis focuses on the determination of stability constants for selected reactions involving cadmium, lead, copper, 2,4,6-trichlorophenol (TCP) and/or pentachlorophenol (PCP). Both the heavy metals and chlorophenols are toxic and commonly occur as groundwater contaminants, and as a result, they are listed as priority pollutants by the United States Environmental Protection Agency (Keith and Telliard, 1979). PCP and TCP may be introduced to the groundwater zone directly, in the form of an insecticide, fungicide or biocide, or unintentionally, during activities such as wood preservation, pulp bleaching, water purification or waste incineration (Makinen et al., 1993). In general, the toxic effects posed by PCP and TCP are severe, as these chemicals are long-lived, carcinogenic, and highly bioaccumulative (Niimi and Palazzo, 1985; Pollard et al., 1993; Kishino and Kobayashi, 1995). There are presently well over 1000 sites world-wide which are known to be contaminated by these chlorophenols (Mueller et al., 1989).

Like the chlorophenols, the heavy metals cadmium, lead and copper are potential groundwater pollutants. These heavy metals are introduced to the groundwater environment from several sources (Alloway, 1995; Baker and Senft, 1995; Davies, 1995). Most notably, these metals reach the subsurface through activities related to the mining, smelting and refining of metalliferous ores. In

addition, cadmium is released to groundwater through the disposal of plastics and batteries, lead through the agricultural application of manures and sewage sludges, and copper through the application of sewage sludges, fungicides and biocides. Lastly, these heavy metals may reach the groundwater zone due to atmospheric deposition associated with the burning of fossil fuels. As a result, the concentrations of cadmium, lead and copper in contaminated soils and soil fluids can exceed several hundred ppm. The toxic effects of these heavy metals are severe and well documented (Fasset, 1980; Nriagu, 1983; Fergusson, 1990).

Due to their toxicity and common co-occurrence, Chapter 2 of this thesis focuses on the determination of stability constants describing the formation of aqueous heavy metal - chlorophenol complexes. Aqueous complexation refers to the reaction by which two or more dissolved species react to form an aqueous compound. Commonly, the reactants carry opposite charges, with the electrostatic attraction between them causing the reaction to occur. Consider, for example, a solution containing the metal M with positive charge $m+$ and the ligand L with negative charge $l-$. The two ions may react to produce a complex as follows:

$$xM^{m+} + yL^{l-} \leftrightarrow M_x L_y^{(xm+yl)} \qquad (1)$$

Note that a number of complexes with different charges may be formed as the values of the stoichiometric coefficients x and y are varied. In a given system at equilibrium, at a fixed temperature and pressure, the activities of the products and

reactants are related by the thermodynamic mass action law and stability constant *K*:

$$K = \frac{[M_x L_y^{(xm+yl)}]}{[M^{m+}]^x [L^{l-}]^y} \qquad (2)$$

where the square brackets represent the activities of the enclosed species. The experimental determination of stability constants is well described by Buffle (1988).

To date, thousands of such stability constants have been measured and tabulated (Martell and Smith, 1977, and other volumes of this series), but complexation reactions involving heavy metals and chlorophenols have not been adequately investigated. Indeed, stability constants are unknown for all but the Fe^{3+}-monochlorophenolate complexes (Martell and Smith, 1977), even though estimation techniques suggest that metal-chlorophenol complexation is probable (Fein, 1996). The possible ramifications of metal-chlorophenol complexation are extensive. The solubilities of both the metals and the chlorophenols may be enhanced where aqueous complexes exist. The electrostatic adsorption of both the metals and the chlorophenols may be affected by the formation of a metal-chlorophenol complex with a different charge. Adsorption onto organic materials may also be affected because the complexed and uncomplexed forms of the metals and the chlorophenols are likely to have different hydrophobicities. Clearly, if the fate of metals and chlorophenols occurring together in groundwaters is to be

accurately modelled, the extent of complexation between them must be investigated. The objectives of Chapter 2, then, are to outline an experimental approach for this investigation and to report stability constants describing the formation of selected aqueous heavy metal - chlorophenol complexes.

The fate of heavy metals and chlorophenols in groundwater is controlled not only by aqueous complexation, but by adsorption onto aquifer materials. Chapters 3, 4 and 5 of this thesis focus on the determination of stability constants describing adsorption reactions involving heavy metals or chlorophenols. In general, adsorption reactions describe the partitioning of a chemical species between the solution and the surface of a solid phase. Recent research indicates that adsorption reactions can be quantified in terms of surface complexation, whereby the species in solution interact with discrete functional groups present on the solid surface (e.g. Hohl and Stumm, 1976; Davis and Kent. 1990; Lövgren et al., 1990; Muller and Sigg, 1991; Gunneriusson et al., 1994; Boily and Fein, 1996). The surface functional groups are analogous to aqueous ligands, and so surface complexation can be quantified using the same theoretical framework as aqueous complexation. A metal M with charge $m+$ may interact with a hydroxyl (or other) surface functional group (S-OH, where S represents the surface to which the functional group is attached):

$$S-OH + M^{m+} \leftrightarrow S-OM^{m+} + H^{+} \qquad (3)$$

Again, a mass action law relates the ratio of the activities of the products and reactants to a stability constant K:

$$K = \frac{[S-OM^{m+}][H^+]}{[S-OH][M^{m+}]} \quad (4)$$

Here, the concentrations of surface species are expressed in moles per liter of aqueous solution. Experimental studies of systems containing both solid and aqueous phases permit the determination of stability constants describing the formation of surface complexes. The stability constants describing adsorption can be included in chemical models describing complexation, in order to predict the fate of metals and chlorophenols in complex systems where a variety of chemical processes are occurring.

The surface complexation approach has been extensively applied to model the adsorption of heavy metals by mineral surfaces (Davis and Kent, 1990; Lövgren et al., 1990; Muller and Sigg, 1991; Gunneriusson et al., 1994; Boily and Fein, 1996; Langmuir, 1997). However, bacterial surfaces are also found in many natural environments (Geesey et al., 1977; Harvey et al., 1982; Ghiorse and Wobber, 1989; Mahmood and Rama, 1993; Mandernack and Tebo, 1993; Baker et al., 1994; Corapcioglu and Kim, 1995; Yakimov et al., 1995). Because organic substances commonly coat mineral surfaces in soils (Davis, 1984; Schlautmann and Morgan, 1994), bacterial cells or cell wall fragments may represent a significant fraction of the surface area exposed to groundwaters. Chapter 3

compares the surface properties and heavy metal binding capacities of *Bacillus subtilis* and *Bacillus licheniformis*, two common species of soil bacteria (Duncan et al., 1994). The objectives of this chapter are to measure stability constants describing the adsorption of heavy metals by specific surface functional groups present on the bacterial cell walls, and to investigate systematic variations in the magnitudes of these stability constants in order to elucidate generalities which may be applied to model acid-base behaviour and metal-bacteria interactions in complex, natural systems.

In Chapter 4, the effect of solution ionic strength on the surface properties and metal binding capacities of *Bacillus subtilis* and *Bacillus licheniformis* is investigated. Bacterial surfaces are often negatively charged in natural environments (Harden and Harris, 1953), and it is well established that ionic strength-dependent electrostatic interactions between metal ions in solution and electrically charged surfaces influence experimentally determined adsorption stability constants (Stumm and Morgan, 1981; Langmuir, 1997). The effect of ionic strength on metal adsorption by mineral surfaces has been described by several different electrostatic double layer models, each describing the distribution of electric charge at the mineral-water interface (Westall and Hohl, 1980; Davis and Kent, 1990). However, it is not clear that these double layer models can be effectively applied to predict the extent of proton and metal adsorption by bacterial surfaces in electrolytes of differing ionic strengths. The objective of Chapter 4 is to quantify the effect of ionic strength on the acid-base properties (i.e.

proton adsorption) and metal-binding capacities of *Bacillus subtilis* and *Bacillus licheniformis*.

Chapter 5 investigates and compares the adsorption of TCP by α-Al_2O_3 and *B. subtilis*. *B. subtilis* is commonly found in soils; although α-Al_2O_3 itself is not a common soil mineral, it is characterized by surface functional groups which are representative of the Al surface sites on many more common alumino-silicate minerals. This study, then, allows the comparison of TCP adsorption by bacterial and mineral surfaces representative of those found in natural aquifers. A number of workers have previously examined the adsorptive behaviour of TCP onto representative soil solids (Schellenberg et al., 1984; Yoshida et al, 1987; Lee et al., 1990; Kung and McBride, 1991; Smejtek et al., 1996; You and Liu, 1996). However, all previous workers have failed to consider the specific interactions between TCP and the functional groups present on the solid surfaces. Such non-specific models for adsorption provide only a semi-quantitative description of the process, and as a result, the non-specific model parameters cannot be used to accurately predict the amount of TCP adsorption that will occur under conditions that differ from those of measurement. In Chapter 5, the non-specific model traditionally used to describe the adsorption of organic compounds is compared to a thermodynamic, site-specific adsorption model. Again, the objective of this study is to determine stability constants that can be applied to predict the extent of TCP adsorption in complex, natural systems.

REFERENCES

Alloway, B. J. In *Heavy Metals in Soils*; Alloway, B. J., Ed.; Chapman and Hall, London, 1995, pp 122-151.

Baker, D. E.; Senft, J. P. In *Heavy Metals in Soils*; Alloway, B. J., Ed.; Chapman and Hall, London, 1995, pp 179-205.

Baker, E. T.; Freely, R. A.; Mottl, M. J.; Sansone, F. T.; Wheat, C. G.; Resing, J. A.; Lupton, J. E. *Earth Planet. Sci. Let.* **1994**, *128*, 1-17.

Boily, J.-F.; Fein, J. B. *Geochim. Cosmochim. Acta* **1996**, *60*, 2929-2938.

Buffle, J. "Complexation Reactions in Aquatic Systems: An Analytical Approach." John Wiley and Sons, N. Y., 1988.

Corapcioglu, M. Y.; Kim, S. *Wat. Res. Research* **1995**, *31*, 2693-2647.

Davies, B. E. In *Heavy Metals in Soils*; Alloway, B. J., Ed.; Chapman and Hall, London, 1995, pp 206-223.

Davis, J. A. *Geochim. Cosmochim Acta* **1984**, *48*, 679-691.

Davis, J. A.; Kent, D. B. In *Mineral-Water Interface Geochemistry*; Hochella, M. F., White, A. F., Eds.; Reviews in Mineralogy, Mineralogical Society of America, 1990; v. 23, pp 177-260.

Domenico, P. A.; Schwartz, F. W. "Physical and Chemical Hydrogeology." John Wiley and Sons, N. Y., 1990.

Duncan, K. E.; Ferguson, N.; Kimura, K.; Zhou, X.; Istock, C. A. *Evolution* **1994**, *48*, 2002-2025.

Fasset, D. W. In *Metals in the Environment*; Waldron, H. A, Ed.; Academic Press, London, 1980, pp. 61-110.

Fein, J. B. *Appl. Geochem.* **1996**, *11*, 735-744.

Fergusson, J. E. "The Heavy Elements: Chemistry, Environmental Impact and Health Effects." Pergamon Press, Toronto, 1990.

Freeze, R. A.; Cherry, J. A. "Groundwater." Prentice-Hall, N. J., 1979.

Geesey, G. G.; Richardson, W. T.; Yeomans, H. G.; Irvin, R. T.; Costerton, J. W. *Can. J. Microbiol.* **1977**, *23*, 1733-1736.

Ghiorse, W. S.; Wobber, F. J. "Deep Subsurface Microbiology." Crane, Russak & Co., N. Y., 1989.

Gunneruisson, L.; Lövgren, L.; Sjöberg, S. *Geochim. Cosmochim. Acta* **1994**, *58*, 4973-4983.

Harden, V.P.; Harris, J.O. *J. Bacteriol.* **1953**, *65*, 198-202.

Harvey, R. W.; Lion, L. W.; Young, L. Y.; Leckie, J. O. *J. Marine Res.* **1982**, *40*, 1201-1211.

Hohl, H.; Stumm, W. *J. Colloid Interface Sci.* **1976**, *55*, 281-228.

Keith, L. H.; Telliard, W. A. *Environ. Sci. Technol.* **1979**, *13*, 416-423

Kishino, T.; Kobayashi, K. *Water Res.* **1995**, *29*, 431-442.

Kung, K.-H. S.; McBride, M. B. *Environ. Sci. Technol.* **1991**, *25*, 702-709.

Langmuir, D. "Aqueous Environmental Geochemistry." Prentice-Hall, N. J., 1997.

Lee, L. S.; Rao, P. S.; Nkedi-Kizza, P.; Delfino, J. J. *Environ. Sci. Technol.* **1990**, *24*, 654-661.

Lövgren, L; Sjöberg, S.; Schindler, P. W. *Geochim. Cosmochim. Acta* **1990**, *54*, 1301-1306.

Mahmood, S. K.; Rama, R. P. *Bull. Environ. Contam. Toxicol.* **1993**, *50*, 486-491.

Makinen, P. M.; Theno, T. J.; Ferguson, J. F.; Ongerth, J. E.; Puhakka, P. M. *Environ. Sci. Technol.* **1993**, *27*, 1434-1439.

Mandernack, K. W.; Tebo, B. M. *Geochim. Cosmochim. Acta* **1993**, *57*, 3907-3923.

Martell, A. E.; Smith, R. M. "Critical Stability Constants: 3. Other Organic Ligands." Plenum, N. Y., 1977.

Mueller, J. G.; Chapman, P. J.; Pritchard, P. H. *Env. Sci. Tech.* **1989**, *23*, 1197-1201.

Müller, B.; Sigg, L. *J. Colloid Interface Sci.* **1991**, *148*, 517-532.

Niimi, A. J.; Palazzo, V. *Water Res.* **1985**, *19*, 205-207.

Nordstrom, D. K.; Munoz, J. L. "Geochemical Thermodynamics." Blackwell Scientific, CA, 1986.

Nriagu J.O. "Lead and Lead Poisoning in Antiquity." John Wiley and Sons, N. Y., 1983.

Pollard, S. J. T.; Hoffman, R. E.; Hrudley, S. E. *Can. J. Civ. Eng.* **1993**, *20*, 787-800.

Schellenberg, K.; Leuenberger, C.; Schwartzenbach, R. P. *Environ. Sci. Technol.* **1984**, *18*, 652-657.

Schlautmann, M. A.; Morgan, J. J. *Geochim. Cosmochim. Acta* **1994**, *58*, 4293-4303.

Smejtek, P.; Blochel, A.; Wang, S. *Chemosphere* **1996**, *33*, 177-201.

Stumm, W., and Morgan, J. J., "Aquatic Chemistry." John Wiley and Sons, N. Y., 1981.

Westall, J.; Hohl, H. *Adv. Colloid Interface Sci.* **1980**, *12*, 265-294.

Yakimov, M. M.; Timmis, K. N.; Wray, V.; Fredrickson, H. L. *Appl. Env. Microbiol.* **1995**, *61*, 1706-1713.

Yoshida, K.; Shigeoka, T.; Yamamuchi, F. *Chemosphere* **1987**, *16*, 2531-2544.

You, C. N.; Liu J. C. *Wat. Sci. Tech.* **1996**, *33*, 263-270.

CHAPTER 2:

AQUEOUS COMPLEXATION OF CADMIUM, LEAD AND COPPER BY 2,4,6-TRICHLOROPHENOLATE AND PENTACHLOROPHENOLATE

Christopher J. Daughney
Jeremy B. Fein

Department of Earth and Planetary Sciences
McGill University
3450 University St.
Montréal, PQ H3A 2A7 Canada

Submitted to:
Geochimica et Cosmochimica Acta
May, 1996

ABSTRACT

The subsurface mobility of metals and polychlorinated phenols occurring together in contaminated groundwaters may be significantly affected by the extent of aqueous complexation between them. However, no previous experimental studies have examined these interactions. In light of this, the aqueous complexation of cadmium, lead and copper by both 2,4,6-trichlorophenolate (TCP^-) and pentachlorophenolate (PCP^-) has been studied at 25°C. Experimental data gathered by ion selective electrode potentiometry and ultraviolet spectrophotometry indicate that metal-chlorophenol complexation occurs, and we interpret the experimental data in terms of a single 1:1 complex in each system. The log stability constants for the complexes, with 2σ errors, are calculated to be: $Cd(TCP)^+$, 2.5±0.3; $Pb(TCP)^+$, 3.0±0.5; $Cu(TCP)^+$, 4.9±0.4; $Cd(PCP)^+$, 2.9±0.3; $Pb(PCP)^+$, 2.8±0.5; and $Cu(PCP)^+$, 4.2±0.4. Based on these values, a simple correlation technique has been applied to estimate stability constants involving other metals and chlorophenols. Calculations using these stability constants suggest that metal-chlorophenolate complexation can drastically alter metal and/or chlorophenol mobilities in contaminated groundwaters.

INTRODUCTION

A great proportion of the water extracted from the subsurface is removed from near-surface aquifers, and anthropogenic contamination of these aquifers is growing increasingly common. In order to remediate contaminated sites and evaluate environmental risk, the subsurface mobilities of the various pollutants must be quantified. In the groundwater environment, the mobility of any contaminant is controlled by its chemical interactions with other dissolved species and with the aquifer materials. Unfortunately, the number of interactions which might affect any given pollutant is virtually limitless, and where more than one type of contaminant is present, predicting their mobilities becomes more difficult. Our ability to model the fate of subsurface contaminants is severely limited by a lack of thermodynamic data pertaining to complex systems.

This study investigates the aqueous complexation of cadmium, lead and copper by 2,4,6-trichlorophenol (TCP) and pentachlorophenol (PCP). These heavy metals and chlorophenols may occur together in contaminated groundwaters, particularly in proximity to wood preservation facilities, where they are used as biocides (Pollard et al., 1993). There are presently several hundred sites world-wide which are known to be contaminated by these chemicals (Mueller et al., 1989). The health risks posed by both the heavy metals and the chlorophenols are severe and well documented (Kishino and Kobayashi, 1995; Pollard et al., 1993; Fergusson, 1990; Niimi and Palazzo, 1985; Nriagu, 1983). Each of these heavy metals and

chlorophenols is recognized as a priority pollutant by the United States Environmental Protection Agency (Keith and Telliard, 1979).

At present, the geochemical interactions between dissolved metals and chlorophenols have not been adequately addressed. TCP and PCP are organic acids, which deprotonate in basic solutions to yield negatively charged chlorophenolate anions, denoted here as TCP^- and PCP^- (Figure 1). Where metals are present in the system, the simple chlorophenol speciation presented in Figure 1 is likely to be altered through the formation of aqueous metal-organic complexes. However, metal-chlorophenolate complexation studies are rare, and thus stability constants are unknown for all but the Fe^{3+}-monochlorophenolate complexes (Martell and Smith, 1977a). Nonetheless, the possible ramifications of aqueous complexation are extensive. The solubility of both the metal and the chlorophenol may be enhanced where complexes exist. Because a metal-chlorophenolate complex carries a different charge than the free chlorophenolate anion, its behaviour in electrostatically driven adsorption reactions may be markedly affected. The presence of metal-chlorophenol complexes may slow the rate of chlorophenol breakdown, as metal-carboxylate complexation slows decarboxylation reactions (Fein et al., 1995; Fein and Hestrin, 1994). Sorption onto organic materials may also be affected because the complexed and uncomplexed forms of a chlorophenol are likely to have different hydrophobicities. All of these effects are likely to be dependent upon pH and ionic strength. Clearly, if the mobility and fate of the chlorophenols are to be accurately modelled, their behaviour in the presence of metals must be examined. The objective of this study, then, is to measure the

Figure 1: Aqueous speciation diagrams for: (a) 2,4,6-trichlorophenol, (b) pentachlorophenol, (c) cadmium, (d) lead and (e) copper systems. Diagrams correspond to total chlorophenol concentrations of $10^{-3.0}$ M and total metal concentrations of $10^{-4.0}$ M. The systems are assumed to be free of dissolved carbon dioxide. Equilibria and stability constants applied in the calculations are listed in Table 1.

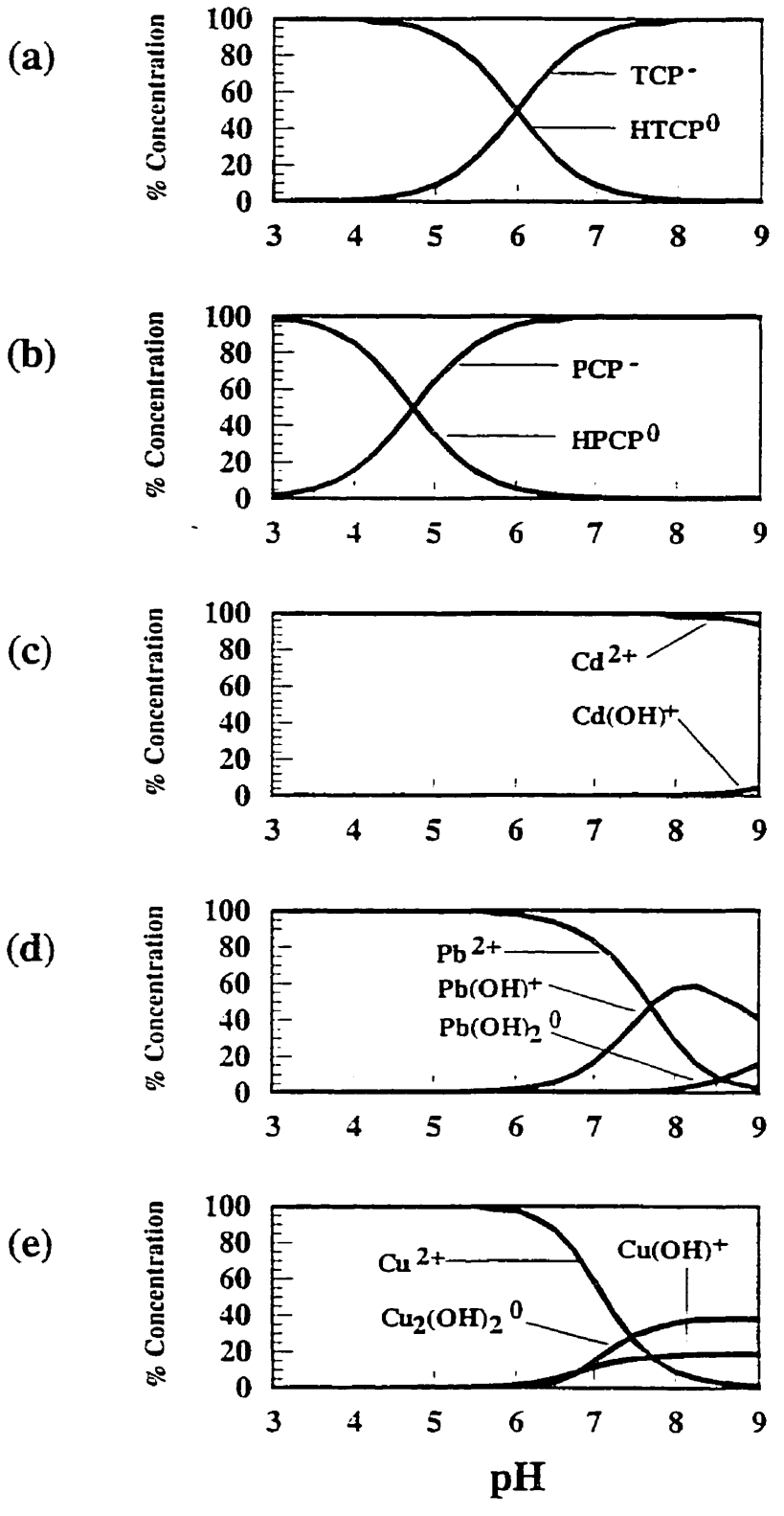
(a)
% Concentration
100
80
60
40
20
0
3
4
5
6
7
8
9
TCP⁻
HTCP⁰
(b)
% Concentration
PCP⁻
HPCP⁰
(c)
% Concentration
Cd 2+
Cd(OH)+
(d)
% Concentration
Pb 2+
Pb(OH)+
Pb(OH)2 0
(e)
% Concentration
Cu 2+
Cu(OH)+
Cu2(OH)2 0
pH

Figure 1

stability constants describing the formation of aqueous metal-chlorophenol complexes.

THEORY

The experimental determination of aqueous stability constants has been reviewed in detail by Buffle (1988). In general, a solution containing known total concentrations of both the metal and the ligand must be prepared. The equilibrium speciation of the system is defined by a series of mass action, mass balance and charge balance equations. However, because the stability constant describing the metal-ligand complex of interest is at this point unknown, the solution speciation can only be explicitly defined if the equilibrium activity of at least one species is accurately measured. This measurement, in combination with the equations described above, provides enough information to calculate the equilibrium activity of each species in solution and, ultimately, the value of the stability constant describing the complex of interest. In theory, only one experimental measurement of activity is required to calculate the value of the stability constant describing a single metal-chlorophenolate complex. In practice, many activity measurements are made during experiments performed as a function of pH and metal:ligand ratio, and so the system is over-determined. As a result, the experimental observations can be compared to several models involving one or more metal-chlorophenolate complexes, each with different stoichiometries, and the fit of the different models can be quantitatively

compared. This permits the value of the stability constant(s) and the stoichiometry of the complex(es) to be tightly constrained.

In the metal-chlorophenol systems studied here, we express the complexation reaction as follows:

$$xM^{2+} + yL^{-} \leftrightarrow M_x L_y^{(2x-y)} \quad (1)$$

where M represents Cd^{2+}, Pb^{2+} or Cu^{2+}, L represents either TCP^- or PCP^-, and x and y are stoichiometric coefficients. Note that a number of complexes with different charges may be formed as the values of x and y are varied. In a given metal-chlorophenol system at equilibrium, at a fixed temperature and pressure, the activities of the products and reactants are related by the mass action law and stability constant (K):

$$K = \frac{[M_x L_y^{(2x-y)}]}{[M^{2+}]^x [L^-]^y} \quad (2)$$

where the square brackets represent the activities of the enclosed species.

In addition to the complexation reaction above, several other equilibria, with previously measured stability constants, are required to fully define speciation in the metal-chlorophenol systems. The previously studied reactions and equilibrium constants used in this study are listed in Table 1. Log K values are reported for the condition of zero ionic strength and 25°C. Literature values reported at other ionic

TABLE 1: Previously Studied Equilibria Used to Model Experimental Systems

Equilibrium	Log K	Equilibrium	Log K
		$HPCP \leftrightarrow PCP^- + H^+$	-4.7[c]
$Cd^{2+} + H_2O \leftrightarrow CdOH^+ + H^+$	-10.1[a]	$HTCP \leftrightarrow TCP^- + H^+$	-6.0[c]
$Cd^{2+} + 2H_2O \leftrightarrow Cd(OH)_2^0 + 2H^+$	-20.4[a]	$HEPES \leftrightarrow HEPES^- + H^+$	-7.6[d]
$Cd^{2+} + 3H_2O \leftrightarrow Cd(OH)_3^- + 3H^+$	-33.3[a]	$Na^+ + H_2O \leftrightarrow NaOH^0 + H^+$	-14.2[b]
$Cd^{2+} + 4H_2O \leftrightarrow Cd(OH)_4^{2-} + 4H^+$	-47.4[a]	$NaOH^0 + NO_3^- \leftrightarrow NaNO_3^0 + OH^-$	-0.4[b]
$2Cd^{2+} + H_2O \leftrightarrow Cd_2OH^{3+} + H^+$	-9.4[a]	$Cd^{2+} + NO_3^- \leftrightarrow CdNO_3^+$	-0.1[b]
$4Cd^{2+} + 4H_2O \leftrightarrow Cd_4(OH)_4^{4+} + 4H^+$	-32.9[a]	$Cd^{2+} + 2NO_3^- \leftrightarrow Cd(NO_3)_2^0$	0.2[b]
		$Pb^{2+} + NO_3^- \leftrightarrow PbNO_3^+$	1.2[b]
$Pb^{2+} + H_2O \leftrightarrow PbOH^+ + H^+$	-7.7[a]	$Pb^{2+} + 2NO_3^- \leftrightarrow Pb(NO_3)_2^0$	1.4[b]
$Pb^{2+} + 2H_2O \leftrightarrow Pb(OH)_2^0 + 2H^+$	-17.1[a]	$Pb^{2+} + 3NO_3^- \leftrightarrow Pb(NO_3)_3^-$	1.3[b]
$Pb^{2+} + 3H_2O \leftrightarrow Pb(OH)_3^- + 3H^+$	-28.1[a]	$Pb^{2+} + 4NO_3^- \leftrightarrow Pb(NO_3)_4^{2-}$	0.3[b]
$2Pb^{2+} + H_2O \leftrightarrow Pb_2OH^{3+} + H^+$	-6.4[a]	$Cu^{2+} + NO_3^- \leftrightarrow CuNO_3^+$	0.5[b]
$3Pb^{2+} + 4H_2O \leftrightarrow Pb_3(OH)_4^{2+} + 4H^+$	-23.9[a]	$Cu^{2+} + 2NO_3^- \leftrightarrow Cu(NO_3)_2^0$	-0.4[b]
$4Pb^{2+} + 4H_2O \leftrightarrow Pb_4(OH)_4^{4+} + 4H^+$	-20.9[a]	$H_2O + CO_{2(g)} \leftrightarrow H_2CO_3^0$	-1.47[b]
$6Pb^{2+} + 8H_2O \leftrightarrow Pb_6(OH)_8^{4+} + 6H^+$	-43.6[a]	$H_2CO_3^0 \leftrightarrow H^+ + HCO_3^-$	-6.35[b]
		$HCO_3^- \leftrightarrow H^+ + CO_3^{2-}$	-10.3[b]
$Cu^{2+} + H_2O \leftrightarrow CuOH^+ + H^+$	-8.0[a]	$Na^+ + HCO_3^- \leftrightarrow NaHCO_3^0$	-0.25[e]
$Cu^{2+} + 2H_2O \leftrightarrow Cu(OH)_2^0 + 2H^+$	-17.3[a]	$Na^+ + CO_3^{2-} \leftrightarrow NaCO_3^-$	1.27[e]
$Cu^{2+} + 3H_2O \leftrightarrow Cu(OH)_3^- + 3H^+$	-27.8[a]	$Pb^{2+} + 2CO_3^{2-} \leftrightarrow Pb(CO_3)_2^{2-}$	-6.4[b]
$Cu^{2+} + 4H_2O \leftrightarrow Cu(OH)_4^{2-} + 4H^+$	-39.6[a]	$Cu^{2+} + CO_3^{2-} \leftrightarrow CuCO_3^0$	6.8[e]
$2Cu^{2+} + 2H_2O \leftrightarrow Cu_2(OH)_2^{2+} + 2H^+$	-10.4[a]	$Cu^{2+} + 2CO_3^{2-} \leftrightarrow Cu(CO_3)_2^{2-}$	10.0[b]
$H_2O \leftrightarrow H^+ + OH^-$	-14.0[b]		

Equilibria [a]from Baes and Mesmer (1976); [b]from Smith and Martell (1976); [c]from Callahan et al. (1979); [d]from Good et al. (1966); and [e]from Martell and Smith (1982). All log K values are reported for the condition of zero ionic strength, at 25°C.

strengths were adjusted using the Debye-Hückel equation with parameters given by Helgeson et al. (1981). Literature values reported at temperatures other than 25°C were adjusted using the isocoulombic approach of Gu et al. (1994).

This study utilizes both ion selective electrode (ISE) potentiometry and ultraviolet spectrophotometry to measure the activity (or in the latter case, the concentration) of a particular species in solution. In the potentiometric studies, an ISE is used to monitor the activity of the free metal (i.e. Cd^{2+}, Pb^{2+} or Cu^{2+}) in a mixed metal-chlorophenol solution during the course of a titration. The complexation of the metal by the chlorophenolate causes the activity of the free metal to decrease, and the magnitude of this decrease is used to calculate the value of the metal-chlorophenolate stability constant. The spectrophotometric technique is used to measure the concentration of the chlorophenolate anion (TCP^- or PCP^-) in mixed metal-chlorophenol systems. Again, the complexation causes the concentration of the chlorophenolate anion to decrease in an amount related to the magnitude of the metal-chlorophenolate stability constant. Both of these experimental techniques are most sensitive when the analyte is present in a lower concentration than its complexing counterpart. Thus, the potentiometric experiments are performed in chlorophenol-dominated systems, and the spectrophotometric experiments are run in metal-dominated systems. In combination, these two analytical techniques are applied to determine the values of x and y in Equation 2, and to place quantitative constraints on the values of K for the most important metal-chlorophenolate complexes.

The computer speciation program FITEQL 2.0 (Westall, 1982a, b) is used extensively in the analysis of the experimental data. The program calculates stability constants from experimental data, and can be used to model speciation in complex systems if all relevant stability constants are provided. In all analytical procedures involving FITEQL, Davies equation activity coefficients are included in the calculations, and the equilibria listed in Table 1 are used to calculate equilibrium speciation. All stability constants determined in this work are thus referenced to the condition of zero ionic strength and 25°C.

In the analysis of the potentiometric titration data, FITEQL is used to optimize for the stability constants of various metal-chlorophenol complexes. The program calculates a variance (V) describing the fit of the model to the experimental data. The variance is normalized with respect to the number of titration data points, the number of species in solution for which total concentrations are known, and the number of stability constants to be optimized. As such, it quantifies the goodness of the fit of a particular model.

FITEQL is also applied to the analysis of the spectrophotometric data. At the wavelength used in this study (289 nm), the chlorophenolate anion, the metal-chlorophenolate complex and the nitrate ion contribute to the observed absorbance:

$$A_{observed} = \varepsilon_{chlorophenolate} c_{chlorophenolate} + \varepsilon_{nitrate} c_{nitrate} + \varepsilon_{complex} c_{complex} \qquad (3)$$

where ε and c represent the extinction coefficient and the concentration of each absorbing species, respectively. The buffer N-(2-hydroxyethyl)piperazine (HEPES)

used here and the neutral form of chlorophenol do not contribute significantly to the absorbance. The nitrate ion is present in the experimental solutions because nitrate salts are used as the source of the metals. The extinction coefficient of the chlorophenolate is determined experimentally by measuring the absorbance of several solutions free of nitrate but containing varying total concentrations of chlorophenol. Because the total chlorophenol concentrations are known, FITEQL can be used to calculate the concentrations of the chlorophenolate anion. The extinction coefficient of the chlorophenolate is then calculated by a linear regression relating the chlorophenolate concentrations to the observed absorbances. The nitrate extinction coefficient is determined similarly from samples free of chlorophenol.

Assuming a particular stoichiometry and stability constant for a metal-chlorophenolate complex, we use FITEQL to calculate a theoretical aqueous speciation. This theoretical speciation is then used in conjunction with the experimentally determined extinction coefficients to calculate a 'computed' absorbance:

$$A_{computed} = \varepsilon_{chlorophenolate} c_{chlorophenolate} + \varepsilon_{nitrate} c_{nitrate} \qquad (4)$$

The speciation calculation considers the proposed metal-chlorophenolate complex, but the computed absorbance does not include its effect, because it is not possible to experimentally determine the extinction coefficient of the complex without also knowing its true concentration. In our analysis, we apply the following χ^2 function

to quantify the difference between the computed and observed absorbances (Holm and Smothers, 1990):

$$\chi^2 = \sum_i (A_{i,\,observed} - A_{i,\,computed})^2 \qquad (5)$$

Here, the summation is performed for i solutions with varying metal:chlorophenol ratios. The χ^2 function is minimized when the stoichiometry and stability constant of the proposed metal-chlorophenol complex are most correct.

MATERIALS AND METHODS

The complexation between each of the three metals and the two chlorophenols has been studied independently in 0.1 M $NaClO_4$ electrolyte solutions. All reagents were obtained from Aldrich and used without further purification. Prior to use, the chlorinated phenols were powdered and passed through a 60 mesh sieve. Hydrated nitrate salts were used as the source of the metals. Distilled, deionized water (with a resistance of 18 MΩ) was used to make all solutions.

Potentiometric studies were performed with cadmium, lead and copper ion selective electrodes supplied by Orion, used in conjunction with an Orion Ag/AgCl double junction reference electrode. Free metal activity was monitored during two different types of titrations. First, the total concentrations of both the chlorophenol and metal were kept constant while the pH was varied through the addition of dilute

NaOH and/or HNO_3. In these pH titrations, total concentrations were $10^{-4.0}$ M for cadmium, $10^{-4.0}$ M for lead, $10^{-5.5}$ M for copper, $10^{-3.0}$ M for TCP and $10^{-5.0}$ M for PCP. Second, the total metal concentration was fixed, the pH was buffered with $10^{-2.0}$ M N-(2-hydroxyethyl)piperazine (HEPES) (Good et al., 1966), and the chlorophenol concentration was varied. For these chlorophenol titrations, the total concentrations were again $10^{-4.0}$ M for cadmium, $10^{-4.0}$ M for lead, and $10^{-5.5}$ M for copper, and the chlorophenol concentrations ranged from $10^{-5.0}$ to $10^{-2.0}$ M. Both the pH and the chlorophenol titrations were repeated in triplicate, with the exception of the lead system, for which only pH titrations in the presence of TCP were performed. Temperature was maintained at 25°C by immersion of the reaction vessels in a water bath, and N_2 gas was bubbled through the solutions in order to purge them of dissolved CO_2. Solution pH was measured with an Orion combination electrode, standardized against Fisher Scientific buffer solutions (2.00, 4.00, 7.00 and 10.00). The responses of the ISEs to the acid and base were characterized by performing pH titrations in the absence of chlorophenol. Similarly, the responses of the ISEs to the HEPES, the electrolyte, and the chlorophenols were tested by independently varying the concentrations of each in the absence of metal.

Spectrophotometric analyses were performed at 289 nm using ten centimetre cells and a Bausch and Lomb Spectronic 21. The study of each metal-chlorophenol system required sixteen combinations of four different total chlorophenol concentrations with four different total metal concentrations. In all cases, the solution pH was buffered to approximately 7 using $10^{-2.0}$ M HEPES, and the ionic

strength was maintained at 0.1 M using $NaClO_4$. Again, experiments in each metal-chlorophenol system were repeated in triplicate.

RESULTS

Ion Selective Electrode Experiments. Data for the titration of cadmium, cadmium-TCP and cadmium-PCP solutions are presented in Figure 2. The cadmium ISE was found to respond ideally to the activity of the Cd^{2+} ion, as indicated by linear calibration plots of electrode potential against log $[Cd^{2+}]$. The slopes of the calibration lines were found to be slightly sub-Nernstian at 25 - 28 mV/decade, in good agreement with the calibration slopes reported by other workers for similar ISEs (Heijne et al., 1978; Kivalo et al., 1976). The slope of the calibration line was found to change only slightly from day to day, whereas the intercept changed more drastically. Midgley (1987) has noted comparable results believed to be caused by degradation and photo-oxidation of the ISE membrane. In order to ensure that the calibration slope and intercept had not changed significantly during the course of a titration, electrode calibrations were performed both before and after each experiment. The cadmium ISE was not affected by pH or chlorophenol concentration, and after corrections for dilution, the experimental results from the chlorophenol-free systems adequately match the predicted changes in $[Cd^{2+}]$ due to hydrolysis (Fig. 2a). Thus, the decline in the electrode potential observed during the titration of the cadmium-chlorophenol systems may be

Figure 2: Cadmium ISE titration data. (a) Acid-base titration of chlorophenol-free solutions, and comparison of electrode response to theoretically predicted response. (b) TCP titration data. (c) PCP titration data. Different symbols represent replicate experiments.

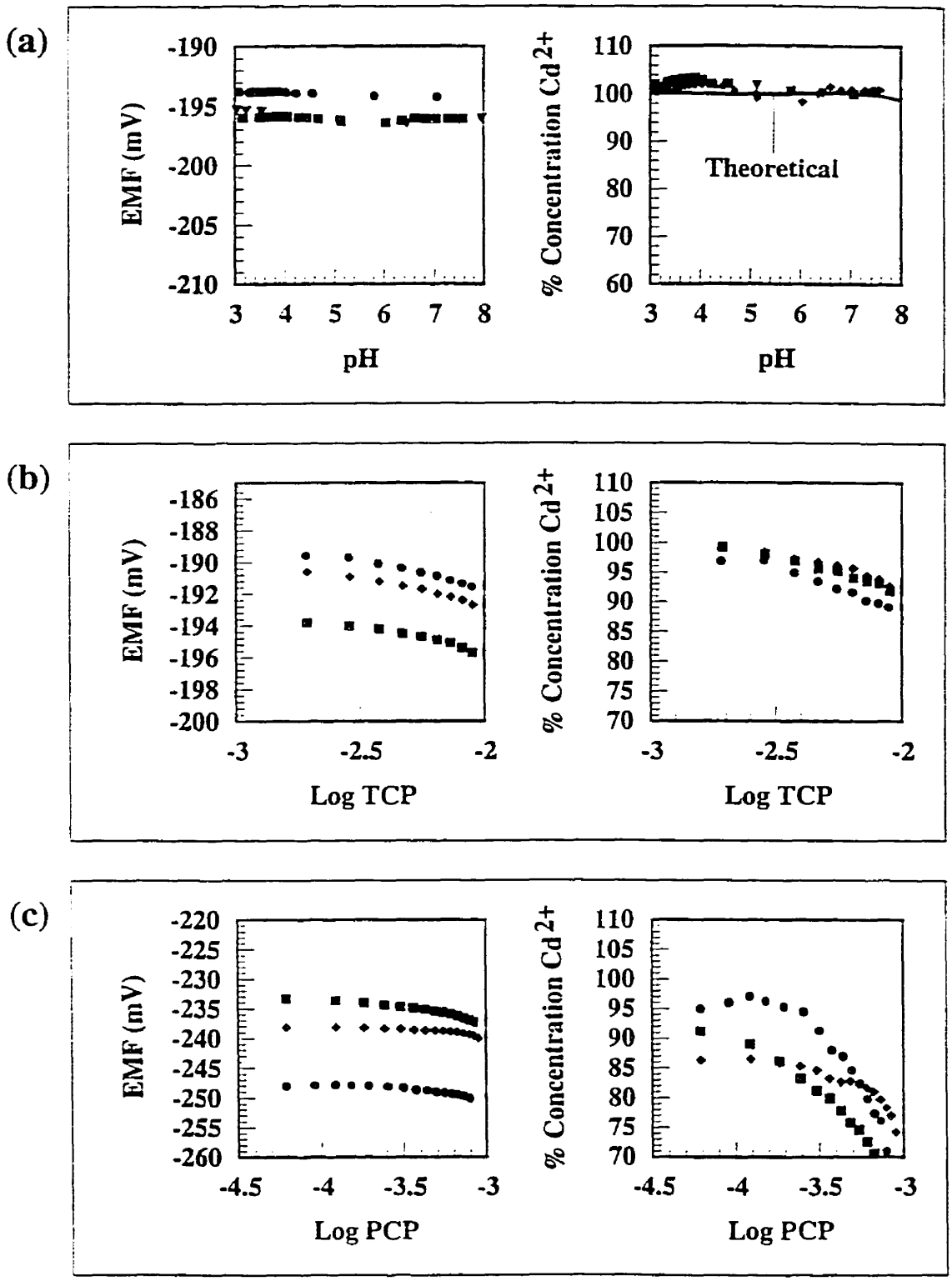
(a)
EMF (mV)
-190
-195
-200
-205
-210
3 4 5 6 7 8
pH
% Concentration Cd 2+
110
100
90
80
70
60
Theoretical
3 4 5 6 7 8
pH
(b)
EMF (mV)
-186
-188
-190
-192
-194
-196
-198
-200
-3 -2.5 -2
Log TCP
% Concentration Cd 2+
110
105
100
95
90
85
80
75
70
-3 -2.5 -2
Log TCP
(c)
EMF (mV)
-220
-225
-230
-235
-240
-245
-250
-255
-260
-4.5 -4 -3.5 -3
Log PCP
% Concentration Cd 2+
110
105
100
95
90
85
80
75
70
-4.5 -4 -3.5 -3
Log PCP

Figure 2

attributed directly and entirely to the complexation between cadmium and the chlorophenol.

Similarly, data for the titration of lead and lead-TCP solutions are presented in Figure 3. The lead ISE was also found to respond ideally to the activity of the Pb^{2+} ion, and similar sub-Nernstian slopes of 25 - 29 mV/decade were observed. The separation between the initial electrode potentials of repeated titrations is again due to daily changes in the calibration slope and intercept. The lead ISE was quite strongly affected by pH, as indicated by its inability to reproduce the predicted changes in the activity of Pb^{2+} due to hydrolysis (Fig. 3a). Even within the working pH range suggested by the electrode supplier (pH 4 - 7), the lead ISE clearly overestimates the concentration of free lead in solution at low pH and underestimates it at higher pH. Because there are no other complexing ions in the solution, it is apparent that the ISE responds to the activity of H^+. A similar effect caused by KNO_3 was reported by Heijne et al. (1978). A correction was applied to the raw titration data in order to calculate the true activity of free lead in solution (see below). The response of the lead ISE was not affected by either the chlorophenol or the HEPES. The slopes of the titration curves obtained in the presence of TCP are more negative than those obtained in the absence of TCP, which indicates significant lead-TCP complexation.

Titration data for the copper, copper-TCP and copper-PCP systems are shown in Figure 4. In order to avoid the precipitation of copper hydroxide in the upper pH range, total copper concentrations were reduced below the level at which the ISE responded in a Nernstian manner, and thus a second order polynomial

Figure 3: Lead ISE titration data. (a) Acid-base titration of chlorophenol-free solutions, and comparison of electrode response to theoretically predicted response. (b) TCP titration data, shown as a function of pH, after the application of the pH correction. Different symbols represent replicate experiments.

(a)

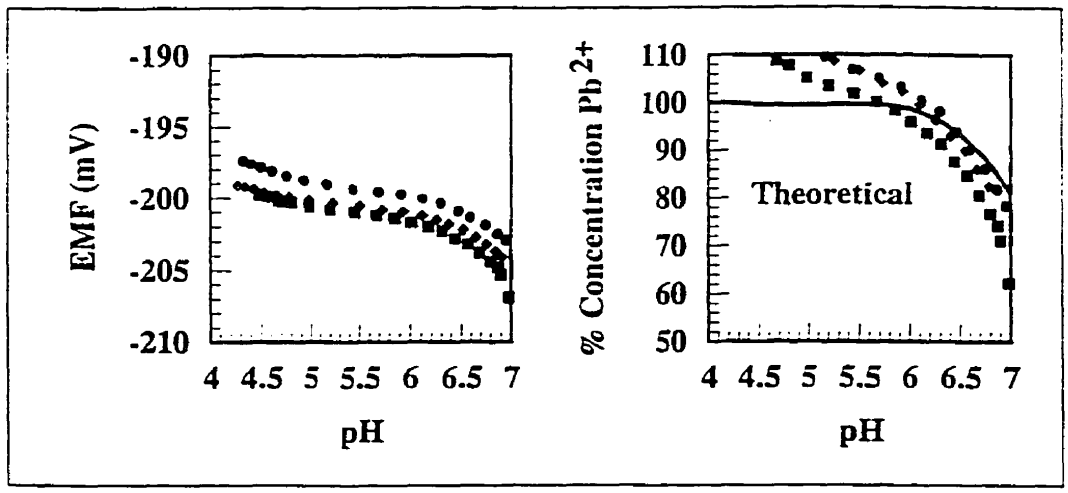
EMF (mV)
-190
-195
-200
-205
-210
4 4.5 5 5.5 6 6.5 7
pH
% Concentration Pb2+
110
100
90
80
70
60
50
Theoretical
4 4.5 5 5.5 6 6.5 7
pH

(b)

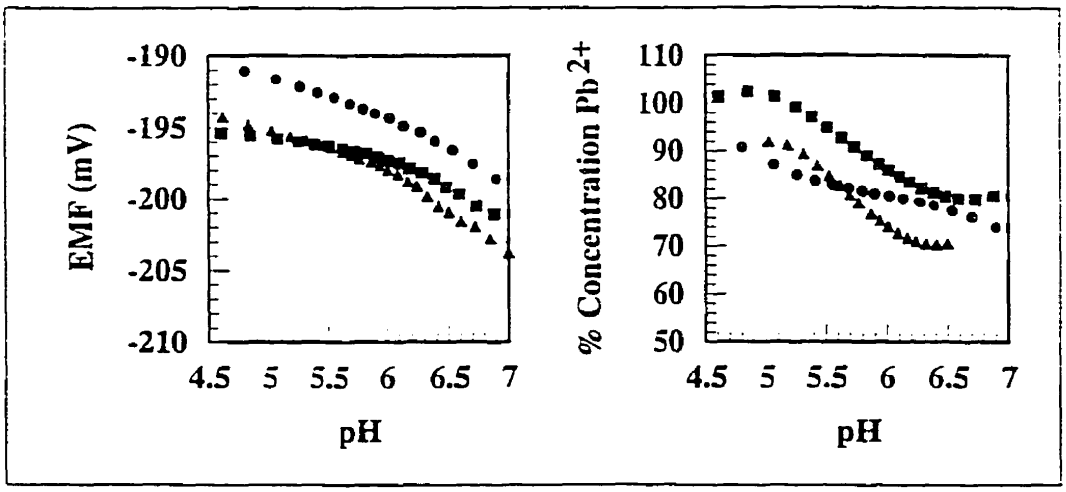
EMF (mV)
-190
-195
-200
-205
-210
4.5 5 5.5 6 6.5 7
pH
% Concentration Pb2+
110
100
90
80
70
60
50
4.5 5 5.5 6 6.5 7
pH

Figure 3

Figure 4: Copper ISE titration data. (a) Acid-base titration of chlorophenol-free solutions, and comparison of electrode response to theoretically predicted response. (b) TCP titration data. (c) PCP titration data. Data shown in (b) and (c) have been adjusted by a pH correction. Different symbols represent replicate experiments.

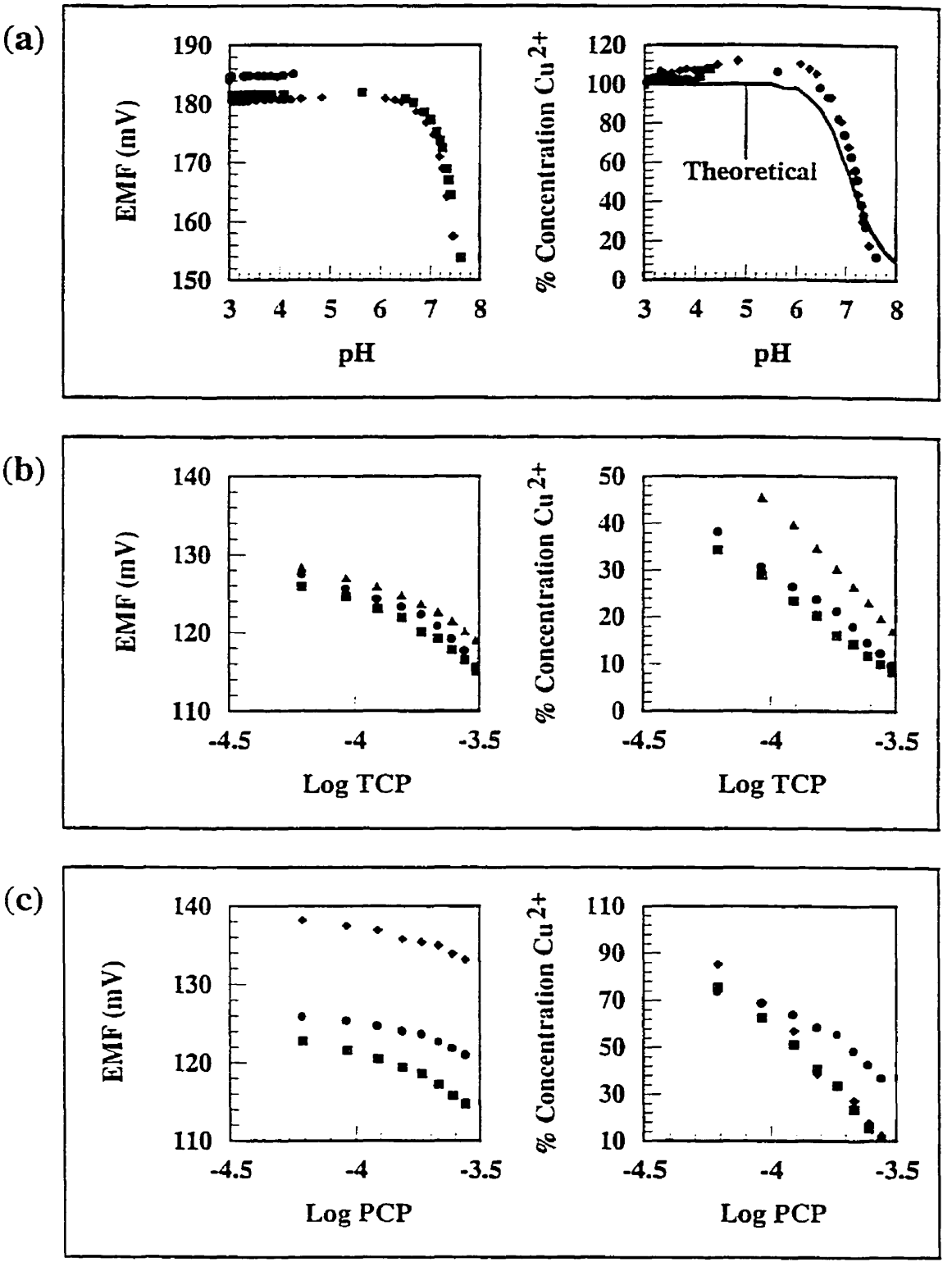
(a)
EMF (mV)
190
180
170
160
150
3 4 5 6 7 8
pH
% Concentration Cu 2+
120
100
80
60
40
20
0
Theoretical
3 4 5 6 7 8
pH
(b)
EMF (mV)
140
130
120
110
-4.5 -4 -3.5
Log TCP
% Concentration Cu 2+
50
40
30
20
10
0
-4.5 -4 -3.5
Log TCP
(c)
EMF (mV)
140
130
120
110
-4.5 -4 -3.5
Log PCP
% Concentration Cu 2+
110
90
70
50
30
10
-4.5 -4 -3.5
Log PCP

Figure 4

calibration curve was used. The copper ISE, like the lead ISE, also responded to the solution pH, although the style of the observed non-ideality was quite different. Again, a pH-based correction function was applied to the ISE response. The response of the copper ISE was also unaffected by the chlorophenols and the HEPES. The decline in the free metal activity with increasing total chlorophenol concentration is attributable to copper-chlorophenolate complexation.

The data in Figures 2 - 4 indicate that although the absolute EMF values of the ISEs changed quite drastically from day to day (due to shifts in the intercept of the electrode calibration line), the shape and slope of the titration lines remained quite constant. In light of this, the effect of pH on the lead and copper ISEs was quantified by examining the slopes of the metal (chlorophenol-free) titration lines, denoted here as $d(\text{EMF})/d(\text{pH})$, instead of the absolute electrode potentials. Figure 5 shows electrode slope plotted as a function of pH for several lead and copper solutions. The 'theoretical' curves represent the free metal activities derived from speciation calculations based on previously measured stability constants; they indicate the amount of free metal which is actually in the solution (see also Figure 1). Empirical regression equations were calculated for the 'observed' and 'theoretical' data, and the two functions were subtracted to quantify the effect of pH on the ISEs. Subsequently, the slope of each lead- and copper-chlorophenol titration line was calculated as a function of pH and then adjusted by the aforementioned pH correction. Using the corrected slope, the corresponding change in Pb^{2+} activity was calculated through division by the electrode calibration slope, S:

Figure 5: Comparison of theoretical (dashed lines) and observed (solid lines) response of (a) the lead and (b) the copper ISEs as a function of pH. Different symbols represent replicate experiments.

(a)

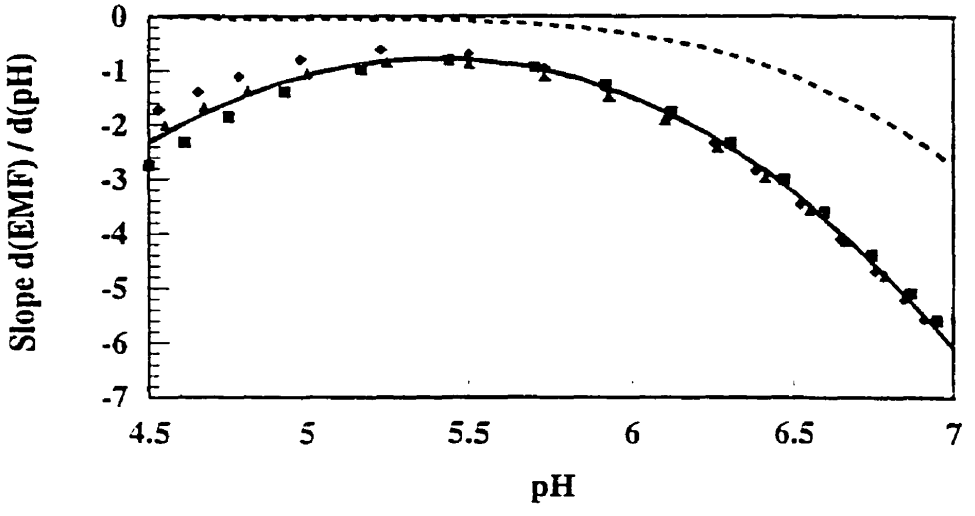
Slope d(EMF) / d(pH)
0
-1
-2
-3
-4
-5
-6
-7
4.5
5
5.5
6
6.5
7
pH

(b)

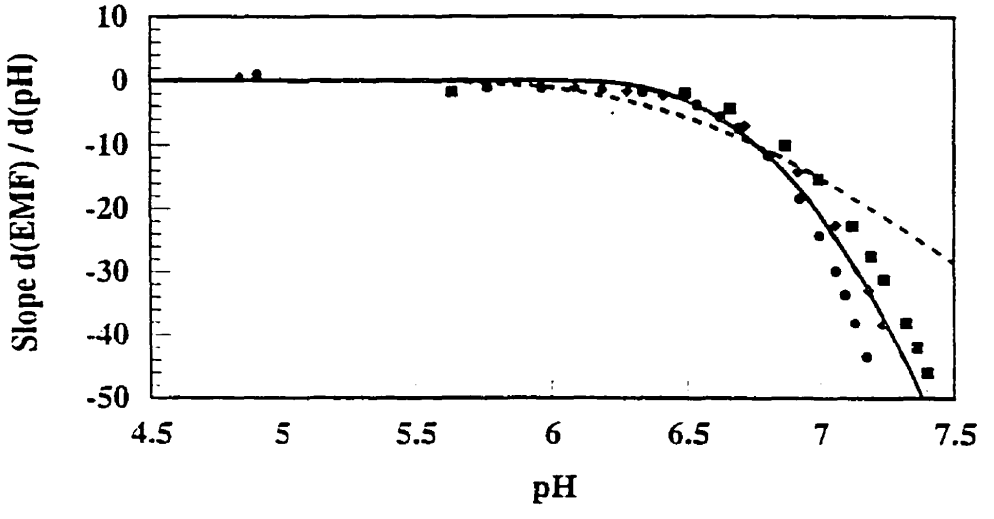
Slope d(EMF) / d(pH)
10
0
-10
-20
-30
-40
-50
4.5
5
5.5
6
6.5
7
7.5
pH

Figure 5

$$\left[\frac{d(\log[Pb^{2+}])}{d(pH)}\right] = \frac{1}{S}\left[\frac{d(EMF)}{d(pH)}\right] \qquad (5)$$

The square brackets denote the activity of the enclosed species. Note that this expression quantifies only the *change* in the activity of the free metal. In other words, the absolute activity of Pb^{2+} or Cu^{2+} cannot be determined unless the activity at the beginning of the titration was known. Here it is necessary to make a critical assumption: at low pH, where the electrode calibrations were performed, virtually all of the metal is in its uncomplexed form, and all of the chlorophenol exists as a neutral species; therefore, the concentration of the metal-chlorophenol complex(es) will be negligible, and the concentration of free metal may be assumed equal to the total metal concentration. This treatment was applied to calculate log $[Pb^{2+}]$ and $[Cu^{2+}]$ as a function of pH. We used these pH corrections to successfully reproduce previously measured stability constants in the lead- and copper-acetate systems, thus justifying their application to the metal-chlorophenol systems.

The FITEQL analyses of separate cadmium-, lead- and copper-chlorophenol titrations are presented in Tables 2, 3 and 4, respectively. These results pertain to the simultaneous analyses of data gathered both at fixed chlorophenol concentrations, as a function of pH, and at a fixed pH, as a function of total chlorophenol concentration. Models involving various combinations of complexes with several stoichiometries have been examined. The most appropriate model is that for which the log K values remain consistent between the repeated titrations,

TABLE 2: Cadmium-Chlorophenol Complexation Results as Modeled by FITEQL

Model[a]	Titration 1[b]		Titration 2[b]		Titration 3[b]	
	log K[c]	V[d]	log K[c]	V[d]	log K[c]	V[d]
$CdTCP^+$	2.41	1.49	2.31	0.99	2.43	9.37
$Cd(TCP)_2^0$	5.70	1.29	5.58	1.09	5.67	10.93
$Cd(OH)TCP^0$	-5.78	2.29	-5.60	3.47	-6.10	13.63
$CdTCP^+$ $Cd(OH)TCP^0$	2.24 -6.04	0.60	2.29 -6.58	1.10	2.40 -6.81	10.00
$CdTCP^+$ $Cd(TCP)_2^0$	no convergence[e]		no convergence[e]		no convergence[e]	
$CdTCP^+$ $Cd(OH)TCP^0$ $Cd(TCP)_2^0$	no convergence[e]		no convergence[e]		no convergence[e]	

Model[a]	Titration 1[b]		Titration 2[b]		Titration 3[b]	
	log K[c]	V[d]	log K[c]	V[d]	log K[c]	V[d]
$CdPCP^+$	3.05	0.02	3.05	0.03	3.27	0.06
$Cd(PCP)_2^0$	6.50	0.02	6.44	0.09	6.73	0.07
$Cd(OH)PCP^0$	-4.46	0.07	-4.71	0.16	-4.42	0.18
$CdPCP^+$ $Cd(OH)PCP^0$	no convergence[e]		no convergence[e]		no convergence[e]	
$CdPCP^+$ $Cd(PCP)_2^0$	2.75 6.22	0.06	no convergence[e]		no convergence[e]	
$CdPCP^+$ $Cd(OH)PCP^0$ $Cd(PCP)_2^0$	no convergence[e]		no convergence[e]		no convergence[e]	

[a]Chemical compositions of experimental solutions are given in the text. [b]Titrations are identical replicates; both pH and chlorophenol titrations are represented. [c]Log K values reported correspond to zero ionic strength. [d]Variance as calculated by FITEQL. [e]Indicates severe misfit between the model and the experimental data.

TABLE 3: Lead-Chlorophenol Complexation Results as Modeled by FITEQL

Model[a]	Titration 1[b]		Titration 2[b]		Titration 3[b]	
	log K[c]	V[d]	log K[c]	V[d]	log K[c]	V[d]
$PbTCP^+$	2.61	3.30	2.90	3.25	3.52	9.86
$Pb(TCP)_2^0$	5.97	3.02	6.24	10.49	7.47	15.69
$Pb(OH)TCP^0$	-4.01	11.75	-3.78	34.76	-3.01	59.16
$PbTCP^+$ $Pb(OH)TCP^0$	2.69 -8.46	3.93	2.97 -9.23	4.52	no convergence[e]	
$PbTCP^+$ $Pb(TCP)_2^0$	1.99 5.86	3.15	3.25 -10.80	45.77	no convergence[e]	
$PbTCP^+$ $Pb(OH)TCP^0$ $Pb(TCP)_2^0$	no convergence[e]		no convergence[e]		no convergence[e]	

[a]Chemical compositions of experimental solutions are given in the text. [b]Titrations are identical replicates: chlorophenol titrations were not performed. [c]Log K values reported correspond to zero ionic strength. [d]Variance as calculated by FITEQL. [e]Indicates severe misfit between the model and the experimental data.

TABLE 4: Copper-Chlorophenol Complexation Results as Modeled by FITEQL

Model[a]	Titration 1[b]		Titration 2[b]		Titration 3[b]	
	log K[c]	V[d]	log K[c]	V[d]	log K[c]	V[d]
$CuTCP^+$	4.88	0.29	5.09	0.40	4.97	0.15
$Cu(TCP)_2^0$	8.79	0.85	9.01	1.19	8.89	0.88
$Cu(OH)TCP^0$	-1.75	0.71	-1.50	1.23	-1.71	0.88
$CuTCP^+$ $Cu(OH)TCP^0$	no convergence[e]		no convergence[e]		no convergence[e]	
$CuTCP^+$ $Cu(TCP)_2^0$	4.84 7.79	0.31	5.05 8.03	0.44	4.93 7.92	0.15
$CuTCP^+$ $Cu(OH)TCP^0$ $Cu(TCP)_2^0$	no convergence[e]		no convergence[e]		no convergence[e]	

Model[a]	Titration 1[b]		Titration 2[b]		Titration 3[b]	
	log K[c]	V[d]	log K[c]	V[d]	log K[c]	V[d]
$CuPCP^+$	4.11	0.03	4.39	0.77	4.43	1.39
$Cu(PCP)_2^0$	8.03	0.11	8.50	0.16	8.53	0.92
$Cu(OH)PCP^0$	-2.66	0.09	-2.15	0.13	-2.11	0.91
$CuPCP^+$ $Cu(OH)PCP^0$	no convergence[e]		no convergence[e]		no convergence[e]	
$CuPCP^+$ $Cu(PCP)_2^0$	4.00 7.39	0.03	no convergence[e]		no convergence[e]	
$CuPCP^+$ $Cu(OH)PCP^0$ $Cu(PCP)_2^0$	no convergence[e]		no convergence[e]		no convergence[e]	

[a]Chemical compositions of experimental solutions are given in the text. [b]Titrations are identical replicates; both pH and chlorophenol titrations are represented. [c]Log K values reported correspond to zero ionic strength. [d]Variance as calculated by FITEQL. [e]Indicates severe misfit between the model and the experimental data.

and the variances calculated by FITEQL are sufficiently low to imply an excellent correlation between the model and the experimental data. Applying these criteria, each of the metal-chlorophenol systems are well modelled by a single complex having either a 1:1 or a 1:2 stoichiometry. Based on the small differences in the calculated variances, there is little statistical basis to choose between these two models. However, in the experiments performed here, where the chlorophenol concentration is gradually increased, it is not likely that the 1:2 complex would become significant before the 1:1 complex. The models involving two types of complex (both 1:1 and 1:2) do not provide a significantly improved fit over the models involving only the 1:1 complex, and commonly, they fail to converge entirely. This suggests that the 1:2 complex is not significant under these experimental conditions. For this reason, and for reasons relating to the spectrophotometric data below, we choose to model the experimental data using a single complex with a 1:1 stoichiometry. This single complex adequately describes the experimental data over all pH ranges and chlorophenol concentrations. Average log K values determined by ISE potentiometry are listed in Table 5.

The errors in the magnitude of the stability constants reported in Table 5 arise from three sources. First, the largest source of error involves the temporal variability in the electrode response itself, as manifested by the difference in the metal-chlorophenol log K values from replicate experiments. From Table 5, we consider the electrode response to cause 2σ errors in the average log K values for the Cd-, Pb- and Cu-chlorophenolate complexes of $\pm$ 0.1, $\pm$ 0.5 and $\pm$ 0.2 log units respectively. Second, errors associated with the ISE pH corrections must be

TABLE 5: Summary of Stability Constants Determined by ISE Potentiometry

Model	Log K			
	Trial 1[a]	Trial 2[a]	Trial 3[a]	Average
$CdTCP^+$	2.41	2.31	2.43	2.4±0.1
$CdPCP^+$	3.05	3.05	3.27	3.1±0.1
$PbTCP^+$	2.61	2.90	3.52	3.0±0.5
$CuTCP^+$	4.88	5.09	4.97	5.0±0.4
$CuPCP^+$	4.11	4.39	4.43	4.3±0.4

[b]Trials are identical replicates.

considered in the Pb and Cu systems. Variability in the Pb pH correction function is minimal across the pH range of the titrations (Figure 5), and thus the associated errors are negligible. By contrast, variability in the Cu pH correction increases slightly with pH. However, the Cu experiments were conducted at or below pH 7.5, where the error associated with the pH correction function is less than 5%. This error imparts an error of ± 0.2 log units to the determination of the Cu-chlorophenolate stability constants. Third, we also consider errors caused by our reliance on literature values for the stability constants listed in Table 1. The first three copper hydrolysis stability constants are maxima, and are not well constrained. However, the omission of these equilibria from the model changes the Cu-chlorophenolate log K values by less than 0.005 log units. The stability constants of the $NaNO_3^0$, $Pb(NO_3)_3^-$, $Pb(NO_3)_4^{2-}$ and $Pb(CO_3)_4^{2-}$ complexes listed in Table 1 have been adjusted from the literature values to zero ionic strength and 25°C. The method of extrapolation imparts some error, but the omission of these equilibria from the model does not change any of the metal-chlorophenolate stability constants by more than 0.005 log units. We thus conclude that the Cd-, Pb-, and Cu-chlorophenolate stability constants determined by ISE potentiometry carry 2σ errors of ± 0.1, ± 0.5 and ± 0.4 log units respectively.

Spectrophotometric Experiments. Representative experimental data for the spectrophotometric analyses of each metal-chlorophenol system are given in Tables 6, 7 and 8. The results of the replicate trials are summarized in Table 9 and displayed in Figure 6. The log K values plotted along the abscissa of Figure 6 describe the strength of the metal-chlorophenol stability constant used to calculate

TABLE 6: Representative Cadmium-Chlorophenol Spectrophotometric Experimental Data

Log M Cd_T	Log M TCP_T	A_{289}[a]	Log M Cd_T	Log M PCP_T	A_{289}[a]
—	-5.751	0.025	—	-5.746	0.032
-4.354	-5.753	0.029	-4.354	-5.749	0.033
-4.038	-5.756	0.034	-4.051	-5.751	0.043
-3.881	-5.758	0.040	-3.887	-5.753	0.051
—	-5.501	0.046	—	-5.504	0.063
-4.354	-5.503	0.056	-4.390	-5.506	0.066
-4.047	-5.505	0.055	-4.055	-5.508	0.070
-3.881	-5.507	0.060	-3.894	-5.510	0.071
—	-5.252	0.090	—	-5.251	0.109
-4.354	-5.254	0.092	-4.372	-5.253	0.110
-4.055	-5.256	0.095	-4.064	-5.256	0.117
-3.881	-5.258	0.108	-3.881	-5.258	0.125
—	—	0.000	—	—	0.000
-4.337	—	0.009	-4.373	—	0.010
-4.055	—	0.012	-4.055	—	0.014
-3.881	—	0.018	-3.879	—	0.019
$\varepsilon_{nitrate}$[b] = 71.66 $\varepsilon_{trichlorophenolate}$[b] = 1646.0			$\varepsilon_{nitrate}$[b] = 78.32 $\varepsilon_{pentachlorophenolate}$[b] = 1950.9		

[a]Absorbance measured in ten centimetre cells at 289 nm.
[b]Extinction coefficients (cm^{-1} M^{-1}) calculated from concentrations of free chlorophenolate and nitrate by linear regression.

TABLE 7: Representative Lead-Chlorophenol Spectrophotometric Experimental Data

Log M Pb_T	Log M TCP_T	A_{289}[a]	Log M Pb_T	Log M PCP_T	A_{289}[a]
—	-5.752	0.031	—	-5.748	0.036
-4.330	-5.756	0.039	-4.637	-5.750	0.040
-4.024	-5.761	pptn[b]	-4.321	-5.753	0.045
-3.849	-5.765	pptn[b]	-4.153	-5.755	0.047
—	-5.501	0.052	—	-5.501	0.061
-4.321	-5.506	0.060	-4.602	-5.503	0.067
-4.024	-5.510	0.068	-4.321	-5.505	0.064
-3.849	-5.514	pptn[b]	-4.164	-5.507	pptn[b]
—	-5.252	0.084	—	-5.255	0.105
-4.312	-5.256	0.097	-4.620	-5.257	pptn[b]
-4.024	-5.260	0.126	-4.321	-5.259	0.116
-3.850	-5.264	0.137	-4.153	-5.261	0.117
—	—	0.000	—	—	0.000
-4.312	—	0.014	-4.620	—	0.013
-4.020	—	0.018	-4.312	—	0.014
-3.850	—	pptn[b]	-4.153	—	0.020
$\varepsilon_{nitrate}$[c] = 106.10 $\varepsilon_{trichlorophenolate}$[c] = 1697.2			$\varepsilon_{nitrate}$[c] = 104.96 $\varepsilon_{pentachlorophenolate}$[c] = 1924.6		

[a]Absorbance measured in ten centimetre cells at 289 nm. [b]Precipitation of metal hydroxide occurred; absorbance values were omitted from calculations. [c]Extinction coefficients (cm^{-1} M^{-1}) calculated from concentrations of free chlorophenolate and nitrate by linear regression.

TABLE 8: Representative Copper-Chlorophenol Spectrophotometric Experimental Data

Log M Cd_T	Log M TCP_T	A_{289}[a]	Log M Cd_T	Log M PCP_T	A_{289}[a]
—	-6.001	0.020	—	-6.001	0.022
-5.226	-6.002	0.034	-5.463	-6.002	0.031
-4.724	-6.002	0.052	-5.204	-6.003	0.038
-4.503	-6.003	pptn[b]	-5.029	-6.003	0.046
—	-5.801	0.031	—	-5.804	0.034
-5.504	-5.802	0.037	-5.504	-5.805	0.040
-5.226	-5.803	0.044	-5.204	-5.806	0.048
-5.014	-5.804	0.055	-5.029	-5.807	0.056
—	-5.601	0.044	—	-5.605	0.049
-5.505	-5.602	0.054	-5.505	-5.606	0.056
-5.204	-5.603	0.061	-5.205	-5.607	0.063
-5.029	-5.603	0.071	-5.028	-5.608	0.073
—	—	0.000	—	—	0.000
-5.504	—	0.013	-5.504	—	0.009
-5.204	—	0.019	-5.204	—	0.016
-5.029	—	0.025	-5.029	—	0.025
$\varepsilon_{nitrate}$[c] = 146.61 $\varepsilon_{trichlorophenolate}$[c] = 1997.9			$\varepsilon_{nitrate}$[c] = 134.93 $\varepsilon_{pentachlorophenolate}$[c] = 2057.8		

[a]Absorbance measured in ten centimetre cells at 289 nm. [b]Precipitation of metal hydroxide occurred; absorbance values were omitted from calculations. [c]Extinction coefficients ($cm^{-1} M^{-1}$) calculated from concentrations of free chlorophenolate and nitrate by linear regression.

TABLE 9: Summary of Stability Constants Determined by Spectrophotometry

Model[a]	Log K			
	Trial 1[b]	Trial 2[b]	Trial 3[b]	Average
$CdTCP^{+}$	2.6	2.5	2.6	2.6±0.3
$CdPCP^{+}$	2.7	2.4	2.7	2.6±0.3
$PbTCP^{+}$	3.0	3.3	3.0	3.1±0.3
$PbPCP^{+}$	2.8	3.0	2.8	2.8±0.3
$CuTCP^{+}$	4.8	4.8	4.8	4.8±0.3
$CuPCP^{+}$	4.1	4.2	4.1	4.1±0.3

[a]Models involving complexes with other stoichiometries fail to converge. [b]Trials are identical replicates.

Figure 6: Stability constants as determined by UV spectrophotometry. All curves are calculated for single metal-chlorophenolate complexes with 1:1 stoichiometries. The numbers at right represent the confidence levels corresponding to selected F-ratios.

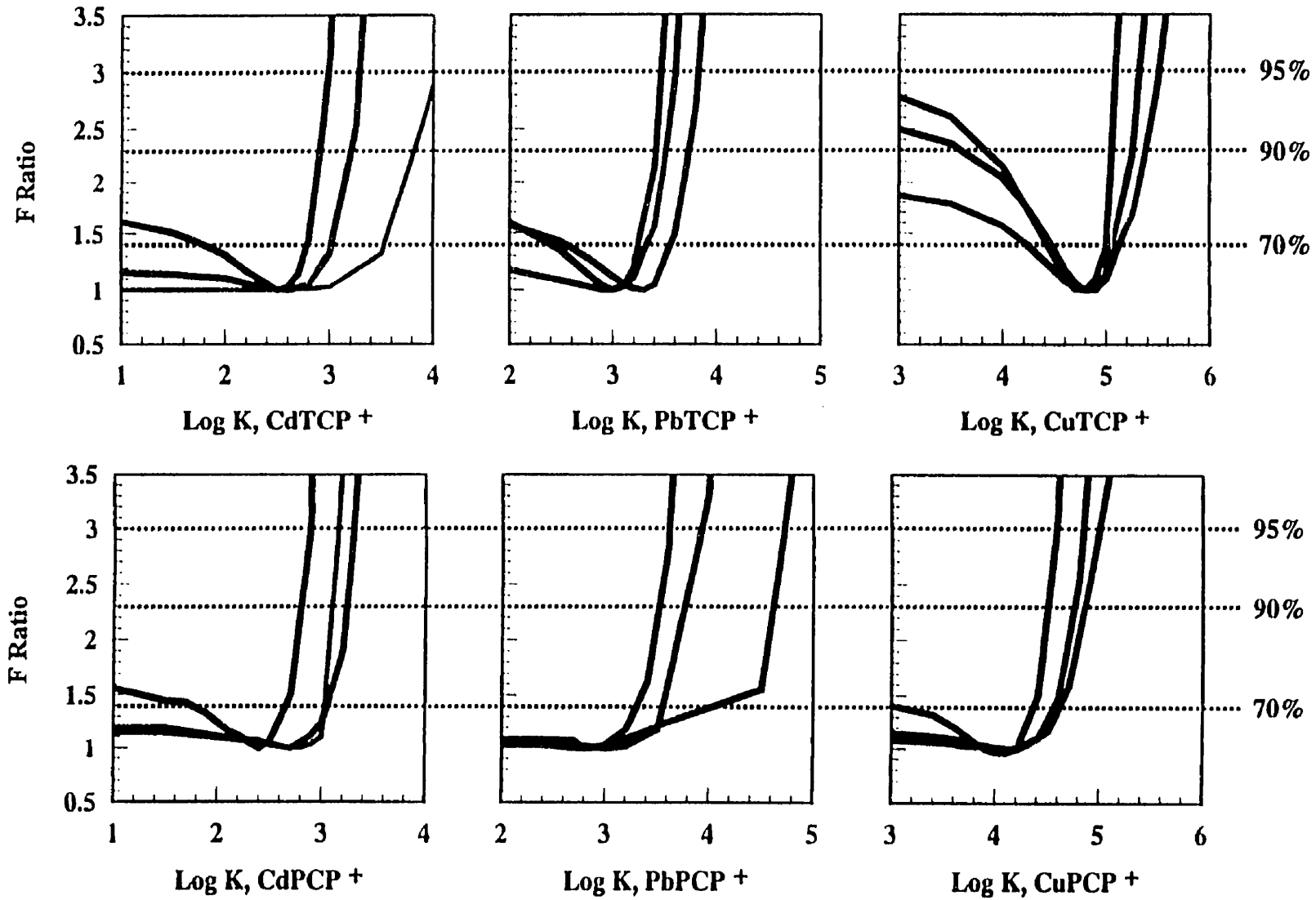
F Ratio
3.5
3
2.5
2
1.5
1
0.5
95%
90%
70%
1
2
3
4
Log K, CdTCP +
2
3
4
5
Log K, PbTCP +
3
4
5
6
Log K, CuTCP +
F Ratio
Log K, CdPCP +
Log K, PbPCP +
Log K, CuPCP +

Figure 6

the solution speciation. The experimentally measured χ^2 function (Equation 5) is normalized such that the minima all occur at unity. The normalization allows the functions to be described by an F-ratio, equal to χ^2/χ^2_{min}. The minima of the normalized χ^2 functions occur at the true value of the stability constant, with increased χ^2 values associated with both under-estimation and over-estimation of the pertinent stability constant. The experimental data are best fit by a model involving a single complex with a 1:1 stoichiometry. Attempts to calculate stability constants for metal-chlorophenolate complexes of other stoichiometries yield χ^2 functions which do not converge to consistent minimum values, or fail to converge entirely. This, and the agreement between the 1:1 stability constant values calculated using the two different analytical techniques strongly suggests that only the 1:1 complex is important under these experimental conditions.

The errors in the log K values reported in Table 9 arise from three sources. First, those caused by instrument noise are manifested by the variability in the position of the χ^2 minima, yielding a 2σ error of $\pm$ 0.1 log units in each metal-chlorophenolate stability constant. Second, the existence of the minima must be statistically verified. We use the normalized F-ratios to show the confidence limit at which a particular minimum can be judged to be statistically significant. Applying the 70% confidence limit, we note that over-estimation of the stability constant produces a statistically significant minimum 0.3 log units above its true value in all the metal-chlorophenolate systems studied. In contrast, the F-ratios involved with under-estimation of the stability constant are lower than those involved with over-estimation, due to the logarithmic nature of the abscissa scale. The F-ratios of

under-estimation ultimately plateau as the proposed metal-chlorophenol complex becomes insignificant as the log K values decrease. In the under-estimation of the stability constants (at the 70% confidence limit), the existence of the minima is verified only in some systems, and then at up to one log unit below their true values. Thus we cannot place accurate lower limits on the value of the stability constants determined by spectrophotometry. A third source of error, the reliance on literature values for the stability constants listed in Table 1, has been discussed above. This does not impart significant error to the determination of the metal-chlorophenol stability constants. We conclude that the metal-chlorophenolate stability constants determined by UV spectrophotometry carry 2σ errors of ± 0.3 log units, though we acknowledge the uncertainty of the lower limits.

CONCLUSION

The data presented above are the first to quantify the extent of aqueous complexation in mixed metal-TCP and -PCP systems. The log stability constants and errors are summarized in Table 10, and Figure 7 displays the speciation of the three metals in the presence of the chlorinated phenols. The speciation is significantly modified in all cases (see Figure 1), and dramatically modified in the copper-chlorophenol systems. At present, the effects of this complexation on other geochemical processes are undetermined, although these potential effects may be substantial. For example, we may consider adsorption onto a mineral surface. The adsorption of a positively charged metal ion, such as Pb^{2+}, onto many mineral

TABLE 10: Summary of the Stability Constants Determined for the Various Metal-Chlorophenol Complexes

Complex	Average Log K		
	ISE Pot.	Spec.	Average
$CdTCP^+$	2.4±0.1	2.6±0.3	2.5±0.3
$CdPCP^+$	3.1±0.1	2.6±0.3	2.9±0.3
$PbTCP^+$	3.0±0.5	3.1±0.3	3.0±0.5
$PbPCP^+$	N/A	2.8±0.3	2.8±0.3
$CuTCP^+$	5.0±0.4	4.8±0.3	4.9±0.4
$CuPCP^+$	4.3±0.4	4.1±0.3	4.2±0.4

Figure 7: Aqueous speciation diagrams for: a) cadmium in the presence of TCP; b) cadmium in the presence of PCP; c) lead in the presence of TCP; d) lead in the presence of PCP; e) copper in the presence of TCP; and f) copper in the presence of PCP. Total chlorophenol = $10^{-3.0}$ M; total metal = $10^{-4.0}$ M. Systems are assumed to be free from dissolved carbon dioxide.

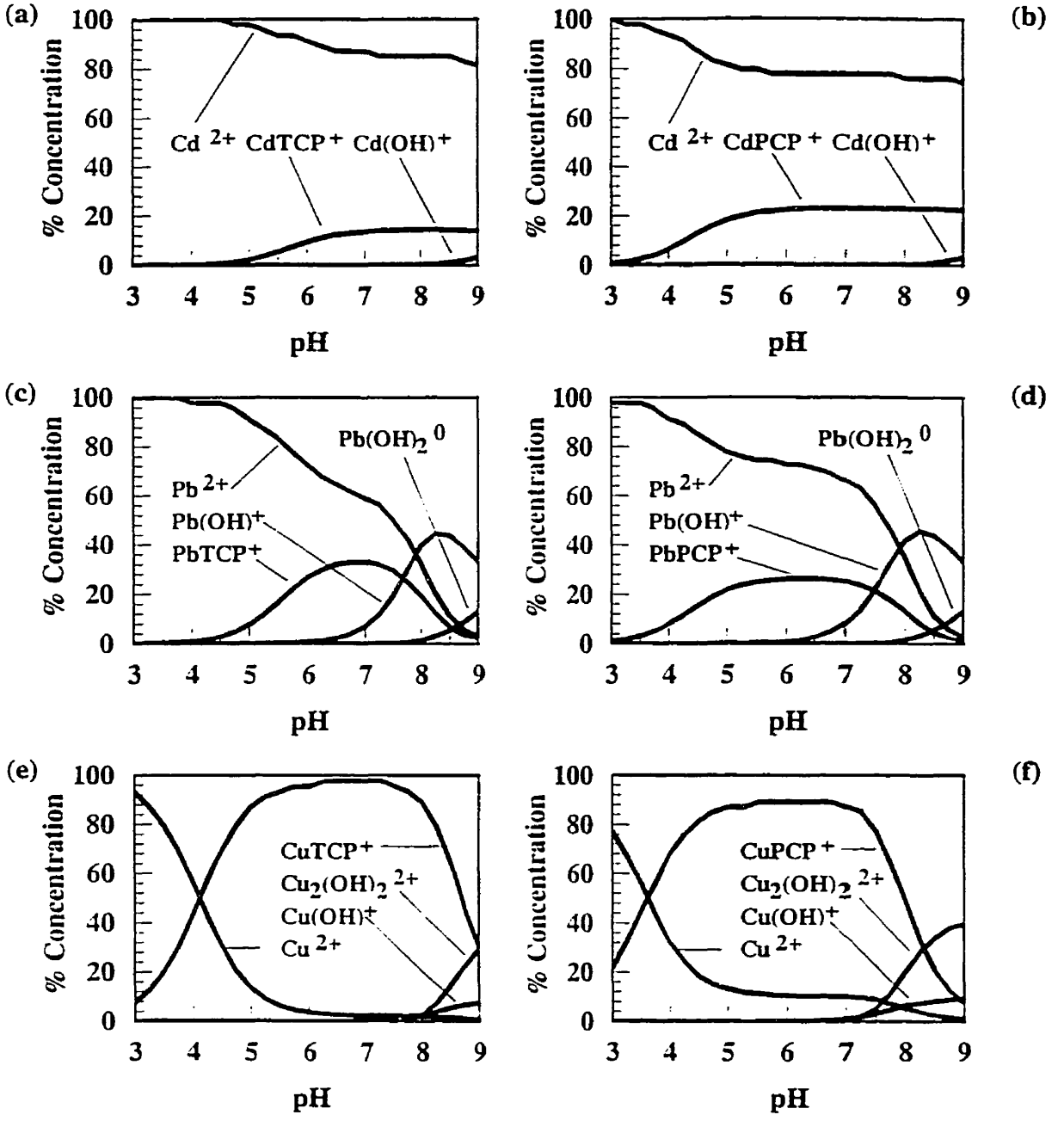
(a)
% Concentration
100
80
60
40
20
0
Cd 2+ CdTCP+ Cd(OH)+
3 4 5 6 7 8 9
pH
(b)
% Concentration
Cd 2+ CdPCP+ Cd(OH)+
pH
(c)
% Concentration
Pb(OH)2 0
Pb 2+
Pb(OH)+
PbTCP+
pH
(d)
% Concentration
Pb(OH)2 0
Pb 2+
Pb(OH)+
PbPCP+
pH
(e)
% Concentration
CuTCP+
Cu2(OH)2 2+
Cu(OH)+
Cu 2+
pH
(f)
% Concentration
CuPCP+
Cu2(OH)2 2+
Cu(OH)+
Cu 2+
pH

Figure 7

surfaces is electrostatically controlled, as evidenced by extensive metal adsorption in basic solutions, where many mineral surfaces are negatively charged (Gunneriusson et al., 1994; Davis and Kent, 1990; Schindler and Stumm, 1987; Hohl and Stumm, 1976). If the adsorption behaviour of the chlorophenols is also electrostatically controlled, they may not adsorb at all in the high pH range, because they will exist as anions. However, the complexation data presented above show that up to 40% of the total TCP may exist as $PbTCP^+$, and hence the complex may adsorb as a whole. Conversely, if the complex tends to remain in solution, the adsorption of the metal may be reduced. Both scenarios may affect the mobility of these chemicals in the groundwater zone. In addition to its effect upon adsorption reactions, metal-chlorophenol complexation may influence other geochemical reactions such as mineral dissolution, (bio)chemical degradation, and organic matter partitioning. Further research is essential if the environmental fate of these pollutants is to be adequately predicted.

The use of the two very different analytical procedures applied here has been extremely useful in the determination of aqueous stability constants. The potentiometric approach, because it measures changes in free metal activity resulting from metal-chlorophenol complexation, requires a chlorophenol-dominated system. By contrast, the spectrophotometric technique requires a metal-dominated system because it measures changes in chlorophenol concentration caused by complexation. The combination of the two methods allows for extensive variation in the total metal to ligand ratio. Additionally, the potentiometric pH titrations allow the ratio of the organic ligand to the hydroxide ion to be varied as well. Interestingly, the data

gathered here suggest that a single complex with a 1:1 metal:chlorophenolate stoichiometry is dominant under all of the chemical conditions used in this study. Further, this range of chemical conditions covers the effective limits expected in natural environments: the metal concentrations range from several ppm to ppb; the pH varies across the range common to most natural waters; the experiments were performed both well below and very close to the saturation of the metal hydroxides; and the highest chlorinated phenol concentrations approached the limit of aqueous solubility. The stability constants reported here may thus be applied to virtually any natural system.

The thermodynamic approach to this work allows the prediction of the relative magnitudes of stability constants describing other metal-chlorophenolate complexes. The measured stability constants are in good agreement with those predicted by Fein (1996). This suggests that a relatively simple linear correlation technique may be effectively used to estimate the values of other metal-chlorophenolate stability constants, even those which differ by several orders of magnitude. Using the technique described by Langmuir (1979), we relate the metal-chlorophenolate stability constants determined in this work to stability constants describing complexation between the same metals and a second anion. If such correlations are valid, then an unknown metal-chlorophenolate stability constant may be estimated from the stability constant of the corresponding metal-anion complex. Here, we compare the stability constants describing the complexation of cadmium, lead and copper by TCP and PCP to those describing complexation of the same metals by hydroxide, oxalate and tiron (1,2-dihydroxybenzene-3,5-disulfonic

acid) (see Table 11). Good correlations between the metal-chlorophenolate and the metal-hydoxide, -oxalate, and -tiron stability constants exist, supporting the use of this technique (Figure 8). In Table 12, we predict the stability constants of TCP and PCP complexes involving other metals. Because this study is the first to measure metal-polychlorophenolate stability constants, Fein (1996) could only predict metal-polychlorophenolate stabilities from metal-phenolate stability constants. Our predictions, although based on only six experimental measurements, should more accurately describe metal-TCP and metal-PCP complexation. For example, Zn^{2+}, a common contaminant at wood treatment sites, should complex strongly with TCP and PCP. Complexation of common rock forming cations will be variable: Al^{3+} probably forms strong polychlorophenolate complexes, whereas complexation by Ca^{2+} is likely to be insignificant. Thus, not only do the data presented above quantify the extent of complexation in the measured systems, but they can be used to predict the strength of complexation in many other metal-chlorophenol systems.

ACKNOWLEDGEMENTS

Funding for this study was provided by N.S.E.R.C. and F.C.A.R. (Nouveaux Chercheurs) research grants to J.B.F. We are indebted to Martin Fey and Peter Linder for assistance provided to C.J.D. at the University of Cape Town. We also thank Lydia Scratch for conducting some of the experiments.

TABLE 11: Measured Metal-Organic Stability Constants

Metal	Log K for 1:1 Metal-Organic Complex[a]		
	Hydroxide	Oxalate	Tiron
Cd	3.9	3.89	10.29
Pb	6.3	4.91	14.97
Cu	6.3	6.23	15.17

[a]Data from Martell and Smith (1977a, b) adjusted, if required, to zero ionic strength and 25°C using the Davies equation.

TABLE 12: Predicted Metal-TCP and Metal-PCP Stability Constants

Complex	Log Stability Constant[a]			
	Hydroxide	Oxalate	Tiron	Average
$CaTCP^{+}$	0.9	1.3	1.0	1.1 ± 0.3
$MgTCP^{+}$	1.7	1.8	1.3	1.6 ± 0.3
$NiTCP^{+}$	2.6	3.6	2.3	2.8 ± 0.8
$ZnTCP^{+}$	3.1	3.3	2.5	3.0 ± 0.5
$FeTCP^{2+}$	7.4	9.0	5.7	7.4 ± 1.7
$AlTCP^{2+}$	6.6	7.4	5.3	6.4 ± 1.1
$(UO_2)TCP^{+}$	5.1	5.8	4.2	5.0 ± 0.8
$HgTCP^{+}$	6.6	9.4	5.3	7.1 ± 2.3
$CaPCP^{+}$	1.8	2.0	1.8	1.8 ± 0.2
$MgPCP^{+}$	2.2	2.2	2.0	2.1 ± 0.1
$NiPCP^{+}$	2.8	3.4	2.6	2.9 ± 0.5
$ZnPCP^{+}$	3.1	3.2	2.7	3.0 ± 0.3
$FePCP^{2+}$	5.5	6.7	4.6	5.6 ± 1.1
$AlPCP^{2+}$	5.1	5.7	4.3	5.0 ± 0.7
$(UO_2)PCP^{+}$	4.2	4.7	3.7	4.2 ± 0.5
$HgPCP^{+}$	5.1	6.9	4.3	5.4 ± 1.5
R^2_{TCP}[b]	0.67	0.97	0.70	
R^2_{PCP}[b]	0.60	0.95	0.63	

[a]Stability constants predicted by linear regression, based upon the metal-organic values given in Table 10. Values correspond to zero ionic strength and 25°C. [b]Correlation coefficent relating log K of metal-chlorophenolate complex to log K of metal-organic complex.

Figure 8: Correlation diagram relating a) metal-trichlorophenolate and b) metal-pentachlorophenolate log stability constants to the metal-hydroxide, metal-oxalate and metal-tiron log stability constants listed in Table 11. Linear correlation coefficients are shown for each relationship.

(a)

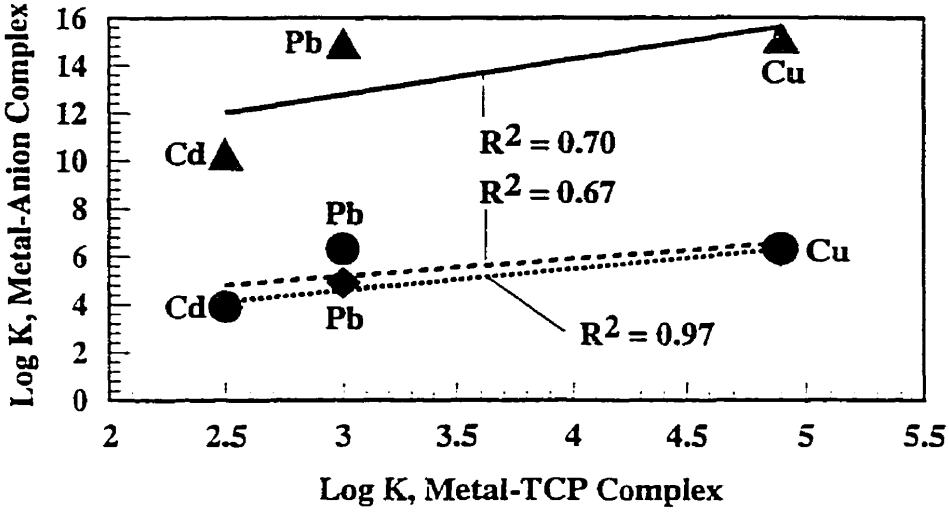

(b)

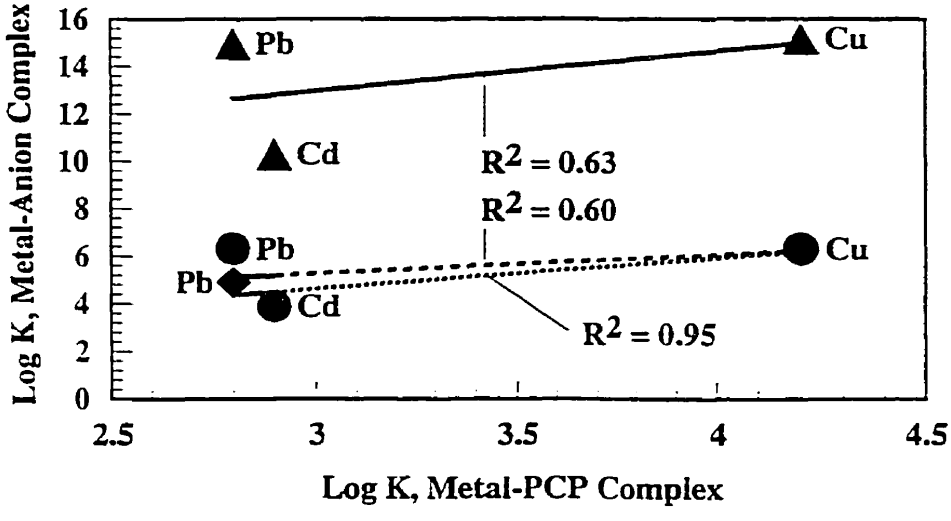

Chlorophenolate-Hydroxide Correlation
Chlorophenolate-Oxalate Correlation
Chlorophenolate-Tiron Correlation
Chlorophenolate-Hydroxide Regression Line
Chlorophenolate-Oxalate Regression Line
Chlorophenolate-Tiron Regression Line

Figure 8

REFERENCES

Baes C. F. Jr. and Mesmer R. E. (1976) *The Hydrolysis of Cations*. John Wiley and Sons.

Buffle J. (1988) *Complexation Reactions in Aquatic Systems: An Analytical Approach*. John Wiley and Sons.

Callahan M. A., Slimak M. W., Gabel N. W., May I. P., Fowler C., Freed J. R., Jennings P., Durfee R. L., Whitmore F. C., Maestri B., Mabey W. R., Holt B. R. and Gould C. (1979) *Water-Related Environmental Fate of 129 Priority Pollutants*, Report EPA-440-4-79-029a. U. S. Environmental Protection Agency.

Davis J. A and Kent D. B. (1990) Surface complexation modeling in aqueous geochemistry. In *Mineral-Water Interface Geochemistry* (ed. M. F. Hochella, Jr. and A. F. White), Reviews in Mineralogy, Vol. 23, pp. 177-260. Mineralogical Society of America.

Fein J. B. (1996) The effect of aqueous metal-chlorophenolate complexation on contaminant transport in groundwater systems. *Applied Geochmistry*, in press.

Fein J.B. and Hestrin J. E. (1994) Experimental studies of oxalate complexation at 80°C: Gibbsite, amorphous silica, and quartz solubilities in oxalate-bearing fluids. *Geochim. Cosmochim. Acta* **58,** 4817-4829.

Fein J.B., Gore N., Marshall D., Yassa L., Loch A., and Brantley S.L. (1995) The effect of aqueous complexation and gibbsite surface sites on the decarboxylation rate of malonate. *Geochim. Cosmochim. Acta* **59,** 5071-5080.

Fergusson J. E. (1990) *The Heavy Elements: Chemistry, Environmental Impact and Health Effects*. Pergamon.

Good N. E., Winget G. D., Winter W., Connolly T. N., Izawa S., and Singh M. M. (1966) Hydrogen ion buffers for biological research. *Biochemistry* **5,** 467-477.

Gu Y., Gammons C. H., and Bloom M. S. (1994) A one-term extrapolation method for estimating equilibrium constants of aqueous reactions at elevated temperatures. *Geochim. Cosmochim. Acta* **58,** 3545-3560.

Gunneriusson L., Lövgren L., and Sjöberg S. (1994) Complexation of Pb(II) at the geothite (α-FeOOH) / fresh water interface: The influence of chloride. *Geochim. Cosmochim. Acta* **58,** 4973-4983.

Heijne G. J. M., van der Linden W. E., and Den Boef G. (1978) The formation and properties of mixed lead sulfide - silver sulfide membranes for lead (II) selective electrodes. *Anal. Chim. Acta* **100,** 193-305.

Helgeson H. C., Kirkham D. H., and Flowers G. C. (1981). Theoretical prediction of the thermodynamic behaviour of aqueous electrolytes at high pressures and temperatures: IV. Calculation of activity coefficients, osmotic coefficients and apparent molal and standard and relative partial molal properties to 600°C and 5 Kb. *Am. J. Sci.* **281,** 1249-1516.

Hohl H. and Stumm W. (1976) Interaction of Pb^{2+} ions with hydrous γ-Al_2O_3. *J. Colloid Interface Sci.* **55,** 281-288.

Holm T. R. and Smothers S. H. (1990) Characterizing the lead-complexing properties of polyphosphate water treatment products by competing-ligand spectrophotometry using 4-(2-pyridylazo)resorcinol. *Intern. J. Environ. Anal. Chem.* **41,** 71-82.

Keith L. H. and Telliard W. A. (1979) Priority pollutants: I. A perspective view. *Env. Sci. Tech.* **13,** 416-423.

Kivalo P., Vurtanen R., Wickstrom K., Wilson M., Pungor E., Horvai G., and Toth K. (1976) An evaluation of some lead (II) - selective electrodes. *Anal. Chim. Acta* **87,** 401-409.

Kishino T. and Kobayashi K. (1995) Relationship between toxicity and accumulation of chlorophenols in fish. *Water Res.* **29,** 431-442.

Langmuir D. (1979) Techniques of estimating thermodynamic properties for some aqueous complexes of geochemical interest. In *Chemical Modeling in Aqueous Systems* (ed E.A. Jeanne) Amer. Chem. Soc., Washington, DC, 353-387.

Martell A. E. and Smith R. M. (1977) *Critical Stability Constants: 3. Other Organic Ligands*. Plenum.

Martell A. E. and Smith R. M. (1982) *Critical Stability Constants: 5. First Supplement*. Plenum.

Midgley D. (1987) Systematic and random errors in known addition potentiometry: A review. *Analyst* **112,** 557-572.

Mueller J. G., Chapman P. J., and Pritchard P. H. (1989) Creosote-contaminated sites. *Env. Sci. Tech.* **23,** 1197-1201.

Niimi A. J. and Palazzo V. (1985) Temperature effects on the elimination of pentachlorophenol, hexachlorobenzene amd Mirex by rainbow trout (Salmo Gairdneri). *Water Res.* **19,** 205-207.

Nriagu J.O. (1983) *Lead and Lead Poisoning in Antiquity.* John Wiley and Sons.

Pollard S. J. T., Hoffman R. E., and Hrudley S. E. (1993) Screening of risk management options for abandoned wood-preserving plant sites in Alberta, Canada. *Can. J. Civ. Eng.* **20,** 787-800.

Schindler P. W., and Stumm W. (1987) The surface chemistry of oxides, hydroxides, and oxide minerals. In *Aquatic Surface Chemistry* (ed. W. Stumm), pp 83-110. John Wiley and Sons.

Smith R. M. and Martell A. E. (1976) *Critical Stability Constants: 4. Inorganic Complexes.* Plenum.

Westall J. C. (1982a) FITEQL: A Computer Program for the Determination of Chemical Equilibrium Constants from Experimental Data; Version 1.2. Department of Chemistry, Oregon State University, Report 82-01.

CHAPTER 3:

A COMPARISON OF THE THERMODYNAMICS OF METAL ADSORPTION ONTO TWO COMMON BACTERIA

Christopher J. Daughney
Jeremy B. Fein
Nathan Yee

Department of Earth and Planetary Sciences
McGill University
3450 University St.
Montréal, PQ H3A 2A7 Canada

Revised manuscript submitted to:
Chemical Geology
May 1997

PREFACE

In Chapter 2 of this thesis, thermodynamic stability constants describing aqueous complexation between selected heavy metals and chlorinated phenols were quantified. These stability constants can be incorporated into a model which describes the speciation of these chemicals in the groundwater environment. The ability to accurately describe speciation is essential to predict the fate, or mobility, of these heavy metals and chlorophenols should aquifer contamination occur. However, aqueous complexation is not the only process which affects speciation. Speciation, and hence subsurface mobility, is strongly affected by adsorption reactions. Adsorption is defined as the binding of an aqueous ion or molecule by a solid surface. Where heavy metals or chlorophenols are strongly adsorbed to soil solids, their subsurface mobility is greatly reduced relative to the flow of the groundwater. Therefore, stability constants describing adsorption onto soil solids must be measured and used in chemical models in concert with stability constants for aqueous complexation to truly predict contaminant mobility. In Chapter 3 of this thesis, the adsorption of heavy metals by bacterial surfaces is investigated, and stability constants are reported.

ABSTRACT

The cell walls of bacteria are known to adsorb a variety of metals, and thus they may control metal mobilities in many low-temperature aqueous systems. In order to quantify metal adsorption onto bacterial surfaces, recent studies have applied equilibrium thermodynamics to the specific chemical and electrostatic interactions occurring at the solution-cell wall interface. However, to date, few studies have used this approach to compare the surface properties and metal affinities of different species of bacteria. In this study, we use acid-base titrations to determine the concentrations and deprotonation constants of specific surface functional groups on *Bacillus licheniformis*. The cell wall displays carboxyl, phosphate and hydroxyl surface functional groups, with pK_a values and 1*s* errors of 5.2 ± 0.3, 7.5 ± 0.4 and 10.2 ± 0.5, respectively. We perform metal-*B. licheniformis* adsorption experiments using Cd, Pb, Cu and Al. The average log K values for the Cd-, Pb-, Cu- and Al-carboxyl stability constants, with 1*s* errors, are 3.9 ± 0.5, 4.6 ± 0.3, 4.9 ± 0.4 and 5.8 ± 0.3, respectively. Finally, we compare the surface characteristics and metal affinities of *B. licheniformis* to those of *Bacillus subtilis*, as determined by Fein et al. (1997). Our investigations indicate that these two species of bacteria have different relative and absolute concentrations of surface sites and slightly different deprotonation and metal adsorption stability constants. We relate these variations in surface properties to variations in metal affinity in order to predict metal mobilities in complex, natural systems.

INTRODUCTION

Bacteria are common in near-surface fluid-rock systems, and may represent a significant portion of the surface area exposed to fluids in many natural environments, including fresh and saline surface waters (Geesey et al., 1977; Harvey et al., 1982), groundwaters (Mahmood and Rama, 1993; Corapcioglu and Kim, 1995), deep-sea hydrothermal systems (Mandernack and Tebo, 1993; Baker et al., 1994), and deep sedimentary basins (Ghiorse and Wobber, 1989; Yakimov et al., 1995). Bacterial cell walls are also known to exhibit a strong affinity for metal cations (Beveridge and Murray, 1980; Gonçalves et al., 1987; Beveridge, 1989; Fein et al., 1997). The ability of bacterial cells to bind metals can play a significant role in several geochemical processes, including the subsurface transport of groundwater contaminants (Corapcioglu and Kim, 1995), the fossilization of microorganisms (Ferris et al., 1988), and the accumulation of some low temperature metal deposits (Savvichev et al., 1986).

Bacterial cell walls are known to display a number of different types of proton-active surface functional groups (Beveridge and Murray, 1980; Beveridge et al., 1982; Beveridge, 1989). Recent research indicates that the interaction between metal cations and these surface functional groups can be effectively described in the framework of equilibrium thermodynamics (Gonçalves et al., 1987; Xue et al., 1988; Fein et al., 1997). The thermodynamic description of any metal-bacteria system requires the determination of 1) the relative and absolute concentrations of the various surface functional groups per unit weight of bacteria;

2) the weight of bacteria per kilogram of fluid; 3) the magnitude of the stability constants describing the deprotonation of each type of bacterial surface functional group; and 4) the magnitude of the stability constants describing the adsorption of the metal onto each different surface functional group. These parameters are determined through the experimental study of isolated systems containing a single metal and a single species of bacteria.

However, hundreds if not thousands of such isolated metal-bacteria experiments would have to be performed in order to collect the data necessary to model all of the possible interactions occurring in a complex natural system, which may contain a variety of metals and several species of bacteria. To date, no research has quantitatively evaluated the variation in the thermodynamic properties between different species of bacteria. In this study, we compare the acid-base properties and metal-binding capacities of two species of gram-positive bacteria, *Bacillus subtilis* and *Bacillus licheniformis*, both of which are common in natural environments (Duncan et al., 1994). The objective of this work is to elucidate generalities which may be applied to model acid-base behaviour and metal-bacteria interactions in complex, natural systems.

THEORY

The cell wall structures of both *B. subtilis* and *B. licheniformis* are known to display active carboxyl, phosphate and hydroxyl functional groups (Beveridge, 1989). The cell wall of *B. subtilis* is composed primarily of peptidoglycan and

teichoic acid (Beveridge and Murray, 1980), wheras the cell wall of *B. licheniformis* contains teichuronic acid as an additional component (Beveridge et al., 1982). Peptidoglycan is a polymer of acetylglucosamine and acetylmuramic acid which displays carboxyl and hydroxyl functional groups. Teichoic acid, a polymer of glycopyranosyl glycerol phosphate, displays phosphate and hydroxyl functional groups. Teichuronic acid is a polymer similar to teichoic acid, but lacking phosphate functional groups. Because the ratio of these three cell wall components differs between the two species, the relative and absolute concentrations of the carboxyl, phosphate and hydroxyl functional groups varies as well (Beveridge, 1989).

The acid-base characteristics displayed by bacteria are due to the sequential deprotonation of the cell wall functional groups with increasing pH (Gonçalves et al., 1987; Plette et al., 1995; Fein et al., 1997). The deprotonation of the carboxyl, phosphate and hydroxyl surface functional groups may be represented by the following equilibria:

$$R-COOH^0 \Leftrightarrow R-COO^- + H^+ \quad (1)$$

$$R-PO_4H^0 \Leftrightarrow R-PO_4^- + H^+ \quad (2)$$

$$R-OH^0 \Leftrightarrow R-O^- + H^+ \quad (3)$$

where R represents the bacterial cell wall. The mass action equations corresponding to the above equilibria are:

$$K_{(1)} = \frac{[R-COO^-]a_{H^+}}{[R-COOH^0]} \quad (4)$$

$$K_{(2)} = \frac{[R-PO_4^-]a_{H^+}}{[R-PO_4H^0]} \quad (5)$$

$$K_{(3)} = \frac{[R-O^-]a_{H^+}}{[R-OH^0]} \quad (6)$$

Here K and a represent the stability constant and the activity, respectively, and the square brackets represent the concentration of the surface species in moles per kg of solution.

The adsorption of metal cations (M^m) can be described by equilibria relating to the specific surface functional groups displayed on the cell wall (Fein et al., 1997):

$$M^m + R-COO^- \Leftrightarrow R-COOM^{(m-1)} \quad (7)$$

$$M^m + R-PO_4^- \Leftrightarrow R-PO_4M^{(m-1)} \quad (8)$$

$$M^m + R-O^- \Leftrightarrow R-OM^{(m-1)} \quad (9)$$

The mass action equations corresponding to the above equilibria are:

$$K_{(4)} = \frac{[R-COOM^{(m-1)}]}{[R-COO^-]a_{M^m}} \quad (10)$$

$$K_{(5)} = \frac{[R-PO_4M^{(m-1)}]}{[R-PO_4^-]a_{M^m}} \quad (11)$$

$$K_{(6)} = \frac{[R-OM^{(m-1)}]}{[R-O^-]a_{M^m}} \tag{12}$$

The bacterial surfaces, when deprotonated, carry a negative charge (Harden and Harris, 1953), and the interaction between the metal cation and the electric charge surrounding the bacterial surface affects the mass action equations above. We account for the electrostatic interactions with the following relationship:

$$K_{intrinsic} = K\exp(F\psi / RT) \tag{13}$$

Here, $K_{intrinsic}$ is the equilibrium constant referenced to the condition of zero surface charge and zero surface coverage. The variables F, ψ, R, and T refer to Faraday's constant, the electric potential of the cell wall surface, the gas constant, and the absolute temperature, respectively. We relate the electric potential (ψ) to the surface charge (σ) using a constant capacitance model for the electric field:

$$C = \frac{\sigma}{\psi} \tag{14}$$

where C is the capacitance of the bacterial surface in Farads/m^2. We assume a surface area of 140 m^2/g, after Fein et al. (1997).

MATERIALS AND METHODS

Growth Procedures. *B. licheniformis* cells were obtained from T. J. Beveridge, University of Guelph, Ontario. The cells were cultured in 3 mL volumes of autoclaved (120°C for 20 minutes) trypticase soy broth (Becton Dickenson) containing 0.5 % yeast extract (Becton Dickenson) by weight. After growing for 24 hours at 32°C, the cells were transferred to 1 L volumes of autoclaved broth and allowed to culture for an additional 24 hours. The cells were removed from the growth medium by centrifugation at 6000 rpm for 15 minutes. The pelleted cells were rinsed two times in distilled, deionized (DDI) water, soaked for one hour in 0.1 M HNO_3, rinsed two times in DDI water, soaked overnight in 0.001 M EDTA, rinsed five times in DDI water, and finally rinsed two times in 0.1 M $NaNO_3$ (the electrolyte used in the experiments). Following each rinse, the cells were pelleted by centrifugation at 6000 rpm for 15 minutes, and the supernatant was discarded. This procedure was followed in order to strip the cell walls of any metals present in the growth medium. It is well established that the cell wall structure of these bacteria varies in response to changing growth conditions (Doyle et al., 1980; Beveridge et al., 1982; Herben et al., 1990). In order to make meaningful comparisons of the cell wall variation between *B. licheniformis* and of *B. subtilis*, we ensured that all cultures were grown in exactly the same controlled and reproducible manner.

Acid-Base Titrations. Acid-base titrations were performed in order to determine the deprotonation constants and absolute concentrations of the specific

functional groups present on the bacterial cell walls. The bacterial cells were suspended in 10 mL of 0.1 M $NaNO_3$, which had been bubbled with N_2 for 60 minutes in order purge it of dissolved CO_2. The titration vessel was sealed immediately, and a positive internal pressure of N_2 was maintained for the duration of the experiment. The titrations were conducted using a Radiometer-Copenhagen TTT85-autotitrator/ABU80-burette assembly. The pH of the bacterial suspension was recorded after each addition of titrant (1.00 or 0.50 M NaOH, standardized against reagent grade K-H-phthalate) only when a stability of 0.1 mV/s had been attained. Following the titration, the bacteria present in the titration vessel were pelleted by centrifugation at 6000 rpm for 60 minutes, and the weight of the dry pellet was recorded (all values for bacterial biomass reported in this communication are given in grams of bacteria, in dry weight equivalent, per unit mass of electrolyte). High Performance Liquid Chromatography (HPLC) was used to analyze the supernatants for dissolved organic exudates. In the HPLC analysis, the filtered supernatants were passed across a Hewlett Packard ODS Hypersil column, with the eluents ramping from 100 % DDI water (adjusted to pH 2 with H_3PO_4) to 100 % acetonitrile over 60 minutes. The suspensions were examined by optical microscopy both before and after the titrations in order to determine the extent of cell wall fragmentation. Seven replicate acid-base titrations were performed.

Metal Adsorption Experiments. Batch experiments were conducted as a function of pH in order to determine site-specific stability constants for Cd, Pb and Cu adsorption onto the bacterial surfaces. The washed bacteria were pelleted

by centrifugation at 6000 rpm for 60 minutes. The bacterial pellet was weighed and then resuspended in a known weight of 0.1 M $NaNO_3$ electrolyte to yield a parent suspension. Homogenous 5.00 g aliquots of this parent suspension together with a known volume of 1000 ppm metal standard (Cd, Pb or Cu) were added to 12 - 24 identical reaction vessels, and the pH of the suspension in each vessel was adjusted to a different value using HNO_3 or NaOH. The reaction vessels were shaken and allowed to equilibrate for 30 minutes. The 30 minute reaction time was chosen based on the kinetic experiments reported by Fein et al. (1997). The contents of each reaction vessel were then filtered through a 0.45 μm cellulose nitrate/acetate filter (Micron Separation Inc.). The filtrate from each reaction vessel was acidified and analyzed for the dissolved metal by flame atomic absorption spectrophotometry. Experiments for the Cd, Pb and Cu systems were repeated in triplicate, with solid:solution ratios ranging from 1.54 - 6.00 g bacteria/L.

Batch experiments were also conducted to characterize the adsorption of Al onto the bacterial surfaces. Because the experimental solutions reach saturation with respect to gibbsite, $Al(OH)_3$, above pH 4, these experiments were conducted as a function of bacteria:metal ratio, over the range $3.2 < pH < 3.8$. Bacterial pellets of different weights were transferred to several identical reaction vessels. Subsequently, 5.00 g of 0.1 M $NaNO_3$ electrolyte containing 10 ppm Al were added to each vessel. Techniques for pH adjustment, experimental equilibration and filtration were identical to those of the Cd, Pb and Cu experiments described above.

RESULTS AND DISCUSSION

Acid-Base Characteristics of *B. licheniformis*. The experimental data indicate that the bacteria impart a significant buffering capacity to the solution, over and above that of the electrolyte alone, with the range of effective buffering extending from pH 3 to 11 (a representative titration is shown in Figure 1). Analyses of the titration supernatants by HPLC and optical microscopy gave no evidence of the presence of dissolved organic exudates or cell wall fragmentation, and so the buffering observed during the titrations is assumed to arise entirely from protonation and deprotonation of surface functional groups on the bacterial cell wall.

For each of the seven titrations, we attempt to fit the experimental data by invoking models involving one, two or three distinct types of surface functional groups, using the computer speciation program FITEQL 2.0 (Westall, 1981a, b). Models involving more than three types of surface functional groups fail to converge, indicating that the addition of a fourth proton-active site is not supported by the data. We use FITEQL to solve for the deprotonation constant and absolute concentration (moles/L) of each distinct type of surface site proposed in the model. The surface site concentrations are normalized with respect to the weight of bacteria per litre of electrolyte, to yield site concentrations in moles per gram of bacteria. FITEQL calculates the variance, V(Y), between the experimental data and the model, which provides a quantitative means of comparing the fit of the different models. Equilibria describing the aqueous

Figure 1. Acid-base titration data from a typical titration of *B. licheniformis*. Results from the FITEQL modeling are depicted for the best-fitting 1pK, 2pK and 3pK models.

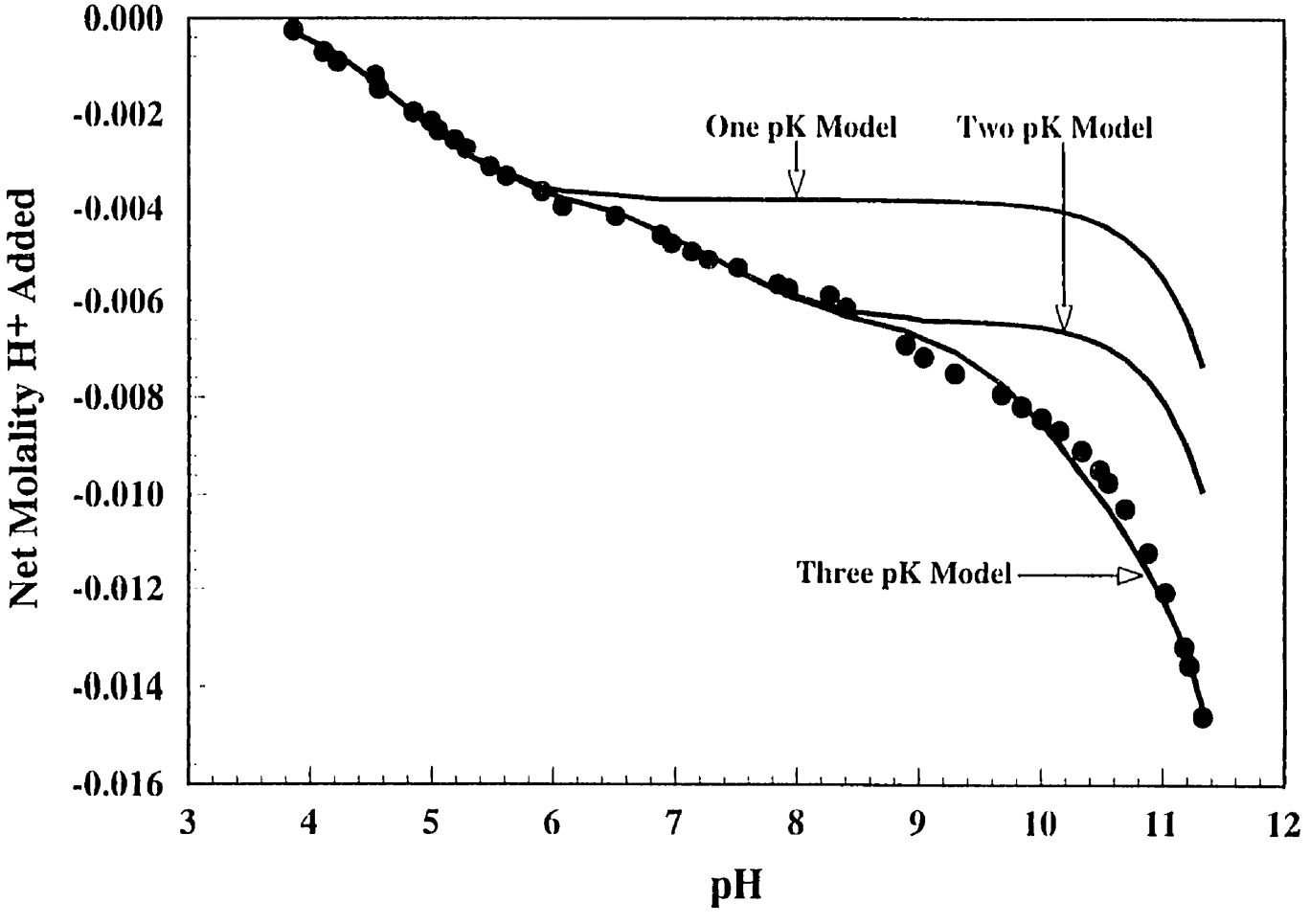
0.000
-0.002
-0.004
-0.006
-0.008
-0.010
-0.012
-0.014
-0.016
Net Molality H+ Added
3
4
5
6
7
8
9
10
11
12
pH
One pK Model
Two pK Model
Three pK Model

Figure 1

dissociation of water, the acid, the base and the electrolyte are included in the model, with stability constants taken from Smith and Martell (1976).

The experimental data are best fit by a model involving three distinct types of surface functional groups (Table 1). Models which include only one or two distinct types of surface functional groups do not adequately fit the experimental data. A one-site model can account for the buffering capacity of the bacterial suspensions only below pH 6 (Figure 1). Above this pH, virtually all of the modeled functional groups are deprotonated. The buffering capacity predicted by the one-site model is thus negligible above pH 6, though the buffering of the bacterial suspensions is substantial. Similarly, a two-site model can only describe the experimental data below pH 8.5. Again, above this pH, the two-site model predicts no further buffering, though significant buffering is displayed by the bacterial suspensions. The experimental data are adequately described only by a model involving three distinct types of surface functional groups; the buffering behaviour of the bacteria is explained by the sequential protonation/deprotonation of these different surface functional groups in response to changes in the solution pH.

Based on the data presented in Table 1 and Figure 1, we select the three-site model to describe the experimental data. The average pK_a values for the three different functional groups, with 1*s* errors, are 5.2 ± 0.3, 7.5 ± 0.4 and 10.2 ± 0.5. Based on the average pK_a values for simple carboxylic ($pK_a \approx 4$-6) and phenolic acids ($pK_a \approx 9$-11) (Perdue, 1985), we assume that these bacterial pK_a values correspond to carboxyl, phosphate and hydroxyl surface functional groups,

TABLE 1: Acid-base titration of *B. licheniformis* as modeled by FITEQL

Trial[a]	g/L[b]	Model[c]	pK_1[d]	AC_1[e]	pK_2[d]	AC_2[e]	pK_3[d]	AC_3[e]	V(Y)[f]
1	162.8	1 pK	5.57	5.76	—	—	—	—	458.2
		2 pK	5.30	4.40	8.57	4.70	—	—	56.44
		3 pK	5.18	3.78	7.29	2.43	10.61	4.16	18.30
2	74.66	1 pK	5.22	5.91	—	—	—	—	302.3
		2 pK	5.03	4.75	8.76	4.11	—	—	25.53
		3 pK	4.99	4.53	7.93	2.28	10.54	6.30	9.89
3	50.4	1 pK	5.68	23.5	—	—	—	—	689.2
		2 pK	5.23	14.9	8.28	21.1	—	—	61.02
		3 pK	5.14	13.6	7.66	14.6	10.22	17.4	9.99
4	42.06	1 pK	no convergence[g]						
		2 pK	no convergence[g]						
		3 pK	5.63	9.07	7.60	10.4	10.92	21.5	8.07
5	36.63	1 pK	5.82	20.9	—	—	—	—	564.6
		2 pK	5.52	15.2	9.01	18.2	—	—	68.52
		3 pK	5.25	10.7	6.83	8.53	9.61	18.1	25.30
6	35.35	1 pK	5.56	13.8	—	—	—	—	647.8
		2 pK	5.13	9.02	9.14	11.4	—	—	69.76
		3 pK	4.98	7.71	7.70	11.5	10.33	7.01	10.21
7	29.95	1 pK	5.31	20.4	—	—	—	—	505.1
		2 pK	5.01	15.0	8.63	15.4	—	—	54.33
		3 pK	4.87	12.8	7.29	8.64	9.98	14.2	13.15
Average[h]		3 pK	5.2 ± 0.3	8.88 ± 3.8	7.5 ± 0.4	8.34 ± 4.6	10.2 ± 0.5	12.7 ± 6.8	N/A

[a]With the exception of the weight of bacteria per unit weight of electrolyte, the trials are identical replicates. [b]Weight of bacteria per unit weight of electrolyte. [c]Models consider one, two or three distinct types of surface functional groups and are termed 1pK, 2pK and 3pK models respectively. [d]pK values for the subscripted surface functional groups, corresponding to the condition of zero ionic strength and zero surface coverage. [e]Absolute concentrations of the subscripted surface functional groups in 10^{-5} moles per gram of bacteria. [f]Variance as calculated by FITEQL. [g]Indicates severe misfit between the model and the experimental data. [h]Average values for 3pK model, with 1*s* errors.

respectively. The surface sites with pK_a values of 10.17 may be amine groups rather than hydroxyl groups, but without direct observation of the surface, it is not possible to make such a distinction. The average values for the absolute concentrations of these surface sites, with 1*s* errors, are $(8.87 \pm 3.8) \times 10^{-5}$ moles of carboxyl sites, $(8.34 \pm 4.6) \times 10^{-5}$ moles of phosphate sites, and $(1.24 \pm 0.7) \times 10^{-4}$ moles of hydroxyl sites per gram of bacteria. A capacitance value of 3.0 F/m^2 provides the best fit to the experimental data. This capacitance value is in good agreement with values for other colloid sized particles (8.0 F/m^2 for *B. subtilis*, Fein et al., (1997); 0.5 - 1.5 F/m^2 for many mineral surfaces, Langmuir, 1997). However, the value of the best-fit surface capacitance depends on the charge-potential relationship chosen to model the electric field surrounding the surface. Various models for the electric field surrounding bacterial surfaces will be compared in a future communication (Daughney et al., 1997).

In this study, we observe a significant variation in the relative and absolute concentrations of cell wall functional groups of *B. licheniformis* (Table 1). The cell wall structure of *B. licheniformis* is known to change if the growth conditions vary (Herben et al., 1990), but our experimental procedure has ensured that the growth conditions are controlled and reproducible. We have verified the accuracy of our method of titration by reproducing the stability constant and absolute concentrations of proton-active sites in a sodium-acetate system. An examination of the bacterial suspensions by HPLC and optical microscopy both before and after titration gives no evidence of organic exudates or cell disruption. The observed variation in cell wall structure may also result from changes in cell shape

or size due to osmotic effects associated with the distilled water rinses (Section 3.1). We have examined this possibility by rinsing the bacteria in 0.1 M $NaNO_3$ rather than distilled water; we observe no significant changes in the titration curves, and so we consider osmotic effects to be negligible. The titrations are reversible (Figure 2), which suggests that the extremes in pH do not cause changes in the cell wall structure through saponification of lipids or destruction of peptide bonds. The reproducibility of the stability constants determined, together with the excellent fit of our models in general, suggests that our use of the thermodynamic framework is valid. We conclude that the observed variation in the relative and absolute concentrations of surface functional groups is in fact evidence of true variation in the structure of the cell wall itself. *B. licheniformis* is capable of forming spores, and the composition of the spore wall is known to differ from that of the cell wall (Brock and Madigan, 1970). The duration of the titrations may be sufficient to allow varying degrees of sporulation in response to changes in solution chemistry. However, because the extent of variation is not systematic for any particular type of site, we conclude that the variations in surface site concentrations are due to essentially random differences in the cell wall structure arising from reproduction. *B. licheniformis* is a sexual species, capable of genetic exchange during reproduction (Duncan et al., 1994). The cell wall structure of descending populations may thus be largely uniform if reproduction is primarily asexual, or significantly different where reproduction is largely sexual. Our results indicate that *B. licheniformis* can develop very different cell wall structures, even when cultured under laboratory conditions.

Figure 2. Representative data gathered during an acid-base titration of B. licheniformis, showing that the proton adsorption-desorption reactions are reversible.

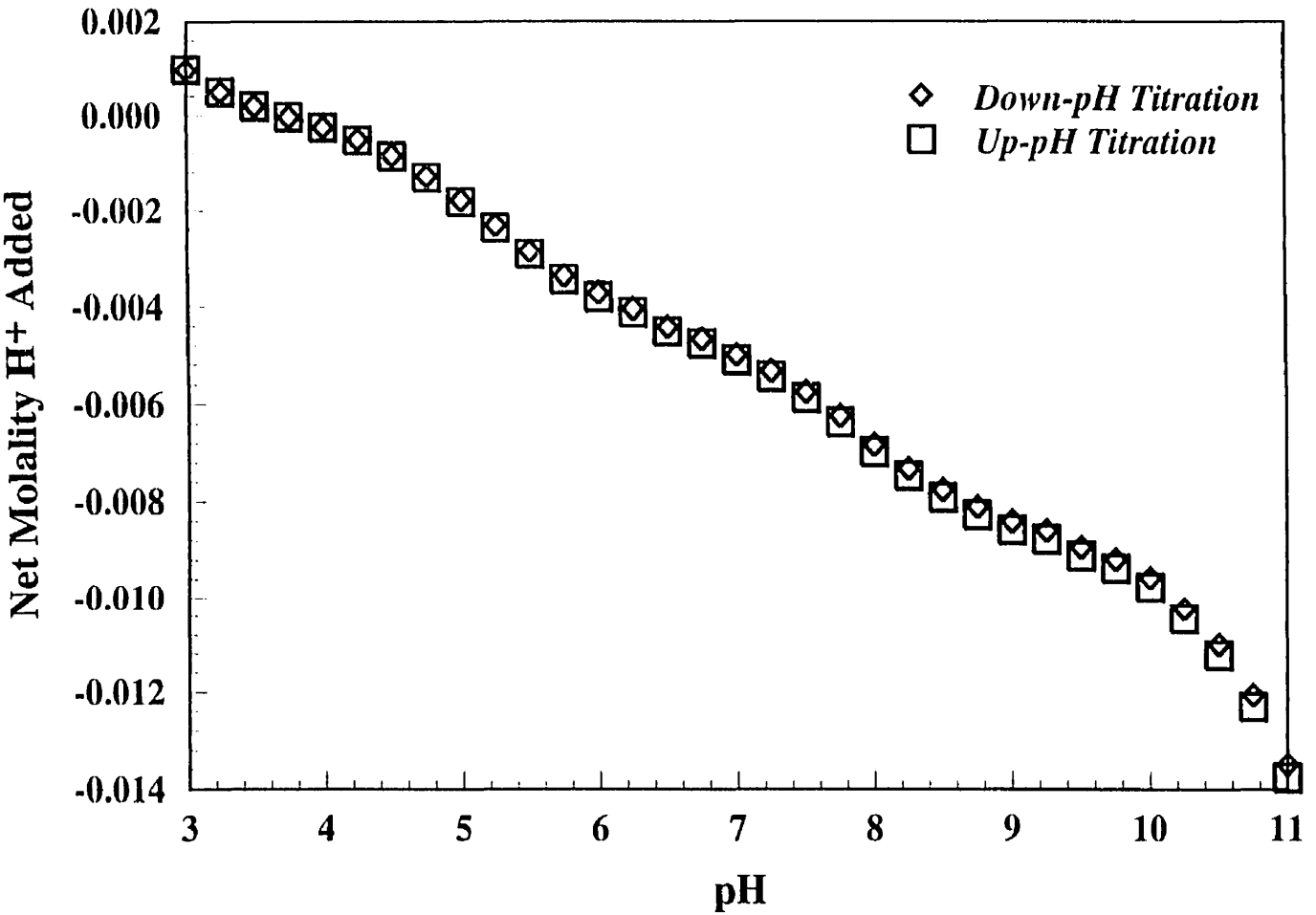
0.002
0.000
-0.002
-0.004
-0.006
-0.008
-0.010
-0.012
-0.014
Net Molality H+ Added
3
4
5
6
7
8
9
10
11
pH
Down-pH Titration
Up-pH Titration

Figure 2

In light of the variability of the cell wall structure, the reproducibility of the equilibrium constants describing deprotonation is remarkable. The pK_a values for each type of functional group are tightly constrained, regardless of how many groups are present on the cell surface, or in what ratio they exist. This result suggests either that the deprotonation of a single surface functional group is not affected by the deprotonation of its neighbouring functional groups, or that there are simply so many functional groups on the cell wall that an average value for the stability constant is appropriate. Regardless, constancy of the pK_a values illustrates that the surface properties of bacteria can be effectively quantified using equilibrium thermodynamics.

Metal Adsorption by *B. licheniformis*. The results of the Cd, Pb, Cu and Al adsorption experiments are displayed in Figures 3 to 6. Because all the adsorption experiments were performed below saturation with respect to any solid metal phase, any observed change in the aqueous metal concentration is attributed entirely to adsorption onto the cell wall. The bacterial cell walls display a strong affinity for the metals used in this study, with the extent of metal adsorption increasing with increasing pH. Further, the proportion of metal adsorbed at a particular pH increases as the ratio of the total concentration of bacterial surface functional groups to the total metal concentration (bacteria:metal ratio) increases.

For each metal-bacteria system, we attempt to fit the experimental data by invoking models involving metal adsorption onto one, two or three distinct types of surface functional groups, and we consider several stoichiometries for the adsorbed metal surface complex. We use FITEQL to solve for site-specific

Figure 3. Percent adsorption of aqueous Cd onto *B. licheniformis* as a function of pH. Data sets Cd1 and Cd2 correspond to 6.00 g bacteria/L and 8.90 x 10^{-5} M total Cd; data set Cd3 corresponds to 1.54 g bacteria/L and 8.90 x 10^{-5} M total Cd. Model fit curves were generated by FITEQL, and are all two-site models.

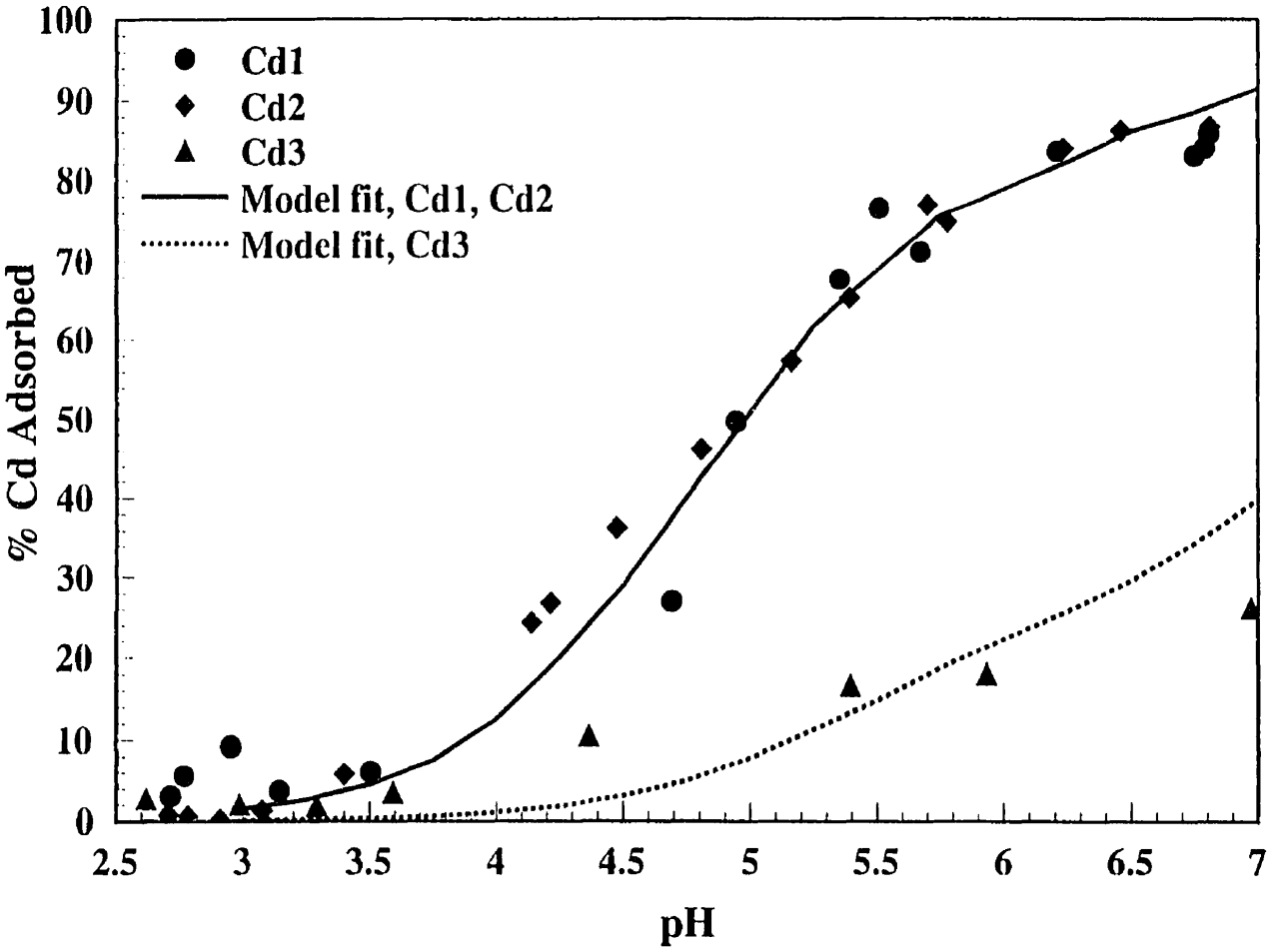
Cd1
Cd2
Cd3
Model fit, Cd1, Cd2
Model fit, Cd3
% Cd Adsorbed
pH
0
10
20
30
40
50
60
70
80
90
100
2.5
3
3.5
4
4.5
5
5.5
6
6.5
7

Figure 3

Figure 4. Percent adsorption of aqueous Pb onto *B. licheniformis* as a function of pH. Data set Pb1 corresponds to 6.00 g bacteria/L and 4.83 x 10^{-5} M total Pb; data set Pb2 corresponds to 3.48 g bacteria/L and 4.83 x 10^{-5} M total Pb; and data set Pb3 corresponds to 1.54 g bacteria/L and 1.94 x 10^{-4} M total Pb. Model fit curves were generated by FITEQL. Curves for Pb1 and Pb2 are one-site models; curve for Pb3 is a two-site model.

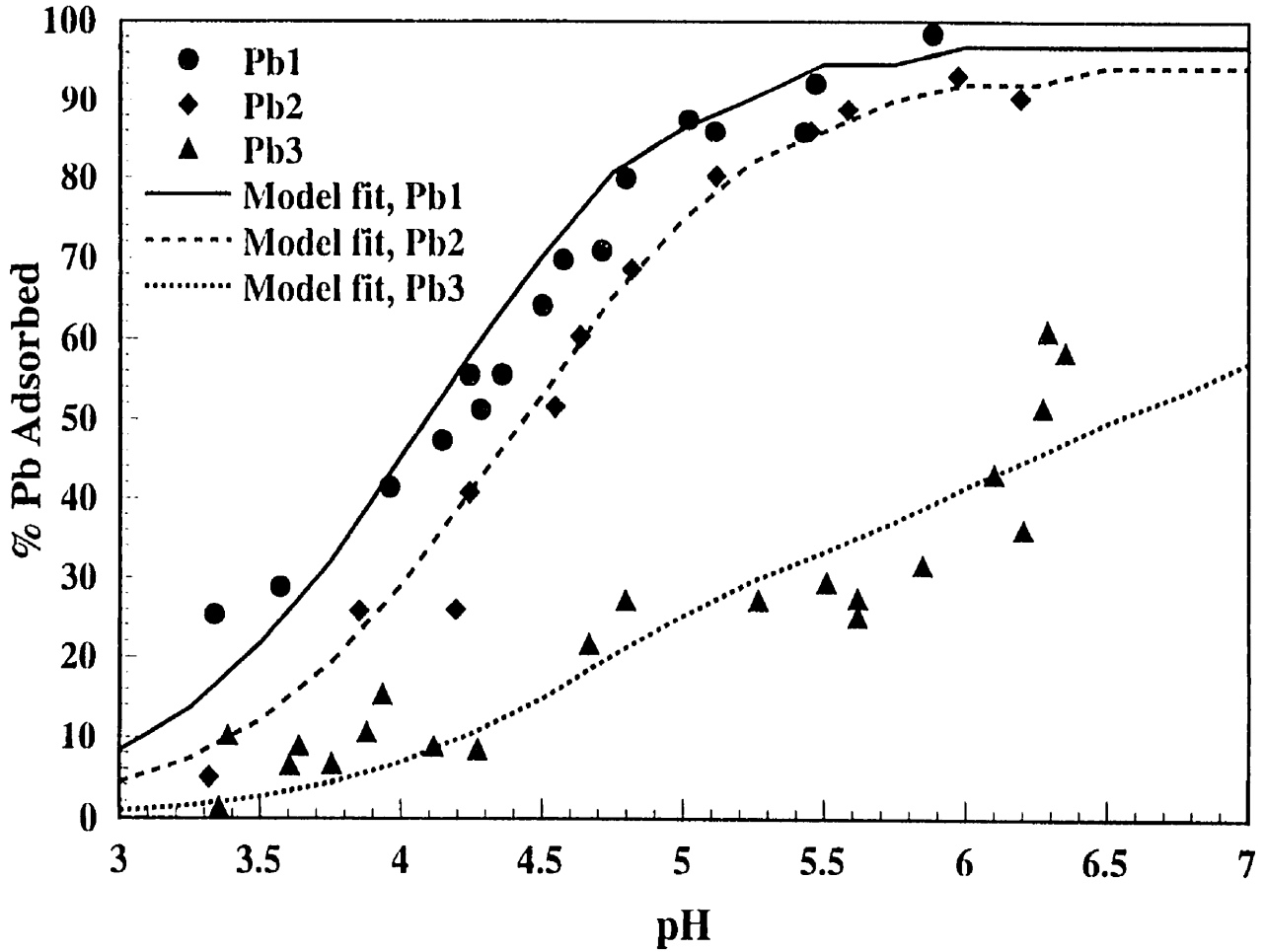
Pb1
Pb2
Pb3
Model fit, Pb1
Model fit, Pb2
Model fit, Pb3
% Pb Adsorbed
pH
0
10
20
30
40
50
60
70
80
90
100
3
3.5
4
4.5
5
5.5
6
6.5
7

Figure 4

Figure 5. Percent adsorption of aqueous Cu onto *B. licheniformis* as a function of pH. Data set Cu1 corresponds to 5.91 g bacteria/L and 1.57 x 10^{-4} M total Cu; data set Cu2 corresponds to 3.44 g bacteria/L and 1.57 x 10^{-4} M total Cu; and data set Cu3 corresponds to 1.54 g bacteria/L and 2.36 x 10^{-4} M total Cu. Model fit curves were generated by FITEQL, and all are one-site models.

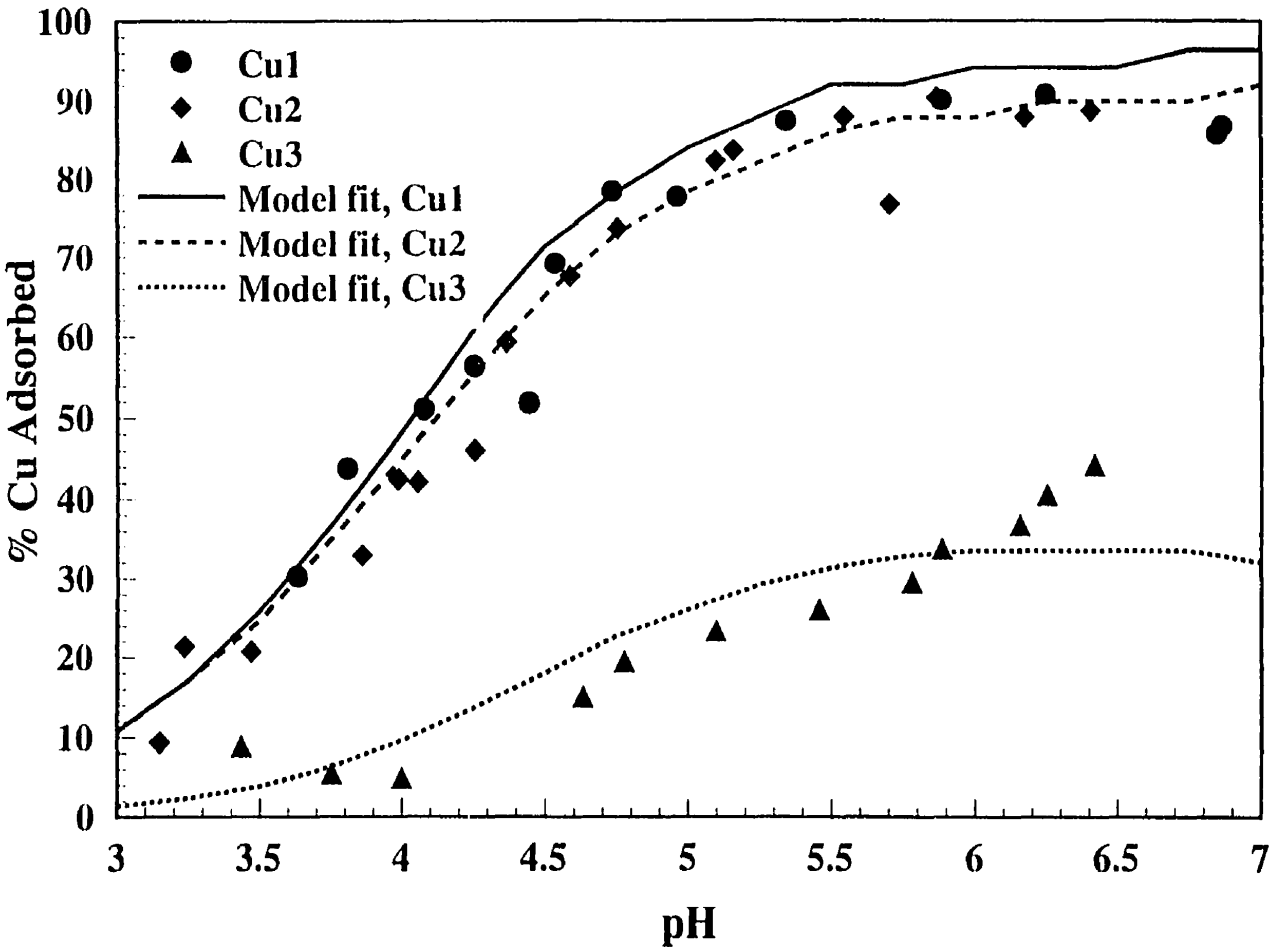
100
90
80
70
60
50
40
30
20
10
0
% Cu Adsorbed
Cu1
Cu2
Cu3
Model fit, Cu1
Model fit, Cu2
Model fit, Cu3
3
3.5
4
4.5
5
5.5
6
6.5
7
pH

Figure 5

Figure 6. Percent adsorption of aqueous Al onto *B. licheniformis* as a function of weight of bacteria per unit weight of electrolyte. One-site model fit curve was generated by FITEQL.

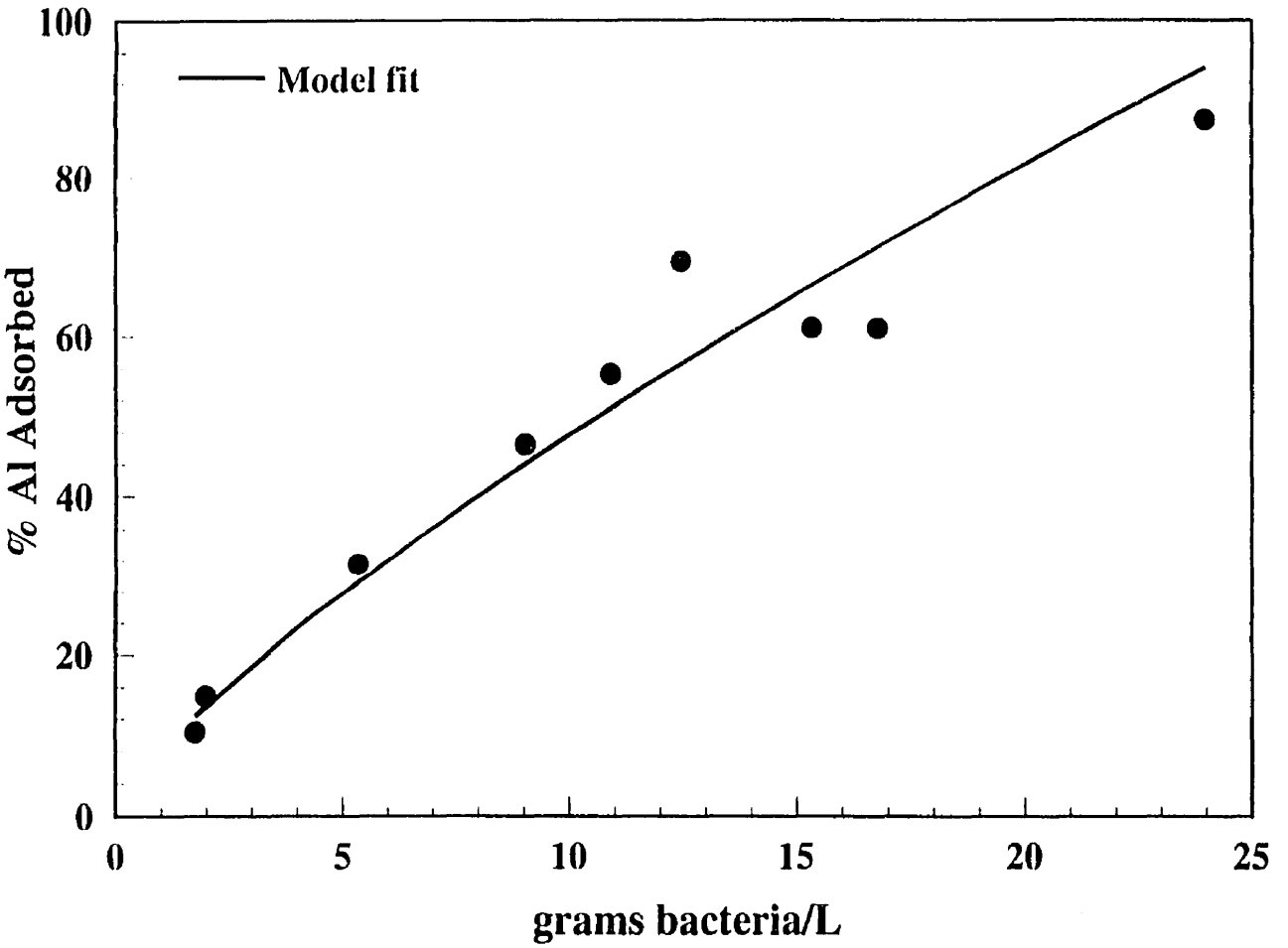
Model fit
% Al Adsorbed
100
80
60
40
20
0
0
5
10
15
20
25
grams bacteria/L

Figure 6

stability constants describing metal adsorption onto the bacterial cell walls. The variance, V(Y), calculated by FITEQL is applied to judge the goodness of the model fit to the experimental data. In the treatment of the Al experiments, which were performed as a function of bacteria:metal ratio, we solve for a stability constant for each data point. As a result, a value for V(Y) cannot be calculated. This is necessary because FITEQL requires a constant value for the weight of bacteria per litre of electrolyte. In the speciation calculations, we use the average acid-base stability constants, the absolute concentrations of surface functional groups, and the cell wall capacitance determined during the surface titrations (Table 1). The errors associated with these parameters are retained during the modeling of the metal-bacteria systems, and thus the stability constants describing metal adsorption are reported with corresponding 1s errors. Equilibria describing metal hydrolysis are included in our models, with stability constants taken from Baes and Mesmer (1976). The results of the FITEQL modeling are listed in Table 2.

The experimental data for some systems are best described by a one-site model involving adsorption only onto the carboxyl functional groups. We assume a 1:1 stoichiometry for the metal-carboxyl surface complex (we support this assumption below). We observe that the appropriateness of this one-site model depends upon the metal involved and the bacteria:metal ratio. In the Cd systems, the one-site model provides a good fit to the data where the bacteria:metal ratio is high (trials Cd1 and Cd2), but a poor fit where the ratio is low (Cd3) (Table 2). Similarly, in the Pb systems, the one-site model fits the experimental data very

TABLE 2: Adsorption of metals by *B. licheniformis* as modeled by FITEQL

Trial[a]	g/L[b]	$M_{T\,met}$[c]	Model[d]	Log K_1[e]	Log K_2[e]	V(Y)[f]
Cd1	6.00	8.90×10^{-5}	one-site	4.00 ± 0.30	—	10.35
			two-site	3.92 ± 0.24	4.56 ± 0.58	9.28
Cd2	6.00	8.90×10^{-5}	one-site	4.26 ± 0.43	—	74.03
			two-site	no convergence[g]		
Cd3	1.54	8.90×10^{-5}	one-site	3.92 ± 0.48	—	74.03
			two-site	3.38 ± 0.36	4.10 ± 0.74	44.44
Avr.[h]	N/A	N/A	two-site	3.9 ± 0.5	4.4 ± 0.7	N/A
Pb1	6.00	4.83×10^{-5}	one-site	4.81 ± 0.20	—	6.25
			two-site	no convergence[g]		
Pb2	3.48	4.83×10^{-5}	one-site	4.75 ± 0.22	—	2.05
			two-site	4.71 ± 0.06	6.26 ± 0.45	2.18
Pb3	1.54	1.93×10^{-4}	one-site	4.65 ± 0.41	—	107.8
			two-site	4.40 ± 0.36	5.17 ± 0.23	75.97
Avr.[h]	N/A	N/A	two-site	4.6 ± 0.3	5.7 ± 0.7	N/A
Cu1	5.91	1.57×10^{-4}	one-site	4.91 ± 0.23	—	15.33
			two-site	no convergence[g]		
Cu2	3.44	1.57×10^{-4}	one-site	5.17 ± 0.28	—	10.70
			two-site	no convergence[g]		
Cu3	1.54	2.36×10^{-4}	one-site	4.56 ± 0.43	—	48.69
			two-site	no convergence[g]		
Avr.[h]	N/A	N/A	one-site	4.9 ± 0.4	—	N/A
Al1	23.98	3.71×10^{-4}	one-site	5.85 ± 0.25	—	N/A
Al2	20.00	3.71×10^{-4}	one-site	5.54 ± 0.23	—	N/A
Al3	16.78	3.71×10^{-4}	one-site	5.71 ± 0.25	—	N/A
Al4	15.34	3.71×10^{-4}	one-site	5.99 ± 0.25	—	N/A
Al5	12.46	3.71×10^{-4}	one-site	6.10 ± 0.33	—	N/A
Al6	10.92	3.71×10^{-4}	one-site	6.02 ± 0.27	—	N/A
Al7	9.04	3.71×10^{-4}	one-site	5.95 ± 0.27	—	N/A
Al8	5.35	3.71×10^{-4}	one-site	6.05 ± 0.29	—	N/A
Al9	1.99	3.71×10^{-4}	one-site	5.52 ± 0.33	—	N/A
Al10	1.87	3.71×10^{-4}	one-site	5.44 ± 0.29	—	N/A
Avr.[h]	N/A	N/A	one-site	5.8 ± 0.3	—	N/A

[a]With the exception of the weight of bacteria per unit weight of electrolyte, the trials are identical replicates. [b]Weight of bacteria per unit weight of electrolyte. [c]Total molarity of metal. [d]Models consider metal adsorption onto one or two distinct types of surface functional groups and are termed one-site and two-site models respectively. [e]Log K values for the subscripted surface functional groups, with 1*s* errors, corresponding to the condition of zero ionic strength and zero surface coverage. [f]Variance as calculated by FITEQL. [g]Indicates severe misfit between the model and the experimental data. [h]Average values for model, with 1*s* errors.

well where the bacteria:metal ratio is moderate or high (Pb1 and Pb2), but poorly where it is low (Pb3). In the Cu and Al systems, the one-site model provides an excellent fit to the experimental data regardless of the bacteria:metal ratio.

The experimental data for other systems are best fit by a two-site model which considers metal adsorption onto both the carboxyl and the phosphate surface functional groups. Again, we assume a 1:1 stoichiometry for the metal-bacteria surface complexes. In the Cd systems, the two-site model provides a slightly improved fit over the one-site model where the bacteria:metal ratio is high (Cd1) and a drastically improved fit where it is low (Cd3). In the Pb system with the highest bacteria:metal ratio (Pb1), the two-site model does not converge. Where the bacteria:metal ratio is moderate (Pb2), the experimental data are fit equally well by the one-site and the two-site models, and thus there is little statistical basis to select one over the other. However, where the bacteria:metal ratio is small (Pb3), the two-site model fits the experimental data much more closely than the one-site model. As stated above, the Cu data are best fit by a one-site model, although the variance increases slightly as the bacteria:metal ratio decreases (Cu3). The two-site model does not improve the model fit of the Al data.

We conclude that the bacteria:metal ratio provides a governing control to the adsorption mechanism. Where the total concentration of bacterial surface functional groups far exceeds the total metal concentration, the chemical driving force behind the adsorption reaction is large, and thus at a given pH, a proportionately large amount of the metal exists in the form of a surface complex.

The adsorption edge is steep, and thus 100% adsorption is attained at a relatively low pH. In general, under these experimental conditions, virtually all of the metal is adsorbed below the pH at which the phosphate sites begin to deprotonate. Thus, the experimental data are well described by a model involving adsorption onto only the carboxyl sites. Under these conditions, a model considering metal adsorption onto both the carboxyl and the phosphate sites does not provide a statistically improved fit to the experimental data, and thus is not supported. In contrast, where the total concentration of bacterial surface sites is much smaller in relation to the total concentration of metal, the adsorption edge is less steep, and 100% adsorption is reached at a higher pH (if at all). A model involving adsorption only onto the carboxyl sites does not adequately fit the experimental data in the mid-pH range, but a model which considers adsorption onto both the carboxyl and the phosphate sites provides an excellent fit to the data. In no case does a model which also involves metal adsorption onto the hydroxyl sites provide a significantly improved fit to the experimental data. Thus, because the ratio of the total concentration of bacterial surface functional groups to the total metal concentration affects the pH range over which adsorption occurs, and because the different bacterial functional groups become active in different pH regions, we must consider metal adsorption onto both the carboxyl and the phosphate sites to fully describe all of the experimental data.

The type of metal involved in the adsorption reaction further constrains our selection of a model. The pH range over which the metal adsorbs is governed not only by the bacteria:metal ratio, but also by the affinity of the metal for the

bacterial surface. At a given pH and at a fixed bacteria:metal ratio, less Cd is adsorbed than Pb, and less Pb is adsorbed than Cu. Even for the highest bacteria:metal ratios used in this study, the pH over which Cd adsorbs coincides with significant deprotonation of the phosphate sites, and hence a two-site model provides a good fit to the data. However, because the two-site model does not offer a greatly improved fit to the data, the Cd-phosphate stability constant calculated from Cd1 is approximate. For accurate determination of the Cd-phosphate stability constant, we model the system with the lowest bacteria:metal ratio (Cd3). The adsorption of Pb is such that the system with an intermediate bacteria:metal ratio (Pb2) is described equally well by either the one-site or the two-site model. The high bacteria:metal ratio system (Pb1) is best fit by a one-site model, while the low bacteria:metal ratio (Pb3) requires a two-site model. Cu has such a high affinity for the surface that even the system with the lowest bacteria:metal ratio (Cu3) does not require a two-site model. Because the Al experiments were performed in acidic solutions ($3.2 < pH < 3.8$) where the phosphate sites are fully protonated, the one-site model is sufficient to describe the experimental data.

In all cases, a 1:1 stoichiometry for the metal-surface site complex is assumed. The agreement between the stability constants determined in systems of differing bacteria:metal ratio supports the 1:1 stoichiometry. The Al experiments, performed as a function of bacteria:metal ratio, show no systematic trend in the magnitude of the Al-carboxyl stability constant, which further supports a 1:1 stoichiometry for the surface complex. Our results are in agreement with those of

Fein et al. (1997), who describe a 1:1 stoichiometry for metal interactions with the cell wall functional groups of *B. subtilis*. Further evidence in support of the 1:1 stoichiometry of metal-bacteria surface complexes is provided by the electrophoretic mobility experiments of Collins and Stotzky (1991), who report that a variety of bacterial cells, which are negatively charged in the absence of metals, become positively charged when metals are present. The negative charge in the metal-free systems likely arises due to the deprotonation of the cell wall functional groups as described above. The positive charge most likely originates from a surface complex having one metal ion coordinated to one surface functional group. Coordination of one metal ion to two surface functional groups would yield a surface complex with a neutral charge.

Based on the discussion above and the FITEQL analyses presented in Table 2, we choose to model metal adsorption onto both the carboxyl and phosphate surface sites. The average log K values for the Cd-, Pb-, Cu- and Al-carboxyl stability constants, with 1s errors, are 3.9 ± 0.5, 4.6 ± 0.3, 4.9 ± 0.4 and 5.8 ± 0.3, respectively. Average values for the Cd- and Pb-phosphate log K values are 4.4 ± 0.7 and 5.7 ± 0.7, respectively. These average stability constants and 1s errors are calculated by modeling all of the experimental data points simultaneously. The metal-phosphate stability constants carry slightly more error because they are determined from fewer data points. In order to better constrain the magnitude of the metal-phosphate stability constants, experiments must be performed at a higher pH and at a lower bacteria:metal ratio. However, under

these conditions, the experimental solutions become saturated with respect to metal oxides or hydroxides.

***B. licheniformis* and *B. subtilis*: Comparison of Thermodynamic Parameters.** In Table 3, we compare the cell wall structure of *B. licheniformis* to that of *B. subtilis* (these two species were cultured and examined using identical techniques). The cell walls of both species display carboxyl, phosphate and hydroxyl surface functional groups. However, our findings indicate that the cell wall of *B. licheniformis* contains fewer carboxyl groups and more phosphate and hydroxyl groups per gram than the cell wall of *B. subtilis*. A student's *t*-test for averages shows the site concentrations listed in Table 3 to be different at a confidence interval of approximately 60% (*t* statistic values for the carboxyl, phosphate and hydroxyl sites are 0.79, 0.86, and 0.96, respectively; the degree of freedom value is 23). The cell wall of *B. licheniformis* is known to contain less peptidoglycan than the cell wall of *B. subtilis*, and it should display fewer carboxyl functional groups. Similarly, the cell wall of *B. licheniformis* contains relatively more teichoic acid and teichuronic acid than *B. subtilis*, and thus it should display more phosphate and hydroxyl functional groups. Thus our results are consistent with the variation in cell wall structure between the two species described by Beveridge and Murray (1980), Beveridge et al. (1982), and Beveridge (1989). However, the difference in cell wall structure between the two species is of limited statistical significance, which suggests that the acid-base characteristics of complex bacterial populations may be modeled using a single,

TABLE 3: Average surface characteristics of *B. licheniformis* and other biological surfaces

Species	*Bacillus licheniformis*	*Bacillus subtilis*	*Rhodococcus erythopolis*	*Chlamydo-monas rheinhardii*	*Klebsiella pneumonia*
Source	This paper	Fein et al. (1997)	Plette et al. (1995)	Xue et al. (1988)	Gonçalves et al. (1987)
Model[a]	3pK	3pK	3pK/Donnan	1pK	2pK
pK_1[b]	5.2 ± 0.3	4.8 ± 0.1	4.62 ± 0.02	5.8 - 7.6	4.7
AC_1[c]	8.88 ± 3.8	12.0 ± 1.0	50.3 ± 1.5	N/A	N/A
pK_2[b]	7.5 ± 0.4	6.9 ± 0.3	7.83 ± 0.1	—	7.8
AC_2[c]	8.34 ± 4.6	4.4 ± 0.2	19.3	—	N/A
pK_3[b]	10.2 ± 0.5	9.4 ± 0.3	9.96 ± 0.1	—	—
AC_3[c]	12.7 ± 6.8	6.2 ± 0.2	23.5 ± 0.7	—	—
C[d]	3.0	8.0	N/A	N/A	N/A

[a]Models consider one, two or three distinct types of surface functional groups and are termed 1pK, 2pK and 3pK models respectively; Donnan model describes surface electric field. [b]Negative log K values for the subscripted surface functional groups, with 1*s* errors, corresponding to the condition of zero ionic strength and zero surface coverage. [c]Absolute concentrations of the subscripted surface functional groups, with 1*s* errors, in 10^{-5} moles per gram of bacteria. [d]Capacitance of surface (F/m^2).

average set of surface site concentrations if species-specific values are not available.

The pK_a values for each type of functional group differ slightly but significantly between *B. licheniformis* and *B. subtilis*, with those of the former consistently roughly 0.5 log units larger (Table 3). A student's *t*-test for averages shows the pK_a values listed in Table 3 to be different at a confidence interval of approximately 80% (*t* statistic values for the carboxyl, phosphate and hydroxyl sites are 1.27, 1.17, and 1.36, respectively. The degree of freedom value is 23). This observation suggests that the magnitude of the deprotonation constant is species-specific. In this sense, the specific functional groups displayed on the cell walls behave very much like short-chain organic acids, with slight variation in the magnitude of the deprotonation constant controlled by the molecule to which the functional group is attached (e.g. succinic acid, $pK_{a1} = 4.2$; glutaric acid, $pK_{a1} = 4.3$; adipic acid, $pK_{a1} = 4.4$; Martell and Smith, 1977). However, the deprotonation of a specific type of cell wall functional group is defined by a single pK_a value, wheras the deprotonation constants for identical functional groups on the same short-chain organic acid are very different (e.g. oxalic acid, $pK_{a1} = 1.3$; $pK_{a2} = 4.3$; Martell and Smith, 1977). Note that an increased separation of identical functional groups on a short-chain organic acid results in more similar pK_a values (e.g. adipic acid, $pK_{a1} = 4.4$; $pK_{a2} = 5.4$; Martell and Smith, 1977). Based on these observations, we conclude that the functional groups on the bacterial cell walls are effectively isolated, such that the deprotonation of a single functional group is not affected by the deprotonation of its neighbouring

functional groups. However, the deprotonation of a single type of functional group is controlled by the surrounding cell wall structure, and thus pK_a values differ slightly between species.

The acid-base behaviour of *B. licheniformis* and *B. subtilis* are compared in Figure 7. The latter species provides greater buffering in the mid-pH region, though the two curves are similarly shaped. Using the correlation technique described by Langmuir (1979), we compare the deprotonation constants of these two species of bacteria (Figure 8). The excellent correlation between the two data sets ($R^2 = 1.00$) shows that Langmuir's approach may be applied to biological surfaces. In this manner, the pK_a values of one bacterial species may be predicted if those of another have been measured.

In Table 3, we compare the surface properties of *B. licheniformis* and *B. subtilis* to those of the bacteria *Rhodococcus erythopolis* and *Klebsiella pneumonia* and the algae *Chlamydomonas rheinhardii.* Each of these latter species has been cultured and examined under different conditions, and so inferences drawn from these comparisons are somewhat limited. Nonetheless, the pK_a values are quite similar between all the species studied, suggesting that the same types of functional groups are present on all the cell walls. Plette et al. (1995) propose that the surface sites with $pK_a \approx 10$ are amino rather than hydroxyl functional groups. However, without a detailed examination of the surface structure, it is impossible to identify the nature of each proton-active surface site, and so this distinction is, at present, quite arbitrary. We report a single pK_a value

Figure 7. FITEQL model output comparing the acid-base behaviour of *B. licheniformis* (solid line) and *B. subtilis* (dashed line). The curves are calculated using the average surface site concentrations and pK_a values summarized in Table 3, assuming 50 grams of bacteria per litre of solution.

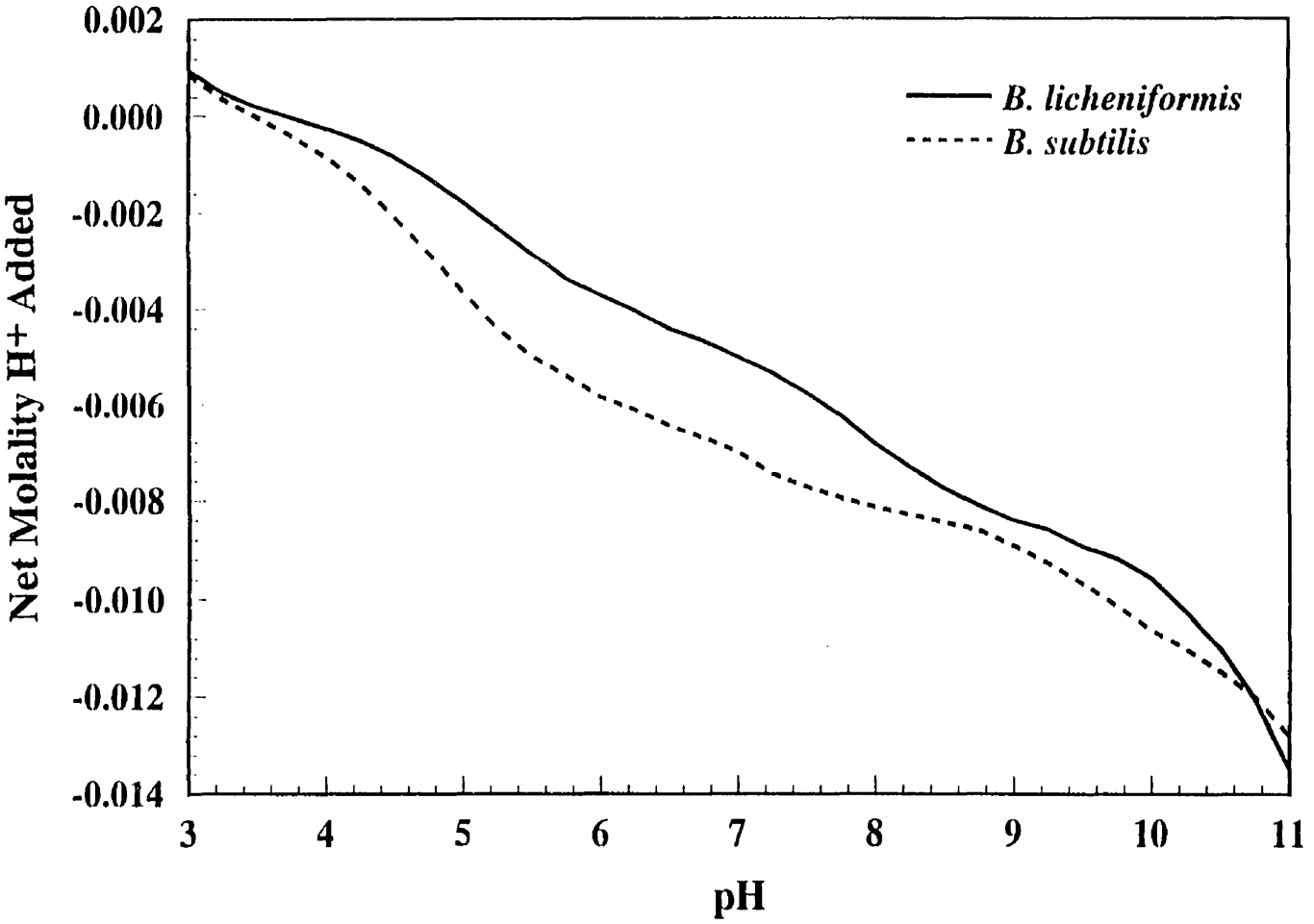
0.002
0.000
-0.002
-0.004
-0.006
-0.008
-0.010
-0.012
-0.014
Net Molality H+ Added
3
4
5
6
7
8
9
10
11
pH
B. licheniformis
B. subtilis

Figure 7

Figure 8. Correlation diagram relating pK_a values of *B. licheniformis* and *B. subtilis*. The equation of the linear regression line and the linear correlation coefficient are shown.

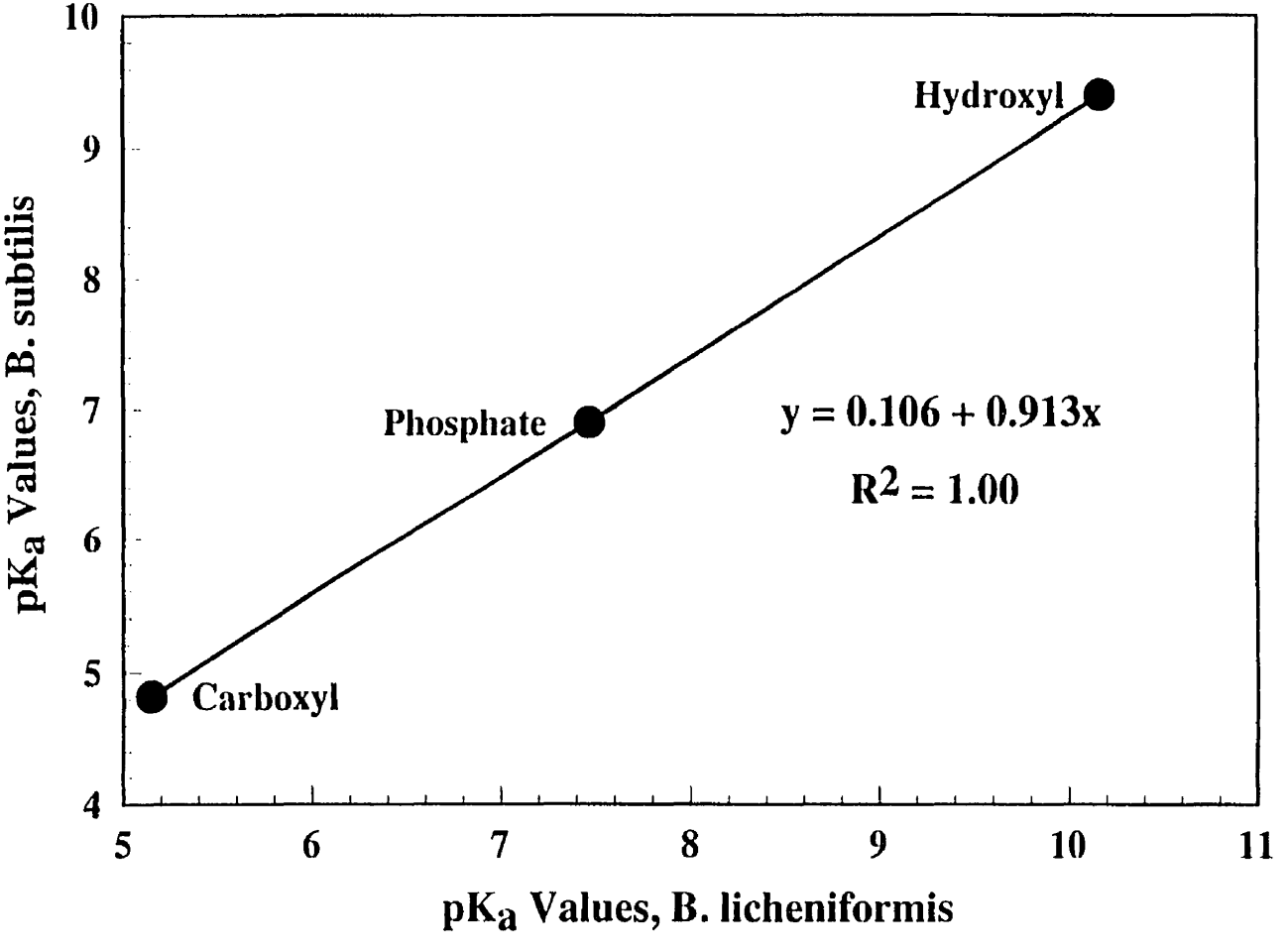
10
9
8
7
6
5
4
5
6
7
8
9
10
11
Hydroxyl
Phosphate
Carboxyl
y = 0.106 + 0.913x
R2 = 1.00
pKa Values, B. subtilis
pKa Values, B. licheniformis

Figure 8

for each type of functional group on *B. licheniformis* and *B. subtilis*, but it as yet unclear that this approach can be applied to all biological surfaces. Plette et al. (1995) choose to model their experimental data using a range of deprotonation constants for each type of surface site, but this decision is affected by their model of the electric field surrounding the cell walls. We have applied a simple constant capacitance model to describe the electric field in our research; the role of electrostatic interactions will be investigated in a future communication (Daughney et al, 1997). Gonçalves et al. (1987) and Xue et al. (1988) report non-site specific deprotonation constants which vary with pH, and thus cannot be directly compared to our results. Variation in cell wall structure between the species is difficult to quantify due to varying growth conditions, but the total concentrations of proton-active surface sites per gram of material are in general agreement. This comparison suggests first that equilibrium thermodynamics can be applied to the study of biological surfaces. Second, the biological surfaces compared here have similar cell wall structures and pK_a values which vary only slightly between species.

In Table 4, we compare our analyses of metal adsorption onto *B. licheniformis* to those reported by Fein et al. (1997) for *B. subtilis*. The thermodynamic parameters presented in Tables 3 and 4 permit us to predict the extent of metal adsorption under any conditions. For both species, the metal-carboxyl stability constants follow a trend, with Cd < Pb < Cu < Al. This affinity series also applies to many short-chain organics. Further, the metal-carboxyl stability constants are of similar magnitude between the two species, with those of

TABLE 4: Average metal binding properties of *B. licheniformis* and other biological surfaces

Species	*Bacillus licheniformis*		*Bacillus subtilis*	
Source	This paper		Fein et al. (1997)	
Metal	Log K M-carboxyl[a]	Log K M-phosphate[b]	Log K M-carboxyl[a]	Log K M-phosphate[b]
Cd	3.9 ± 0.5	4.4 ± 0.7	3.4 ± 0.1	5.4 ± 0.2
Pb	4.7 ± 0.3	5.7 ± 0.7	4.2 ± 0.1	5.6 ± 0.1
Cu	4.9 ± 0.4	—	4.4 ± 0.1	6.0 ± 0.2
Al	5.8 ± 0.3	—	5.0 ± 0.2	—

[a]Log stability constants describing adsorption of metal onto carboxyl sites, with 1*s* errors. [b]Log stability constants describing adsorption of metal onto phosphate sites, with 1*s* errors.

B. licheniformis consistently about 0.5 log units higher. A student's *t*-test for averages indicates that the metal-surface site stability constants differ between the two species at confidence intervals of approximately 80%, with the exception of the Pb-phosphate stability constants, which are not significantly different (*t* statistic values for the Cd-, Pb-, Cu-, and Al-carboxyl stability constants are 0.88, 1.55, 1.19, and 2.82, respectively. *t* statistic values for the Cd- and Pb-phosphate stability constants are 1.44 and 0.16, respectively. The degree of freedom values for the Cd, Pb, Cu and Al trials are 6, 4, 2 and 21, respectively). Again, we apply the correlation technique of Langmuir (1979) to compare the metal-carboxyl stability constants of the two species (Figure 9). The correlation between the two data sets is excellent (R^2 = 0.96). Using this type of correlation, the metal-carboxyl stability constant for one bacteria can be estimated if the stability constant describing adsorption of the same metal onto a different bacteria has been measured, if a sufficient number of other metal-carboxyl stability constants have been determined to define the slope and intercept of the correlation line. Figure 9 also includes the carboxyl pK_a values for the two species, showing that H^+ behaves similarly to the metals on this type of correlation plot. Although we have investigated only two bacterial species in this study, the quality of the correlation suggests that it may be possible to estimate metal-surface stability constants with reasonable accuracy from a pK_a measurement alone, where the slope and intercept of the correlation line are known.

In Figure 10, we predict the percentage of aqueous metal adsorbed to the two species, assuming a total metal concentration of 10^{-4} M and 6 grams of

Figure 9. Correlation diagram relating log proton- and metal-carboxyl stability constants of *B. licheniformis* and *B. subtilis*. The equation of the linear regression line and the linear correlation coefficient are shown.

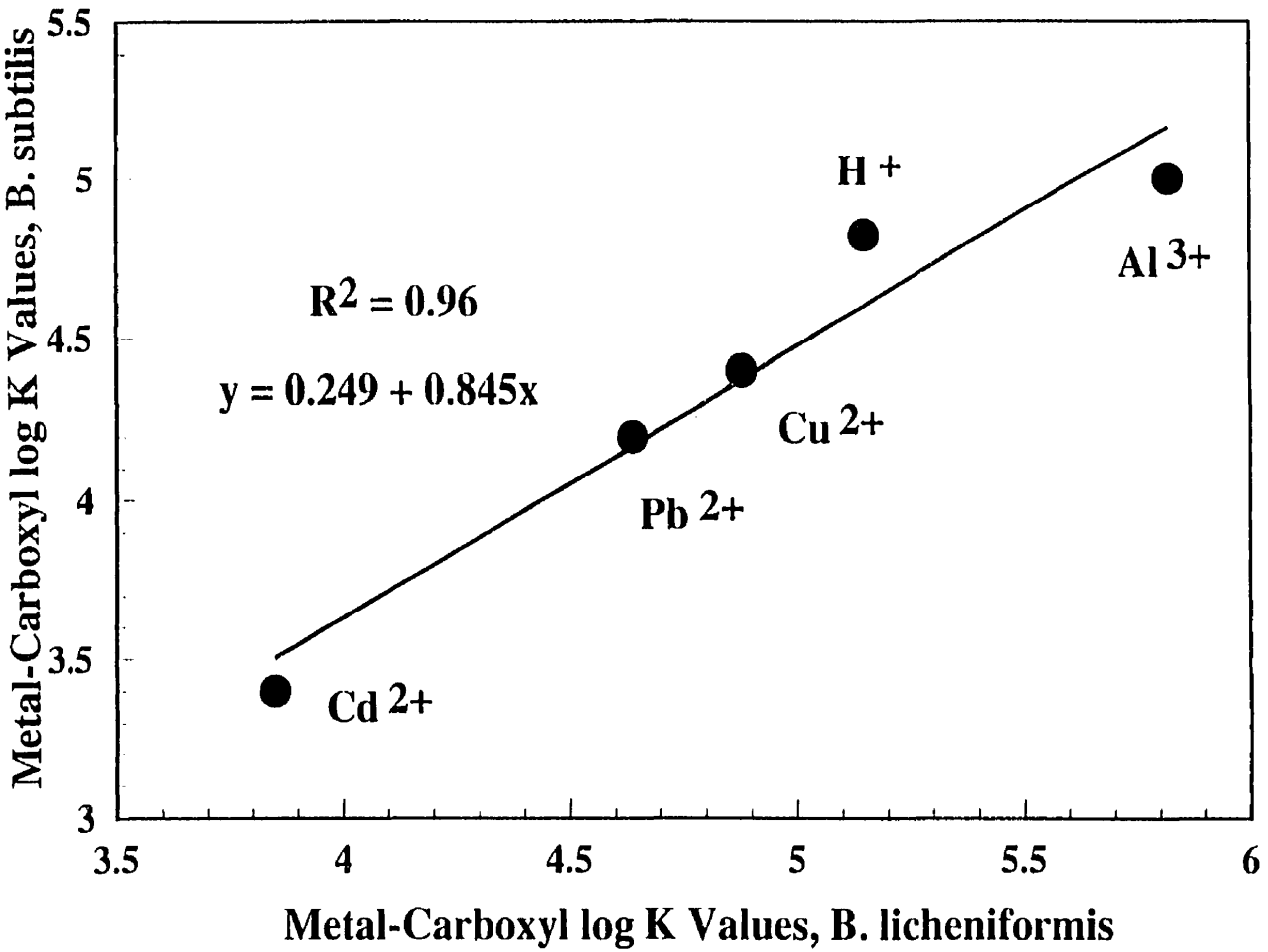
Metal-Carboxyl log K Values, B. subtilis
5.5
5
4.5
4
3.5
3
3.5
4
4.5
5
5.5
6
Metal-Carboxyl log K Values, B. licheniformis
H +
Al 3+
R2 = 0.96
y = 0.249 + 0.845x
Cu 2+
Pb 2+
Cd 2+

Figure 9

Figure 10. FITEQL model output comparing the adsorption of a) Cd, b) Pb, c) Cu and d) Al onto *B. licheniformis* (solid line) and *B. subtilis* (dashed line). The model curves are calculated from the average surface site concentrations, pK_a values, metal-carboxyl and metal-phosphate stability constants presented in Tables 3 and 4, assuming a total metal concentration of 10^{-4} M and 6 grams of bacteria per litre of solution.

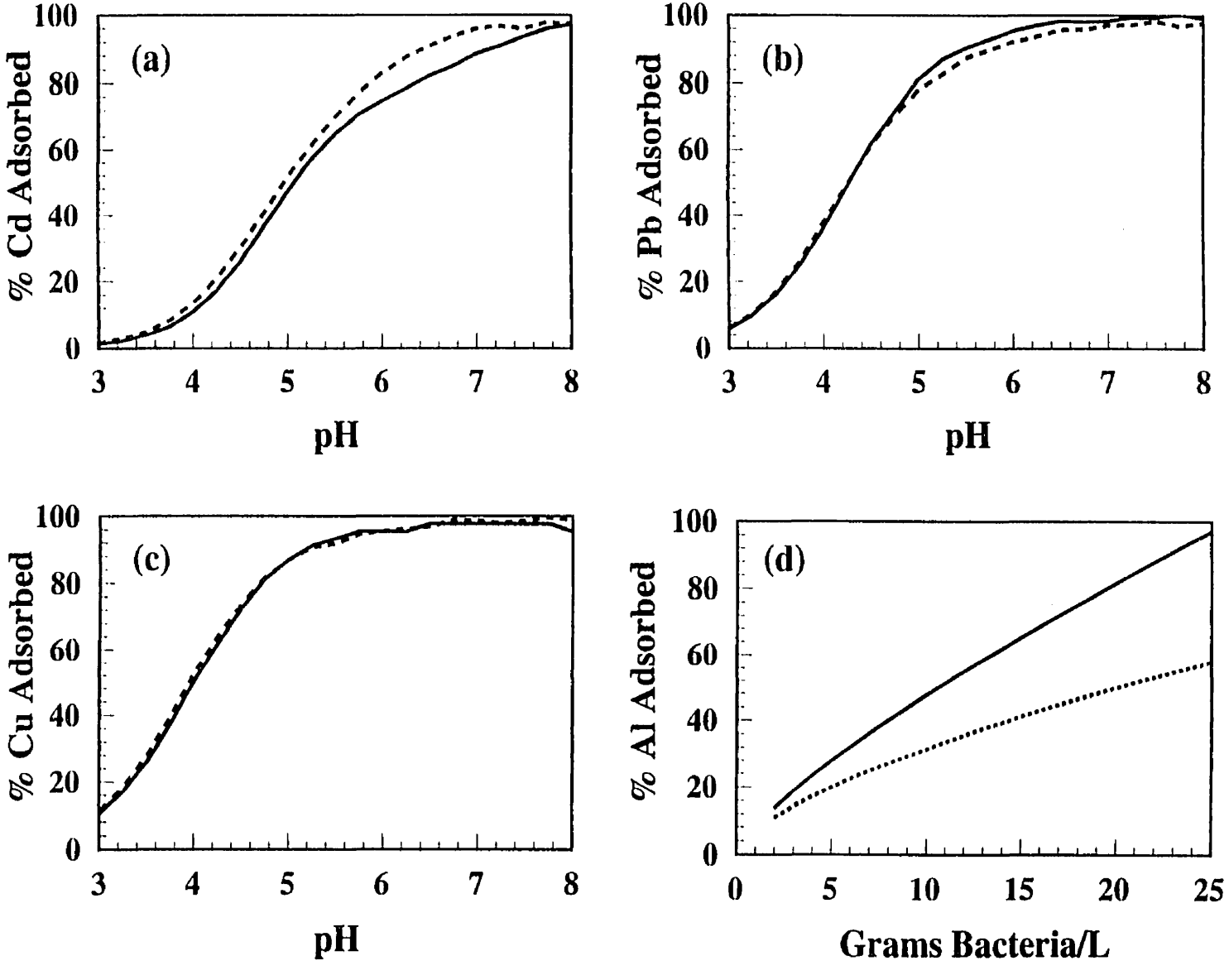
(a)
% Cd Adsorbed
pH
(b)
% Pb Adsorbed
pH
(c)
% Cu Adsorbed
pH
(d)
% Al Adsorbed
Grams Bacteria/L

Figure 10

bacteria/L. Interestingly, the slight differences in the surface characteristics are offset by the slight differences in the metal-surface stability constants, such that *B. licheniformis* and *B. subtilis* adsorb virtually identical quantities of Cd, Pb and Cu as a function of pH. It is important to note that this agreement in metal-binding capacity may arise because the thermodynamic parameters of the two species are statistically similar. Nonetheless, if future research shows that this relationship holds for all *Bacillus* species or all gram-positive bacteria, it can be used to greatly simplify the modeling of bacteria-metal interactions in natural systems. The Al adsorption curves for the two bacteria do not coincide because the experiments were performed as a function of the weight of bacteria present, rather than as a function of pH. The two bacterial species have different concentrations of functional groups per unit weight, giving rise to the difference in Al adsorption behaviour shown in Figure 10.

CONCLUSION

This study illustrates that equilibrium thermodynamics may be applied to describe both deprotonation and metal adsorption reactions involving bacterial surfaces. Biological surfaces display several types of active surface functional groups. The absolute concentrations of these surface functional groups varies slightly between species, and may be correlated to differences in cell wall structure. The deprotonation of each type of surface functional group also varies slightly between species, suggesting that the pK_a values are affected by the structure of the

surrounding cell wall. However, the deprotonation of each functional group is described by a single pK_a value, implying that the functional groups are electrochemically isolated on the cell wall, such that the deprotonation of one functional group is not affected by the deprotonation of its neighbouring functional groups. There exists an excellent correlation between the deprotonation constants of *B. licheniformis* and *B. subtilis*, suggesting that the pK_a values of one bacterial species may be predicted from those of another species. Metal adsorption onto bacterial surfaces involves more than one distinct type of surface functional group, depending upon the ratio of total bacterial surface sites to the total concentration of metal. A recognizable affinity series exists, with Cd (weak affinity) < Pb < Cu < Al (strong affinity). Metal-surface site stability constants are also well correlated between species. In general, the surface characteristics and metal adsorption behaviour of various biological surfaces appear broadly similar, such that it may be possible to apply the thermodynamic parameters reported here to model metal adsorption by complex bacterial populations.

ACKNOWLEDGMENTS

This work was funded by an NSERC Operating Grant and a FCAR Nouveaux Chercheurs Grant to J.B.F. We thank Jean-François Boily, Peter Wightman and Lawrence Yane for their assistance in the early stages of this work. We also thank Alfonso Mucci and Jeanne Paquette for the use of their auto-titrators and Terry

Beveridge for supplying the bacterial cultures. This manuscript was greatly improved by the careful reviews of L. Warren and an anonymous editor.

REFERENCES

Baes, C.F. and Mesmer, R.E., 1976. *The Hydrolysis of Cations.* Wiley-Interscience, N.Y.

Baker, E.T., Freely, R.A., Mottl, M.J., Sansone, F.T., Wheat, C.G., Resing, J.A. and Lupton, J.E., 1994. Hydrothermal plumes along the East Pacific Rise, 8° 40' to 11° 40'N: Plume distribution and relationship to the apparent magmatic budget. Earth Planet. Sci. Let., 128: 1-17.

Beveridge, T.J., 1989. Role of cellular design in bacterial metal accumulation and mineralization. Annu. Rev. Microbiol., 43: 147-171.

Beveridge, T.J., Forsberg, C.W. and Doyle, R.J., 1982. Major sites of metal binding in *Bacillus licheniformis* walls. J. Bacteriol., 150: 1438-1448.

Beveridge, T.J. and Murray, R.G.E., 1980. Sites of metal deposition on the cell wall of *Bacillus subtilis*. J. Bacteriol., 141: 876-887.

Brock, T.D. and Madigan, M.T., 1970. *Biology of Microorganisms.* Prentice-Hall, N.J.

Collins, Y.E and Stotzky, G., 1991. Heavy metals alter the electrokinetic properties of bacteria, yeasts and clay minerals. Appl. Env. Microbiol., 58: 1592-1600.

Corapcioglu, M.Y. and Kim, S., 1995. Modeling facilitated contaminant transport by mobile bacteria. Wat. Res. Research, 31: 2693-2647.

Daughney, C.J., Fein, J.B. and Yee, N., 1997 (submitted). The effect of ionic strength on the adsorption of H^+, Cd^{2+}, Pb^{2+} and Cu^{2+} by *Bacillus subtilis* and *Bacillus licheniformis*: A chemical equilibrium model. J. Coll. Interface Sci.

Doyle, R.J., Matthews, T.H. and Streips, U.N., 1980. Chemical basis for selectivity of metal ions by the *Bacillus subtilis* cell wall. J. Bacteriol., 143: 471-480.

Duncan, K.E., Ferguson, N., Kimura, K., Zhou, X. and Istock, C.A., 1994. Fine-scale genetic and phenotypic structure in natural populations of *Bacillus subtilis* and *Bacillus licheniformis*: Implications for bacterial evolution and speciation. Evolution, 48: 2002-2025.

Fein, J.B., Daughney, C.J., Yee, N. and Davis, T., 1997 (in press). A chemical equilibrium model of metal adsorption onto bacterial surfaces. Geochim. Cosmochim. Acta.

Ferris, F.G., Fyfe, W.S. and Beveridge, T.J., 1988. Metallic ion binding by *Bacillus subtilis*: Implications for the fossilization of microorganisms. Geology, 16: 149-152.

Geesey, G.G., Richardson, W.T., Yeomans, H.G., Irvin, R.T. and Costerton, J.W., 1977. Microscopic examination of natural sessile bacterial populations from an alpine stream. Can. J. Microbiol., 23: 1733-1736.

Ghiorse, W.S. and Wobber, F.J., 1989. *Deep Subsurface Microbiology.* Geomicrobiology J., 7. Crane, Russak & Co., N.Y. 130 p.

Gonçalves, M.L.S., Sigg, L., Reutlinger, M. and Stumm, W., 1987. Metal ion binding by biological surfaces: Voltametric assessment in the presence of bacteria. Sci. Tot. Environ., 60: 105-119.

Harden, V.P. and Harris, J.O., 1953. The isoelectric point of bacterial cells. J. Bacteriol., 65: 198-202.

Harvey, R.W., Lion, L.W., Young, L.Y. and Leckie, J.O., 1982. Enrichment and association of lead and bacteria at particulate surfaces in a salt-marsh surface layer. J. Marine Res., 40: 1201-1211.

Herben, P.F.G., Mozes, N. and Rouxhet, P.G., 1990. Variation of the surface properties of *Bacillus licheniformis* according to age, temperature and aeration. Biochim. Biophys. Acta, 1033: 184-188.

Langmuir, D., 1997. *Aqueous Environmental Geochemistry*. Prentice-Hall, N.J.

Langmuir, D., 1979. Techniques of estimating thermodynamic properties for some aqueous complexes of geochemical interest. In *Chemical Modeling in Aqueous Systems* (ed. E. A. Jeanne) Amer. Chem. Soc., Washington, DC, 353-387.

Mahmood, S.K. and Rama, R.P., 1993. Microbial abundance and degradation of polycyclic aromatic hydrocarbons in soil. Bull. Environ. Contam. Toxicol., 50: 486-491.

Mandernack, K.W. and Tebo, B.M., 1993. Manganese scavenging and oxidation at hydrothermal vents and in vent plumes. Geochim. Cosmochim. Acta, 57: 3907-3923.

Martell, A.E. and Smith, R.M., 1977. *Critical Stability Constants. III: Other Organic Ligands*. Plenum Press, N.Y.

Perdue, E.M., 1985. Acidic functional groups of humic substances. In *Humic Substances in Soil, Sediment and Water* (ed. G.R. Aiken et al.) Wiley-Interscience, N.Y., 493-526.

Plette, A.C.C., Van Reimsdijk, W.H., Bendetti, M.F. and Van der Wal, A., 1995. pH dependent charging behaviour of isolated cell walls of a gram-positive soil bacterium. J. Coll. Int. Sci., 173: 354-363.

Savvichev, A.S., Nikitin, D.I. and Oranskaya, M.S., 1986. The two phases of colloidal gold accumulation by immobilized microorganisms. Geochem. Int., 23: 60-62.

Smith, R.M. and Martell, A.E., 1976. *Critical Stability Constants. IV: Inorganic Complexes*. Plenum Press, N.Y.

Westall, J.C., 1982a. *FITEQL. A computer program for determination of chemical equilibrium constants from experimental data.* Version 2.0. Report 82-01, Dept. Chem. Oregon St. Univ., Corvallis, OR, USA.

Westall, J.C., 1982b. *FITEQL. A computer program for determination of chemical equilibrium constants from experimental data.* Version 2.0. Report 82-02, Dept. Chem. Oregon St. Univ., Corvallis, OR, USA.

Xue, H.-B., Stumm, W. and Sigg, L., 1988. The binding of heavy metals to algal surfaces. Wat. Res., 22: 917-926.

Yakimov, M.M., Timmis, K.N., Wray, V. and Fredrickson, H.L., 1995. Characterization of a new lipopeptide surfactant produced by therotolerant and halotolerant subsurface *Bacillus licheniformis BA S50*. Appl. Env. Microbiol., 61: 1706-1713.

CHAPTER 4:

THE EFFECT OF IONIC STRENGTH ON THE ADSORPTION OF H^+, Cd^{2+}, Pb^{2+} AND Cu^{2+} BY *Bacillus subtilis* AND *Bacillus licheniformis*: A CHEMICAL EQUILIBRIUM MODEL

Christopher J. Daughney
Jeremy B. Fein
Nathan Yee

Department of Earth and Planetary Sciences
McGill University
3450 University St.
Montréal, PQ H3A 2A7 Canada

Submitted to:
Journal of Colloid and Interface Science
June 1997

PREFACE

Chapter 3 of this thesis showed that metal adsorption by bacterial surfaces can be described by discrete stability constants, within the framework of equilibrium thermodynamics. Because the same theoretical framework was applied in Chapter 2 to quantify aqueous complexation, the stability constants presented in both of these chapters may be incorporated into a single chemical model in order to predict the speciation of heavy metals in groundwaters, if all other relevant stability constants are available. However, it is possible that a change in solution ionic strength may affect the stability constants presented here. The stability constants presented in Chapter 3 were determined in 0.1 M $NaNO_3$, which has an ionic strength that is much higher than most groundwaters. Therefore, if the stability constants given in Chapter 3 are to be effectively applied to describe speciation in groundwaters, the role played by ionic strength must be investigated. This role is examined in Chapter 4.

ABSTRACT

In order to quantify metal adsorption onto bacterial surfaces, recent studies have applied surface complexation theory to model the specific chemical and electrostatic interactions occurring at the solution-cell wall interface. However, to date, the effect of ionic strength on these interactions has not been investigated. In this study, we perform acid-base titrations of suspensions containing *Bacillus subtilis* or *Bacillus licheniformis* in 0.01 or 0.1 M $NaNO_3$, and we evaluate the Constant Capacitance and Basic Stern double layer models in their ability to describe ionic strength dependent behaviour. The Constant Capacitance model provides the best description of the experimental data, and can be applied to predict the acid-base behaviour of bacterial suspensions in conditions different from those of this study. The Constant Capacitance model parameters vary between independently grown bacterial cultures, possibly due to cell wall variation arising from genetic exchange during reproduction. We perform metal-*B. subtilis* and metal-*B. licheniformis* adsorption experiments using Cd, Pb, and Cu, and we solve for stability constants describing metal adsorption onto distinct functional groups on the bacterial cell walls. We find that these stability constants vary substantially but systematically between the two bacterial species at the two different ionic strengths. As a result, the metal adsorption stability constants provided here can be applied to predict metal adsorption in systems with ionic strengths that are different from those of this study.

INTRODUCTION

Bacteria and their cell wall fragments are ubiquitous in natural fluid-rock systems (1 - 9). Organic material often coats the mineral solids in such systems (10, 11), and so bacterial cell walls may represent a significant portion of the surface area exposed to both surface waters and soil fluids. Bacterial cell walls are known to exhibit a strong affinity for metal cations (12 - 18). The ubiquity of bacterial cells in near-surface fluid-rock systems and their ability to bind metals may play an important role in the subsurface transport of metals occurring as groundwater contaminants (19), the fossilization of microorganisms (20), and the accumulation of metal deposits (21). If such geochemical processes are to be quantified, a suitable model describing metal-bacteria interactions in natural environments must be developed.

Recent research indicates that the binding of protons and metal ions onto bacterial surfaces can be effectively described in terms of surface complexation, within the framework of equilibrium thermodynamics (15, 17, 18, 22). Acid-base titrations of bacterial suspensions enable the determination of the absolute concentrations and deprotonation constants of specific proton-active surface sites on the cell walls. Experimental studies of isolated systems containing a single metal and a single species of bacteria permit the determination of site-specific thermodynamic stability constants describing the formation of metal-bacteria surface complexes. For example, Fein et al. (17) have shown that the cell walls of *B. subtilis* display carboxyl, phosphate and hydroxyl functional groups, each in a

different absolute concentration, and each with a distinct deprotonation constant (Table 1). Fein et al. (17) also report stability constants describing the binding of various metals onto specific functional groups on the *B. subtilis* surface (Table 1). Daughney et al. (18) have performed a similar study using *B. licheniformis*, and noted that the concentrations of the functional groups, their deprotonation constants, and their metal binding constants are slightly, but systematically, different than those of *B. subtilis* (Table 1). However, Fein et al. (17) and Daughney et al. (18) have performed all of their experiments at a single, fixed ionic strength of 0.1 M, and so the effect of ionic strength on proton and metal adsorption by bacterial surfaces remains unclear.

The adsorption of ions by bacterial surfaces is likely a function of ionic strength. Bacterial surfaces are often negatively charged in natural environments (23), and it is well established that ionic strength-dependent electrostatic interactions influence the adsorption of ions onto electrically charged surfaces (24, 25). The ionic strength dependence of ion adsorption onto mineral surfaces can be quantified by several different electrostatic double layer models, each describing the distribution of electric charge at the mineral-water interface (26, 27). It is not clear, *a priori*, that these double layer models can be effectively applied to predict the extent of proton and metal adsorption by bacterial surfaces in electrolytes of differing ionic strengths.

The objective of this study, then, is to examine the effect of ionic strength on the acid-base properties (i.e. proton adsorption) and metal-binding capacities of two species of gram-positive bacteria, *Bacillus subtilis* and *Bacillus licheniformis*,

TABLE 1. Average surface characteristics and metal binding constants of *B. subtilis* and *B. licheniformis* as determined by Fein et al. (1997) and Daughney et al. (1997).

Species	*B. subtilis*	*B. licheniformis*
Source	Fein et al. (1997)	Daughney et al. (1997)
Electrolyte	0.1 M $NaNO_3$	0.1 M $NaNO_3$
C_1[a]	8.0	3.0
pK_1[b]	4.8 ± 0.1	5.15 ± 0.3
$Conc_1$[c]	12.0 ± 1.0	8.88 ± 3.8
pK_2	6.9 ± 0.3	7.47 ± 0.4
$Conc_2$	4.4 ± 0.2	8.34 ± 4.6
pK_3	9.4 ± 0.3	10.17 ± 0.5
$Conc_3$	6.2 ± 0.2	12.7 ± 6.8
Log K Cd-carboxyl[d]	3.4 ± 0.1	3.85 ± 0.5
Log K Cd-phosphate	5.4 ± 0.2	4.35 ± 0.7
Log K Pb-carboxyl	4.2 ± 0.1	4.64 ± 0.3
Log K Pb-phosphate	5.6 ± 0.1	5.71 ± 0.7
Log K Cu-carboxyl	4.4 ± 0.1	4.88 ± 0.4
Log K Cu-phosphate	6.0 ± 0.2	—

[a]Capacitance of the bacterial surface (F/m^2). [b]Negative logarithm and 1*s* error of the subscripted surface site, referenced to the condition of zero surface charge, zero surface coverage, and zero ionic strength. Subscripts 1, 2, and 3 correspond to carboxyl, phosphate and hydroxyl functional groups, respectively. [c]Concentration and 1*s* error of the subscripted surface functional group, expressed in $x10^{-5}$ moles per gram of bacteria. [d]Logarithm and 1*s* error of stability constant describing adsorption of metal onto a particular surface functional group.

both of which are common in natural environments (28). Using *B. subtilis* and *B. licheniformis* we perform acid-base titrations and batch metal adsorption experiments (with Cd, Pb, and Cu) in 0.01 M $NaNO_3$ electrolyte solutions. In conjunction with data from Fein et al. (17) and Daughney et al. (18), we compare the Constant Capacitance and Basic Stern double layer models in their ability to quantify ionic strength dependent adsorption behaviour.

BACKGROUND AND THEORY

The cell walls of both *B. subtilis* and *B. licheniformis* are known to display active carboxyl, phosphate and hydroxyl functional groups (16). The acid-base behaviour displayed by these bacteria results from the sequential deprotonation of the cell wall functional groups with increasing pH (15, 17, 18, 22). The deprotonation of the carboxyl, phosphate and hydroxyl surface functional groups may be represented by the following equilibria:

$$R-COOH^0 \Leftrightarrow R-COO^- + H^+ \qquad [1]$$

$$R-PO_4H^0 \Leftrightarrow R-PO_4^- + H^+ \qquad [2]$$

$$R-OH^0 \Leftrightarrow R-O^- + H^+ \qquad [3]$$

where R represents the bacterial cell wall to which the functional group is attached. The mass action equations corresponding to the above equilibria are:

$$K_{carb} = \frac{[R-COO^-]a_{H^+}}{[R-COOH^0]} \quad [4]$$

$$K_{phos} = \frac{[R-PO_4^-]a_{H^+}}{[R-PO_4H^0]} \quad [5]$$

$$K_{hydr} = \frac{[R-O^-]a_{H^+}}{[R-OH^0]} \quad [6]$$

Here K and a represent the stability constant and the activity, respectively, and the square brackets represent the concentration of the surface species in moles per kg of solution. Stability constants for Eqs. [4] - [6] and total surface site concentrations for each type of cell wall functional group for *B. subtilis* (17) and *B. licheniformis* (18) are presented in Table 1.

The adsorption of metal cations can be described by equilibria relating to the specific surface functional groups displayed on the cell wall:

$$M^m + R-COO^- \Leftrightarrow R-COOM^{(m-1)} \quad [7]$$

$$M^m + R-PO_4^- \Leftrightarrow R-PO_4M^{(m-1)} \quad [8]$$

$$M^m + R-O^- \Leftrightarrow R-OM^{(m-1)} \quad [9]$$

The mass action equations corresponding to the above equilibria are:

$$K_{M-carb} = \frac{[R-COOM^{(m-1)}]}{[R-COO^-]a_{M^m}} \quad [10]$$

$$K_{M-phos} = \frac{[R-PO_4M^{(m-1)}]}{[R-PO_4^-]a_{M^m}} \quad [11]$$

$$K_{M-hydr} = \frac{[R-OM^{(m-1)}]}{[R-O^-]a_{M^m}} \quad [12]$$

The metal binding stability constants for Eqs. [10] - [12], applicable to *B. subtilis* (17) and *B. licheniformis* (18) are also presented in Table 1. Fein et al. (17) and Daughney et al. (18) conclude that all surface complexes have a 1:1 stoichiometry, based on agreement between stability constant values determined in systems of differing bacteria to metal ratios. Further evidence in support of the 1:1 stoichiometry for the metal-bacteria surface complexes is provided by the electrophoretic mobility experiments of Collins and Stotzky (29), who report that bacterial cells, which are negatively charged in the absence of metals, become positively charged when divalent metals are present. The positive charge likely originates from a surface complex having one metal ion coordinated to one surface functional group. Coordination of one metal ion to two surface functional groups, for example, would yield a surface complex with a neutral charge.

The bacterial surfaces, when deprotonated, carry a negative charge (23). The interaction between the metal cation and the electric charge surrounding the bacterial surface will affect all experimentally observed equilibrium constants ($K_{observed}$). We account for the electrostatic interactions with the following relationship:

$$K_{intrinsic} = K_{observed} \exp(zF\psi / RT) \qquad [13]$$

Here, $K_{intrinsic}$ is the equilibrium constant referenced to the condition of zero surface charge and zero surface coverage, but to a distinct, finite ionic strength. The variables F, ψ, R, T and z refer to Faraday's constant, the electric potential of the cell wall surface, the gas constant, the absolute temperature, and the charge of the adsorbing ion, respectively. The Boltzmann factor, $\exp(zF\psi/RT)$, quantifies the activity difference between an ion near the bacterial surface and the same ion in the bulk solution.

Several different electrostatic double layer models have been developed to describe the configuration of the electric field surrounding charged surfaces in solution. In this study, we consider the Constant Capacitance model (30), and the Basic Stern model (31). Schematic representations of the charge-potential relationships for the Constant Capacitance and Basic Stern models are shown in Figure 1. Both the Constant Capacitance and Basic Stern models have been used to describe metal and proton adsorption onto oxide mineral surfaces (26), and the Constant Capacitance model has been used to describe metal adsorption onto bacterial surfaces (17, 18). Both the Constant Capacitance and Basic Stern models are valid for the range of ionic strengths considered here, but they require optimization of a different number of parameters in order to describe experimental proton or metal adsorption data (32, 33).

The Constant Capacitance model assumes that all adsorbed ions occupy an adsorption plane immediately adjacent to the solid surface (Figure 1). The surface

Figure 1. Schematic representations of the distribution of electric potential (ψ) and electric charge (σ) at the bacterial surface - solution interface, for a) the Constant Capacitance model and b) the Basic Stern model.

A.

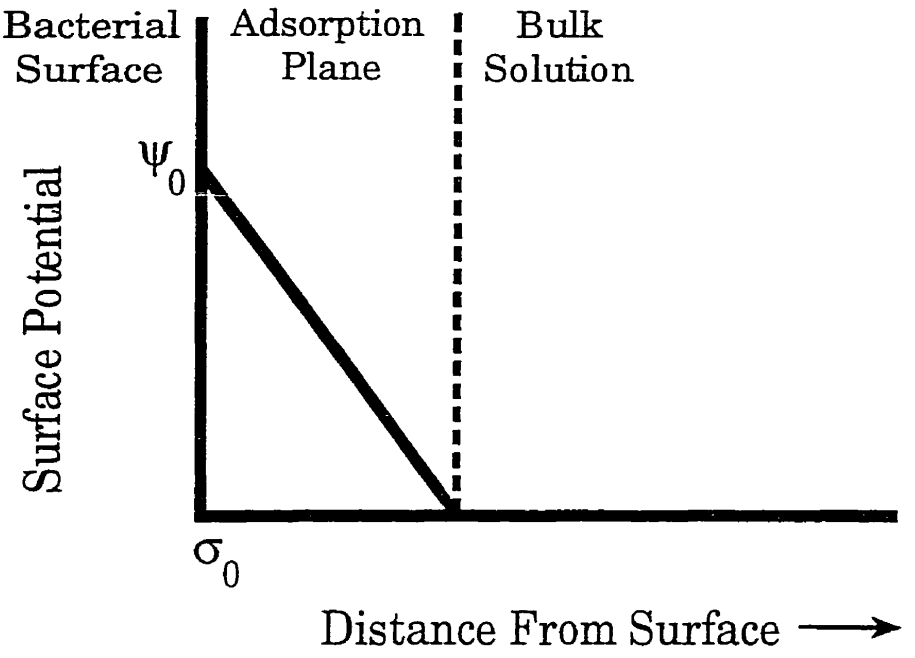
Bacterial Surface
Adsorption Plane
Bulk Solution
ψ_0
Surface Potential
σ_0
Distance From Surface

B.

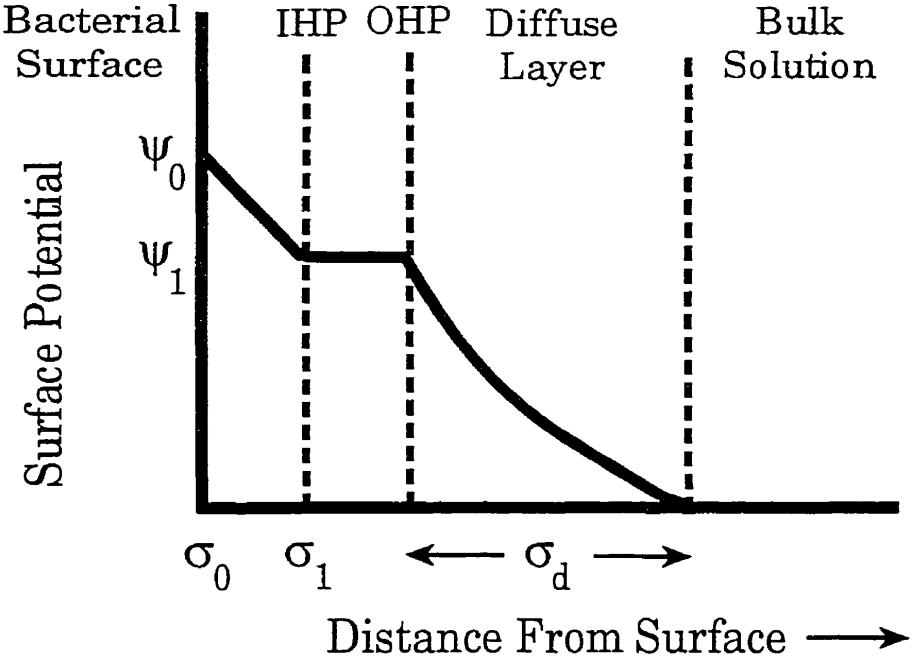
Bacterial Surface
IHP
OHP
Diffuse Layer
Bulk Solution
ψ_0
ψ_1
Surface Potential
σ_0
σ_1
σ_d
Distance From Surface

Figure 1

complexes formed are thus analogous to inner-sphere aqueous complexes. The electric potential in the zero plane (ψ_0) is related to the electric charge (σ_0) by the capacitance of the bacterial surface (C_1) (30):

$$C_1 = \frac{\sigma_0}{\psi_0} \qquad [14]$$

Here, the surface potential is independent of ionic strength, and so the Constant Capacitance model cannot be used to predict changes in ion adsorption resulting from changes in ionic strength. Instead, the Constant Capacitance model requires a different set of surface deprotonation constants (Eqs. [4] - [6]) and metal binding constants (Eqs. [10] - [12]) for each ionic strength considered. In addition to the determination of pertinent stability constants, a description of metal-bacteria adsorption with the Constant Capacitance model requires determination of the total concentrations of the carboxyl, phosphate and hydroxyl functional groups. Lastly, because the capacitance (C_1) cannot be measured directly, it must be considered a parameter for optimization, and determined experimentally.

The Basic Stern model considers specifically adsorbed species to occupy either the Inner Helmholtz Plane (IHP), with capacitance C_1, or the Outer Helmholtz Plane (OHP), which is some distance away from the surface (the capacitance of OHP is omitted in the Basic Stern model). Surface complexes in the IHP are again analogous to inner-sphere aqueous complexes, wheras surface complexes in the OHP are more akin to aqueous ion-pairs, as the ions are only

electrostatically bound to the surface. The OHP is the inner-most plane of the diffuse layer. The relationships between charge (σ) and potential (ψ) in these planes are (31):

$$\sigma_0 = C_1(\psi_0 - \psi_1) \quad [15]$$

$$\sigma_1 = -\sigma_0 + \sigma_d = C_1(\psi_1 - \psi_0) + \sigma_d \quad [16]$$

$$\sigma_d = -0.1174\sqrt{I}\sinh(zF\psi_d / 2RT) \quad [17]$$

Here, the subscripts *0*, *1* and *d* denote the charge or potential at the surface, the IHP and the OHP, respectively, and *I* is the ionic strength of the solution. Unlike the Constant Capacitance model, the Basic Stern model can predict adsorption over a wide range of ionic strengths with only one set of surface deprotonation constants. The Stern model accounts for changing ionic strength through Eq. [17], and by considering adsorption of electrolyte ions into the OHP. Because the bacterial surfaces are neutral or negatively charged, we consider adsorption of only the Na^+ electrolyte cations:

$$Na^+ + R-COO^- \Leftrightarrow R-COONa^0 \quad [18]$$

$$Na^+ + R-PO_4^- \Leftrightarrow R-PO_4Na^0 \quad [19]$$

$$Na^+ + R-O^- \Leftrightarrow R-ONa^0 \quad [20]$$

Corresponding stability constants for the above reactions are:

$$K_{Na-carb} = \frac{[R-COONa^0]}{[R-COO^-]a_{Na^+}} \quad [21]$$

$$K_{Na-phos} = \frac{[R-PO_4Na^0]}{[R-PO_4^-]a_{Na^+}} \quad [22]$$

$$K_{Na-hydr} = \frac{[R-ONa^+]}{[R-O^-]a_{Na^+}} \quad [23]$$

A full description of the adsorption of a single aqueous metal cation by the bacterial surface using the Basic Stern model may require the determination of up to nine stability constants (Eqs. [4] - [6], [10] - [12] and [21] - [23]), one capacitance (C_1), and the total concentrations of the carboxyl, phosphate and hydroxyl functional groups. It is not possible to determine stability constants for Eqs. [4] - [6] and [21] - [23] simultaneously, and as a result, several sets of stability constant values may fit the experimental data equally well (32).

In this study, we use the computer speciation program FITEQL 2.0 (34, 35) to calculate stability constants (Eqs. [4] - [6], [10] - [12] and [21] - [23]) from experimental acid-base titration data. The FITEQL program used here has been modified by Johannes Lützenkirchen (Department of Inorganic Chemistry, Umea University, Sweden; pers. comm.) to accept a greater number of input data points and to consider input data for several different solid:solution ratios simultaneously. We attempt to describe the experimental data with several models involving different adsorption reactions, and FITEQL is used to compute a variance, V(Y), which quantifies the fit of each model. The variance is

normalized with respect to the number of experimental data points, the number of chemical components for which the total concentration is known, and the number of equilibrium constants to be determined, and so it provides a quantitative means of assessing the goodness of fit of the various models.

The thermodynamic standard states employed in this study for the solid phases and liquid water are taken to be the pure substance at 25°C and 1 atm. The standard state for aqueous species is a hypothetical one molal solution which exhibits the behaviour of infinite dilution at the temperature and pressure of interest. Departures from this standard state are quantified by Davies equation activity coefficients. Neutral aqueous species are assigned activity coefficients of unity. The standard state for surface complexes is one of zero coverage and zero surface potential. Departures from this standard state are corrected with the Boltzmann equation, as outlined above. All equilibrium constants reported in this work are referenced to 25°C, zero surface potential, and the ionic strength of the background electrolyte.

MATERIALS AND METHODS

Growth Procedures. The bacteria were cultured as described by Fein et al. (17) and Daughney et al. (18). *B. licheniformis* and *B. subtilis* cells were obtained from T. J. Beveridge (University of Guelph, Ontario). The cells were cultured in 3 mL volumes of autoclaved (120°C for 20 minutes) trypticase soy broth (Becton Dickenson) containing 0.5 wt. % yeast extract (Becton Dickenson). After

growing for 24 hours at 32°C, the cells were transferred to 1 L volumes of autoclaved broth and allowed to culture for an additional 24 hours at 32°C. The cells were removed from the growth medium by centrifugation at 6000 rpm for 15 minutes. The pelleted cells were rinsed two times in distilled, deionized (DDI) water, soaked for one hour in 0.1 M HNO_3, rinsed two times in DDI water, soaked overnight in 0.001 M EDTA, rinsed five times in DDI water, and finally rinsed two times in 0.01 M $NaNO_3$ (the electrolyte used in the experiments). Following each rinse, the cells were pelleted by centrifugation at 6000 rpm for 15 minutes, and the supernatant was discarded. This procedure was followed in order to strip the cell walls of any metals present in the growth medium.

Acid-base Titrations. Acid-base titrations were performed in order to determine the deprotonation constants and absolute concentrations of the specific functional groups present on the bacterial cell walls. The bacterial cells were suspended in 10.0 mL of 0.1 M or 0.01 M $NaNO_3$, which had been bubbled with N_2 for 60 minutes in order purge it of dissolved CO_2. The titration vessel was sealed immediately, and a positive internal pressure of N_2 was maintained for the duration of the experiment. The titrations were conducted using a Radiometer-Copenhagen TTT85-autotitrator/ABU80-burette assembly. The pH of the bacterial suspension was recorded after each addition of titrant (1.00 or 0.50 M NaOH, standardized against reagent grade K-H-phthalate) only when a stability of 0.1 mV/s had been attained. Following the titration, the bacteria present in the titration vessel were pelleted by centrifugation at 6000 rpm for 60 minutes, and the weight of the dry pellet was recorded. High Performance Liquid

Chromatography (HPLC) was used to analyze the supernatants for dissolved organic exudates. Four titrations were performed for each bacterial species at each ionic strength.

Adsorption Experiments. Batch experiments were conducted as a function of pH in order to determine site-specific stability constants for Cd, Pb and Cu adsorption onto the bacterial surfaces. The washed bacteria were pelleted by centrifugation at 6000 rpm for 60 minutes. The bacterial pellet was weighed and then resuspended in a known weight of 0.1 M or 0.01 M $NaNO_3$ electrolyte to yield a parent suspension. Homogenous 5.00 g aliquots of this parent suspension together with a known volume of 1000 ppm aqueous metal standard (Cd, Pb or Cu) were added to several identical reaction vessels, and the pH of the suspension in each vessel was adjusted to a different value using 1.0 M HNO_3 or NaOH. The reaction vessels were shaken and allowed to equilibrate for 30 minutes. The 30 minute reaction time was chosen based on the kinetic experiments reported by Fein et al. (17). The contents of each reaction vessel were then filtered through a 0.45 μm cellulose nitrate/acetate filter (Micron Separation Inc.). The filtrate from each reaction vessel was acidified and analyzed for the dissolved metal by flame atomic absorption spectrophotometry. Experiments for the Cd, Pb and Cu systems were repeated in duplicate, with 1.5, 3.5 or 6.0 grams of bacteria per litre of suspension, and total metal concentrations ranging from 10 - 35 ppm.

PROTON ADSORPTION RESULTS AND DISCUSSION

Experimental data collected during acid-base titrations of *B. subtilis* and *B. licheniformis* in 0.1 and 0.01 M $NaNO_3$ indicate that the bacteria impart significant buffering capacity to the suspensions between pH 3 and 12, and that this buffering capacity increases with the quantity of bacteria present (Figure 2). In the following section, we compare the Constant Capacitance and Basic Stern models in their ability to describe the experimental titration data and predict ionic strength dependent behaviour. We begin by modeling each of the sixteen titrations individually, examining the extent to which the optimizable model parameters vary between the different trials. Next, we model subsets of the titrations simultaneously. The four titrations of a given bacteria in a particular electrolyte can be modeled simultaneously in order to derive a single set of optimizable model parameters applicable to all solid:solution ratios (but a single ionic strength). This set of parameters should, in theory, correspond closely to the average of the parameters determined by modeling the four titrations individually. Further, it is possible to model all eight titrations of each bacteria simultaneously, in order to determine a parameter set which can be applied to all solid:solution ratios and both ionic strengths. Note that the Basic Stern model can be applied in this last case, because the charge-potential relationship is ionic strength dependent, but the Constant Capacitance model can not.

For each model proposed, we use FITEQL to solve for up to ten optimizable parameters: the capacitance of the bacterial surface, and the

Figure 2. Experimental data gathered during acid-base titration of a) *B. subtilis* in 0.1 M $NaNO_3$ from Fein et al. (17), b) *B. subtilis* in 0.01 M $NaNO_3$, c) *B. licheniformis* in 0.1 M $NaNO_3$ from Daughney et al. (18), and d) *B. licheniformis* in 0.01 M $NaNO_3$.

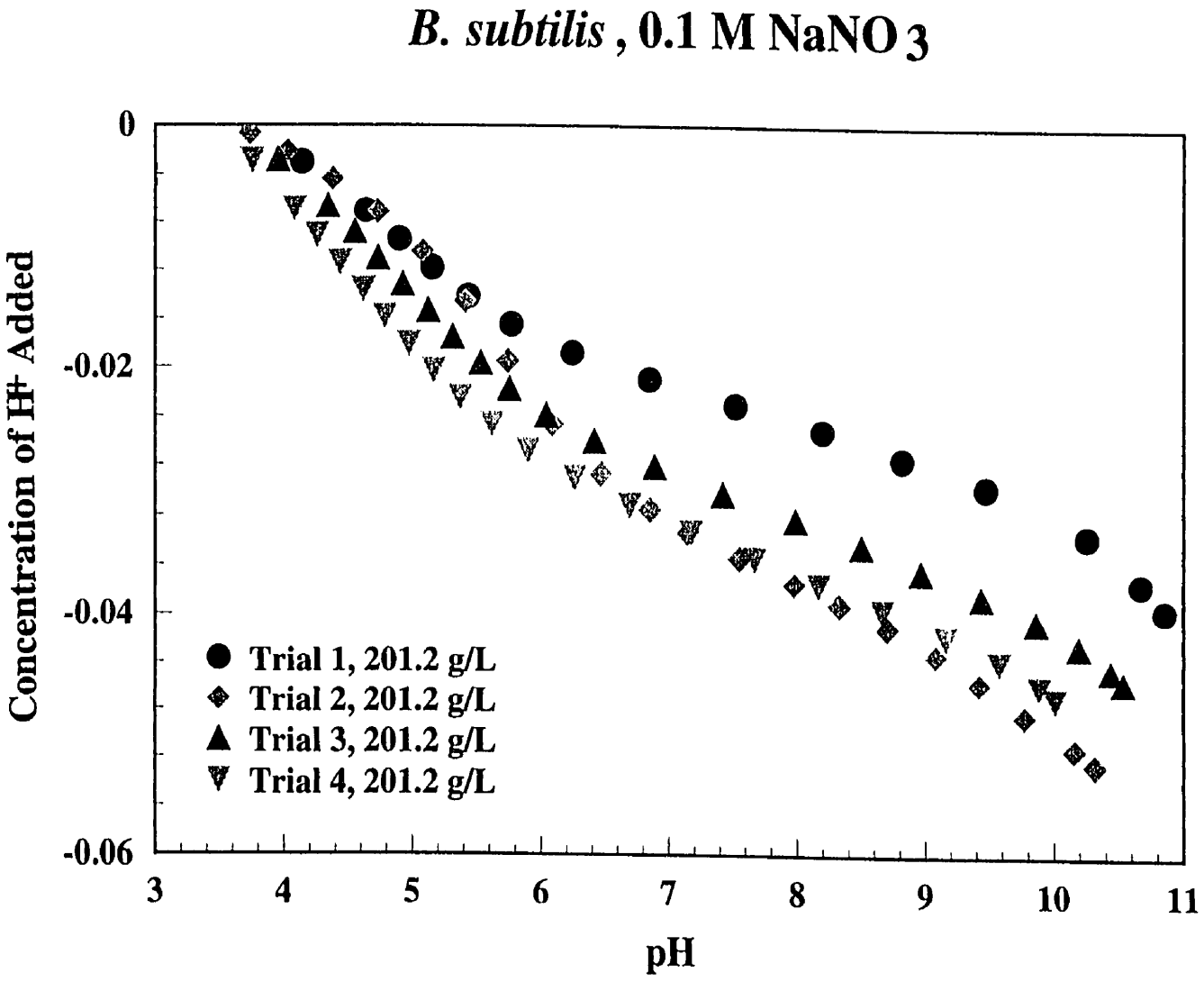
B. subtilis, 0.1 M $NaNO_3$
Concentration of H^+ Added
0
-0.02
-0.04
-0.06
3
4
5
6
7
8
9
10
11
pH
Trial 1, 201.2 g/L
Trial 2, 201.2 g/L
Trial 3, 201.2 g/L
Trial 4, 201.2 g/L

Figure 2a

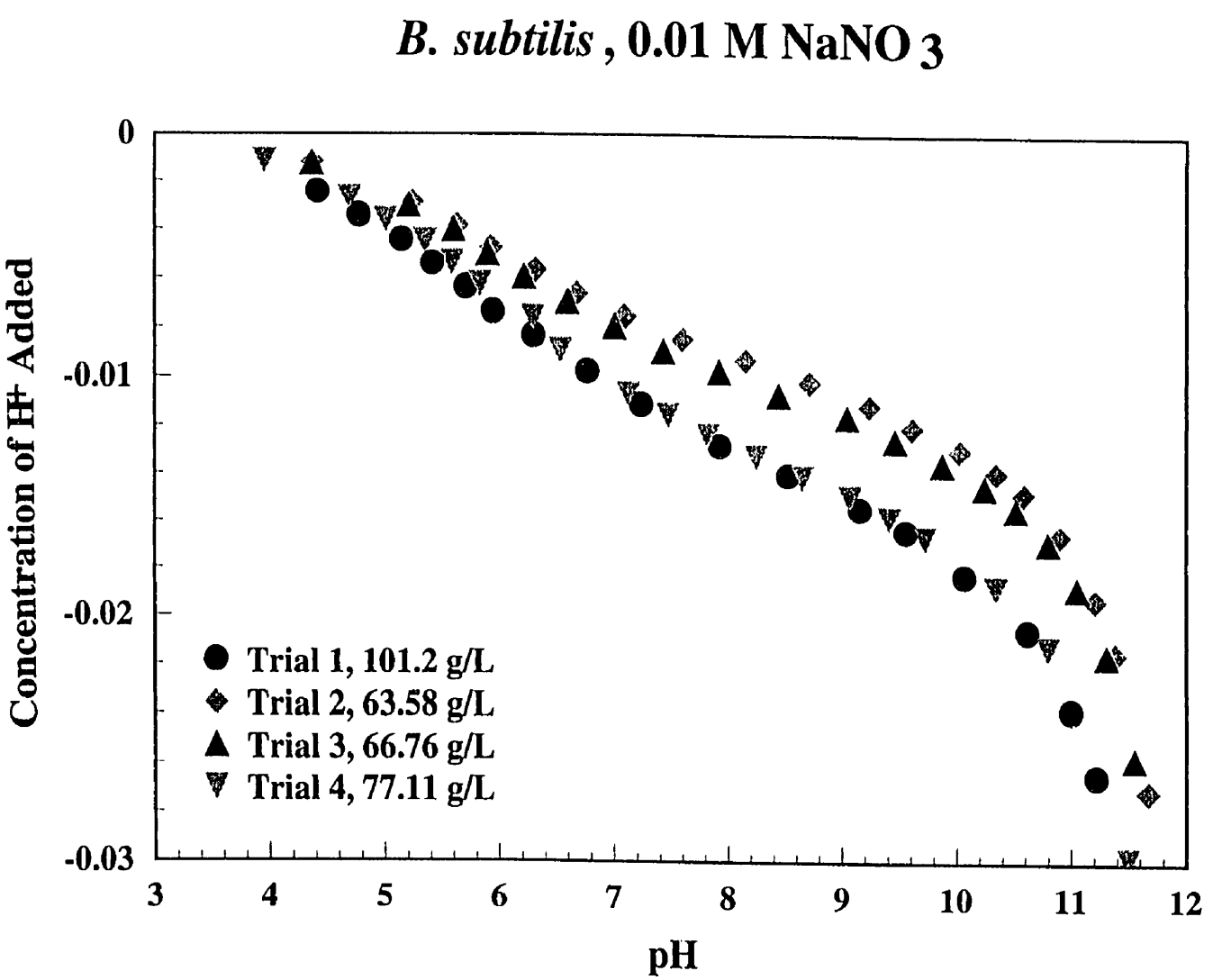
B. subtilis , 0.01 M $NaNO_3$
Concentration of H^+ Added
0
-0.01
-0.02
-0.03
3
4
5
6
7
8
9
10
11
12
pH
Trial 1, 101.2 g/L
Trial 2, 63.58 g/L
Trial 3, 66.76 g/L
Trial 4, 77.11 g/L

Figure 2b

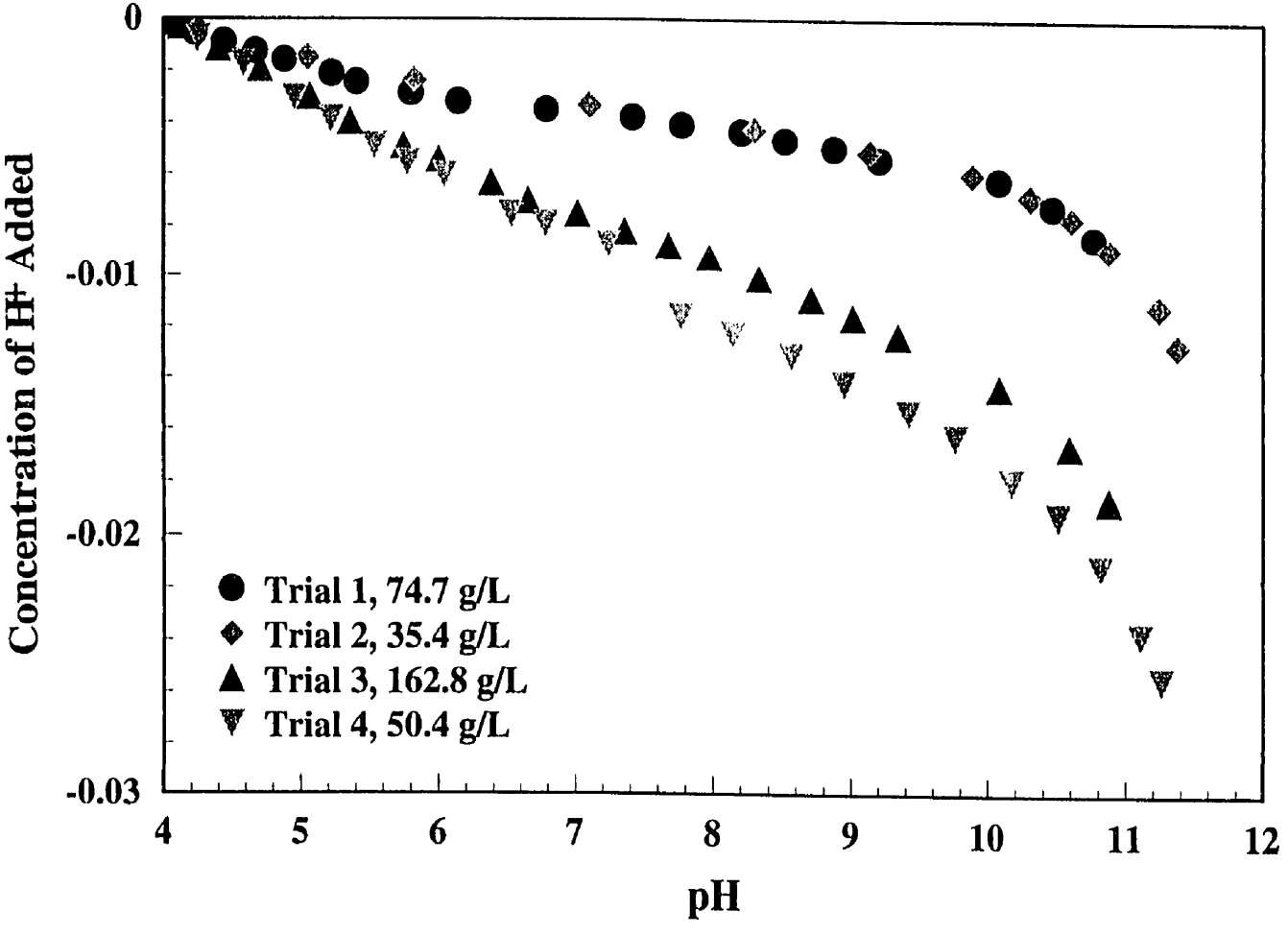
B. licheniformi s, 0.1 M $NaNO_3$
Concentration of H^+ Added
0
-0.01
-0.02
-0.03
4
5
6
7
8
9
10
11
12
pH
Trial 1, 74.7 g/L
Trial 2, 35.4 g/L
Trial 3, 162.8 g/L
Trial 4, 50.4 g/L

Figure 2c

B. licheniformi s, 0.01 M $NaNO_3$

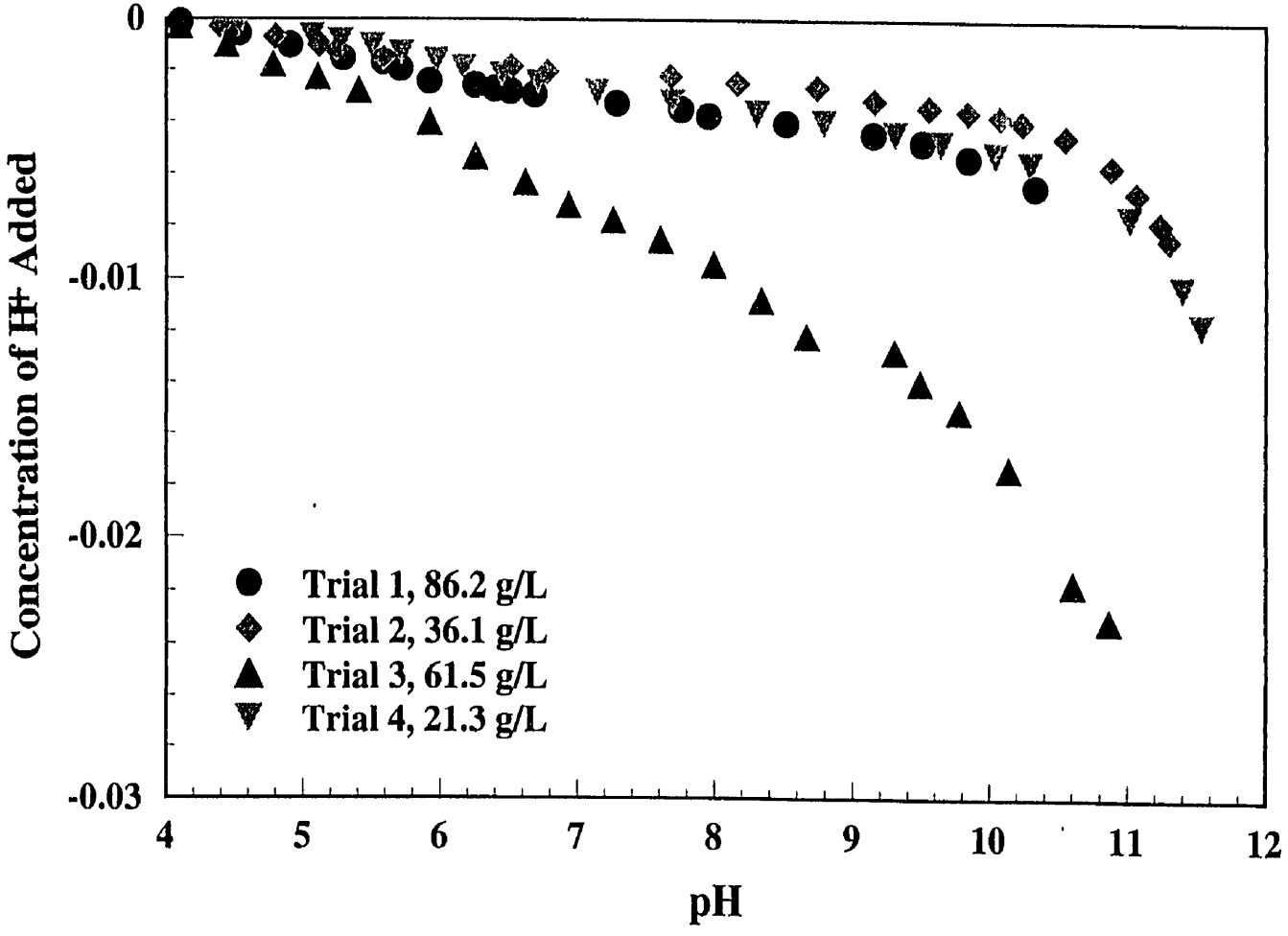

Figure 2d

deprotonation constants (Eqs. [4] - [6] for the Constant Capacitance model, Eqs. [4] - [6] and [21] - [23] for the Basic Stern model) and absolute concentrations (moles/L) of each of the three types of surface functional groups. The concentrations of the functional groups can be normalized with respect to the weight of bacteria per unit weight of electrolyte, to yield concentrations in moles per gram of bacteria. Equilibria describing the aqueous dissociation of water, the acid, the base and the electrolyte are included in the model, with stability constants taken from Smith and Martell (36).

Constant Capacitance Models. We first model the acid-base behaviour of the 16 titrations individually, using the Constant Capacitance model (FITEQL models are summarized in Table 2 and compared to the experimental data in Figure 3). Fein et al. (17) and Daughney et al. (18) used the Constant Capacitance model to describe the acid-base behaviour of *B. subtilis* and *B. licheniformis* in 0.1 M $NaNO_3$, applying models which consider three distinct types of proton-active surface functional groups, as described above. Similarly, the experimental data presented here are better described by models involving three distinct proton-active sites than by models considering only one or two types of proton-active sites, and so parameters for the one-site and two-site models are not tabulated here.

The variances for these individual Constant Capacitance models are small, indicating an excellent correlation between the model and the experimental data. However, because each titration is modeled independently, the optimizable parameters can vary between trials. The average values and 1s errors displayed in

TABLE 2. Acid-base titration data as described by individual Constant Capacitance models.

Trial[a]	g/L[b]	C_1[c]	pK_1[d]	$Conc_1$[e]	pK_2	$Conc_2$	pK_3	$Conc_3$	V(Y)[f]
***B. subtilis*, 0.1 M $NaNO_3$**									
1	201.2	3.3	4.80	1.01	7.38	3.67	9.82	7.38	1.4
2	201.2	4.4	4.98	9.45	5.88	8.60	8.60	8.03	9.3
3	201.2	4.1	4.73	12.8	6.88	40.8	9.14	5.90	1.4
4	201.2	8.0	4.51	13.2	6.44	4.68	8.75	5.48	1.6
	Avr[g]	5.0	4.76	9.12	6.65	14.4	9.08	6.70	
	1*s*[h]	2.1	0.2	5.7	0.6	18	0.5	1.2	
***B. subtilis*, 0.01 M $NaNO_3$**									
1	101.2	1.6	4.56	7.05	6.36	7.64	10.32	84.2	9.8
2	63.6	1.8	4.83	7.81	6.34	8.46	9.79	39.2	11.2
3	66.8	1.5	4.65	5.87	5.88	10.6	9.54	48.5	8.9
4	77.1	1.6	4.40	6.15	5.84	12.0	9.33	42.5	7.1
	Avr	1.6	4.61	6.72	6.11	9.68	9.75	53.6	
	1*s*	0.1	0.2	0.9	0.3	2.0	0.4	21	
***B. licheniformis*, 0.1 M $NaNO_3$**									
1	74.7	4.0	4.89	4.52	7.83	2.28	10.45	6.34	5.3
2	35.4	2.2	4.82	8.33	7.38	5.59	9.67	14.2	2.2
3	162.8	3.5	5.08	3.86	7.22	2.45	9.50	4.17	6.9
4	50.4	6.8	5.01	14.0	7.38	14.6	9.88	18.5	7.7
	Avr[g]	4.1	4.95	7.68	7.45	6.23	9.85	10.8	
	1*s*[h]	1.9	0.1	4.7	0.3	5.8	0.4	6.7	
***B. licheniformis*, 0.01 M $NaNO_3$**									
1	86.2	2.8	5.07	3.09	6.99	1.46	9.67	3.54	14.6
2	36.1	4.3	5.11	5.86	8.61	3.73	11.60	41.8	6.8
3	61.5	2.5	4.96	6.96	6.53	10.3	9.26	71.6	26.8
4	21.3	3.4	5.43	11.5	6.99	6.79	9.44	151	4.3
	Avr	3.8	5.14	6.85	7.28	5.57	9.99	67.0	
	1*s*	1.4	0.2	3.5	0.9	3.8	1.1	63	

[a]With the exception of the weight of bacteria per unit weight of electrolyte, the trials in each subset are identical replicates. [b]Weight of bacteria per unit weight of electrolyte. [c]Capacitance of the bacterial surface (Farads/m^2), treated as an optimizable parameter and adjusted to yield the lowest variance. [d]Negative logarithm of the subscripted surface site, referenced to the ionic strength of the background electrolyte and zero surface charge. [e]Concentration of the subcripted surface site, expressed in $x10^{-5}$ moles per gram of bacteria. [f]Variance as calculated by FITEQL. [g]Average values for all trials. [h]1*s* error corresponding to each average value.

Figure 3. FITEQL model curves describing acid-base behaviour of B. subtilis in 0.01 M $NaNO_3$, for a) individual Constant Capacitance models, b) Net Constant Capacitance models, c) individual Basic Stern Models, and d) Net Basic Stern Models. The experimental data shown in all four graphs are identical to that of Figure 2b.

B. subtilis , 0.01 M $NaNO_3$: Individual CC Models

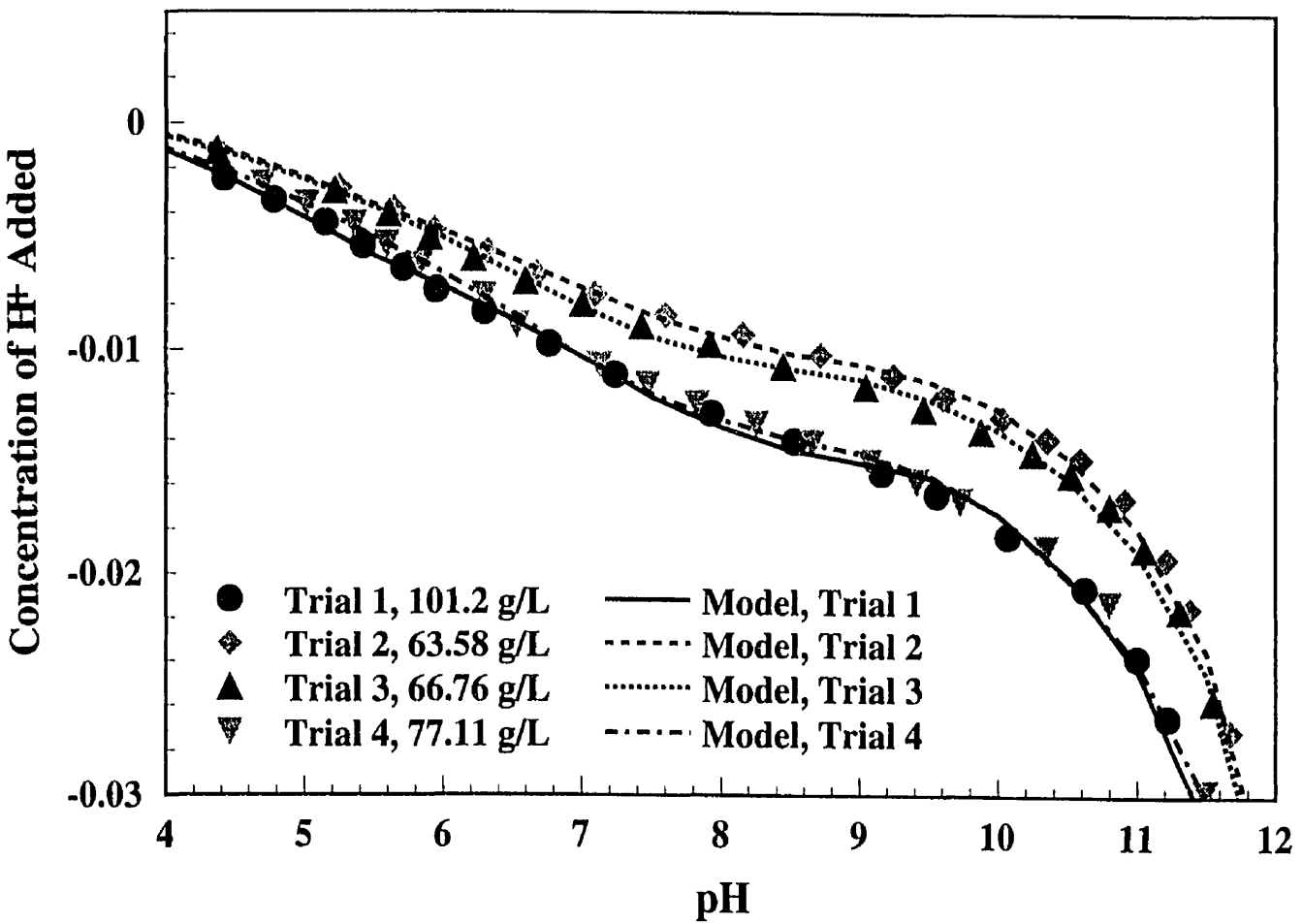

Figure 3a

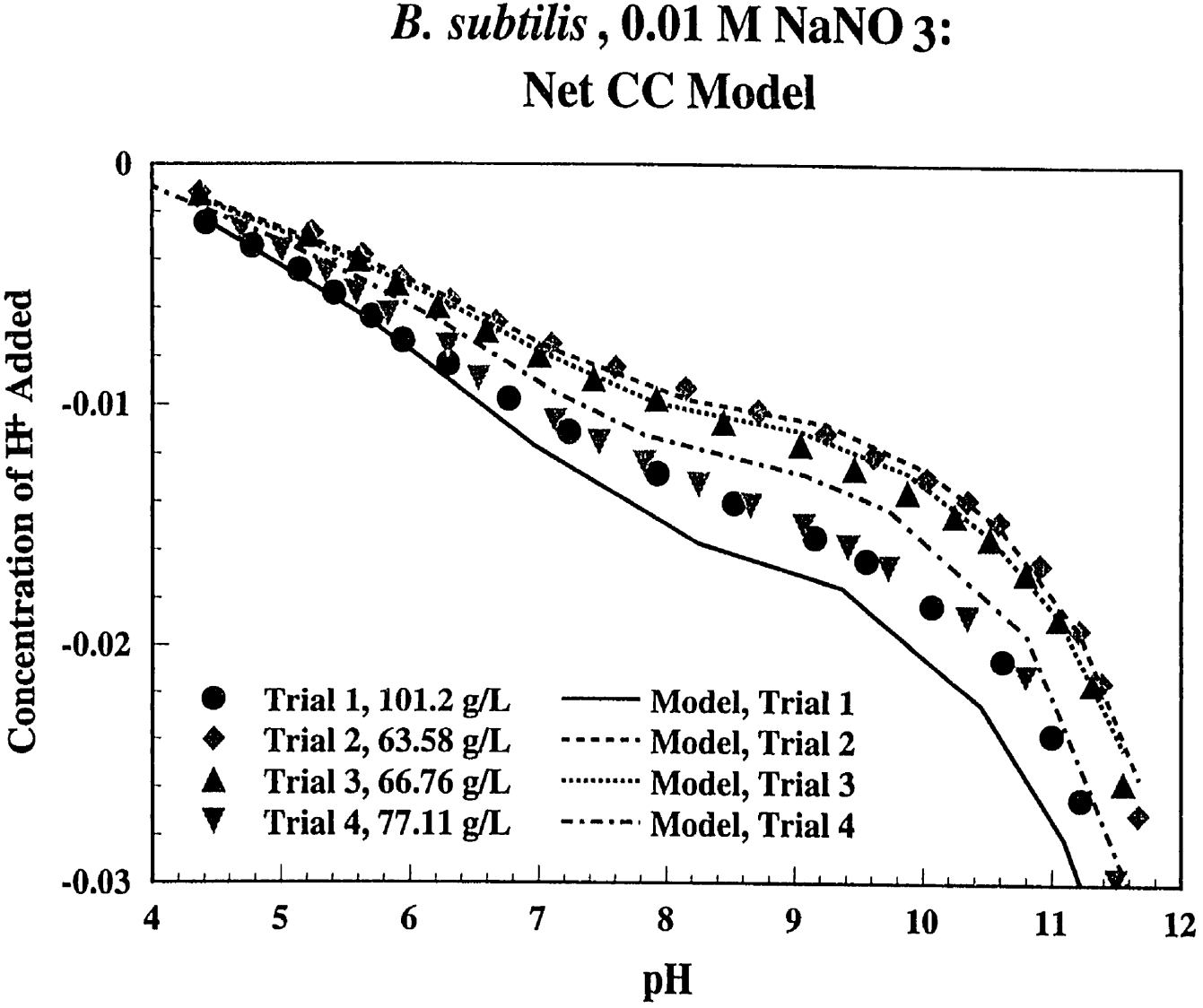
B. subtilis, 0.01 M $NaNO_3$:
Net CC Model
Concentration of H^+ Added
0
-0.01
-0.02
-0.03
4
5
6
7
8
9
10
11
12
pH
Trial 1, 101.2 g/L
Trial 2, 63.58 g/L
Trial 3, 66.76 g/L
Trial 4, 77.11 g/L
Model, Trial 1
Model, Trial 2
Model, Trial 3
Model, Trial 4

Figure 3b

B. subtilis , 0.01 M $NaNO_3$: Individual Stern Models

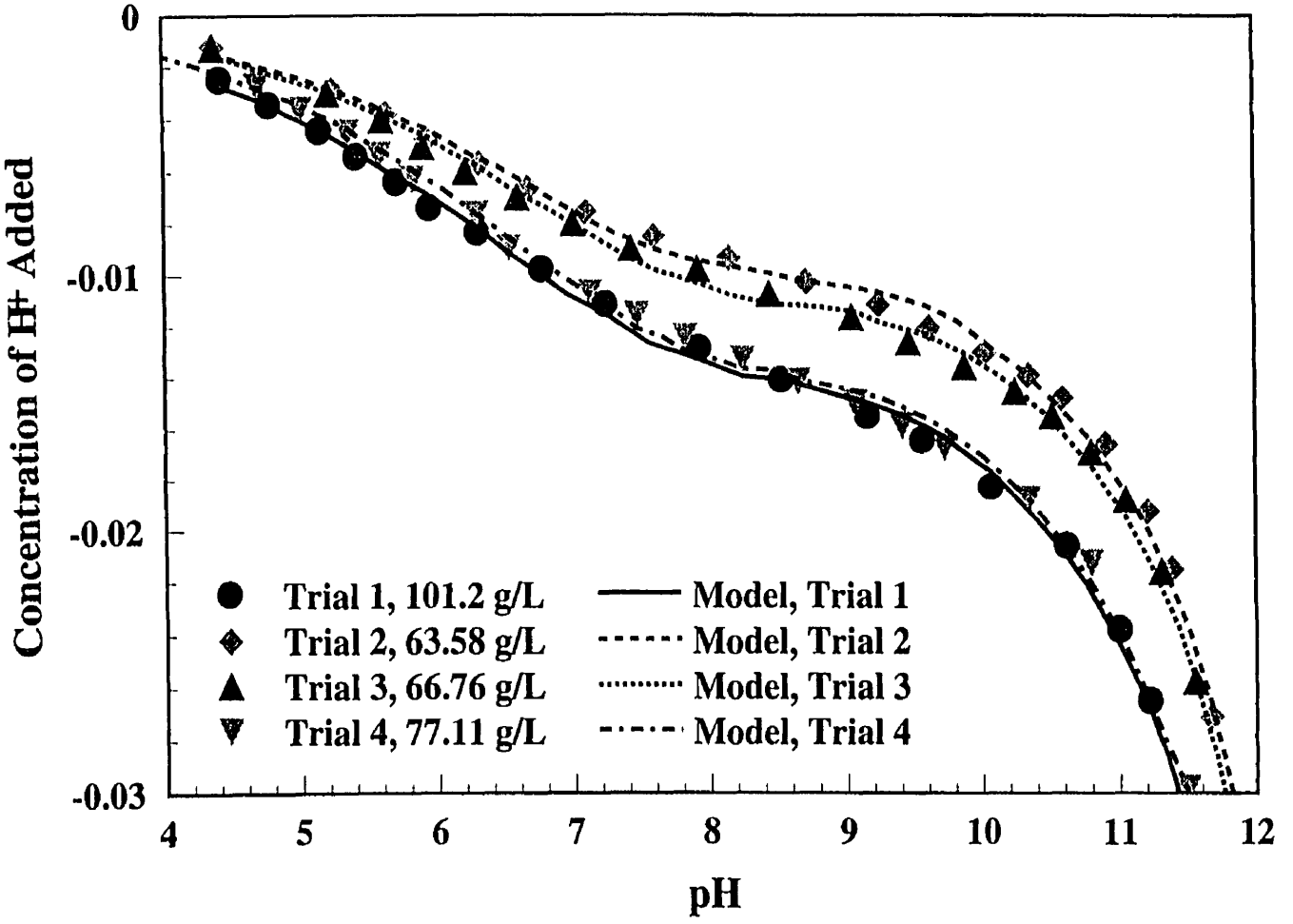

Figure 3c

B. subtilis , 0.01 M $NaNO_3$: Net Stern Model

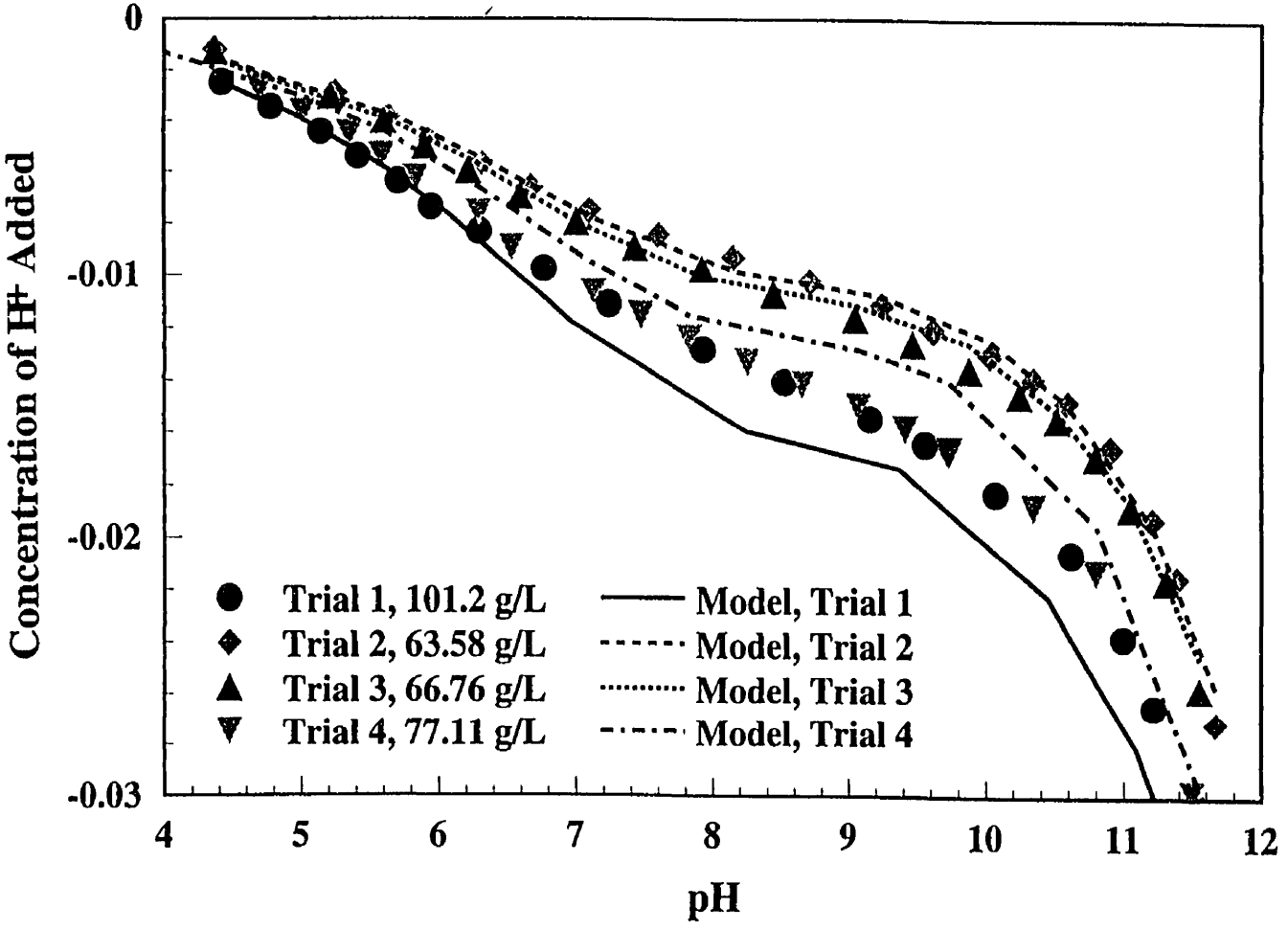

Figure 3d

Table 2 indicate that there is substantial variation in the relative and absolute concentrations of the cell wall functional groups of both *B. subtilis* and *B. licheniformis*. The cell wall structures of both species are known to change if the growth conditions are varied (37), but our experimental procedure ensures that growth conditions are controlled and reproducible. We have verified our method of titration by reproducing the stability constant and absolute concentration of functional groups in a sodium acetate system. An examination of the bacterial suspensions by HPLC and optical microscopy both before and after the titration gives no evidence of organic exudates or cell wall disruption. Further, the titrations are reversible (Figure 4), suggesting that the extremes in pH do not cause changes in the cell wall structure through saponification of lipids or destruction of peptide bonds. Thus we conclude that the observed variation in surface site concentrations is due to true variation in the cell wall structure. Both *B. subtilis* and *B. licheniformis* are capable of forming spores, and the composition of the spore wall is known to differ from that of the cell wall (38). The duration of the titrations may be sufficient to allow varying degrees of sporulation in response to changes in solution chemistry, giving rise to the observed variation in surface site concentration. However, because the extent of variation is not systematic for a given type of site, a given ionic strength or a given bacterial species, we suggest that the variations in surface site concentrations are due to essentially random differences in cell wall structure arising from genetic exchange during reproduction.

Figure 4. Representative data gathered during an acid-base titration (of *B. subtilis* in 0.01 M $NaNO_3$) intended to test the reversibility of the proton adsorption - desorption reactions.

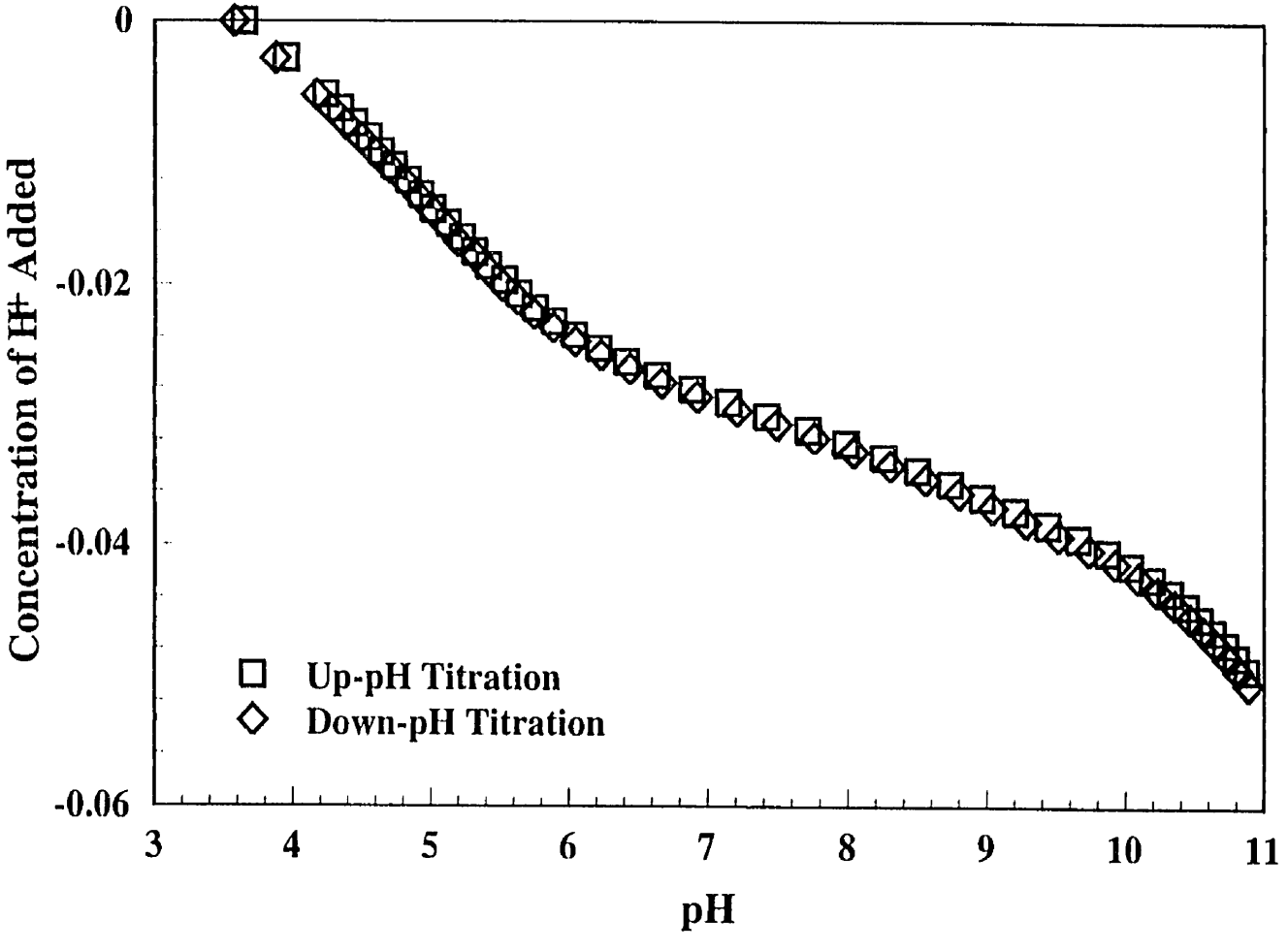
0
-0.02
-0.04
-0.06
Concentration of H+ Added
Up-pH Titration
Down-pH Titration
3
4
5
6
7
8
9
10
11
pH

Figure 4

The variations in the log stability constants are small relative to the variations in the surface site concentrations. This limited variability suggests either that the deprotonation of a given functional group is not affected by changes in the surrounding cell wall structure, or that there are simply so many functional groups on the cell wall that an average value is appropriate. The variation in the deprotonation constants is smallest for the carboxyl sites and largest for the hydroxyl sites. This trend may reflect greater local cell wall variation around the hydroxyl sites. However, because the hydroxyl site concentrations do not vary significantly more than the concentrations of the other sites, this trend is more likely to be caused by experimental errors, which increase with pH due to a decrease in the buffering capacity of the bacterial suspensions.

The capacitance of the bacterial surface is also treated as an optimizable parameter, and so can vary between each titration. However, this variation is of questionable significance, because the values of the best-fit capacitance and the total concentrations of surface sites are not independently resolvable. The concentrations of the functional groups can be inferred from the experimental data describing proton adsorption, and thus the bacterial surface charge can be calculated. However, it is the electric potential of the surface, rather than the charge, which directly affects the observed proton adsorption, through Eq. [13]. The surface electric potential cannot be determined directly, and so must be related to the surface charge through the surface capacitance, using Eq. [14]. Thus, a change in the total concentration of proton active sites will cause a corresponding change in the value of the model capacitance. Therefore, we

conclude that the observed variation in the best-fit capacitance is due to true variation in the relative and absolute concentrations of the cell wall functional groups. The range of capacitance values used here (1.5 - 8.0 Farads/m^2) alters the model determination of site concentrations and deprotonation constants by less than 5%.

We apply the student's t-test (39) for averages to evaluate the significance of the parameter variation between individually modeled titrations:

$$t = \frac{X_1 - X_2}{\sqrt{s_1^2 + s_2^2}} \qquad [24]$$

where X and s are the mean value and the variance of the subscripted population, respectively. For a given degree of freedom (f, where $f = n_1 + n_2 - 2$, and n represents the number of observations of the subscripted population) the value of the t- statistic can be compared to the t-distribution to determine the confidence interval at which the two means can be considered to be different. Here, a confidence interval of 80% or above indicates a statistically significant difference between the mean values of the two populations being compared; a confidence interval of less than 80% suggests that the two population means are not statistically different.

The concentrations of the functional groups change dramatically between the individual trials, and as a result, large 1s errors arise. Because the 1s errors are large, a t-test indicates an insignificant difference in the site concentrations of the

two species, and an insignificant effect of ionic strength (Table 3). In contrast, the values of the deprotonation constants vary only slightly between trials, and thus they have small corresponding 1*s* errors. However, because the average values are similar for all titrations modeled, the t-test indicates that ionic strength has an insignificant effect, relative to experimental uncertainties, on the magnitudes of the deprotonation constants for both bacterial species. In contrast, the change in the deprotonation constants between the two species at a fixed ionic strength appears significant. In summary, the t-test suggests that a single set of parameter values may be adequately applied to all titrations of a given bacteria, regardless of ionic strength, but that the deprotonation constants are species-specific.

Subsequently, we attempt to use a single Constant Capacitance model to simultaneously fit all four titrations of a given species at a particular ionic strength. The FITEQL results for these Net Constant Capacitance models are listed in Table 4, and in Figure 3b they are compared to the *B. subtilis* experimental data collected at 0.01 M ionic strength. The model variances are substantially larger when the titrations are modeled simultaneously. This is due to the large variability in the concentrations of surface functional groups observed between the trials. It is apparent from the model variances that *B. licheniformis* is more prone to cell wall variation than *B. subtilis*, as noted by Daughney et al. (18). In spite of the apparently poorer fit of these Net Constant Capacitance models, they provide an adequate approximation of the acid-base behaviour of each species at each ionic strength. Further, because the Net Constant Capacitance model parameters are essentially averages of the parameters applicable to the

TABLE 3: Statistical comparison of individual Constant Capacitance model parameters.

Comparison of *B. subtilis* model parameters at 0.1[a] and 0.01[b] M							
Parameter	Avr_1[c]	$1s_1$[d]	Avr_2[c]	$1s_2$[d]	f[e]	t[f]	C.I.[g]
C_1	5.0	2.1	1.6	0.1	6	1.617	< 90%
pK_1	4.76	0.2	4.61	0.2	6	0.573	< 60%
pK_2	6.65	0.6	6.11	0.3	6	0.773	< 60%
pK_3	9.08	0.5	9.75	0.4	6	-0.971	< 80%
$Conc_1$	9.12	5.7	6.72	0.9	6	0.419	< 40%
$Conc_2$	14.4	18	9.68	2.0	6	0.265	< 20%
$Conc_3$	6.70	1.2	53.6	21	6	-2.251	< 95%
Comparison of *B. licheniformis* model parameters at 0.1[a] and 0.01[b] M							
C_1	4.1	1.9	3.8	1.4	6	0.127	< 20%
pK_1	4.95	0.1	5.14	0.2	6	-0.815	< 60%
pK_2	7.45	0.3	7.28	0.9	6	0.180	< 20%
pK_3	9.85	0.4	9.99	1.1	6	-0.121	< 20%
$Conc_1$	7.68	4.7	6.85	3.5	6	0.143	< 20%
$Conc_2$	6.23	5.8	5.57	3.8	6	0.095	< 20%
$Conc_3$	10.8	6.7	67.0	63	6	-0.893	< 60%
Comparison of *B. subtilis*[a] and *B. licheniformis*[b] model parameters at 0.1 M							
C_1	5.0	2.1	4.1	1.9	6	0.318	< 40%
pK_1	4.76	0.2	4.95	0.1	6	-0.845	< 60%
pK_2	6.65	0.6	7.45	0.3	6	-1.158	< 80%
pK_3	9.08	0.5	9.85	0.4	6	-1.136	< 80%
$Conc_1$	9.12	5.7	7.68	4.7	6	0.197	< 20%
$Conc_2$	14.4	18	6.23	5.8	6	0.439	< 40%
$Conc_3$	6.70	1.2	10.8	6.7	6	-0.602	< 60%
Comparison of *B. subtilis*[a] and *B. licheniformis*[b] model parameters at 0.01 M							
C_1	1.6	0.1	3.8	1.4	6	-1.567	< 90%
pK_1	4.61	0.2	5.14	0.2	6	-1.970	< 95%
pK_2	6.11	0.3	7.28	0.9	6	-1.229	< 80%
pK_3	9.75	0.4	9.99	1.1	6	-0.206	< 20%
$Conc_1$	6.72	0.9	6.85	3.5	6	-0.036	< 20%
$Conc_2$	9.68	2.0	5.57	3.8	6	0.950	< 80%
$Conc_3$	53.6	21	67.0	63	6	-0.203	< 20%

[a]First and [b]second variable sets. [c]Average value and [d]1s error for each parameter in the subscripted variable set. [e]Degrees of freedom. [f]Value of the t distribution. [g]Upper confidence level at which the average values can be considered statistically different.

TABLE 4. Summary of Net Constant Capacitance model parameters computed from simultaneous modeling of all titrations.

Sp.[a]	I[b]	C_1[c]	pK_1[d]	$Conc_1$[e]	pK_2	$Conc_2$	pK_3	$Conc_3$	V(Y)[f]
B. sub.	0.1	8.0	4.76	11.0	6.65	5.35	9.08	4.22	334
	0.01	1.4	4.45	5.85	5.88	10.2	9.38	38.9	72.6
B. lich.	0.1	4.1	4.95	4.88	7.45	2.23	9.85	8.56	1540
	0.01	4.0	4.96	4.15	7.25	2.68	10.64	22.2	1798
	Avr[g]	4.4	4.78	6.47	6.81	5.12	9.74	18.5	
	1*s*[h]	2.7	0.2	3.1	0.8	3.7	0.7	16	

[a]Bacterial species. [b]Ionic strength of $NaNO_3$ electrolyte. [c]Capacitance of the bacterial surface (Farads/m^2), treated as an optimizable parameter. [d]Negative logarithm of the subscripted surface site, referenced to the ionic strength of the background electrolyte and zero surface charge. [e]Concentration of the subcripted surface site, expressed in $x10^{-5}$ moles per gram of bacteria. [f]Variance as calculated by FITEQL. [g]Average values for all models. [h]1*s* error corresponding to each average value.

individual Constant Capacitance models, they can be appropriately used to model the average acid-base behaviour. As noted above, the Constant Capacitance model parameters are, in theory, applicable only to the ionic strength conditions in which they were determined. However, we have shown that the variation in the majority of these parameters is insignificant under the conditions of this study, and thus an average of the parameter values presented in Table 4 may be effectively used to approximate acid-base behaviour where species-specific deprotonation constants are not available.

Basic Stern Models. We also attempt to model the acid-base behaviour of the 16 titrations individually using the Basic Stern model. Although Fein et al. (17) and Daughney et al. (18) have shown that three distinct types of surface sites are required to describe the acid-base behaviour of *B. subtilis* and *B. licheniformis*, this conclusion is restricted to the Constant Capacitance model. Therefore, when using the Basic Stern model, we attempt to fit the experimental data by considering proton adsorption onto one, two or three distinct types of surface functional groups, both with and without equilibria describing Na^+ adsorption. As noted above, it is not possible to optimize for the stability constants describing Na^+ adsorption (Eqs. [21] - [23]) and proton adsorption (Eqs. [4] - [6]) simultaneously, in the absence of data describing changes in aqueous Na^+ concentration. Therefore, to test for the effects of Na^+ adsorption, we consider Na^+ adsorption onto the carboxyl, phosphate and hydroxyl surface sites independently. We fix the values of the deprotonation constants in Eqs. [21] - [23] and optimize for the values of the stability constants in Eqs. [4] - [6]. This

procedure is repeated for a range of values for the Na^+ adsorption constants, and the parameter set which best fits the experimental data can be identified.

In Table 5 we provide representative results for the FITEQL Basic Stern modeling of two individual *B. subtilis* titrations. Where Na^+ adsorption is not considered, a model involving two proton-active sites best fits the experimental data. Models considering proton adsorption onto only one type of surface site are characterized by high variances, indicating a poor fit between the model and the experimental data, and models considering proton adsorption onto three types of surface sites fail to converge, indicating that the inclusion of the third site is not warranted by the data. The variances for the two-site Basic Stern models are comparable to those of the three-site Constant Capacitance models given in Table 2, though the Basic Stern models predict a much more negative surface potential.

Basic Stern models which consider Na^+ adsorption generally fit the experimental data better than those which do not (Table 5). The experimental data are described equally well by models considering Na^+ adsorption onto any of the three different types of surface sites. However, the log K values describing Na^+ adsorption onto the phosphate and hydroxyl sites are unreasonably large (compared to non-specific (outer sphere) aqueous Na^+ complexes), and so we consider only Na^+-carboxyl adsorption. In no instance is Na^+ adsorption onto more than one type of surface site required to describe the data. The Basic Stern model prediction of surface potential is made less negative if Na^+ adsorption is considered, although the values are still more negative than those predicted by the Constant Capacticance model. This suggests that low negative surface potential

TABLE 5. Representative FITEQL Basic Stern modeling for two individual *B. subtilis* titrations.

B. subtilis, 0.1 M $NaNO_3$, 201.2 g bacteria/L									
Model[a]	C_1[b]	pK_1[c]	$Conc_1$[d]	pK_2	$Conc_2$	pK_3	$Conc_3$	log K_{Na}	V(Y)[e]
1pK	8.0	5.45	27.5	—	—	—	—	—	1614
1pK + Na	6.0	5.58	22.3	—	—	—	—	1.2	978
2pK	8.0	3.78	17.2	6.81	6.15	—	—	—	14.9
2pK + Na	5.9	4.31	15.2	6.77	7.15	—	—	0.4	3.6
3pK	no convergence[f]								
3pK + Na	3.9	5.05	14.4	6.20	4.80	8.16	7.82	1.55	0.1

B. subtilis, 0.01 M $NaNO_3$, 63.6 g bacteria/L									
1pK	8.0	6.13	43.8	—	—	—	—	—	1183
1pK + Na	6.1	5.91	50.6	—	—	—	—	-2.7	1056
2pK	8.0	4.06	15.7	7.75	24.0	—	—	—	12.5
2pK + Na	4.0	3.98	15.9	7.65	33.6	—	—	-2.4	12.7
3pK	no convergence								
3pK + Na	no convergence								

[a]Models consider proton adsorption onto one, two or three distinct types of surface functional groups, and are termed 1pK, 2pK and 3pK respectively. Models considering Na^+ adsorption are indicated. [b]Capacitance of the bacterial surface (Farads/m^2), treated as an optimizable parameter. [c]Negative logarithm of the subscripted surface site, referenced to the ionic strength of the background electrolyte and zero surface charge. [d]Concentration of the subcripted surface site, expressed in $x10^{-5}$ moles per gram of bacteria. [e]Variance as calculated by FITEQL. [f]Indicates severe misfit between the model and the experimental data

values are required to describe the experimental data. Where Na^+-carboxyl adsorption is considered, the 0.1 M titration data are well described by a model invoking three types of proton-active sites; however, for the 0.01 M titrations, the data are better described by a model involving only two proton-active sites. This difference implies that the Basic Stern model invoking Na^+ adsorption cannot account for the observed ionic strength-dependent changes in proton adsorption. This is further demonstrated in Figure 5, where a Basic Stern model using fit parameters determined from a titration in the 0.1 M electrolyte fails to match the 0.01 M titration data, when adjustments for ionic strength are made. Although Na^+ adsorption may be occurring, and although this may be effectively described by a more complex double layer model, Basic Stern models considering Na^+ adsorption do not effectively describe the data gathered here. Therefore, we select the model with two types of proton-active sites, but without Na^+ adsorption, as the Basic Stern model which best describes the experimental data.

Using this two-site Basic Stern model, we model each of the 16 individual titrations (Table 6), and we compare the individual model curves to the *B. subtilis* experimental data gathered in the 0.01 M electrolyte (Figure 3c). The optimizable parameters vary between the individual titrations, for reasons that have been discussed above. Again, we use the student's t-test for averages to compare the variation in model parameters for the two species in the two different electrolytes (Table 7). The first deprotonation constant appears to be species-specific (at the 95% confidence interval). Variation in the second deprotonation constant between the two species is statistically insignificant. Variation in the surface site

TABLE 6. Acid-base titration data as described by individual Basic Stern models.

Trial[a]	g/L[b]	C_1[c]	pK_1[d]	$Conc_1$[e]	pK_2	$Conc_2$	V(Y)[f]
***B. subtilis*, 0.1 M $NaNO_3$**							
1	201.2	8.0	4.42	12.1	7.97	7.18	43.9
2	201.2	no convergence[i]					
3	201.2	8.0	4.26	16.4	7.61	6.51	70.7
4	201.2	8.0	3.97	18.2	7.25	6.23	98.6
	Avr[g]	8.0	4.22	15.6	7.61	6.64	
	1s[h]	0.0	0.2	3.1	0.4	0.5	
***B. subtilis*, 0.01 M $NaNO_3$**							
1	101.2	2.7	3.85	14.1	7.91	57.9	11.3
2	63.6	8.0	4.11	15.9	7.81	25.3	19.8
3	66.8	8.0	4.12	16.7	7.83	25.2	20.0
4	77.1	8.0	3.95	18.1	7.55	24.1	20.2
	Avr	6.7	4.01	16.2	7.73	33.1	
	1s	2.7	0.1	1.7	0.3	17	
***B. licheniformis*, 0.1 M $NaNO_3$**							
1	74.7	8.0	4.76	5.19	8.19	4.17	35.3
2	35.4	4.5	4.61	10.8	7.95	13.7	17.3
3	162.8	5.5	5.08	5.04	8.02	4.90	33.8
4	50.4	8.0	4.66	24.5	7.29	19.8	86.3
	Avr	6.5	4.78	11.4	7.86	10.6	
	1s	1.8	0.2	9.2	0.4	7.5	
***B. licheniformis*, 0.01 M $NaNO_3$**							
1	86.2	8.0	4.76	4.38	8.18	4.33	78.4
2	36.1	8.0	4.30	6.79	7.96	9.26	89.8
3	61.5	12.0	4.57	19.4	7.84	8.99	135
4	21.3	8.0	4.38	19.6	7.36	17.9	112
	Avr	9.0	4.50	12.5	7.84	10.1	
	1s	2.0	0.2	8.1	0.4	5.7	

[a]With the exception of the weight of bacteria per unit weight of electrolyte, the trials in each subset are identical replicates. [b]Weight of bacteria per unit weight of electrolyte. [c]Capacitance of the bacterial surface (Farads/m^2). [d]Negative logarithm of the subscripted surface site, referenced to the ionic strength of the background electrolyte and zero surface charge. [e]Concentration of the subcripted surface site, in $x10^{-5}$ moles per gram of bacteria. [f]Variance as calculated by FITEQL. [g]Average values for all trials. [h]1s error corresponding to each average value.

TABLE 7: Statistical comparison of individual Basic Stern model parameters.

Comparison of *B. subtilis* model parameters at 0.1[a] and 0.01[b] M							
Parameter	Avr_1[c]	$1s_1$[d]	Avr_2[c]	$1s_2$[d]	f[e]	t[f]	C.I.[g]
C_1	8.0	0.0	6.7	2.7	6	0.481	< 40%
pK_1	4.22	0.2	4.01	0.1	6	0.939	< 80%
pK_2	7.61	0.4	7.73	0.3	6	-0.254	< 20%
$Conc_1$	15.6	3.1	16.2	1.7	6	0.419	< 40%
$Conc_2$	6.64	0.5	33.1	17	6	0.265	< 20%

Comparison of *B. licheniformis* model parameters at 0.1[a] and 0.01[b] M							
C_1	6.5	1.8	9.0	2.0	6	-0.929	< 80%
pK_1	4.78	0.2	4.50	0.2	6	0.990	< 80%
pK_2	7.86	0.4	7.84	0.4	6	0.035	< 20%
$Conc_1$	11.4	9.2	12.5	8.1	6	-0.090	< 20%
$Conc_2$	10.6	7.5	10.1	5.7	6	0.053	< 20%

Comparison of *B. subtilis*[a] and *B. licheniformis*[b] model parameters at 0.1 M							
C_1	8.0	0.0	6.5	1.8	6	0.833	< 60%
pK_1	4.22	0.2	4.78	0.2	6	-1.980	< 95%
pK_2	7.61	0.4	7.86	0.4	6	-0.442	< 40%
$Conc_1$	15.6	3.1	11.4	9.2	6	0.433	< 40%
$Conc_2$	6.64	0.5	10.6	7.5	6	-0.527	< 40%

Comparison of *B. subtilis*[a] and *B. licheniformis*[b] model parameters at 0.01 M							
C_1	6.7	2.7	9.0	2.0	6	-0.685	< 60%
pK_1	4.01	0.1	4.50	0.2	6	-2.191	< 95%
pK_2	7.73	0.3	7.84	0.4	6	-0.220	< 20%
$Conc_1$	16.2	1.7	12.5	8.1	6	0.447	< 40%
$Conc_2$	33.1	16.5	10.1	5.7	6	1.318	< 80%

[a]First and [b]second variable sets. [c]Average value and [d]1s error for each parameter in the subscripted variable set. [e]Degrees of freedom. [f]Value of the t distribution. [g]Upper confidence level at which the average values can be considered statistically different.

Figure 5. Comparison of Basic Stern model predictions and experimental data for two *B. subtilis* titrations. Model parameters were determined by fitting titration data for 0.1 M electrolyte; this model fails to match the 0.01 M titration data, when adjustments for ionic strength are made.

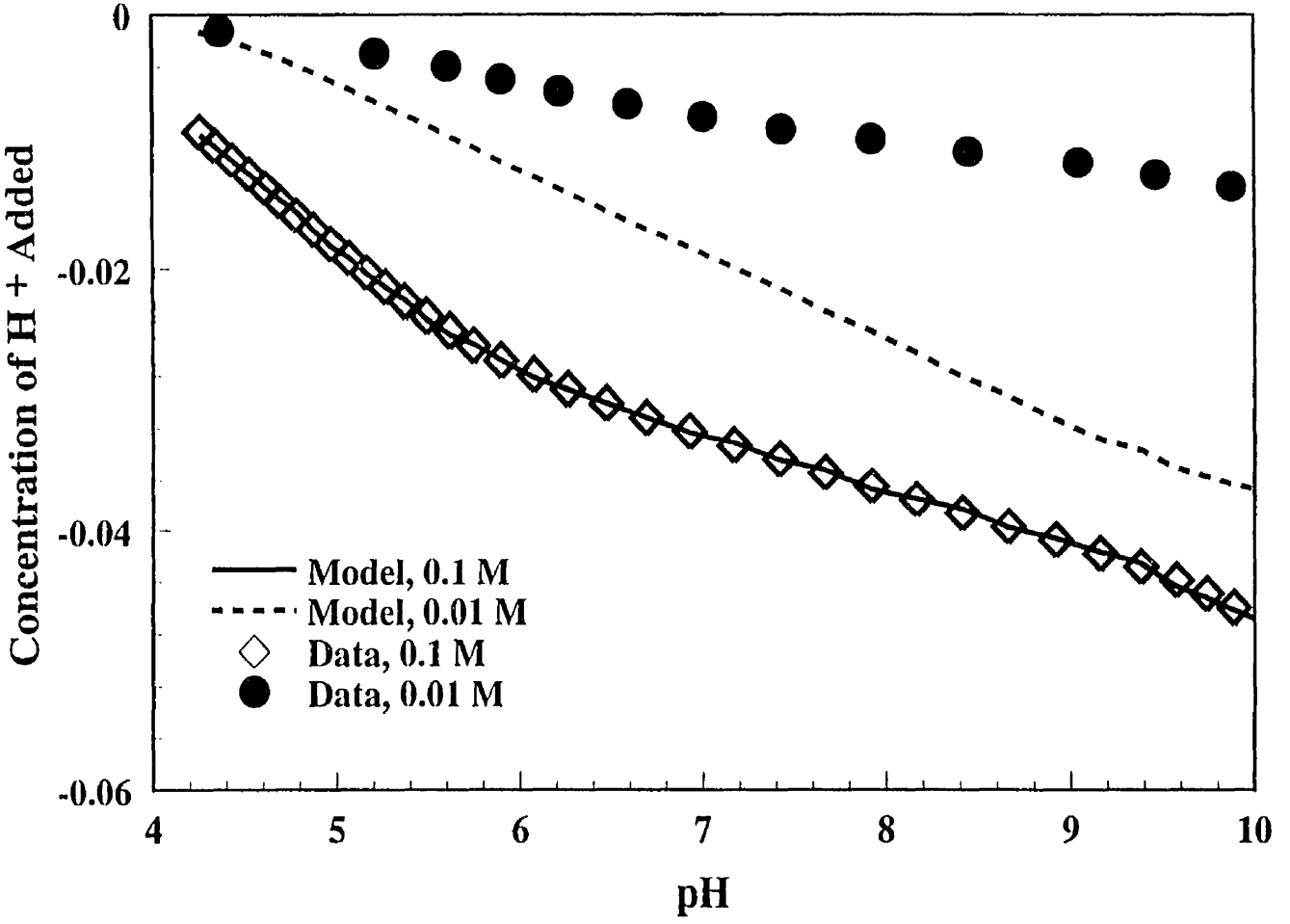
0
-0.02
-0.04
-0.06
Concentration of H + Added
4
5
6
7
8
9
10
pH
Model, 0.1 M
Model, 0.01 M
Data, 0.1 M
Data, 0.01 M

Figure 5

concentrations is also insignificant between the species and between the different ionic strengths. Although some parameters vary significantly between the different titrations, in general, parameter variation between the species and ionic strengths is insignificant, and in this regard, the two-site Basic Stern model is in agreement with the Constant Capacitance model.

We also attempt to use a single two-site Basic Stern model to simultaneously fit all four titrations of a given species at a particular ionic strength. The FITEQL results for these Net Basic Stern models are given in Table 8, and in Figure 3d they are compared to the *B. subtilis* experimental data collected at 0.01 M ionic strength. Again, the model variances are substantially larger when the titrations are modeled simultaneously, due to the variability in the concentrations of surface functional groups. However, the variation in the model parameters cannot be considered significant, and thus average values (Table 6) can be applied to predict acid-base behaviour of the two bacteria in the range of chemical conditions of this study. The Net Basic Stern model does not describe the experimental data as well as the Net Constant Capacitance model, as indicated by its slightly higher variances. However, because the variances are large in both cases, there is little statistical basis to choose between them.

Lastly, we attempt to use the two-site Basic Stern model to simultaneously describe all eight titrations for each species, including trials performed at different solid:solution ratios and both ionic strengths. Such a model fails to converge for the *B. subtilis* titration data, although it provides a slightly improved fit for the *B.*

TABLE 8. Summary of Net Basic Stern model parameters computed from simultaneous modeling of all titrations.

Sp.[a]	I[b]	C_1[c]	pK_1[d]	$Conc_1$[e]	pK_2	$Conc_2$	V(Y)[f]
B. sub.	0.1	8.0	4.22	14.5	7.61	7.37	563
	0.01	8.0	4.10	16.4	7.78	21.4	84.8
	All	no convergence[g]					
B. lich.	0.1	8.0	4.87	6.06	9.07	17.2	1650
	0.01	8.0	4.50	5.72	9.30	5.28	1772
	All	8.0	4.84	5.61	9.75	5.60	1582
Avr[h]	All	8.0	4.51	9.66	8.70	11.4	
$1s$[i]			0.4	5.3	1.0	7.4	

[a]Bacterial species. [b]Ionic strength of $NaNO_3$ electrolyte. 'All' refers to FITEQL model which considers both ionic strengths and all solid:solution ratios. [c]Negative logarithm of the subscripted surface site, referenced to the ionic strength of the background electrolyte and zero surface charge. [d]Concentration of the subcripted surface site, expressed in $x10^{-5}$ moles per gram of bacteria. [e]Capacitance for the bacterial surface (Farads/m^2). [g]Indicates severe misfit between the model and the experimental data. [h]Average values for all models. [i]$1s$ error corresponding to each average value.

licheniformis data. Because the applicability of this model is not adequate for both species, we favour the Net Constant Capacitance model.

Consideration of Errors. The relative 1*s* errors associated with the log deprotonation constants and site concentrations reported here are approximately ± 6% and ± 60%, respectively. These errors arise from three principal sources. First, we consider the analytical error associated with our method of titration. We have examined the accuracy of this experimental technique by reproducing the deprotonation constant and total concentration of functional groups in a sodium acetate system, to within 2% of the expected values (the literature pK_a value and initial acetate concentration, respectively). We conclude that the deprotonation constants and concentrations of the bacterial functional groups reported here carry maximum relative 1*s* errors of ± 2% due to analytical uncertainties.

Second, the variables required for the electric double layer models (surface area and mass of bacteria per unit weight of electrolyte) are difficult to quantify, and so give rise to errors in the model parameters. The BET and organic adsorption techniques commonly used to determine surface area cannot be applied to bacteria because both techniques markedly alter the cell wall. We determine the bacterial surface area from cell geometry. The cell surface area of these rod-shaped species is approximately equal to that of a right circular cylinder with spherical ends, of length 5.0 μm and radius 0.5 μm. There are approximately 4 x 10^9 cells per gram of bacteria (17). These values yield a bacterial surface area of approximately 140 m^2/g, although errors in the cell dimensions, surface roughness and quantity of cells per gram cause this estimate to vary over roughly one order

of magnitude. Changes in the model surface area values between 50 and 500 m^2/g cause the surface site concentrations to vary by approximately ± 5% and the deprotonation constants to change by roughly ± 1%. Additionally, the bacteria may multiply during the course of the experiments, giving rise to an error in the mass or surface area of bacteria per unit mass of suspension that we apply in our modeling. We have examined this possibility by separating and drying the bacteria in the suspension both prior to and following the titrations. We observe no increase in the weight of bacteria present, and thus we consider this error to be negligible. Lastly, the bacterial biomass per unit weight of electrolyte is determined by separating the bacteria from a known weight of electrolyte through centrifugation (6000 rpm for 60 minutes) and weighing the pellet produced. The centrifugation may not effectively remove all the electrolyte solution, or alternatively, fluids may be driven out of the cells, and so the weight of bacteria determined carries a 1s error of roughly ± 5%. This error in bacterial biomass, when propagated through the FITEQL models, causes errors in the log deprotonation constants and site concentrations of ± 2% and ± 5%, respectively. Thus the surface site concentrations determined here carry 1s errors of ± 10% due to inaccuracies in the values of bacterial mass and surface area applied in the modeling, whereas the log deprotonation constants carry errors of ± 4%.

Third, the accuracy of the models developed here depends upon the extent of cell wall variation between cultures. As described above, the cell wall characteristics of independently grown cultures of *B. subtilis* and *B. licheniformis* appear to vary substantially. Cell wall variation seems to cause little variation in

the log deprotonation constants (± 2%), but is likely responsible for the majority of the error (± 45 - 50%) in the surface site concentrations. Variations in the surface site concentrations are large and essentially random, and they are the greatest limitation to the development of a single predictive model to describe the acid-base behaviour of these bacterial surfaces.

Summary and Choice of Model. A comparison of the variances listed in Tables 2 and 6 indicates that the three-site Constant Capacitance model provides a better description of acid-base behaviour than the two-site Basic Stern model, when the titrations are modeled independently. Further, the addition of the third surface site in the Constant Capacitance model is justified by experimental studies which indicate that the cell walls of these bacteria display carboxyl, phosphate and hydroxyl functional groups (13). Thus we favour the Constant Capacitance model over the Basic Stern model where the titrations are modeled individually.

The experimental data are better described if the titrations are modeled individually than if several titrations are modeled simultaneously, but because the optimizable parameters of individual titrations vary substantially, an average set of parameter values is better used to predict the acid-base behaviour of the bacterial suspensions. A comparison of the variances listed in Tables 2, 4, 6, and 8 shows that simultaneous modeling of several titrations yields a set of parameters that closely agrees with the averages of the parameters determined when the titrations are modeled individually. Further, the Net Constant Capacitance models describe the experimental data slightly better than the Net Basic Stern models. It has also been shown above that the deprotonation constants are species-specific.

Therefore, we choose to model acid-base behaviour using the four parameter sets given in Table 4, one set corresponding to each bacteria in each electrolyte, rather than applying average parameter values.

METAL ADSORPTION RESULTS AND DISCUSSION

The results of the Cd^{2+}, Pb^{2+} and Cu^{2+} adsorption experiments are displayed in Figures 6 to 8, respectively. All of the adsorption experiments were performed below saturation with respect to any solid metal phase, and so any change in the aqueous metal concentration observed during the course of the experiment is attributed entirely to adsorption onto the cell wall. It is evident that the bacterial cell walls display a strong affinity for the metals used in this study, with the extent of metal adsorption increasing with increasing pH. Further, the proportion of metal adsorbed at a particular pH increases as the ratio between the total concentration of bacterial surface functional groups and the total metal concentration (bacteria:metal ratio) increases. These results are in excellent agreement with those of Fein et al. (17) and Daughney et al. (18). It is also apparent that the position of the metal-*B. subtilis* adsorption edges are shifted to lower pH values when the ionic strength is decreased. In contrast, the metal-*B. licheniformis* adsorption edges are shifted to higher pH values when the ionic strength is decreased.

For each metal-bacteria system, we use FITEQL to solve for site-specific stability constants describing metal adsorption onto the bacterial cell walls (Tables

Figure 6. Percent adsorption of Cd^{2+} onto *B. subtilis* and *B. licheniformis* in 0.1 M $NaNO_3$ (black symbols) and 0.01 M $NaNO_3$ (grey symbols). Experiments are performed with two, independently grown bacterial cultures. Experimental solutions contain 10 ppm Cd.

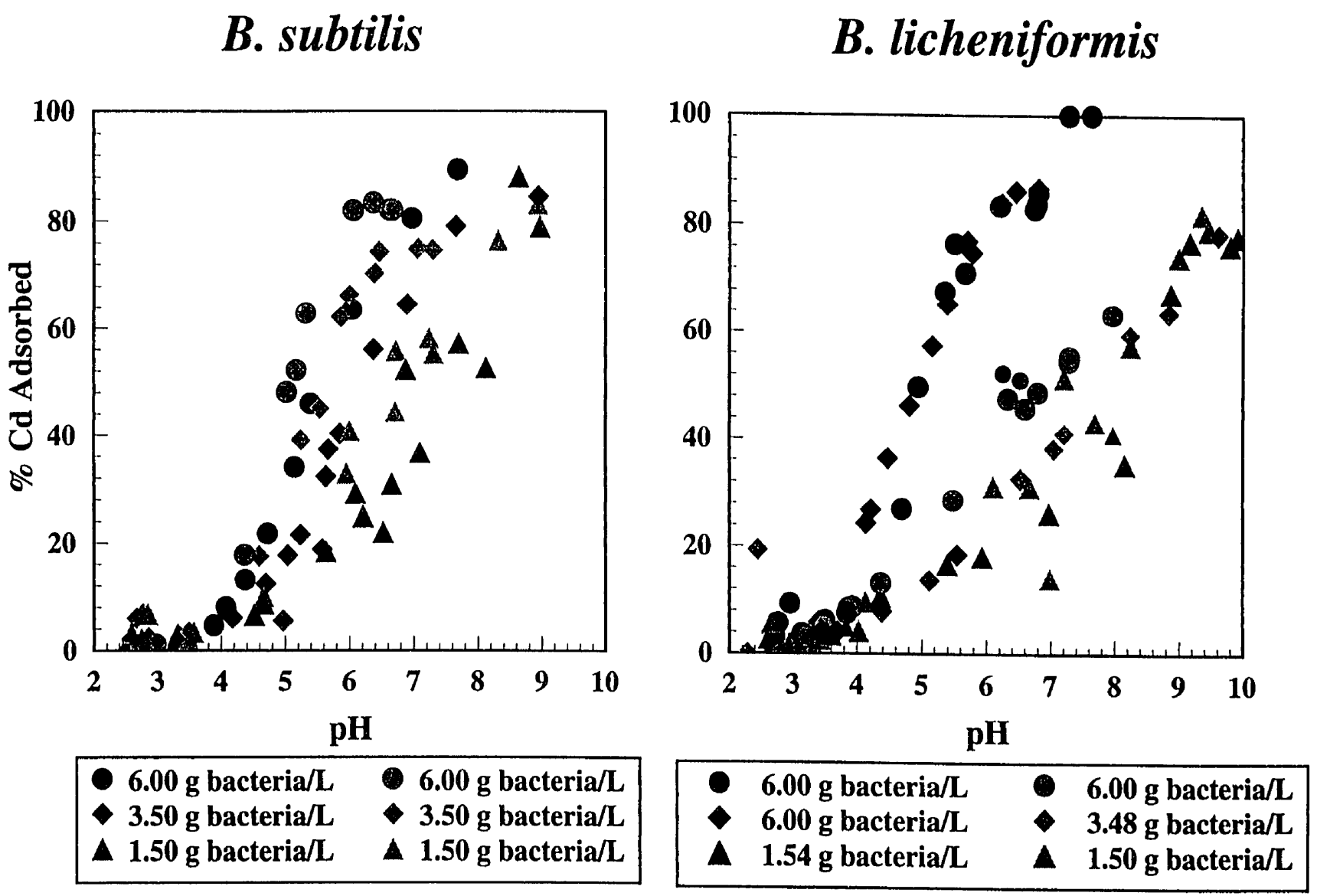
B. subtilis
B. licheniformis
% Cd Adsorbed
pH
pH
100
80
60
40
20
0
2
3
4
5
6
7
8
9
10
6.00 g bacteria/L
3.50 g bacteria/L
1.50 g bacteria/L
6.00 g bacteria/L
3.50 g bacteria/L
1.50 g bacteria/L
6.00 g bacteria/L
6.00 g bacteria/L
1.54 g bacteria/L
3.48 g bacteria/L
1.50 g bacteria/L

Figure 6

Figure 7. Percent adsorption of Pb^{2+} onto *B. subtilis* and *B. licheniformis* in 0.1 M $NaNO_3$ (black symbols) and 0.01 M $NaNO_3$ (grey symbols). Experiments are performed with two, independently grown bacterial cultures. Experimental solutions contain 10 ppm Pb unless otherwise noted.

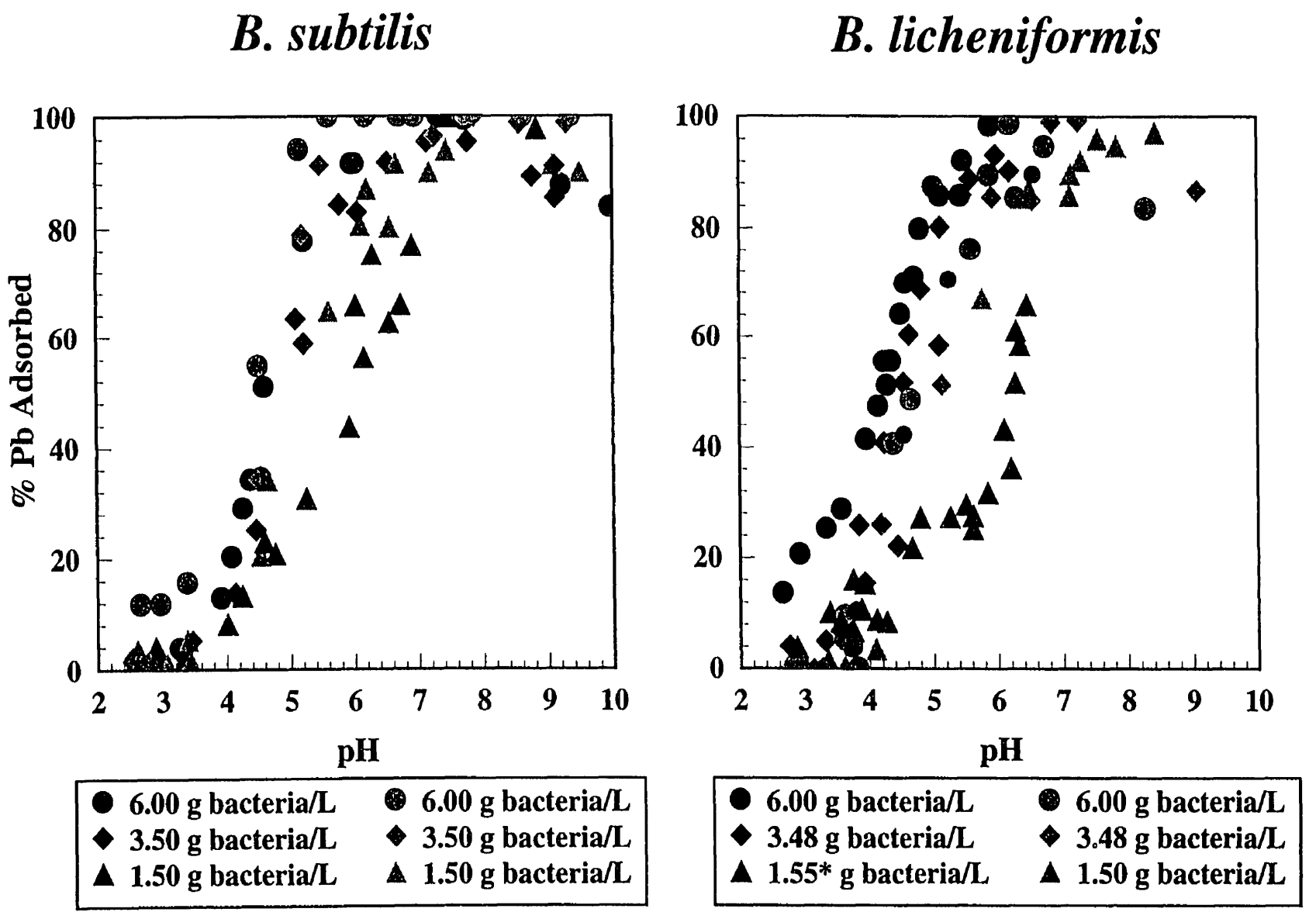
B. subtilis
B. licheniformis
% Pb Adsorbed
100
80
60
40
20
0
2
3
4
5
6
7
8
9
10
pH
6.00 g bacteria/L
3.50 g bacteria/L
1.50 g bacteria/L
6.00 g bacteria/L
3.50 g bacteria/L
1.50 g bacteria/L
6.00 g bacteria/L
3.48 g bacteria/L
1.55* g bacteria/L
6.00 g bacteria/L
3.48 g bacteria/L
1.50 g bacteria/L
* Total Pb = 35 ppm

Figure 7

Figure 8. Percent adsorption of Cu^{2+} onto *B. subtilis* and *B. licheniformis* in 0.1 M $NaNO_3$ (black symbols) and 0.01 M $NaNO_3$ (grey symbols). Experiments are performed with two, independently grown bacterial cultures. Experimental solutions contain 10 ppm Cu unless otherwise noted.

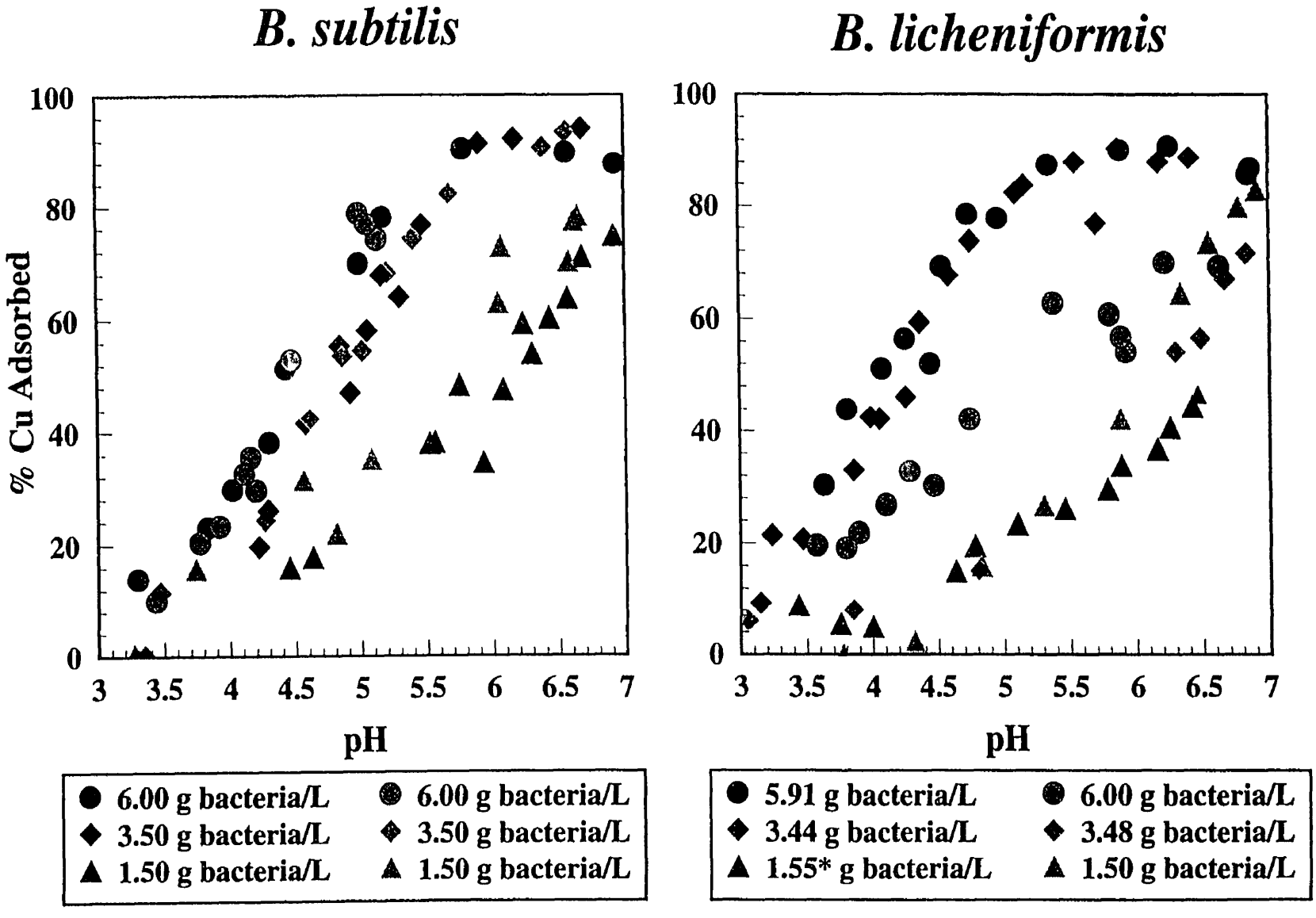
B. subtilis
B. licheniformis
% Cu Adsorbed
100
80
60
40
20
0
3
3.5
4
4.5
5
5.5
6
6.5
7
pH
6.00 g bacteria/L
3.50 g bacteria/L
1.50 g bacteria/L
6.00 g bacteria/L
3.50 g bacteria/L
1.50 g bacteria/L
5.91 g bacteria/L
3.44 g bacteria/L
1.55* g bacteria/L
6.00 g bacteria/L
3.48 g bacteria/L
1.50 g bacteria/L
* Total Cu = 15 ppm

Figure 8

9 - 11). We attempt to fit the experimental data by invoking models involving metal adsorption onto one, two or three distinct types of surface functional groups. Models considering adsorption onto three distinct surface sites generally fail to converge, suggesting that the inclusion of the third equilibrium does not improve the goodness of fit, and therefore such models are not tabulated here. We consider only the 1:1 stoichiometry for the adsorbed metal surface complex, after Fein et al. (17) and Daughney et al. (18). Equilibria describing metal hydrolysis are included in our models, with stability constants taken from Baes and Mesmer (40). In our FITEQL modeling, we use the Net Constant Capacitance model parameters given in Table 4, applying a separate parameter set for each bacterial species at each ionic strength. For each metal, we first model the experimental data for the suspensions of 1.5, 3.5 and 6.0 g bacteria/L independently. Subsequently we model the experimental data for all three bacteria:solution ratios simultaneously, in order to determine a single set of stability constants describing metal adsorption in systems of different bacteria:solution ratios. The metal adsorption stability constants reported here are referenced to zero surface charge, zero surface coverage, and the ionic strength of the background electrolyte.

One-Site Metal Adsorption Models. We first describe the experimental data by considering metal adsorption onto only one type of surface functional group. It is important to note that the fit of any given model depends upon three mathematical and logistical constraints, over and above its relationship to the chemical processes that it attempts to describe. As a result, the fit of any one-site model is variable, as indicated by the range of variances listed in Tables 9 - 11.

TABLE 9a. Adsorption of Cd^{2+} by *B. subtilis* as modeled by FITEQL, treating each bacteria:metal ratio independently

Cd^{2+}-*B. subtilis* Adsorption, 0.1 M $NaNO_3$									
	6.0 g bacteria/L, 10 ppm Cd[a]			3.5 g bacteria/L, 10 ppm Cd[a]			1.5 g bacteria/L, 10 ppm Cd[a]		
Model[b]	Log K_1[c]	Log K_2[d]	V(Y)[e]	Log K_1[c]	Log K_2[d]	V(Y)[e]	Log K_1[c]	Log K_2[d]	V(Y)[e]
C	3.05	—	26.6	3.08	—	39.7	3.54	—	76.9
P	4.67	—	9.5	4.39	—	12.0	4.43	—	27.7
H	7.21	—	11.9	6.89	—	20.9	6.66	—	23.2
C + P	2.78	4.09	0.6	2.69	4.02	1.5	2.34	4.36	29.7
C + H	2.84	6.38	2.23	2.81	6.21	4.0	3.07	5.85	14.6
P + H	no convergence[f]			no convergence[f]			no convergence[f]		

Cd^{2+}-*B. subtilis* Adsorption, 0.01 M $NaNO_3$									
	6.0 g bacteria/L, 10 ppm Cd[a]			3.5 g bacteria/L, 10 ppm Cd[a]			1.5 g bacteria/L, 10 ppm Cd[a]		
Model[b]	Log K_1[c]	Log K_2[d]	V(Y)[e]	Log K_1[c]	Log K_2[d]	V(Y)[e]	Log K_1[c]	Log K_2[d]	V(Y)[e]
C	2.97	—	4.1	2.95	—	39.7	3.18	—	18.1
P	3.42	—	10.7	3.11	—	12.0	2.90	—	17.8
H	6.56	—	14.2	6.17	—	20.9	5.29	—	76.2
C + P	no convergence[f]			no convergence[f]			2.91	2.28	14.6
C + H	no convergence[f]			no convergence[f]			3.06	3.50	7.9
P + H	no convergence[f]			no convergence[f]			2.84	3.27	15.6

[a]Composition of experimental solutions, indicating mass of bacteria per unit weight of electrolyte and total concentration of metal. [b]Models consider adsorption onto one or two distinct types of surface functional groups. C = carboxyl site; P = phosphate site, H = hydroxyl site. [c]Log K value for metal adsorption onto the first type of surface site included in the model column, referenced to the condition of zero surface charge, zero surface coverage and the ionic strength of the background electrolyte. [d]Log K value for metal adsorption onto the second type of surface site considered in the model column. [e]Variance as calculated by FITEQL. [f]Indicates severe misfit between the model and the experimental data.

TABLE 9b. Adsorption of Cd^{2+} by *B. licheniformis* as modeled by FITEQL, treating each bacteria:metal ratio independently

Cd^{2+}-*B. licheniformis* Adsorption, 0.1 M $NaNO_3$									
	6.0 g bacteria/L, 10 ppm Cd[a]			3.5 g bacteria/L, 10 ppm Cd[a]			1.5 g bacteria/L, 10 ppm Cd[a]		
Model[b]	Log K_1[c]	Log K_2[d]	V(Y)[e]	Log K_1[c]	Log K_2[d]	V(Y)[e]	Log K_1[c]	Log K_2[d]	V(Y)[e]
C	4.00	—	26.6	3.98	—	6.4	4.25	—	131
P	6.39	—	11.7	6.59	—	8.7	5.92	—	155
H	8.07	—	13.0	8.31	—	14.9	5.37	—	51.7
C + P	3.62	5.79	10.7	3.86	5.48	1.2	no convergence[f]		
C + H	3.73	7.29	11.6	3.88	7.16	1.3	3.58	5.09	5.6
P + H	no convergence[f]			no convergence[f]			5.63	4.73	18.6

Cd^{2+}-*B. licheniformis* Adsorption, 0.01 M $NaNO_3$									
	6.0 g bacteria/L, 10 ppm Cd[a]			3.5 g bacteria/L, 10 ppm Cd[a]			1.5 g bacteria/L, 10 ppm Cd[a]		
Model[b]	Log K_1[c]	Log K_2[d]	V(Y)[e]	Log K_1[c]	Log K_2[d]	V(Y)[e]	Log K_1[c]	Log K_2[d]	V(Y)[e]
C	3.49	—	7.1	3.71	—	56.2	4.37	—	100
P	4.43	—	47.4	4.45	—	30.6	5.42	—	100
H	6.71	—	71.2	6.41	—	63.3	6.56	—	78.4
C + P	3.39	3.50	4.8	3.10	4.20	26.5	no convergence[f]		
C + H	3.43	5.31	5.0	3.49	4.97	24.3	3.98	5.69	28.2
P + H	no convergence[f]			4.37	4.24	28.3	5.04	5.39	43.0

[a]Composition of experimental solutions, indicating mass of bacteria per unit weight of electrolyte and total concentration of metal. [b]Models consider adsorption onto one or two distinct types of surface functional groups. C = carboxyl site; P = phosphate site, H = hydroxyl site. [c]Log K value for metal adsorption onto the first type of surface site included in the model column, referenced to the condition of zero surface charge, zero surface coverage and the ionic strength of the background electrolyte. [d]Log K value for metal adsorption onto the second type of surface site considered in the model column. [e]Variance as calculated by FITEQL. [f]Indicates severe misfit between the model and the experimental data.

TABLE 9c. Adsorption of Cd^{2+} by *B. subtilis* and *B. licheniformis* as modeled by FITEQL, with all bacteria:metal ratios modeled simultaneously

Cd^{2+}-*B. subtilis* Adsorption						
	0.1 M $NaNO_3$			0.01 M $NaNO_3$		
Model[a]	Log K_1[b]	Log K_2[c]	V(Y)[d]	Log K_1	Log K_2	V(Y)
C	3.19	—	68.7	3.02	—	12.1
P	4.48	—	18.2	3.44	—	25.4
H	6.95	—	23.6	6.16	—	65.6
C + P	2.67	4.19	11.1	2.93	2.39	9.9
C + H	2.86	6.16	7.0	2.98	3.54	7.3
P + H	4.44	4.45	16.3	3.43	2.65	26.1

Cd^{2+}-*B. licheniformis* Adsorption						
	0.1 M $NaNO_3$			0.01 M $NaNO_3$		
Model	Log K_1	Log K_2	V(Y)	Log K_1	Log K_2	V(Y)
C	4.06	—	54.4	3.75	—	83.7
P	6.48	—	56.2	4.64	—	72.5
H	7.98	—	68.1	6.56	—	69.4
C + P	3.87	5.06	28.1	3.36	4.24	54.9
C + H	3.94	5.02	16.0	3.49	2.26	29.2
P + H	6.47	4.72	16.1	4.49	5.28	49.0

[a]Models consider adsorption onto one or two distinct types of surface functional groups. C = carboxyl site; P = phosphate site, H = hydroxyl site. [b]Log K value for metal adsorption onto the first type of surface site included in the model column, referenced to the condition of zero surface charge, zero surface coverage and the ionic strength of the background electrolyte. [c]Log K value for metal adsorption onto the second type of surface site considered in the model column. [d]Variance as calculated by FITEQL.

TABLE 10a. Adsorption of Pb^{2+} by *B. subtilis* as modeled by FITEQL, treating each bacteria:metal ratio independently

Pb^{2+}-*B. subtilis* Adsorption, 0.1 M $NaNO_3$									
	6.0 g bacteria/L, 10 ppm Pb[a]			3.5 g bacteria/L, 10 ppm Pb[a]			1.5 g bacteria/L, 35 ppm Pb[a]		
Model[b]	Log K_1[c]	Log K_2[d]	V(Y)[e]	Log K_1[c]	Log K_2[d]	V(Y)[e]	Log K_1[c]	Log K_2[d]	V(Y)[e]
C	3.48	—	10.8	4.03	—	58.3	3.93	—	149
P	5.44	—	10.7	5.55	—	0.6	5.75	—	119
H	7.98	—	1.1	8.04	—	2.2	8.37	—	204
C + P	2.69	5.33	1.1	2.76	5.41	0.6	no convergence[f]		
C + H	2.74	7.85	1.1	2.96	7.88	2.3	no convergence[f]		
P + H	no convergence[f]			no convergence[f]			4.58	8.14	37.9

Pb^{2+}-*B. subtilis* Adsorption, 0.01 M $NaNO_3$									
	6.0 g bacteria/L, 10 ppm Pb[a]			3.5 g bacteria/L, 10 ppm Pb[a]			1.5 g bacteria/L, 10 ppm Pb[a]		
Model[b]	Log K_1[c]	Log K_2[d]	V(Y)[e]	Log K_1[c]	Log K_2[d]	V(Y)[e]	Log K_1[c]	Log K_2[d]	V(Y)[e]
C	3.79	—	3.7	3.66	—	4.6	4.02	—	16.5
P	4.41	—	4.5	4.13	—	0.3	4.11	—	5.1
H	7.58	—	4.7	7.28	—	0.2	6.96	—	5.8
C + P	no convergence[f]			no convergence[f]			no convergence[f]		
C + H	no convergence[f]			2.49	3.43	0.3	no convergence[f]		
P + H	no convergence[f]			no convergence[f]			3.93	4.73	2.8

[a]Composition of experimental solutions, indicating mass of bacteria per unit weight of electrolyte and total concentration of metal. [b]Models consider adsorption onto one or two distinct types of surface functional groups. C = carboxyl site; P = phosphate site, H = hydroxyl site. [c]Log K value for metal adsorption onto the first type of surface site included in the model column, referenced to the condition of zero surface charge, zero surface coverage and the ionic strength of the background electrolyte. [d]Log K value for metal adsorption onto the second type of surface site considered in the model column. [e]Variance as calculated by FITEQL. [f]Indicates severe misfit between the model and the experimental data.

TABLE 10b. Adsorption of Pb^{2+} by *B. licheniformis* as modeled by FITEQL, treating each bacteria:metal ratio independently

Pb^{2+}-*B. licheniformis* Adsorption, 0.1 M $NaNO_3$									
	6.0 g bacteria/L, 10 ppm Pb[a]			3.5 g bacteria/L, 10 ppm Pb[a]			1.5 g bacteria/L, 35 ppm Pb[a]		
Model[b]	Log K_1[c]	Log K_2[d]	V(Y)[e]	Log K_1[c]	Log K_2[d]	V(Y)[e]	Log K_1[c]	Log K_2[d]	V(Y)[e]
C	4.48	—	5.4	4.46	—	5.3	4.54	—	124
P	7.27	—	6.1	7.21	—	2.3	7.43	—	267
H	9.01	—	7.4	8.91	—	2.4	8.07	—	103
C + P	no convergence[f]			no convergence[f]			no convergence[f]		
C + H	no convergence[f]			4.06	8.60	2.3	4.24	7.36	46.5
P + H	no convergence[f]			no convergence[f]			7.34	7.40	38.0

Pb^{2+}-*B. licheniformis* Adsorption, 0.01 M $NaNO_3$									
	6.0 g bacteria/L, 10 ppm Pb[a]			3.5 g bacteria/L, 10 ppm Pb[a]			1.5 g bacteria/L, 10 ppm Pb[a]		
Model[b]	Log K_1[c]	Log K_2[d]	V(Y)[e]	Log K_1[c]	Log K_2[d]	V(Y)[e]	Log K_1[c]	Log K_2[d]	V(Y)[e]
C	4.11	—	24.9	4.71	—	48.9	4.83	—	48.8
P	6.32	—	20.9	6.25	—	0.7	6.79	—	6.5
H	8.76	—	21.1	8.59	—	1.7	8.58	—	1.1
C + P	4.04	4.57	23.0	2.12	6.24	0.8	no convergence[f]		
C + H	3.87	8.05	22.4	3.69	8.35	1.7	3.30	8.54	1.2
P + H	no convergence[f]			6.24	5.63	0.8	6.37	7.77	0.9

[a]Composition of experimental solutions, indicating mass of bacteria per unit weight of electrolyte and total concentration of metal. [b]Models consider adsorption onto one or two distinct types of surface functional groups. C = carboxyl site; P = phosphate site, H = hydroxyl site. [c]Log K value for metal adsorption onto the first type of surface site included in the model column, referenced to the condition of zero surface charge, zero surface coverage and the ionic strength of the background electrolyte. [d]Log K value for metal adsorption onto the second type of surface site considered in the model column. [e]Variance as calculated by FITEQL. [f]Indicates severe misfit between the model and the experimental data.

TABLE 10c. Adsorption of Pb^{2+} by *B. subtilis* and *B. licheniformis* as modeled by FITEQL, with all bacteria:metal ratios modeled simultaneously

Pb^{2+}-*B. subtilis* Adsorption						
	0.1 M $NaNO_3$			0.01 M $NaNO_3$		
Model[a]	Log K_1[b]	Log K_2[c]	V(Y)[d]	Log K_1	Log K_2	V(Y)
C	3.86	—	82.3	3.85	—	9.3
P	5.60	—	43.0	4.48	—	3.5
H	8.14	—	72.8	7.31	—	4.3
C + P	3.41	5.06	23.2	3.00	4.36	3.6
C + H	3.56	7.22	22.8	3.61	6.07	2.8
P + H	5.50	6.71	10.0	4.45	4.64	3.2

Pb^{2+}-*B. licheniformis* Adsorption						
	0.1 M $NaNO_3$			0.01 M $NaNO_3$		
Model	Log K_1	Log K_2	V(Y)	Log K_1	Log K_2	V(Y)
C	4.53	—	56.7	4.62	—	62.0
P	7.32	—	120	6.42	—	11.5
H	8.45	—	81.6	8.69	—	8.6
C + P	4.40	5.67	33.6	3.41	6.32	11.3
C + H	4.36	4.74	22.9	3.67	8.42	8.3
P + H	no convergence[e]			6.25	7.78	8.4

[a]Models consider adsorption onto one or two distinct types of surface functional groups. C = carboxyl site; P = phosphate site, H = hydroxyl site. [b]Log K value for metal adsorption onto the first type of surface site included in the model column, referenced to the condition of zero surface charge, zero surface coverage and the ionic strength of the background electrolyte. [c]Log K value for metal adsorption onto the second type of surface site considered in the model column. [d]Variance as calculated by FITEQL. [e]Indicates severe misfit between the model and the experimental data.

TABLE 11a. Adsorption of Cu^{2+} by *B. subtilis* as modeled by FITEQL, treating each bacteria:metal ratio independently

Cu^{2+}-*B. subtilis* Adsorption, 0.1 M $NaNO_3$									
	6.0 g bacteria/L, 10 ppm Cu[a]			3.5 g bacteria/L, 10 ppm Cu[a]			1.5 g bacteria/L, 10 ppm Cu[a]		
Model[b]	Log K_1[c]	Log K_2[d]	V(Y)[e]	Log K_1[c]	Log K_2[d]	V(Y)[e]	Log K_1[c]	Log K_2[d]	V(Y)[e]
C	3.73	—	21.2	3.80	—	75.1	4.00	—	115
P	5.82	—	24.6	5.71	—	10.8	5.68	—	86.2
H	8.38	—	22.9	8.33	—	18.9	8.36	—	178
C + P	3.67	4.53	19.4	no convergence[f]			no convergence[f]		
C + H	3.68	6.88	20.1	no convergence[f]			no convergence[f]		
P + H	no convergence[f]			5.54	7.40	9.5	5.34	6.51	26.2

Cu^{2+}-*B. subtilis* Adsorption, 0.01 M $NaNO_3$									
	6.0 g bacteria/L, 10 ppm Cu[a]			3.5 g bacteria/L, 10 ppm Cu[a]			1.5 g bacteria/L, 10 ppm Cu[a]		
Model[b]	Log K_1[c]	Log K_2[d]	V(Y)[e]	Log K_1[c]	Log K_2[d]	V(Y)[e]	Log K_1[c]	Log K_2[d]	V(Y)[e]
C	3.67	—	21.8	3.95	—	44.3	4.22	—	323
P	4.61	—	11.3	4.51	—	12.7	4.22	—	108
H	7.49	—	14.5	7.31	—	21.5	7.05	—	129
C + P	3.37	4.21	8.3	3.47	4.15	7.6	no convergence[f]		
C + H	3.42	7.02	8.3	3.57	6.88	8.4	3.62	6.48	115
P + H	no convergence[f]			no convergence[f]			4.07	5.98	101

[a]Composition of experimental solutions, indicating mass of bacteria per unit weight of electrolyte and total concentration of metal. [b]Models consider adsorption onto one or two distinct types of surface functional groups. C = carboxyl site; P = phosphate site, H = hydroxyl site. [c]Log K value for metal adsorption onto the first type of surface site included in the model column, referenced to the condition of zero surface charge, zero surface coverage and the ionic strength of the background electrolyte. [d]Log K value for metal adsorption onto the second type of surface site considered in the model column. [e]Variance as calculated by FITEQL. [f]Indicates severe misfit between the model and the experimental data.

TABLE 11b. Adsorption of Cu^{2+} by *B. licheniformis* as modeled by FITEQL, treating each bacteria:metal ratio independently

Cu^{2+}-*B. licheniformis* Adsorption, 0.1 M $NaNO_3$									
	6.0 g bacteria/L, 10 ppm Cu[a]			3.5 g bacteria/L, 10 ppm Cu[a]			1.5 g bacteria/L, 15 ppm Cu[a]		
Model[b]	Log K_1[c]	Log K_2[d]	V(Y)[e]	Log K_1[c]	Log K_2[d]	V(Y)[e]	Log K_1[c]	Log K_2[d]	V(Y)[e]
C	4.68	—	18.4	4.93	—	33.6	4.54	—	133
P	7.71	—	19.8	8.02	—	307	7.43	—	411
H	9.18	—	36.8	9.37	—	18.9	8.19	—	76.3
C + P	no convergence[f]			no convergence[f]			no convergence[f]		
C + H	no convergence[f]			4.79	8.42	13.5	4.18	7.37	18.5
P + H	7.71	5.58	21.0	7.67	8.74	15.8	no convergence[f]		

Cu^{2+}-*B. licheniformis* Adsorption, 0.01 M $NaNO_3$									
	6.0 g bacteria/L, 10 ppm Cu[a]			3.5 g bacteria/L, 10 ppm Cu[a]			1.5 g bacteria/L, 10 ppm Cu[a]		
Model[b]	Log K_1[c]	Log K_2[d]	V(Y)[e]	Log K_1[c]	Log K_2[d]	V(Y)[e]	Log K_1[c]	Log K_2[d]	V(Y)[e]
C	4.15	—	23.8	4.90	—	390	3.05	—	14.1
P	6.46	—	139	6.84	—	91.2	4.20	—	6.8
H	8.87	—	150	7.36	—	47.3	6.36	—	3.4
C + P	4.12	3.72	24.1	3.06	6.81	97.8	no convergence[f]		
C + H	4.13	5.82	24.4	4.11	7.02	14.1	no convergence[f]		
P + H	no convergence[f]			6.50	6.49	18.7	no convergence[f]		

[a]Composition of experimental solutions, indicating mass of bacteria per unit weight of electrolyte and total concentration of metal. [b]Models consider adsorption onto one or two distinct types of surface functional groups. C = carboxyl site; P = phosphate site, H = hydroxyl site. [c]Log K value for metal adsorption onto the first type of surface site included in the model column, referenced to the condition of zero surface charge, zero surface coverage and the ionic strength of the background electrolyte. [d]Log K value for metal adsorption onto the second type of surface site considered in the model column. [e]Variance as calculated by FITEQL. [f]Indicates severe misfit between the model and the experimental data.

TABLE 11c. Adsorption of Cu^{2+} by *B. subtilis* and *B. licheniformis* as modeled by FITEQL, with all bacteria:metal ratios modeled simultaneously

Cu^{2+}-*B. subtilis* Adsorption						
	0.1 M $NaNO_3$			0.01 M $NaNO_3$		
Model[a]	log K_1[b]	Log K_2[c]	V(Y)[d]	log K_1	Log K_2	V(Y)
C	3.83	—	76.0	3.84	—	145
P	5.75	—	39.5	4.56	—	42.2
H	8.35	—	69.5	7.35	—	61.2
C + P	3.55	4.94	28.8	3.20	4.36	42.0
C + H	3.59	7.34	28.1	5.01	6.68	41.6
P + H	4.25	8.30	23.5	4.53	5.79	40.0

Cu^{2+}-*B. licheniformis* Adsorption						
	0.1 M $NaNO_3$			0.01 M $NaNO_3$		
Model	log K_1	Log K_2	V(Y)	log K_1	Log K_2	V(Y)
C	4.82	—	69.2	4.30	—	224
P	7.06	—	240	6.40	—	146
H	9.05	—	128	8.69	—	164
C + P	4.73	5.70	47.8	3.93	5.51	138
C + H	4.75	7.19	45.0	6.31	6.89	51.9
P + H	no convergence[e]			9.70	6.47	120

[a]Models consider adsorption onto one or two distinct types of surface functional groups. C = carboxyl site; P = phosphate site, H = hydroxyl site. [b]log K value for metal adsorption onto the first type of surface site included in the model column, referenced to the condition of zero surface charge, zero surface coverage and the ionic strength of the background electrolyte. [c]Log K value for metal adsorption onto the second type of surface site considered in the model column. [d]Variance as calculated by FITEQL. [e]Indicates severe misfit between the model and the experimental data.

First, the fit of these models is largely controlled by the concentration of bacteria present. Where the concentration of bacteria is highest, the adsorption edge is steep, and a one-site model can provide a good fit to the experimental data. In contrast, where the bacterial concentration is low, the metal can saturate one type of surface site, with excess metal available to adsorb onto the next surface site which deprotonates. Under these conditions, adsorption occurs over a pH range in which two types of surface functional groups actively deprotonate, and the metal adsorption edge is less steep. In such cases, the one-site models fit the data poorly. Because of this, where the data for all bacteria concentrations are considered simultaneously, the one-site models often indicate a relatively poor fit to the data (the variance and best-fit stability constant for these models are essentially averages of the values determined when the different bacteria concentrations are modeled independently). Therefore, the appropriateness of any one-site model is best evaluated by considering its fit to the data for the highest bacteria concentration, before considering its fit to the data for all bacteria concentrations modeled simultaneously.

Second, the fit of any one-site model is controlled by the position of the metal adsorption edge as a function of pH. For example, the 0.1 M Cd^{2+}-*B. subtilis* adsorption edge occurs over a pH range where the phosphate surface sites are significantly deprotonated, and thus a model considering Cd^{2+} adsorption onto the phosphate sites fits the data well. By contrast, the 0.01 M Cd^{2+}-*B.subtilis* adsorption edge occurs at a slightly lower pH, and so the experimental data are better described by adsorption onto the carboxyl surface sites. For similar

reasons, Cd^{2+} adsorption onto *B. licheniformis* in the 0.1 M electrolyte can be modeled by adsorption onto the phosphate sites, but because a decrease in ionic strength causes the adsorption edge to shift up with respect to pH, the 0.01 M Cd^{2+}-*B. licheniformis* data are better described by adsorption onto the hydroxyl sites.

Third, it is also important to note that the two species of bacteria have different deprotonation constants for each type of surface functional group. The phosphate sites on *B. subtilis* begin to deprotonate at a lower pH than those on *B. licheniformis*, and as a result, metal-phosphate adsorption models will only fit the *B. licheniformis* data if the metal adsorption edge occurs over a pH of approximately 5.5 - 6.5. With the above discussion in mind, it is possible to compare the appropriateness of the various one-site models.

The one-site models invoking metal adsorption onto either the carboxyl or the phosphate surface sites fit the experimental data equally well. However, research indicates that Cu^{2+} and other hard metal cations (Na^{+}, Mg^{2+}, Mn^{2+}, Fe^{3+}) are preferentially bound to carboxyl sites on the cell walls of both *B. subtilis* and *B. licheniformis* (13, 41, 42). Further, it is known that metal ions display a similar affinity series for a given group of ligands regardless of whether the ligands exist as surface functional groups or as aqueous species (25). For the systems examined here, the magnitudes of the metal adsorption constants indicate that Cd^{2+} has the lowest affinity for the bacterial surface, while Pb^{2+} and Cu^{2+} have greater but roughly equal affinities for the bacterial surface. This same affinity series also describes the complexation of Cd^{2+}, Pb^{2+} and Cu^{2+} by aqueous

carboxylate anions (36). This agreement between the affinity series for metal-bacteria adsorption and metal-carboxylate complexation suggests that metal-bacteria adsorption involves carboxyl surface functional groups. An examination of the adsorption data (Figures 6 to 8) indicates that adsorption is generally initiated well below the pH at which the phosphate sites are significantly deprotonated. Therefore, it is most likely that metal-carboxyl interactions are responsible for the observed adsorption behaviour. Note that the association of an adsorbed metal ion with a particular type of functional group has not been directly observed in this study, but rather inferred from the experimental data. Confirmation of the model selected here requires direct observation of the adsorbed metals.

Two-Site Metal Adsorption Models. Although some of the experimental data can be described by models considering adsorption onto only the carboxyl surface sites, for the majority of metal-bacteria systems examined here, a better fit to the data is obtained by a model which considers metal adsorption onto two types of surface functional groups (Tables 9 - 11). Note that the improved fit may be the result of the addition of an additional optimizable parameter to the model. Two types of two-site models provide close fits to the experimental data, the first considering adsorption onto the carboxyl and phosphate sites, and the second considering adsorption onto the carboxyl and hydroxyl sites. The former type of model is more chemically meaningful, because the phosphate sites are significantly deprotonated in the pH range where the adsorption edge occurs, while the hydroxyl sites are not. We therefore select the model considering

adsorption onto the carboxyl and phosphate sites as the two-site model which best describes the experimental data, in agreement with Fein et al. (17) and Daughney et al. (18). These models are compared to the experimental data in Figure 9.

Three trends are recognizable in the magnitudes of the stability constants presented in Tables 9 - 11. First, for both bacterial species, at both ionic strengths, Cd^{2+} has the lowest affinity for the surface, followed by Pb^{2+}, followed by Cu^{2+}, which has the highest affinity for the surface. The stability constants reported here are in good general agreement with those reported by Fein et al. (17) and Daughney et al. (18) (Table 1). The discrepancy in the values of the stability constants given in Tables 1 and 9 - 11 is likely due to differences in the parameters used to characterize the acid-base behaviour of the bacterial surfaces. The metal adsorption stability constants given here should therefore be applied in combination with the surface parameters provided in Table 4.

Second, for a given ionic strength, the metal-carboxyl and metal-phosphate stability constants for *B. licheniformis* are greater than those for *B. subtilis*. As noted by Daughney et al. (18), there is an excellent correlation between the magnitudes of the metal-carboxyl stability constants describing adsorption onto *B. subtilis* and *B. licheniformis* (Figure 10). The correlation between the metal-phosphate stability constants is also very good. This correlation suggests that metal-carboxyl stability constants for one species of bacteria can be estimated if the stability constant describing adsorption of the same metal onto a different type of bacteria has been measured. The slopes of the majority of the correlation lines

Figure 9. FITEQL model curves describing adsorption of a) Cd^{2+}, b) Pb^{2+}, and c) Cu^{2+} onto *B. subtilis* and *B. licheniformis* in 0.1 M $NaNO_3$ (black symbols) and 0.01 M $NaNO_3$ (grey symbols). Model curves consider metal adsorption onto carboxyl and phosphate sites.

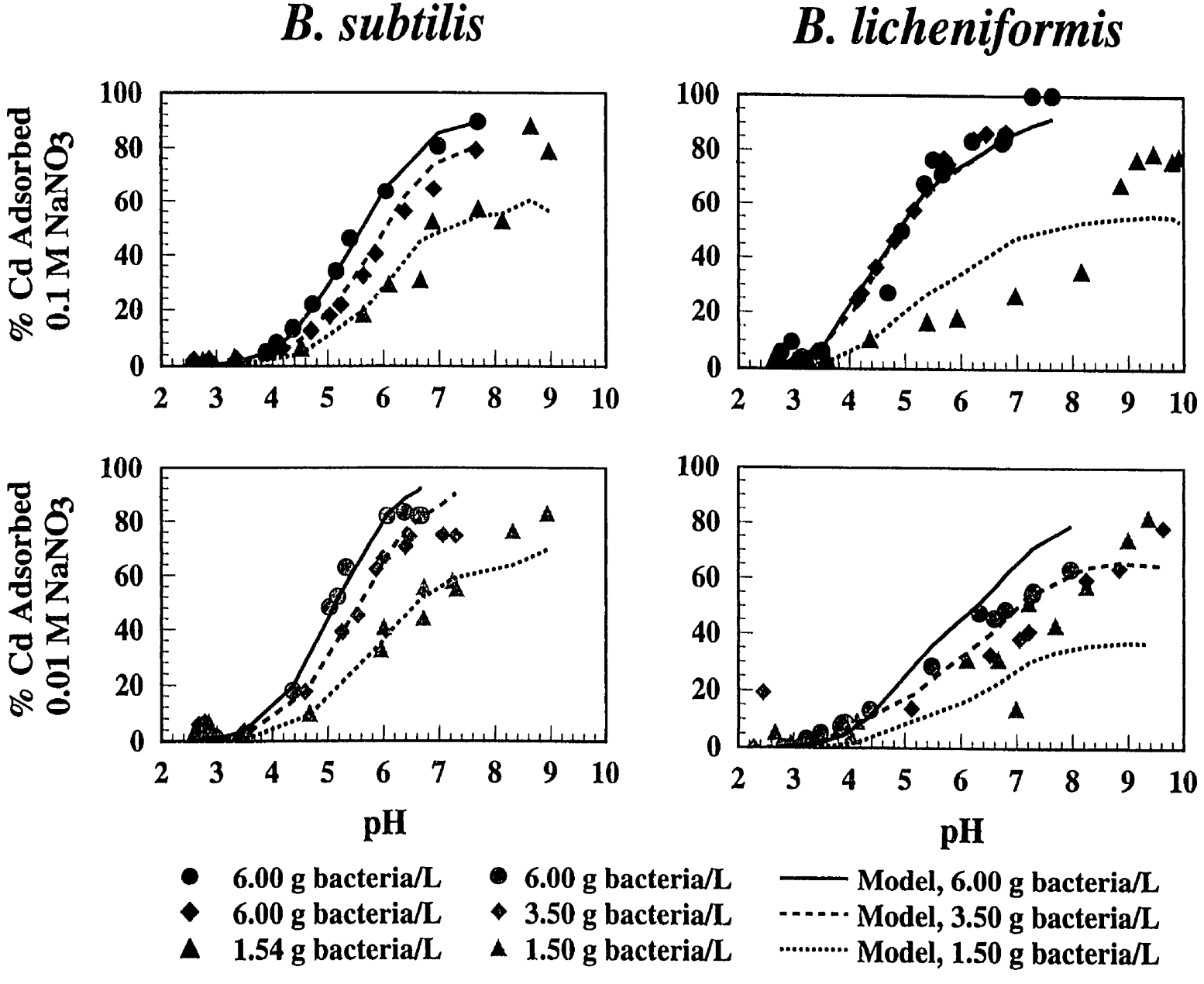
B. subtilis
B. licheniformis
% Cd Adsorbed 0.1 M NaNO3
% Cd Adsorbed 0.01 M NaNO3
pH
pH
6.00 g bacteria/L
6.00 g bacteria/L
6.00 g bacteria/L
3.50 g bacteria/L
1.54 g bacteria/L
1.50 g bacteria/L
Model, 6.00 g bacteria/L
Model, 3.50 g bacteria/L
Model, 1.50 g bacteria/L

Figure 9a

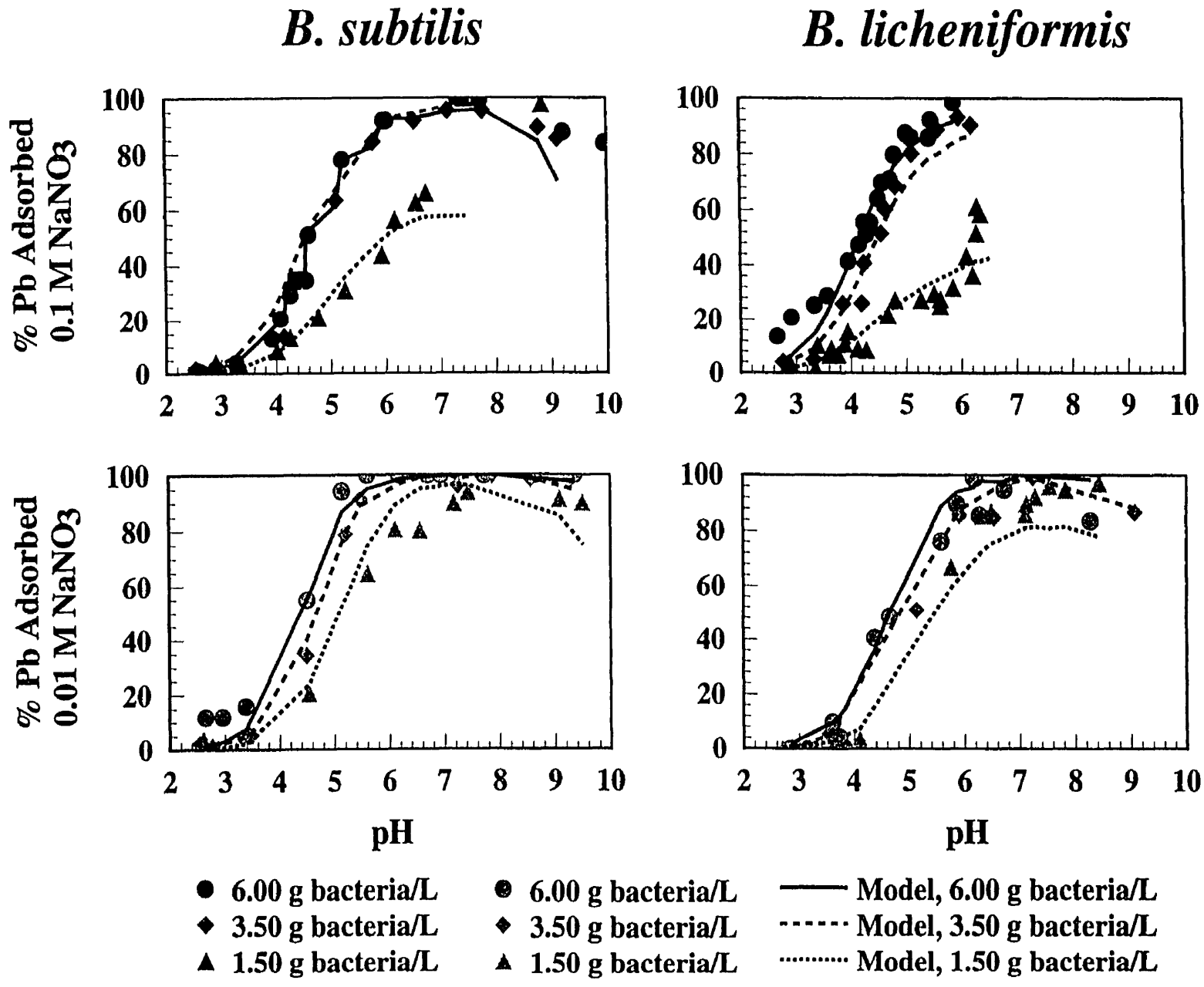
B. subtilis
B. licheniformis
% Pb Adsorbed 0.1 M NaNO3
% Pb Adsorbed 0.01 M NaNO3
100
80
60
40
20
0
2 3 4 5 6 7 8 9 10
pH
6.00 g bacteria/L
3.50 g bacteria/L
1.50 g bacteria/L
6.00 g bacteria/L
3.50 g bacteria/L
1.50 g bacteria/L
Model, 6.00 g bacteria/L
Model, 3.50 g bacteria/L
Model, 1.50 g bacteria/L

Figure 9b

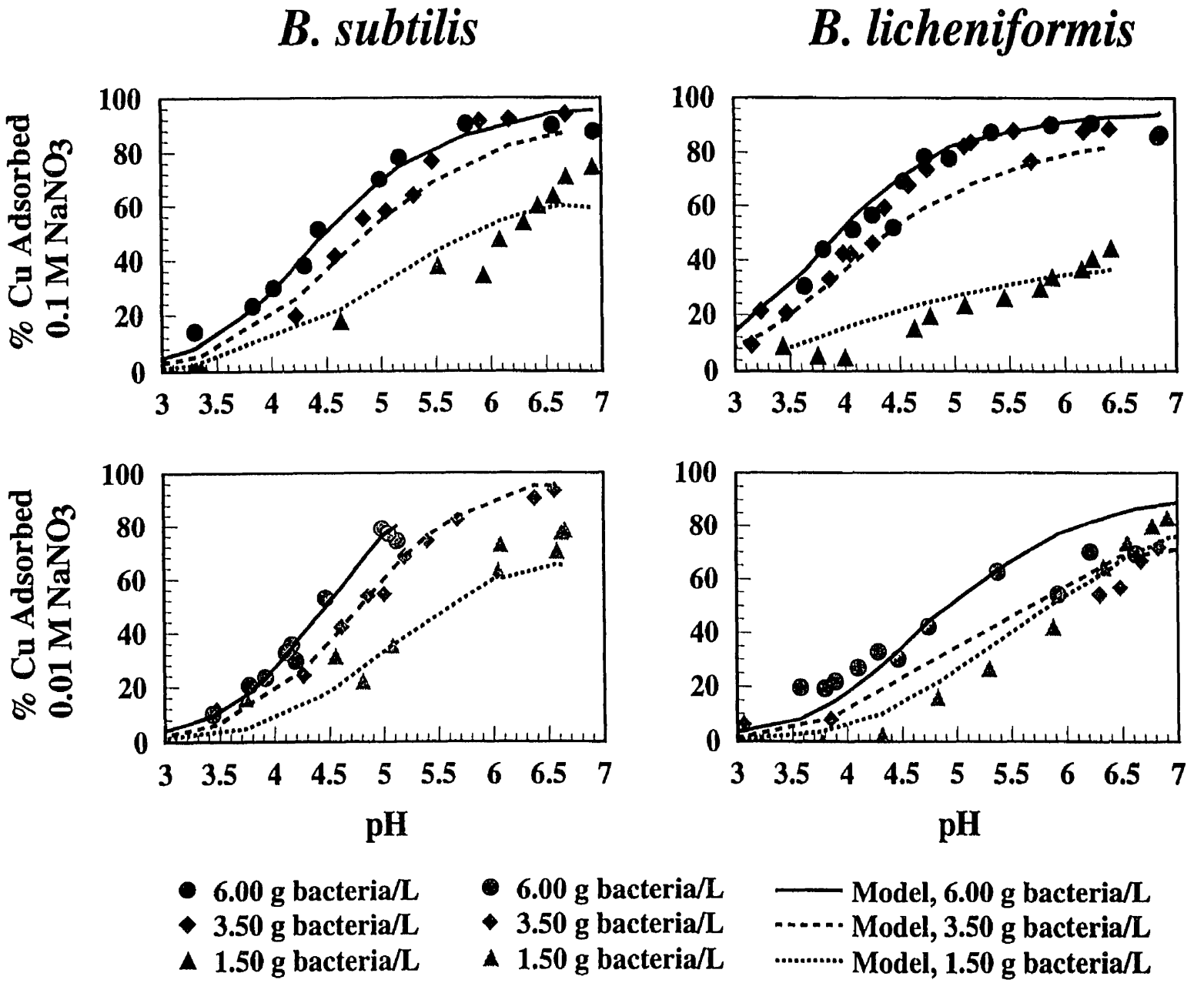
B. subtilis
B. licheniformis
% Cu Adsorbed 0.1 M NaNO3
% Cu Adsorbed 0.01 M NaNO3
100
80
60
40
20
0
3
3.5
4
4.5
5
5.5
6
6.5
7
pH
6.00 g bacteria/L
3.50 g bacteria/L
1.50 g bacteria/L
Model, 6.00 g bacteria/L
Model, 3.50 g bacteria/L
Model, 1.50 g bacteria/L

Figure 9c

Figure 10. Correlation diagram relating metal-carboxyl and metal-phosphate stability constants of *B. subtilis* and *B. licheniformis*, at 0.1 M and 0.01 M $NaNO_3$. The equation of the linear regression line and the linear correlation coefficient are shown.

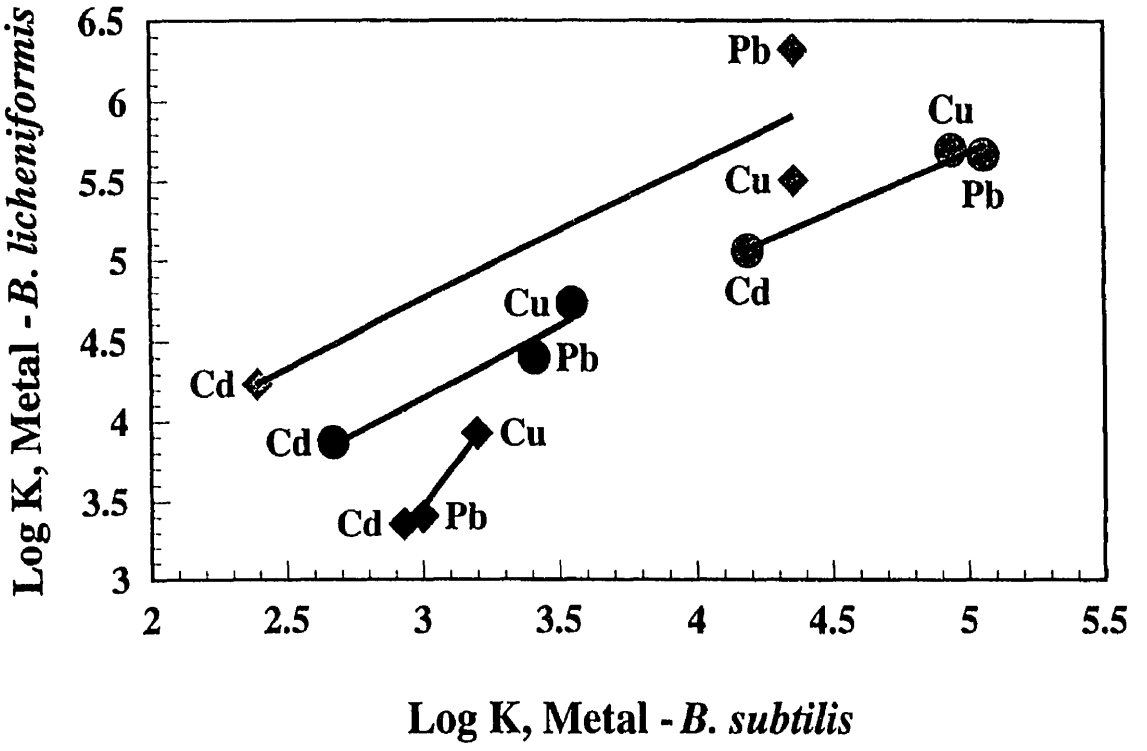

●	Metal-Carboxyl Correlation, 0.1 M	y = 1.474 + 0.891x	R^2 = 0.97
◆	Metal-Carboxyl Correlation, 0.01 M	y = -3.187 + 2.219x	R^2 = 0.99
●	Metal-Phosphate Correlation, 0.1 M	y = 1.905 + 0.755x	R^2 = 0.99
◆	Metal-Phosphate Correlation, 0.01 M	y = 2.208 + 0.850x	R^2 = 0.92

Figure 10

are similar, suggesting that the correlation parameters presented in Figure 10 may be applied to ionic strengths different from those used here.

Third, for both bacterial species, the metal-carboxyl and metal-phosphate stability constants generally decrease with decreasing ionic strength. This ionic strength dependence suggests that metal adsorption is affected by the bacterial surface charge, which, if compared to studies of ion adsorption by mineral surfaces (27, 43), may indicate that the adsorbed metals exist as outer-sphere surface complexes. However, the decrease in the values of the metal-bacteria stability constants with decreasing ionic strength is a trend opposite to that observed for metal adsorption onto most mineral surfaces (27, 43), which implies that the surface complexes may have a different form or structure than that assumed here. Further, the two species of bacteria behave differently in terms of the extent of metal they adsorb as ionic strength is changed. The *B. licheniformis* experimental data indicate that, at a given pH, adsorption decreases with decreasing ionic strength. The *B. subtilis* adsorption data, however, show an opposite trend, which is not reflected as a change in stability constants as a function of ionic strength. The magnitude of the change in the stability constants is too large and too variable to be caused by changes in the activity of the metal ion in the different electrolyte solutions. Again, this suggests that the adsorbed metals may have a different structure than assumed here. Spectroscopic studies are required to clarify the structure of the adsorbed metals. Pending the collection of such data, we model metal adsorption onto the carboxyl and phosphate surface sites, with the stability constant values summarized in Table 12.

TABLE 12. Summary of stability constants describing adsorption of Cd, Pb and Cu onto *B. subtilis* and *B. licheniformis*.

B. subtilis				
Metal[a]	0.1 M $NaNO_3$		0.01 M $NaNO_3$	
	Log K M-carboxyl[a]	Log K M-phosphate[b]	Log K M-carboxyl	Log K M-phosphate
Cd	2.67	4.19	2.93	2.39
Pb	3.41	5.06	3.00	4.36
Cu	3.55	4.94	3.20	4.36
B. licheniformis				
Cd	3.87	5.06	3.36	4.24
Pb	4.40	5.67	3.41	6.32
Cu	4.73	5.70	3.93	5.51

[a]log K value for metal adsorption onto the carboxyl surface sites, referenced to the condition of zero surface charge, zero surface coverage and the ionic strength of the background electrolyte. [b]log K value for metal adsorption onto the phosphate surface sites. Stability constants are determined by modeling all bacteria:metal ratios simultaneously.

CONCLUSIONS

This results of this study illustrate that the surface characteristics of *B. subtilis* and *B. licheniformis* are affected by changes in solution ionic strength. The surface properties and acid-base behaviour of the two bacterial species can be modeled in the framework of chemical thermodynamics, with a different set of stability constants describing interactions between protons and the distinct functional groups on the cell walls. The changes in surface characteristics and metal binding capacities associated with changes in solution ionic strength are manifested by changes in the magnitudes of the site concentrations and deprotonation constants included in the chemical models. We find that the Constant Capacitance model is more effective than the Basic Stern model in its ability to describe ionic strength dependent acid-base behaviour.

The adsorption of Cd^{2+}, Pb^{2+} and Cu^{2+} onto *B. subtilis* and *B. licheniformis* is also controlled by ionic strength, as indicated by variation in the stability constants describing metal adsorption in different electrolytes. Metal adsorption is best described by models considering adsorption onto both the carboxyl and phosphate functional groups. The changes in the metal adsorption stability constants show systematic variation with ionic strength, bacterial species and metal involved. Therefore, the model parameters provided here may be applied to predict metal adsorption in solutions which are different from those of this study. Spectroscopic studies of the bacterial surfaces are recommended in order to elucidate more precisely the nature of the adsorbed metal complexes.

ACKNOWLEDGMENTS

This work was funded by an NSERC Operating Grant and a FCAR Nouveaux Chercheurs Grant to J.B.F. We thank Alfonso Mucci for the use of his autotitrator and Nathan Yee for performing some of the metal adsorption experiments.

REFERENCES

1. Geesey, G.G., Richardson, W.T., Yeomans, H.G., Irvin, R.T. and Costerton, J.W., *Can. J. Microbiol.* **23,** 1733 (1977).

2. Harvey, R. W., and Young, L. Y., *Appl. Environ. Microbiol.* **39**, 894 (1980).

3. Lion, L. W. and Leckie, J. O. *Ann. Rev. Earth Planet. Sci.* **9**, 449 (1981).

4. Jannasch, H. W. and Mottl, M. J. *Science,* **229**, 717 (1985).

5. Yayanos, A. A. *Proc. Natl. Acad. Sci. USA* **83**, 9542 (1986).

6. Ghiorse, W. S. and Wilson, J. T. *Adv. Appl. Microbiol.* **33**, 197 (1988).

7. Huber, R., Stoffers, P., Cheminee, J. L., Richnow, H. H. and Stetter, K. O. *Nature* **345**, 179 (1990).

8. Mahmood, S.K., and Rama, R.P., *Environ. Contam. Toxicol.* **50,** 486 (1993).

9. Yakimov, M.M., Timmis, K.N., Wray, V., and Fredrickson, H.L., *Appl. Env. Microbiol.* **61,** 1706 (1995).

10. Davis, J. A., *Geochim. Cosmochim. Acta* **48,** 679 (1984).

11. Schlautman, M. A., and Morgan, J. J., *Geochim. Cosmochim. Acta* **58,** 4293 (1994).

12. Beveridge, T. J., and Murray, R. G. E., *J. Bacteriol.* **127,** 1502 (1976).

13. Beveridge, T. J., and Murray, R. G. E., *J. Bacteriol.* **141,** 876 (1980).

14. Beveridge, T. J. and Koval, S. F., *Appl. Environ. Microbiol.* **42**, 325 (1981).

15. Gonçalves, M.L.S., Sigg, L., Reutlinger, M., and Stumm, W., *Sci. Tot. Environ.* **60,** 105 (1987).

16. Beveridge, T. J. *Annu. Rev. Microbiol.* **43**, 147 (1989).

17. Fein, J. B., Daughney, C. J., Yee, N., and Davis, T., *Geochim. Cosmochim. Acta* submitted.

18. Daughney, C. J., Fein, J. B., and Yee, N., *Chem. Geol.* submitted.

19. Corapcioglu, M. Y. and Kim, S., *Wat. Res. Research* **31**, 2693 (1995).

20. Ferris, F.G., Fyfe, W.S., and Beveridge, T.J., *Geology,* **16,** 149 (1988).

21. Savvichev, A.S., Nikitin, D.I., and Oranskaya, M.S., *Geochem. Int.* **23,** 60 (1986).

22. Plette, A.C.C., Van Reimsdijk, W.H., Bendetti, M.F., and Van der Wal, A., *J. Coll. Int. Sci.* **173,** 354 (1995).

23. Harden, V.P., and Harris, J.O., *J. Bacteriol.* **65,** 198 (1953).

24. Stumm, W., and Morgan, J. J., "Aquatic Chemistry, Third Edition." John Wiley and Sons, N. Y., 1996.

25. Langmuir, D., "Aqueous Environmental Geochemistry." Prentice-Hall, N. J., 1997.

26. Westall, J., and Hohl, H., *Adv. Colloid Interface Sci.* **12,** 265 (1980).

27. Davis, J. A., and Kent, D. B., *in* "Mineral-Water Interface Geochemistry" (M. F. Hochella and A. F. White, Eds.), Reviews in Mineralogy v. 23, p. 177. Mineralogical Society of America, 1990.

28. Duncan, K. E., Ferguson, N., Kimura, K., Zhou, X., and Istock, C. A., *Evolution* **48,** 2002 (1994).

29. Collins, Y. E. and Stotzky, G., *Appl. Environ. Microbiol.* **58**, 1592 (1991).

30. Hohl, H. and Stumm, W., *J. Colloid Interface Sci.* **55,** 281 (1976).

31. Stern, O. *Z. für Elektrochemie* **30**, 508 (1924).

32. Hayes, K. F., Redden, G., Wendell, E., amd Leckie, J. O., *J. Colloid Interface Sci.* **142,** 448 (1991).

33. Katz, L. E., and Hayes, K. F., *J. Colloid Interface Sci.* **170,** 477 (1995).

34. Westall, J., "FITEQL. A Computer Program for Determination of Chemical Equilibrium Constants from Experimental Data". Department of Chemistry, Oregon State University, Report 82-01, 1982a.

35. Westall, J., "FITEQL. A Computer Program for Determination of Chemical Equilibrium Constants from Experimental Data". Department of Chemistry, Oregon State University, Report 82-02, 1982b.

36. Smith, R.M., and Martell, A.E., "Critical Stability Constants. IV: Inorganic Complexes." Plenum Press, N.Y., 1976.

37. Herben, P. F. G., Mozes, N., and Rouxhet, P. G., *Biochem. Biophys. Acta* **1033,** 184 (1990).

38. Brock, T. D., and Madigan, M. T., "Biology of Microorganisms." Prentice Hall, N. J., 1970.

39. Neter, J., Wasserman, W., and Whitmore, G.A., "Applied Statistics." Allyn and Bacon, Inc., MA, 1988.

40. Baes, C.F., and Mesmer, R.E., "The Hydrolysis of Cations." Wiley-Interscience, N.Y., 1976.

41. Doyle, R. J., Matthews, T, H., and Strepis, U. N., *J. Bacteriol.* **143,** 471 (1980).

42. Beveridge, T. J., Forsberg, C. W., and Doyle, R. J., *J. Bacteriol.* **150,** 1438 (1982).

43. Parks, G. A. *in* "Mineral-Water Interface Geochemistry" (M. F. Hochella and A. F. White, Eds.), Reviews in Mineralogy v. 23, p. 133. Mineralogical Society of America, 1990.

CHAPTER 5:

A COMPARISON OF MODELS DESCRIBING THE ADSORPTION OF 2,4,6-TRICHLOROPHENOL ONTO α-Al_2O_3 AND *Bacillus subtilis*

Christopher J. Daughney
Jeremy B. Fein

Department of Earth and Planetary Sciences
McGill University
3450 University St.
Montréal, PQ H3A 2A7 Canada

Submitted to:
Environmental Science and Technology
March 1997

PREFACE

Chapters 3 and 4 of this thesis investigated heavy metal adsorption by bacterial surfaces, while Chapter 2 examined heavy metal-chlorophenol complexation. In order to model speciation in ternary systems containing metals, chlorophenols and bacteria, the binary chlorophenol-bacteria system must be examined. The following chapter considers the adsorption of TCP onto the cell walls of *Bacillus subtilis*, in order to measure stability constants that can be combined with those presented in the preceding chapters. Further, this chapter compares the adsorption of TCP by bacterial surfaces and mineral surfaces, both of which may be exposed to soil fluids in natural groundwaters.

ABSTRACT

The mobility of 2,4,6-trichlorophenol (TCP) in groundwater is controlled, in part, by its adsorption onto soil mineral and bacterial surfaces. In this study, we perform batch experiments as a function of pH, time and solid:solution ratio to investigate the adsorption of TCP onto representative mineral (α-Al_2O_3) and bacterial (*Bacillus subtilis*) surfaces. We first describe the experimental data with site-specific models, in which we determine stability constants describing the adsorption of both the negative and neutral forms of TCP onto specific functional groups present on the α-Al_2O_3 and *B. subtilis* surfaces. We then compare the site-specific models to non-specific models, in which the TCP partitions onto the surface without interacting with distinct functional groups.

Our experimental data indicate insignificant adsorption of TCP to α-Al_2O_3, but a strong affinity between TCP and *B. subtilis*. The TCP-*B. subtilis* adsorption data are best described by a site-specific model in which the negative form of TCP forms a 1:1 surface complex with the neutral hydroxyl functional groups of the bacteria:

$$TCP^- + R-OH^0 \leftrightarrow (R-OH^0)(TCP^-)$$

$$\log K = 2.33 \pm 0.25$$

and the neutral form of TCP forms a 1:1 surface complex with the neutral hydroxyl surface functional groups:

$$HTCP^0 + R-OH^0 \leftrightarrow (R-OH^0)(HTCP^0)$$

$$\log K = 3.69 \pm 0.25$$

The stability constants reported here may be readily incorporated into thermodynamic models to predict the fate of TCP in complex, natural systems.

INTRODUCTION

Chlorinated phenols, including 2,4,6-trichlorophenol (TCP), have been widely used in agriculture, wood preservation, pulp bleaching, water purification and waste incineration (*1-3*). There are presently several hundred sites worldwide known to be contaminated by TCP (*4, 5*). Due to its wide-spread occurrence, its toxicity (*6, 7*) and its persistence in the environment, TCP is listed as an E.P.A. priority pollutant (*8*). In order to evaluate the environmental risk associated with TCP contamination and develop effective strategies for remediation, the chemical reactions affecting TCP in the natural environment must be quantified. Among these chemical reactions, those involving the adsorption of TCP onto solid surfaces are critical.

A number of workers have examined the adsorptive behaviour of TCP onto common soil solids. In general, the extent of chlorophenol adsorption increases with the increasing hydrophobicity of the adsorbent. The adsorption of TCP onto lipid membranes is extensive (*9*), whereas its adsorption onto pure (hydr)oxide surfaces is small or undetectable (*10, 11*). In soils, TCP adsorption is well correlated with organic carbon content (*3, 4, 12*). Additionally, many workers have reported that TCP adsorption is pH dependent (*3, 4, 10, 11*). This is because TCP is ionizable within the pH range of natural waters ($pK_a \approx 6$, see below), and thus can exist as either a neutrally or a negatively charged species, depending on the solution pH. Both species of TCP are hydrophobic, though the

negative form is less so, and as a result, the extent of adsorption is generally observed to decrease where $pH > pK_a$.

Although the adsorptive behaviour of TCP has been studied in the past, all previous workers have failed to consider the specific interactions between TCP and the functional groups present on the solid surface. This non-specific model for adsorption provides only a semi-quantitative description of the process. For example, because the neutral and negative forms of TCP have different hydrophobicities, the non-specific bulk partition coefficients reported in the literature vary with pH. Some workers have accounted for this pH dependent behaviour by reporting different partition coefficients for the neutral and negative forms of TCP. However, even partition coefficients unique to either the neutral or negative form of TCP vary with the solid:solution ratio. Further, without characterizing the surface chemistry of the adsorbents it is impossible to determine which surface functional groups are responsible for the adsorption of TCP. Due to these limitations, non-specific partition coefficients cannot be used to accurately predict the amount of TCP adsorption that will occur under conditions that differ from those of measurement.

In this communication, we compare the non-specific adsorption model described above to a thermodynamic, site-specific adsorption model. The site-specific model requires the determination of stability constants describing interactions between the neutral and negative forms of TCP and the different functional groups present on the solid surface. These thermodynamic stability constants, once determined, can be easily adjusted to reflect conditions other than

those of the experiments, and they can be combined with other previously determined stability constants. As such, the site-specific adsorption model is able to predict the extent of TCP adsorption in complex, natural systems.

In this study, we compare the adsorption of TCP onto two different surfaces which are representative of the solids found in soils. We select *B. subtilis* and α-Al_2O_3 as adsorbents. *B. subtilis* is a common soil bacteria (*13*) with a surface chemistry that has been examined in the thermodynamic framework (*14*). Bacteria, or bacterial cell wall fragments, comprise a significant fraction of the organic matter in many soils, and because they frequently coat mineral surfaces, they may represent a significant fraction of the surface area exposed to soil fluids. α-Al_2O_3 itself is not a common soil mineral, but it is characterized by surface functional groups which are representative of the Al surface sites on many more common alumino-silicate minerals.

THEORY

The surface chemistry of oxide minerals is commonly characterized by the presence of amphoteric hydrated functional groups, such as the aluminol (≡AlOH) functional groups on the surface of α-Al_2O_3 (*15-17*). These aluminol functional groups protonate or deprotonate depending on the solution pH:

$$\equiv AlOH_2^+ \leftrightarrow \equiv AlOH^0 + H^+ \qquad (1)$$

$$\equiv AlOH^0 \leftrightarrow \equiv AlO^- + H^+ \qquad (2)$$

For the purpose of this study, we characterize the surface chemistry of α-Al_2O_3 as described by Boily and Fein (*15*), because we use the same material treated in the same manner. The mass action expressions for reactions 1 and 2, and corresponding equilibrium constants are as follows:

$$\frac{[\equiv AlOH^0]a_{H^+}}{[\equiv AlOH_2^+]} = K_{aluminol\,1} = 10^{-6.76} \quad (3)$$

$$\frac{[\equiv AlO^-]a_{H^+}}{[\equiv AlOH^0]} = K_{aluminol\,2} = 10^{-9.50} \quad (4)$$

Here, and for the remainder of this paper, the square brackets represent the concentration of the enclosed surface species in moles per kg of solution, *a* represents the activity of the subscripted species, and K is the equilibrium constant. The α-Al_2O_3 surface is neutrally charged at pH $\approx$ 9; below this pH it is positively charged, while above this pH it is negatively charged. The powdered α-Al_2O_3 prepared in the manner of Boily and Fein (*15*) has a surface area of 9.3 m^2/g and a surface site concentration of 2.72 x 10^{-5} moles per gram.

Recent research (*14, 18*) illustrates that the surfaces of various gram-positive bacteria behave in an analogous manner, and are well described by equilibrium thermodynamics. The cell wall of *B. subtilis* is primarily composed of peptidoglycan and teichoic acid (*19*), and it displays active carboxyl, phosphate and hyrdoxyl functional groups (*20*). The deprotonation of these three types of surface functional groups may be represented by the following equilibria (*14*):

$$R-COOH^0 \leftrightarrow R-COO^- + H^+ \quad (5)$$

$$R-PO_4H^0 \leftrightarrow R-PO_4^- + H^+ \quad (6)$$

$$R-OH^0 \leftrightarrow R-O^- + H^+ \quad (7)$$

where R represents the bacterium to which the functional group is attached. The mass action equations and equilibrium constants corresponding to the above equilibria are as follows (*14*):

$$\frac{[R-COO^-]a_{H^+}}{[R-COOH^0]} = K_{carboxyl} = 10^{-4.82} \quad (8)$$

$$\frac{[R-PO_4^-]a_{H^+}}{[R-PO_4H^0]} = K_{phosphate} = 10^{-6.9} \quad (9)$$

$$\frac{[R-O^-]a_{H^+}}{[R-OH^0]} = K_{hydroxyl} = 10^{-9.4} \quad (10)$$

The cell walls of *B. subtilis* have 1.2 x 10^{-4} moles of carboxyl sites, 4.4 x 10^{-5} moles of phosphate sites and 6.2 x 10^{-4} moles of hydroxyl sites per gram. The surface is essentially electrically neutral below pH $\approx$ 3, but due to the sequential deprotonation of the surface sites, it becomes increasingly negative with increasing pH.

2,4,6-Trichlorophenol is a hydrophobic, ionizable compound with a pK_a of 5.99 (*21*). Below a pH of 5.99, the majority of the TCP is present as a protonated,

neutral molecule ($HTCP^0$), whereas above this pH, the majority of the TCP exists as a deprotonated, negative species (TCP^-):

$$HTCP^0 \leftrightarrow H^+ + TCP^- \tag{11}$$

$$\frac{a_{TCP^-} a_{H^+}}{a_{HTCP^0}} = K_{TCP} = 10^{-5.99} \tag{12}$$

The adsorption of dissolved species onto mineral or bacterial surfaces can be quantified in terms of site-specific surface complexation, whereby the reactions between the functional groups on the surface and the species in solution are described by fixed stoichiometries and thermodynamic mass action laws (e.g. *14, 15, 18, 22-25*). This approach permits the derivation of stability constants for simple surface complexation reactions which can subsequently be applied to model adsorption in more complex systems. In general form, the adsorption of TCP onto the aluminol sites of α-Al_2O_3 may be described by the following equilibrium:

$$a(\equiv AlO^-) + b(TCP^-) + cH^+ \leftrightarrow \left((\equiv AlO^-)_a (TCP^-)_b (H^+)_c\right)^{(c-b-a)} \tag{13}$$

where *a*, *b* and *c* are stoichiometric coefficients. This general reaction allows for the protonation and deprotonation of the aluminol functional groups, the adsorption of either the neutral or the negative form of TCP, and the formation of

multidentate surface complexes. A mass action law relates the stability constant $K_{TCP\text{-}aluminol}$ to the activities of the species involved in the reaction:

$$\frac{[\left((\equiv AlO^-)_a(TCP^-)_b(H^+)_c\right)^{(c-b-a)}]}{[\equiv AlO^-]^a[TCP^-]^b[H^+]^c} = K_{TCP-aluminol} \tag{14}$$

Similarly, the adsorption of TCP onto the carboxyl, phosphate and hydroxyl bacterial surface sites may be represented as follows:

$$a(R-CO^-)+b(TCP^-)+cH^+ \leftrightarrow \left((R-CO^-)_a(TCP^-)_b(H^+)_c\right)^{(c-b-a)} \tag{15}$$

$$a(R-PO_4^-)+b(TCP^-)+cH^+ \leftrightarrow \left((R-PO_4^-)_a(TCP^-)_b(H^+)_c\right)^{(c-b-a)} \tag{16}$$

$$a(R-O^-)+b(TCP^-)+cH^+ \leftrightarrow \left((R-O^-)_a(TCP^-)_b(H^+)_c\right)^{(c-b-a)} \tag{17}$$

Mass action laws for the above equilibria are, respectively:

$$\frac{[\left((R-CO^-)_a(TCP^-)_b(H^+)_c\right)^{(c-b-a)}]}{[R-CO^-]^a[TCP^-]^b[H^+]^c} = K_{TCP-carboxyl} \tag{18}$$

$$\frac{[\left((R-PO_4^-)_a(TCP^-)_b(H^+)_c\right)^{(c-b-a)}]}{[R-PO_4^-]^a[TCP^-]^b[H^+]^c} = K_{TCP-phosphate} \tag{19}$$

$$\frac{[\left((R-O^-)_a(TCP^-)_b(H^+)_c\right)^{(c-b-a)}]}{[R-O^-]^a[TCP^-]^b[H^+]^c} = K_{TCP-hydroxyl} \tag{20}$$

Alternatively, the adsorption of dissolved species onto mineral or bacterial surfaces can be quantified with a non-specific model. This model is essentially a bulk partitioning or isotherm model, with adsorption controlled by the mutual affinities and hydrophobicities of the reactants:

$$a(TCP^-)_{aq} + bH^+_{aq} \leftrightarrow \left((TCP^-)_a(H^+)_b\right)^{b-a}_{adsorbed} \tag{21}$$

Here, the TCP partitions onto the mineral surface or the bacterial cell wall, but not onto a specific ionizable surface site. A partition coefficient for the above reaction relates the concentration of TCP in solution to the concentration of TCP on the solid surface:

$$\frac{[\left((TCP^-)_a(H^+)_b\right)^{b-a}_{adsorbed}]}{[TCP^-]^a[H^+]^b} = K_{TCP-surface} \tag{22}$$

This model allows the adsorption of the neutral and negative forms of TCP to be considered independently. Note that the partition coefficient will vary with the total concentration of TCP and the total mass of solid present in the system.

As noted above, a mineral or bacterial surface may develop a positive or negative electric potential due to protonation or deprotonation of its surface functional groups (Figure 1). This charge affects the hydrophobicity of the surface, and it influences interactions between the surface and charged species in

Figure 1. Surface potential of *B. subtilis* (12 g/L) and α-Al_2O_3 (100 g/L) in a 0.1 M $NaNO_3$ electrolyte solution as a function of pH, as calculated with the constant capacitance model.

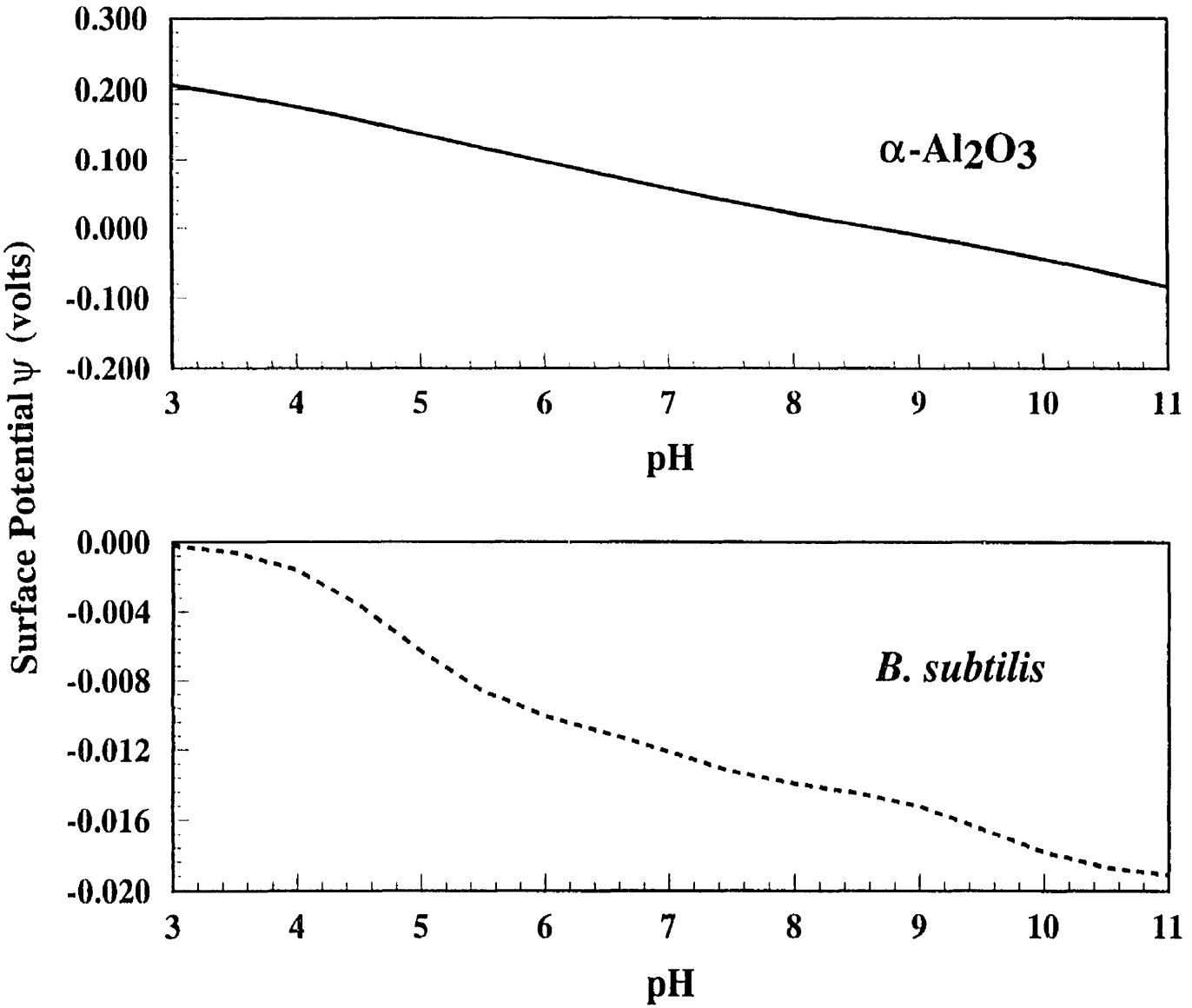
Surface Potential ψ (volts)
0.300
0.200
0.100
0.000
-0.100
-0.200
α-Al2O3
3
4
5
6
7
8
9
10
11
pH
0.000
-0.004
-0.008
-0.012
-0.016
-0.020
B. subtilis
3
4
5
6
7
8
9
10
11
pH

Figure 1

solution. As such, the mass action expressions above must be adjusted by the following relationship:

$$K_{intrinsic} = K_{observed} \exp(-zF\psi / RT) \quad (23)$$

$K_{observed}$ is the experimentally determined equilibrium constant, $K_{intrinsic}$ is the equilibrium constant referenced to the condition of zero charge and zero surface coverage. The variables F, ψ, R, T and z represent Faraday's constant, the electric potential of the solid surface, the gas constant, the absolute temperature and the charge of the adsorbing ion, respectively. This equation accounts for the interactions between an ion in solution and a charged surface, and therefore it is applicable to both the site-specific and non-specific models. The surface electric potential (ψ) can be related to the solid surface charge (σ) by a simple constant capacitance model (*26*):

$$C = \frac{\sigma}{\psi} \quad (24)$$

The capacitance (C) of the α-Al_2O_3 surface is 1.9 Farads/m^2 (*15*), while the capacitance of the *B. subtilis* surface is 8.0 Farads/m^2 (*14*).

The computer speciation program FITEQL 2.0 (*27, 28*) is used to calculate equilibrium constants from experimental data (Equation 14 for TCP-α-Al_2O_3 site-specific adsorption, Equations 18 - 20 for the TCP-*B. subtilis* site-specific

adsorption, and Equation 22 for non-specific adsorption). In the development of a chemical model to describe the experimental data, we consider TCP-surface complexes of various stoichiometries. FITEQL is used to compute a variance (V) which quantifies the fit of the model to the experimental data. The variance is normalized with respect to the number of experimental data points, the number of chemical components for which the total concentration is known, and the number of equilibrium constants to be determined.

The thermodynamic standard states employed for the solid phases and liquid water are taken to be the pure substance at 25°C and 1 bar. The standard state for aqueous species is a hypothetical one molal solution which exhibits the behaviour of infinite dilution. Departures from this standard state are quantified by Davies equation activity coefficients. Neutral aqueous species are assigned activity coefficients of unity. The standard state for surface complexes is one of zero coverage and zero surface potential. Departures from this standard state are corrected with the Boltzmann equation, as outlined above. All equilibrium constants reported in this work are referenced to 25°C, zero ionic strength, and zero surface potential.

MATERIALS AND METHODS

Materials. The adsorption of TCP onto the two solids has been studied independently in 0.1 M $NaNO_3$ electrolyte solutions. The 2,4,6-trichlorophenol and $NaNO_3$ were obtained from Aldrich and used without further purification. Prior to use, the TCP was powdered and passed through a 60 mesh sieve. Reagent grade HNO_3 and NaOH were used to adjust the pH of the experimental solutions where required. Distilled, deionized (DDI) water (resistance = 18 MΩ) was used for all solutions.

Powdered α-Al_2O_3 was obtained from Aldrich and pre-treated with the method of Boily and Fein (*15*). The mineral powder was washed first in 10% HNO_3 and then in 10% NaOH. It was then rinsed 15 - 20 times with DDI water, until the supernatant pH was approximately 8, and then it was oven-dried at 80°C to constant weight. This washing procedure was intended to remove the finest mineral grains and homogenize the surface characteristics of the remaining fraction.

B. subtilis cells were obtained from T. J. Beveridge (University of Guelph, Ontario), and cultured and washed as described by Fein et al. (*14*). The cells were cultured in autoclaved (120°C for 20 minutes) trypticase soy broth extract (Becton Dickenson) containing 0.5 wt. % yeast extract (Becton Dickenson). The cells were allowed to grow in 3 mL volumes of broth at 32°C for 24 hours, then they were transferred to 1 L volumes of broth and cultured at 32°C for an additional 24 hours. The cells were removed from the broth by centrifugation (6000 rpm for 15

minutes), washed twice in DDI water, rinsed once in 0.1 M HNO_3, soaked overnight in 0.001 M EDTA, and finally rinsed five times in 0.1 M $NaNO_3$. Following each rinse, the cells were pelleted by centrifugation (6000 rpm for 15 minutes) and the supernatant was discarded. This rinsing procedure was followed in order to strip the cell walls of any ions present in the growth medium. Further, we ensure that the growth procedure remains constant in order to minimize any potential variation in the cell wall structure (*29*).

Adsorption Experiments. Batch experiments were conducted as a function of pH and solid:solution ratio in order to determine stability constants for the adsorption of TCP onto α-Al_2O_3. These adsorption experiments were performed in Teflon reaction vessels at 25 ± 1°C. Each vessel contained a 100 mL suspension of 0.1 M $NaNO_3$, 0.0001 M TCP and either 50 or 100 g/L α-Al_2O_3. The suspensions were mixed with a Teflon-coated stirring bar and bubbled with nitrogen gas in order to purge them of dissolved CO_2. The pH of each suspension was adjusted to a different value with 0.3 M HNO_3 or 0.3 M NaOH, and allowed to equilibrate for 30 minutes (this equilibration time was based on the results of the kinetic experiments described below). The equilibrium pH was recorded and the suspensions were passed through a 0.45 μm cellulose acetate filter. The filtrate was then basified and analysed for TCP by ultraviolet spectrophotometry.

Batch experiments were also conducted as a function of pH and solid:solution ratio in order to quantify adsorption of TCP onto *B. subtilis*. The washed bacteria were pelleted by centrifugation (6000 rpm for 60 minutes). The

pellet was weighed and then resuspended in a solution containing 0.1 M $NaNO_3$ and 0.0001 M TCP to yield a parent suspension of either 6.0, 9.0 or 12.0 g bacteria/L. Homogenous 5.00 g aliquots of this suspension were placed in several identical reaction vessels, and the pH of each was adjusted to a different value with 0.1 M HNO_3 or 0.1 M NaOH. The reaction vessels were placed on a rotary shaker and allowed to equilibrate for 90 minutes (again, this equilibration time was based on the results of the kinetic experiments described below). The equilibrium pH of each suspension was recorded and then it was passed through a 0.45 μm cellulose acetate filter. The filtered samples were basified and analysed for TCP by ultraviolet spectrophotometry. In order to better constrain the choice of model, adsorption experiments were also performed at pH > 11, with approximately 30 g bacteria/L.

Kinetic Experiments. In order to determine the time required to reach equilibrium in the systems studied here, two series of batch adsorption experiments were conducted as a function of time. In the TCP-α-Al_2O_3 system, the initial solution pH of approximately 8.8 was adjusted to pH 6.9, so that the mineral surface would be positively charged and the TCP would be predominantly TCP^-. This pH adjustment was performed in order to maximize the potential for adsorption. The initial pH of the TCP-*B. subtilis* suspensions was roughly 4.5. Two kinetic experiments were performed in this system, one in which the initial pH was reduced to 2.6, the other in which it was increased to 7.1. Other experimental procedures were as described above.

Desorption Experiments. A series of desorption experiments was conducted in order to evaluate the reversibility of the adsorption reactions. The adsorbents were placed in contact with aqueous TCP in several identical reaction vessels, as described above. The pH of the solutions were adjusted to a value where significant adsorption was expected to occur (pH $\approx$ 2.6, based on the results of the adsorption experiments described above). All suspensions were allowed to equilibrate for 90 minutes, and the equilibrium pH of each solution was measured. The solid present in each reaction vessel was pelleted by centrifugation (6000 rpm for 15 minutes) and the supernatant was analysed for TCP, then discarded. The bacteria were then resuspended in 0.1 M $NaNO_3$, and the solution pH was adjusted to a value favouring the desorption of the TCP (pH $\approx$ 8.5). The suspensions were allowed to equilibrate for different amounts of time (30 - 230 minutes). Finally, the pH of each solution was measured, and the samples were filtered, basified and analysed for TCP as described above.

TCP-α-Al_2O_3 ADSORPTION RESULTS AND DISCUSSION

The results of the TCP-α-Al_2O_3 adsorption experiments are presented in Figure 2. The data displayed here indicate that TCP does not adsorb appreciably to α-Al_2O_3 under the chemical conditions of this investigation. The kinetic experiments (Figure 3) show that TCP adsorption is not significant even for equilibration times as long as two hours.

Figure 2. Percent adsorption of TCP onto α-Al_2O_3 as a function of pH. Solutions contain $10^{-4.00}$ M TCP, $10^{-1.00}$ M $NaNO_3$ and either 50 or 100 g α-Al_2O_3 per L.

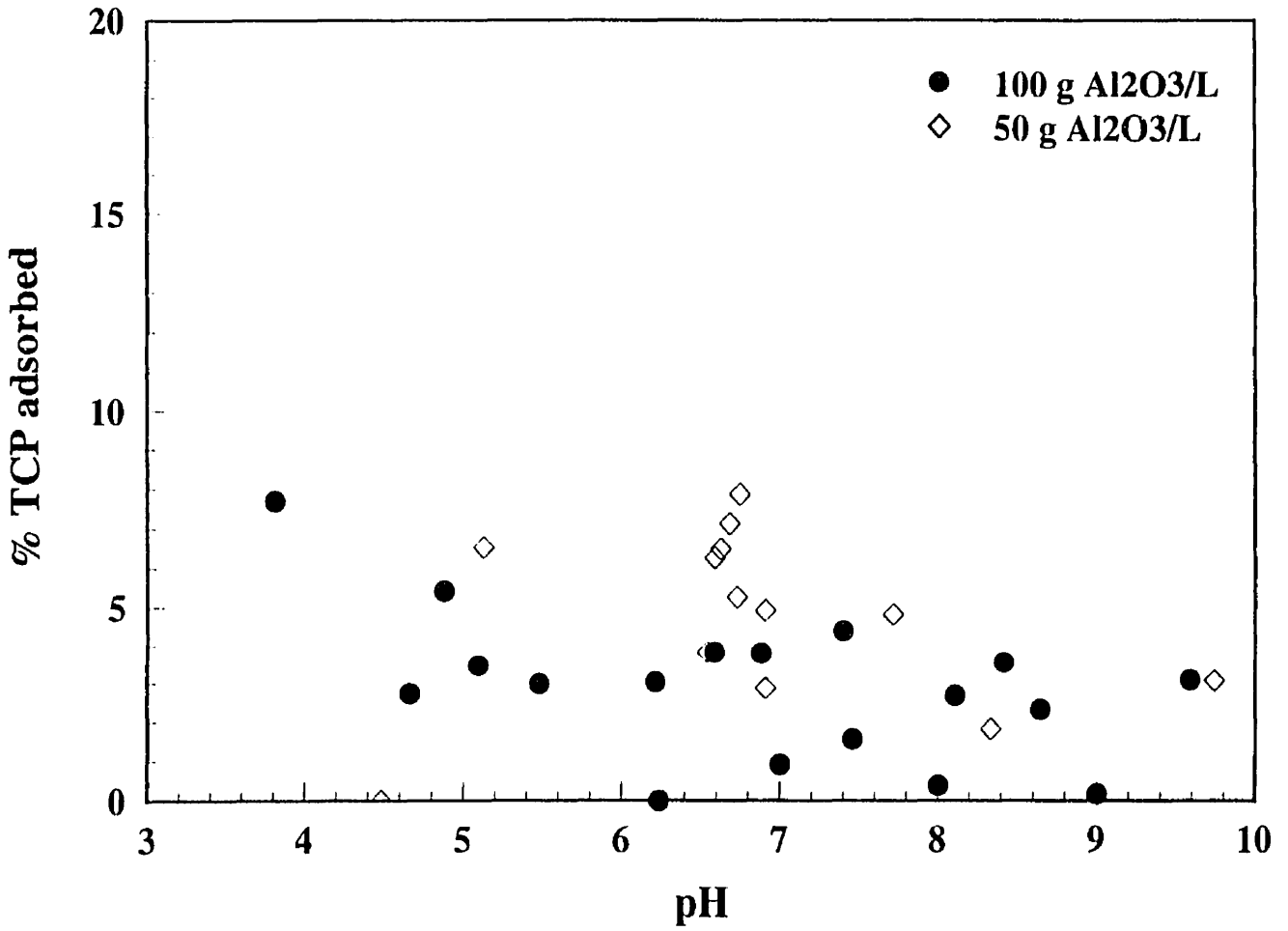

Figure 2

Figure 3. Percent adsorption of TCP onto α-Al_2O_3 as a function of time. Solutions contain $10^{-4.00}$ M TCP, $10^{-1.00}$ M $NaNO_3$ and 100 g α-Al_2O_3 per L.

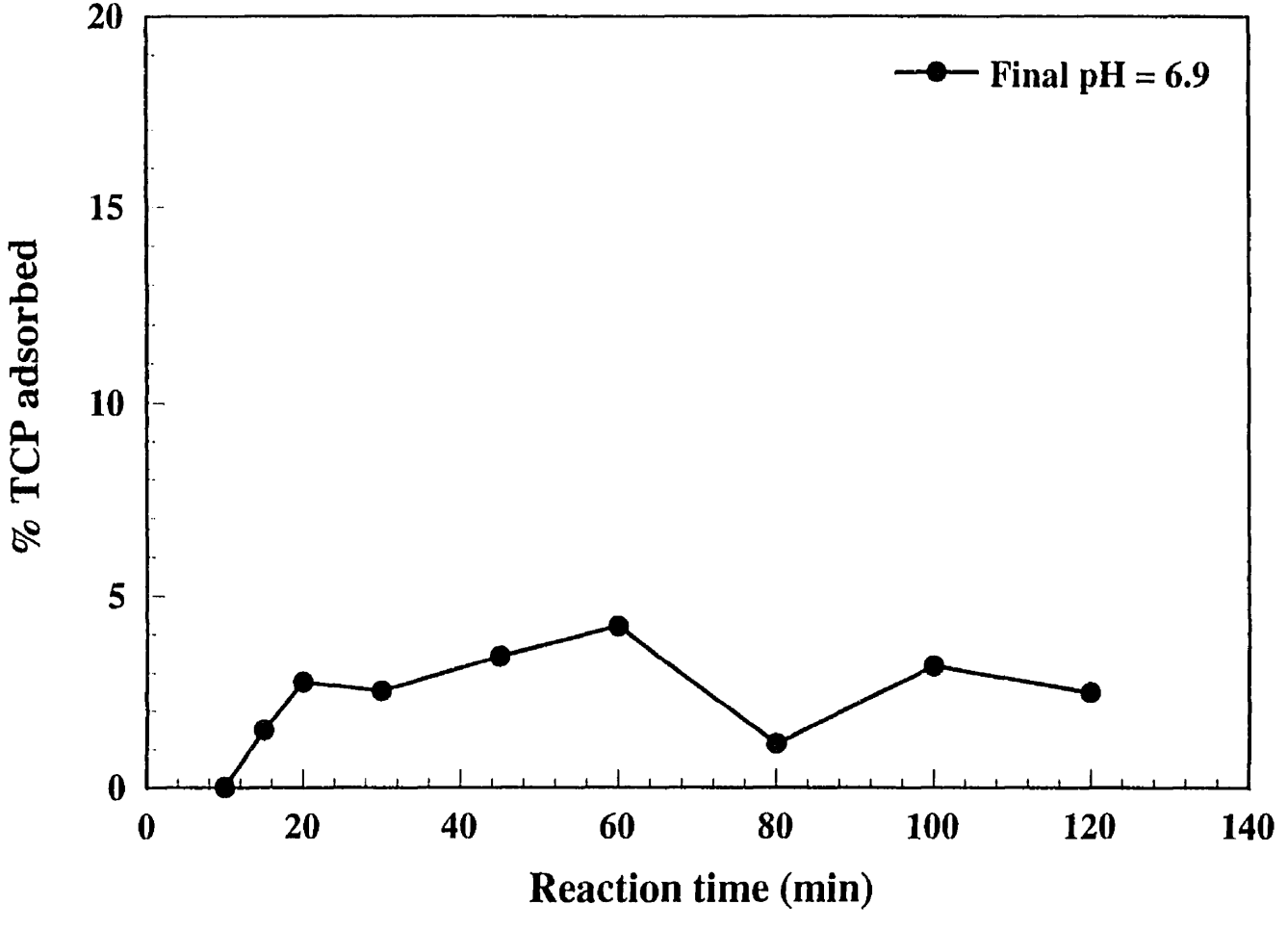
Final pH = 6.9
% TCP adsorbed
Reaction time (min)
0
5
10
15
20
0
20
40
60
80
100
120
140

Figure 3

TCP-*B. subtilis* ADSORPTION RESULTS AND DISCUSSION

The results of the TCP-*B. subtilis* adsorption experiments are displayed in Figure 4. Upon examination of the experimental data, five trends are revealed. First, it is immediately apparent that TCP displays a much greater affinity for the cell walls of *B. subtilis* than for the surface of α-Al_2O_3. Second, the extent of TCP adsorption decreases with increasing pH, reaching zero above pH 10. Third, the extent of adsorption reaches a constant value at pH less than 5. Fourth, the adsorption experiments performed at pH > 11 and high solid:solution ratio indicate that less than 5% adsorption occurs under these conditions. Finally, it is apparent that the fraction of the TCP adsorbed at a given pH increases as the ratio of bacteria to the total TCP concentration increases. These five trends must be considered during the development of a chemical model describing the adsorption of TCP onto *B. subtilis*.

The results of the TCP-*B. subtilis* kinetic experiments are presented in Figure 5. Although we observe small changes in the extent of TCP adsorption during the first hour of equilibration, these are within experimental uncertainties (discussed below), and thus we suggest that equilibrium is reached within approximately 30 minutes. In order to allow for experimental errors and trials involving more extreme pH adjustments, all adsorption and desorption experiments were permitted to equilibrate for 90 minutes.

The results of the TCP-*B. subtilis* desorption experiments are shown in Figure 6. The extent of TCP adsorption following the acidification and

Figure 4. Percent adsorption of TCP onto *B. subtilis* as a function of pH. Solutions contain $10^{-4.00}$ M TCP, $10^{-1.00}$ M $NaNO_3$ and either 6, 9, or 12 g bacteria per L. Model curves were generated by FITEQL, assuming site-specific adsorption of TCP^- onto the neutral hydroxyl sites and of $HTCP^0$ onto the neutral hydroxyl sites. Data points represented by stars have increased solid:solution ratios, with approximately 30 g bacteria per L.

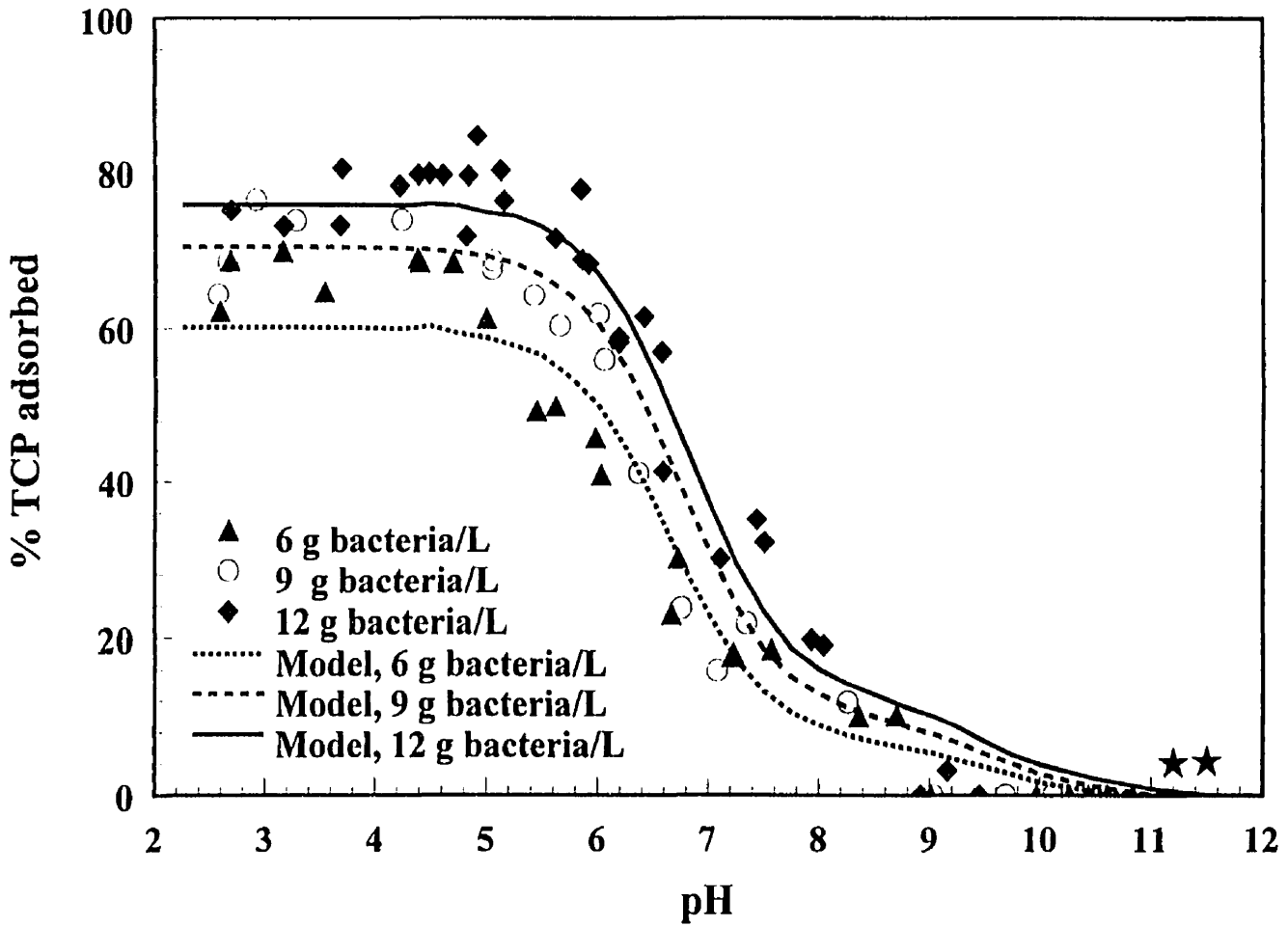
100
80
60
40
20
0
% TCP adsorbed
2
3
4
5
6
7
8
9
10
11
12
pH
6 g bacteria/L
9 g bacteria/L
12 g bacteria/L
Model, 6 g bacteria/L
Model, 9 g bacteria/L
Model, 12 g bacteria/L

Figure 4

Figure 5. Percent adsorption of TCP onto *B. subtilis* as a function of time. Solutions contain $10^{-4.00}$ M TCP, $10^{-1.00}$ M $NaNO_3$ and 12 g bacteria per L. Initial pH $\approx$ 4.5.

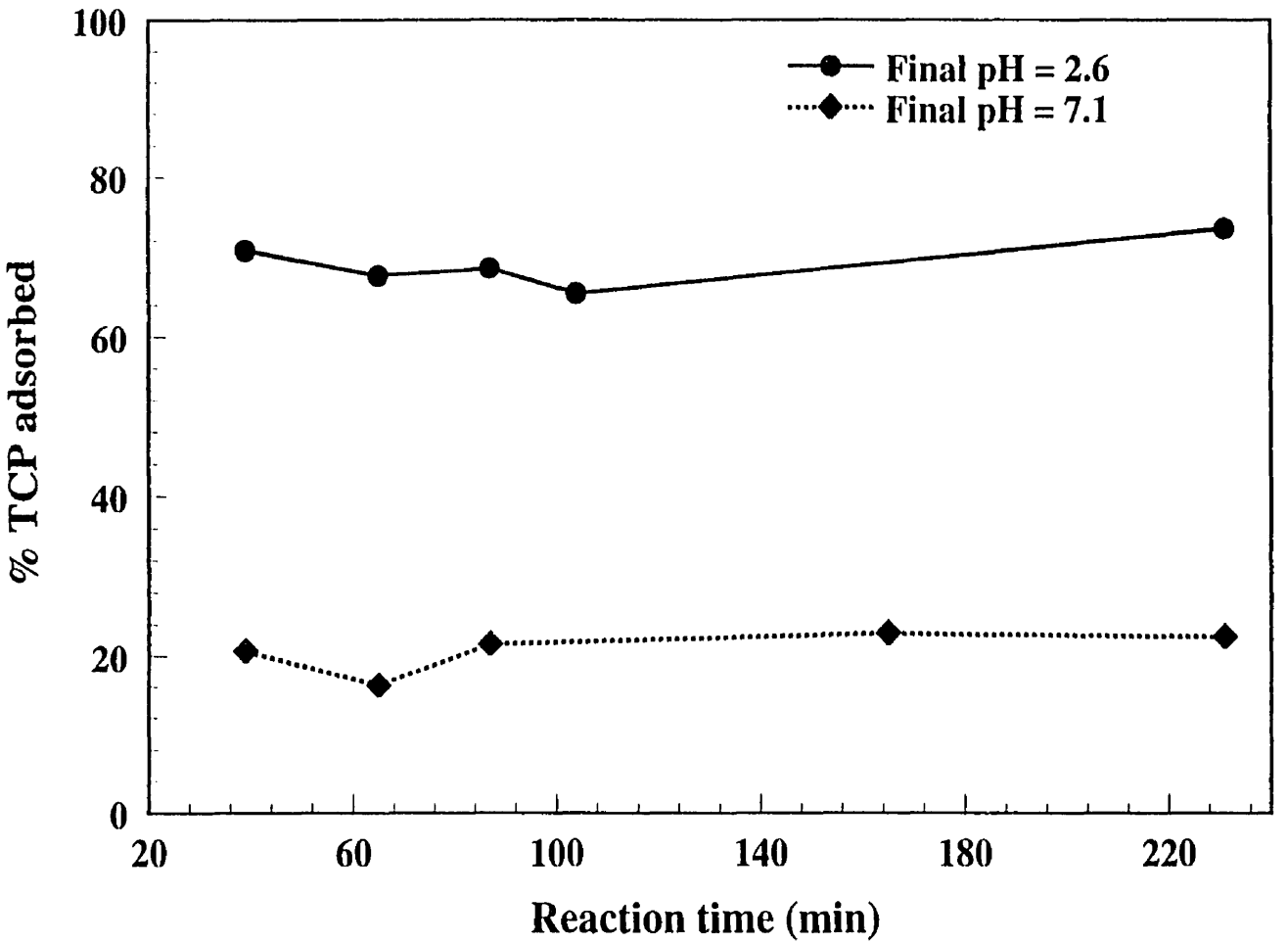
100
80
60
40
20
0
% TCP adsorbed
20
60
100
140
180
220
Reaction time (min)
Final pH = 2.6
Final pH = 7.1

Figure 5

Figure 6. Percent desorption of TCP from *B. subtilis* as a function of time. Initial solutions contained $10^{-4.00}$ M TCP, $10^{-1.00}$ M $NaNO_3$ and 12 g bacteria per L. Open circles show percent TCP initially adsorbed after 90 minutes at pH 2.6. The bacteria were removed from the solution, resuspended in $10^{-1.00}$ M $NaNO_3$ adjusted to a pH of 8.5, and allowed to equilibrate for varied times, as indicated by the arrows. Model curve was generated by FITEQL, assuming site-specific adsorption of TCP^- onto the neutral hydroxyl sites and adsorption of $HTCP^0$ onto the neutral hydroxyl sites.

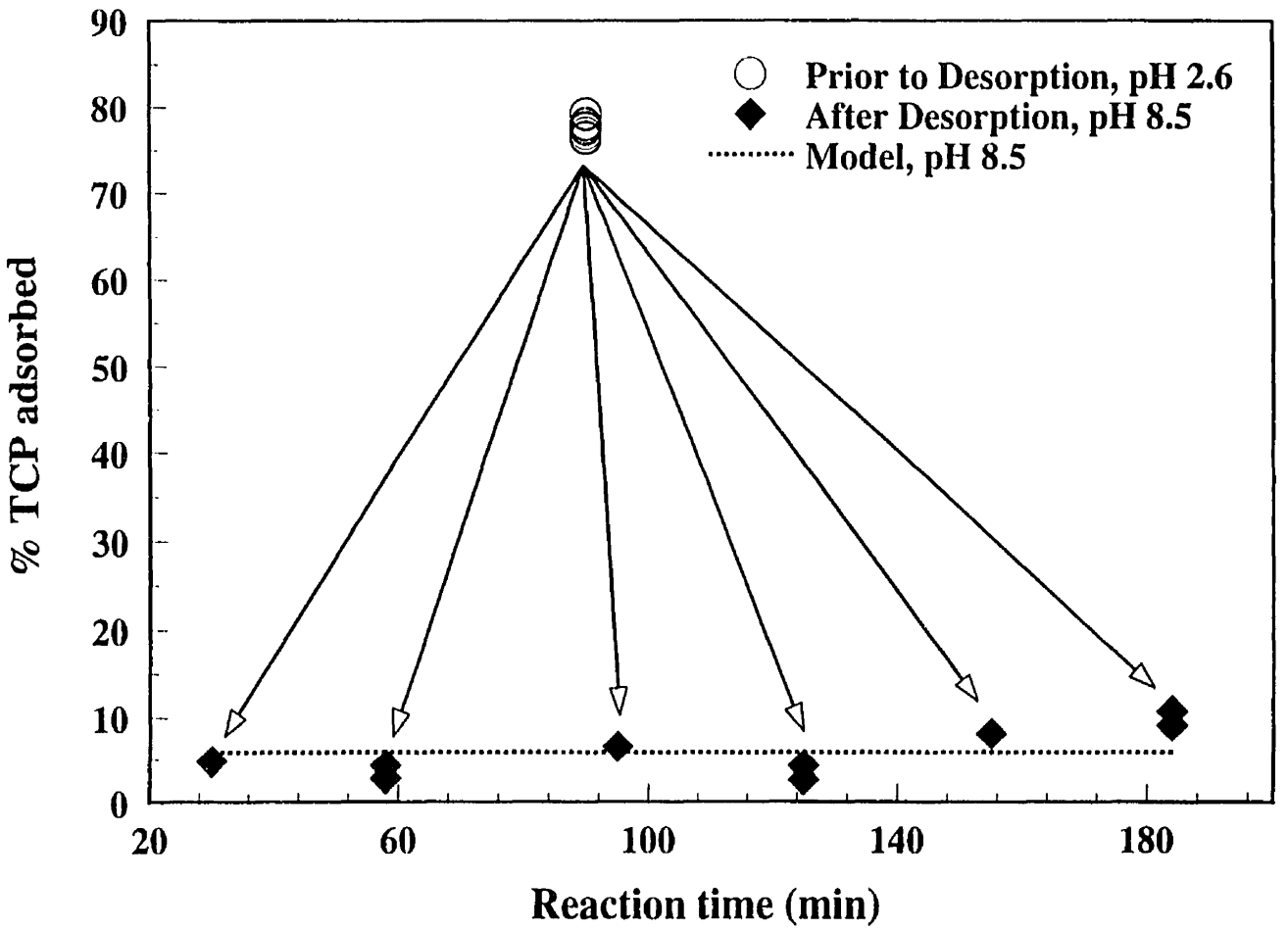
90
80
70
60
50
40
30
20
10
0
% TCP adsorbed
20
60
100
140
180
Reaction time (min)
Prior to Desorption, pH 2.6
After Desorption, pH 8.5
Model, pH 8.5

Figure 6

equilibration of the experimental solutions is in excellent agreement with that noted in the previous adsorption and kinetics experiments. Both the adsorption and desorption reactions are rapid, reversible and effectively predicted by the model developed below, justifying the application of the thermodynamic framework.

Prior to the development of a chemical model, we first consider the possibility that the behaviour observed here (Figures 4 - 6) is the result of anything other than the adsorption of TCP onto *B. subtilis*. All experimental solutions were undersaturated with respect to solid TCP, and so precipitation did not occur. Blank adsorption runs were performed in the absence of the bacteria, but no adsorption of TCP to the walls of the reaction vessels was revealed. An examination of the TCP-*B. subtilis* suspensions (by HPLC and optical microscopy) both before and after the experiments gave no evidence of organic exudates or of cell disruption, and so the adsorption of TCP was not affected by aqueous complexation with any dissolved organic. Lastly, our kinetic and desorption experiments show that the changes in aqueous TCP concentration are rapid and reversible and therefore not representative of bacterial consumption or degradation. Because of this reversibility, application of the thermodynamic framework to this system is justified. We conclude that all observed changes in aqueous TCP concentration can be attributed completely to adsorption onto *B. subtilis*.

Site-Specific Model. We first describe the adsorption of TCP onto the bacterial surface by invoking a site-specific model. We attempt to fit the

experimental adsorption data considering the adsorption of $HTCP^0$ and/or TCP^- onto both neutral and negative carboxyl, phosphate and hydroxyl surface sites. We use FITEQL to solve for site-specific equilibrium constants, and we use the variance calculated by the program as a quantitative measure of goodness of fit of each model. Because FITEQL requires a fixed value for the weight of bacteria per unit weight of electrolyte, we process the data from the 6.0, 9.0 and 12.0 g bacteria/L experiments separately. The most appropriate model is that for which the calculated values of the equilibrium constants are independent of the bacteria:TCP ratio, and for which the variances calculated by FITEQL are sufficiently low to imply an excellent correlation between the model and the experimental data. The results of the FITEQL modeling are summarized in Table 1 and compared to the experimental data in Figure 4.

We first consider site-specific models describing the adsorption of only the neutral form of TCP onto neutral bacterial surface functional groups. This type of adsorption is quite likely, because at pH < 6, where the observed adsorption is greatest, both the TCP and the surface functional groups are largely protonated and neutrally charged. While these models can match the experimental data in acidic solutions, they cannot adequately describe the extent of adsorption observed to occur in basic solutions, where TCP exists predominantly as TCP^-. The variances for these models, listed in Table 1, are relatively large, and indicate that models which do not account for the adsorption of TCP^- do not effectively match the experimental data. Because we observe 5 - 10 % adsorption even at pH

TABLE I: TCP-*B. subtilis* Site-Specific Adsorption Models.

Model[a]	6 g bacteria/L		9 g bacteria/L		12 g bacteria/L	
	Log K[b]	V[c]	Log K[b]	V[c]	Log K[b]	V[c]
(R-COOH)(HTCP^0)	4.07	106.2	4.84	84.3	4.93	100.7
(R-PO$_4$H)(HTCP^0)	3.95	31.5	3.89	24.4	4.02	48.0
(R-OH)(HTCP^0)	3.73	19.7	3.65	19.6	3.80	20.0
(R-COOH)(HTCP^0)	3.50	19.2	3.43	19.1	3.35	19.7
(R-COOH)(TCP$^-$)	4.62		4.56		4.81	
(R-COOH)(HTCP^0)	3.73	19.8	3.85	40.0	3.86	18.5
(R-PO$_4$H)(TCP$^-$)	3.57		3.43		3.67	
(R-COOH)(HTCP^0)	3.91	46.0	4.27	53.5	4.66	56.0
(R-OH)(TCP$^-$)	2.78		2.51		2.55	
(R-PO$_4$H)(HTCP^0)	3.91	32.3	3.83	24.9	3.66	26.9
(R-COOH)(TCP$^-$)	3.84		3.83		4.72	
(R-PO$_4$H)(HTCP^0)	3.89	19.7	3.83	20.6	3.84	10.6
(R-PO$_4$H)(TCP$^-$)	3.24		2.93		3.48	
(R-PO$_4$H)(HTCP^0)	3.91	13.0	3.85	12.0	3.93	19.4
(R-OH)(TCP$^-$)	2.53		2.29		2.44	
(R-OH)(HTCP^0)	no convergence[d]		no convergence[d]		3.68	19.9
(R-COOH)(TCP$^-$)					4.27	
(R-OH)(HTCP^0)	3.70	20.0	no convergence[d]		3.67	11.3
(R-PO$_4$H)(TCP$^-$)	2.65				3.26	
(R-OH)(HTCP^0)	3.70	12.8	3.63	15.0	3.74	11.7
(R-OH)(TCP$^-$)	2.39		2.13		2.22	
(R-OH)(HTCP^0)	3.71	15.8	3.63	16.2	3.76	14.7
(R-COO$^-$)(TCP$^-$)	4.07		3.84		3.88	
(R-OH)(HTCP^0)	3.72	14.6	3.64	15.5	3.77	15.6
(R-PO$_4^-$)(TCP$^-$)	2.49		2.27		2.29	
(R-OH)(HTCP^0)	3.73	20.11	3.65	19.82	3.80	20.4
(R-O$^-$)(TCP$^-$)	-0.26		-0.34		-0.61	

[a]Models consider formation of surface complexes due to adsorption of HTCP^0 and/or TCP$^-$ onto carboxyl, phosphate, and/or hydroxyl surface sites; compositions of experimental solutions are given in the text. Parentheses are included for clarity. [b]Log K values calculated for the various surface complexes, referenced to the condition of zero ionic strength, zero surface charge and zero surface coverage. Log K values have 1*s* errors of ± 0.25. [c]Variance as calculated by FITEQL. [d]Indicates severe misfit between the model and the experimental data.

> 8, where less than 1 % of the TCP is present as $HTCP^0$, we invoke models involving the adsorption of TCP^-.

The experimental data are better described by site-specific models involving adsorption of both $HTCP^0$ and TCP^-. We first consider models in which both forms of the TCP adsorb onto neutral surface functional groups. The adsorption of $HTCP^0$ onto the neutral surface functional groups is probable, because the neutral sites dominate at low pH, as discussed above. The TCP^- likely also adsorbs onto neutral surface functional groups, because electrostatic repulsion would limit its adsorption onto negatively charged sites. It is probable that the $HTCP^0$ adsorbs exclusively to the neutral hydroxyl sites. Models considering the adsorption of $HTCP^0$ onto the neutral phosphate sites yield similar variances, but the $HTCP^0$-phosphate model cannot accurately predict the sharp decline in observed adsorption above pH 9.4. It is possible that the $HTCP^0$-phosphate model yields a relatively low variance because the surface sites deprotonate over the same pH range as the TCP. The choice of model considering TCP^- adsorption is constrained by changes in the speciation of the bacterial surface as a function of pH. At pH > 4.8 the majority of the carboxyl sites are deprotonated; because the extent of adsorption remains constant from pH 2.5 to approximately pH 5.0, models considering adsorption of TCP^- onto neutral carboxyl sites fit the data poorly. Similarly, models considering the adsorption of TCP^- onto neutral phosphate sites are associated with relatively large variances, and often fail to converge altogether.

We also invoke models in which $HTCP^0$ adsorbs onto neutral hydroxyl functional groups while TCP^- is adsorbed onto negatively charged surface sites. A consideration of such models is warranted because TCP deprotonates over the same pH range as the bacterial surface groups, and so the two have the potential to interact, particularly at high pH. We use Equation 23 to account for the electric interaction between TCP^- and the negatively charged surface. However, if the adsorption of TCP^- is controlled more by hydrophobicity than by electrostatics, then the negative surface charge will have a relatively small effect. The best fit to the data is obtained from a model which considers adsorption of $HTCP^0$ onto neutral hydroxyl sites, in combination with adsorption of TCP^- onto negative phosphate sites. This model fits the experimental data well, but not as well as the model invoking adsorption of TCP^- onto neutral hydroxyl sites as described above, particularly at high pH. The difference between these two site-specific models occurs at pH > 9.5, where the model considering the adsorption of TCP^- onto neutral hydroxyl sites predicts no adsorption, whereas the model involving TCP^- adsorption onto negative phosphate sites predicts a plateau at roughly 5 - 10% adsorption. Because the difference between these two site-specific models occurs only at high pH and is generally less than 10%, we perform additional adsorption experiments at higher pH in order to better constrain our choice of model (see below).

Non-Specific Model. We also attempt to model the experimental adsorption data using non-specific models. We consider independent adsorption of $HTCP^0$ and/or TCP^- onto the bacterial surface. Again, we use FITEQL to solve

for partition coefficients, and we use the variance calculated by the program as a quantitative measure of goodness of fit of each model. We use Equation 23 to calculate intrinsic equilibrium constants applicable to zero surface charge and coverage. The results of the FITEQL modeling are summarized in Table 2 and compared to the experimental data in Figure 7.

The non-specific adsorption models fit the experimental data adequately, but not as well as the site-specific model invoking TCP^- adsorption onto neutral hydroxyl sites. The discrepency between the non-specific model and the experimental data is most clearly seen at high pH, where the non-specific model plateaus at approximately 5 - 10 % adsorption, whereas the data drop to zero. This plateau is expected, because the partition coefficient describes a fixed ratio of aqueous to adsorbed TCP^-; the model would predict zero adsorption at high pH only if the partition coefficient was infinitely small. The presence of the model plateaus at high pH suggests that the negative electric potential of the surface has little effect on the hydrophobic adsorption of TCP^-. The same type of plateau is expected in the low pH range, where the ratio of aqueous to adsorbed $HTCP^0$ is fixed by the value of a second partition coefficient. In order to accurately predict the shape of the adsorption edge, the values of the partition coefficients describing $HTCP^0$ and TCP^- adsorption must be optimized simultaneously. This simultaneous optimization of the two partition coefficients permits the non-specific model to match the adsorption edge and the position of one of the two adsorption plateaus, but never the adsorption edge and the position of both plateaus. However, because the difference between the site-specific and non-

TABLE II: TCP-*B. subtilis* Non-Specific Adsorption Models.

	6 g bacteria/L		9 g bacteria/L		12 g bacteria/L	
Model[a]	Log K[b]	V[c]	Log K[b]	V[c]	Log K[b]	V[c]
$HTCP^0$	0.23	20.23	0.34	19.2	0.62	21.2
$HTCP^0$	0.21	14.3	0.33	15.5	0.58	15.6
TCP^-	-1.24		-1.30		-1.18	

[a]Models consider adsorption of $HTCP^0$ and/or TCP^- onto the surface; compositions of experimental solutions are given in the text. [b]Log K values calculated for the various forms of TCP, referenced to the condition of zero ionic strength, zero surface charge and zero surface coverage. Log K values have 1*s* errors of ± 0.25. [c]Variance as calculated by FITEQL.

Figure 7. Percent adsorption of TCP onto *B. subtilis* as a function of pH. Solutions contain $10^{-4.00}$ M TCP, $10^{-1.00}$ M $NaNO_3$ and either 6, 9, or 12 g bacteria per L. Experimental data are identical to Figure 4. Model curves were generated by FITEQL, assuming non-specific adsorption of TCP^- and $HTCP^0$ onto the bacterial surface. Data points represented by stars have increased solid:solution ratios, with g bacteria per L indicated by their labels.

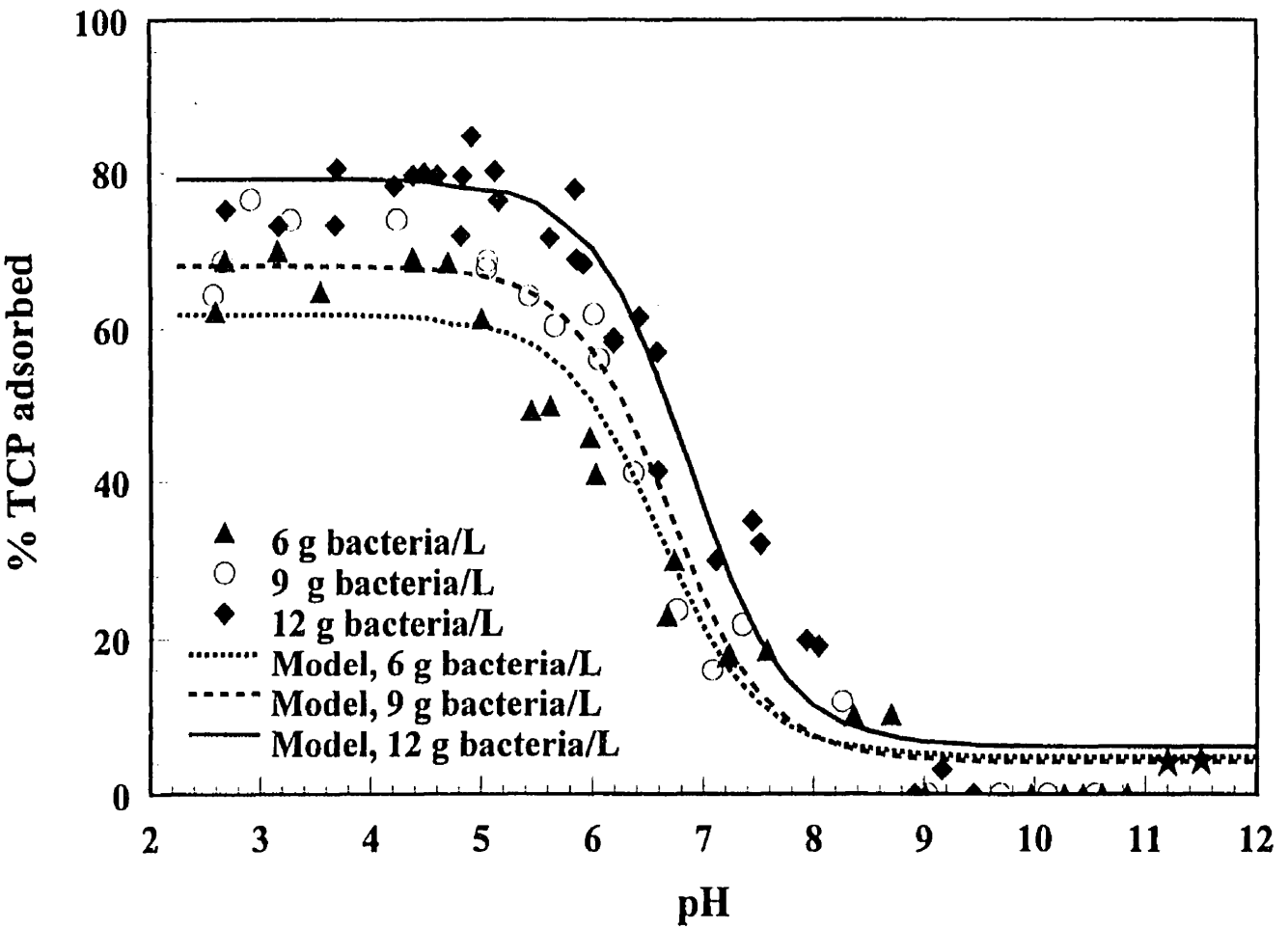
100
80
60
40
20
0
% TCP adsorbed
2
3
4
5
6
7
8
9
10
11
12
pH
6 g bacteria/L
9 g bacteria/L
12 g bacteria/L
Model, 6 g bacteria/L
Model, 9 g bacteria/L
Model, 12 g bacteria/L

Figure 7

specific models is apparent only at high pH and is less than 10%, we perform additional adsorption experiments at high pH, with greater solid:solution ratios in order to better constrain our choice of model.

Comparison of Models. Both the site-specific and the non-specific adsorption models fit the experimental data adequately over the range of conditions used in this study, with the only difference between them occurring at high pH. The difference between the site-specific and non-specific model curves is generally less than 10%, and given the experimental uncertainties (see below), neither model is unequivocally better. Further, two types of site-specific models can be applied to describe the data: one in which the TCP^- adsorbs exclusively onto neutral hydroxyl surface sites; the other in which the TCP^- adsorbs onto negative phosphate sites. In order to better constrain our choice of model, we perform TCP-*B. subtilis* adsorption experiments at pH > 11, with approximately 30 g bacteria/L. If TCP^- adsorbs onto neutral hydroxyl sites, under these conditions, negligible adsorption should occur, because the majority of the sites will be deprotonated. By contrast, if the TCP^- adsorbs onto negative hydroxyl sites, measurable adsorption of TCP should occur. If the site-specific model is valid, the extent of adsorption should be consistent with the model prediction, because the equilibrium constants reported here are independent of solution chemistry and solid:solution ratio. If the site-specific model cannot predict the extent of adsorption observed at high pH and high solid:solution ratio, the non-specific model is more appropriate.

The results of these experiments are shown in Figures 4 and 7, where it is apparent that less than 5% adsorption of TCP^- occurs under these experimental conditions. Both the non-specific and site-specific models can be used to describe these data. The non-specific model predicts increased adsorption with increased solid:solution ratio, because the extent of adsorption depends on the amount of the surface that is present, relative to the total concentration of TCP. The TCP^- partition coefficients listed in Table 2 show a poor correlation with solid:solution ratio, and so it is not possible to report a single partition coefficient, normalized with respect to the weight (or surface area) of bacteria present. As a result, it is difficult to use the non-specific model to predict the adsorption that will occur at pH 11, with 30 g bacteria per L. Nonetheless, if a linear relationship between the partition coefficients (Table 2) and the weight of bacteria per L is assumed, 30 g bacteria per L corresponds to a partition coeffificent of $10^{-1.03}$. Using this value for the TCP^- partition coefficient, under these conditions, approximately 9% adsorption should occur, though given the uncertainties in the extrapolation, 6 - 12% adsorption may be reasonably expected. We conclude that the difference between the model prediction and the experimental data is not large enough to disregard the non-specific model.

The high pH, high solid:solution ratio data can also be predicted with the site-specific model. The equilibrium constants reported in Table 1 apply to all solid:solution ratios, and so can be used to predict the extent of adsorption that will occur at pH 11, with 30 g bacteria per L. The site-specific model considering adsorption of TCP^- onto the negative phosphate sites predicts 12.8% adsorption

under these conditions. Because less than 5% adsorption is observed, the site-specific model considering adsorption of TCP^- onto the neutral hydroxyl sites must be invoked. The experimental data indicate that some adsorption occurs, whereas the TCP^--neutral hydroxyl site model predicts none; however, the observed adsorption is small and within the error of the prediction. Therefore, the site-specific model which best fits the experimental data considers adsorption of both $HTCP^0$ and TCP^- onto neutral hydroxyl sites.

Based on the discussion above and the FITEQL analyses presented in Tables 1 and 2, we choose to model TCP adsorption onto *B. subtilis* with a site-specific two-equilibria model. The experimental data do not unequivocally exclude the non-specific model, but it does not fit the data as well, and the partition coefficients show a poor correlation with the weight of bacteria present. The non-specific model is therefore completely empirical, and cannot be adapted to conditions other than those investigated here. By contrast, the site-specific model accounts for the dependence of adsorption on pH and weight of bacteria per L, and so can be applied to predict the adsorption of TCP under a range of conditions.

In the site-specific model which best describes the data, the negative form of TCP adsorbs onto the neutral hydroxyl sites:

$$TCP^- + R-OH^0 \leftrightarrow (R-OH^0)(TCP^-) \qquad K = 10^{2.33} \qquad (25)$$

Here, the parentheses are included only for clarity. The neutral form of TCP adsorbs onto the neutral hydroxyl sites. This reaction, with corresponding stability constant, may be expressed as follows:

$$HTCP^0 + R-OH^0 \leftrightarrow (R-OH)(HTCP^0) \qquad K = 10^{3.69} \qquad (26)$$

In all cases, a 1:1 stoichiometry for the TCP-surface site complex is assumed. This stoichiometry is supported by the constancy of the stability constants between the systems with different bacteria:TCP ratios. Additionally, a 1:1 stoichiometry has been reported for a variety of metal-bacteria surface complexes (*14, 18*). The experimental data gathered under the chemical conditions of this study are well described by two adsorption reactions, but it is also possible that TCP adsorbs as a mulitdentate complex when the solid:solution ratio is very large.

The site-specific model curves are compared to the experimental data in Figure 4. Note that the variances presented in Table 1 are more indicative of the model fit than the visual correlation shown in Figure 4. This is because the model curves were computed for fixed total concentrations of TCP and bacteria, while the experimental solutions, prepared as individual batch experiments, had slight variations in solution composition due to dilution (we consider all variations in solution composition during our modeling).

Consideration of Errors. Errors associated with the values of the stability constants reported here may arise from four sources. First, the bacteria

may multiply during the course of the experiments, giving rise to an error in the value of the mass of bacteria per unit mass of suspension applied in our modeling. We have examined this possibility by separating and drying the bacteria in the parent suspension both prior to and following the adsorption experiments. We observe no increase in the weight of bacteria present, and thus we consider this error to be negligible.

Second, errors in the stability constants reported here may arise if the mass of bacteria in an aliquot of the parent suspension is variable, as we have assumed that it is constant. We have quantified the homogeneity of the parent suspension by separating and drying the bacteria present in several aliquots of identical weight. Here, we find an error of ± 15 wt. % in the mass of bacteria present in each reaction vessel. This error likely arises due to clumping of the bacteria in the parent suspension, which is made slightly acidic by the presence of the TCP. However, because this error is essentially random (each data point represents a separate experiment), and because we model all experimental data points simultaneously, the corresponding error in the value of the stability constant is quite small. This error, when propagated through our FITEQL models, yields a maximum 1*s* error in the TCP-*B. subtilis* log K values of ± 0.10.

Third, the accuracy of the stability constants reported here depends upon the accuracy of the previously measured stability constants and surface site concentrations that we have used in our FITEQL calculations. Literature values of the pK_a of TCP range from 5.99 (*21*) to 6.15 (*11*). Work by Fein et al. (*14*) indicates that the cell wall characteristics of independently grown cultures of *B.*

subtilis may change slightly: 1*s* errors in the concentrations of surface sites per gram of bacteria are reported as ± 1.0 x 10^{-4}, 1.5 x 10^{-6}, and 2.0 x 10^{-6} for the carboxyl, phosphate and hydroxyl sites, respectively; 1*s* errors in the pK_a values for these sites are ± 0.07, 0.33 and 0.30. In order to minimize errors arising from cell wall variation, we have performed our experiments using at least two independent cultures for each bacteria:TCP ratio, and we have modeled all the experimental data simultaneously. We propagate these uncertainties through our FITEQL calculations, and find that they yield maximum 1*s* errors in the TCP-*B. subtilis* log K values of ± 0.15.

Fourth, we consider the error associated with the analysis of TCP concentration by UV spectrophotometry. A comparison of replicate standards indicates an analytical uncertainty of ± 2 % in the determination of each aqueous TCP concentration. However, this error is essentially random, and each data point involves an independent analysis, and so the corresponding error in the log K values reported here is negligible. A consideration of all the errors discussed above illustrates that the log stability constants reported here carry maximum 1*s* errors of ± 0.25.

CONCLUSION

The chemical model that is developed here is in good general agreement with other studies describing the fate of TCP in natural systems. We note a strong affinity between the TCP and the bacterial surface. A similar association between

TCP with hydrophobic phases such as octanol and organic carbon is well documented in the literature (*3, 4, 12*). By contrast, we observe no interaction between TCP and the mineral surface, in agreement with the findings Kung and McBride (*10*) and Schellenberg et al. (*11*). Our findings are supported by a number of field studies, which indicate that the transport of TCP in groundwater is controlled more by the presence of organic material (*30, 31*) or a non-aqueous phase (*32*) than by the nature of the mineral surfaces present.

The results reported here are the first to quantify the adsorption of TCP onto a bacterial surface in the framework of equilibrium thermodynamics. Our results indicate that both the site-specific and non-specific models describe the experimental data effectively for fixed solid:solution ratios. However, the partition coefficients used in the non-specific models are poorly correlated with the weight of bacteria present, and so cannot be normalized to yield a single partition coefficient applicable to all solid:solution ratios. In contrast, the equilibrium constants used in the site-specific model are fixed regardless of solution composition or solid:solution ratio, and so can be used to predict the extent of adsorption that will occur under widely differing chemical conditions. Further, the site-specific equilibrium constants reported here can be combined with other previously measured stability constants to develop a thermodynamic, quantitative geochemical model describing the fate of TCP in complex, natural systems.

ACKNOWLEDGEMENTS

This study was funded by an NSERC Operating Grant and a FCAR Nouveaux Chercheurs Grant to J.B.F. We thank Dave Yiptong, Krystyne Blaikie, Christian Gravel and Pascal Benalil for conducting some of the experiments. We also thank Alfonso Mucci for the use of his spectrophotometer.

REFERENCES

(1) Makinen, P. M.; Theno, T. J.; Ferguson, J. F.; Ongerth, J. E.; Puhakka, P. M. *Environ. Sci. Technol.* **1993**, *27*, 1434-1439.

(2) Suntio, L. R.; Shiu, W. Y.; Mackay, D. *Chemosphere* **1988**, *17*, 1249-1290.

(3) Yoshida, K.; Shigeoka, T.; Yamamuchi, F. *Chemosphere* **1987**, *16*, 2531-2544.

(4) You, C. N.; Liu J. C. *Wat. Sci. Tech.* **1996**, *33*, 263-270.

(5) Mueller, J. G.; Chapman, P. J.; Pritchard, P. H. *Environ. Sci. Technol.* **1989**, *23*, 1197-1201.

(6) Kishino, T.; Kobayashi, K. *Water Res.* **1995**, *29*, 431-442.

(7) Niimi, A. J.; Palazzo, V. *Water Res.* **1985**, *19*, 205-207.

(8) Keith, L. H.; Telliard, W. A. *Environ. Sci. Technol.* **1979**, *13*, 416-423.

(9) Smejtek, P.; Blochel, A.; Wang, S. *Chemosphere* **1996**, *33*, 177-201.

(10) Kung, K.-H. S.; McBride, M. B. *Environ. Sci. Technol.* **1991**, *25*, 702-709.

(11) Schellenberg, K.; Leuenberger, C.; Schwartzenbach, R. P. *Environ. Sci. Technol.* **1984**, *18*, 652-657.

(12) Lee, L. S.; Rao, P. S.; Nkedi-Kizza, P.; Delfino, J. J. *Environ. Sci. Technol.* **1990**, *24*, 654-661.

(13) Duncan, K. E.; Ferguson, N.; Kimura, K.; Zhou, X.; Istock, C. A. *Evolution* **1994**, *48*, 2002-2025.

(14) Fein, J. B.; Daughney, C. J.; Yee, N.; Davis, T. *Geochim. Cosmochim. Acta submitted.*

(15) Boily, J.-F.; Fein, J. B. *Geochim. Cosmochim. Acta* **1996**, *60*, 2929-2938.

(16) Davis, J. A.; Kent, D. B. In *Mineral-Water Interface Geochemistry*; Hochella, M. F., White, A. F., Eds.; Reviews in Mineralogy, Mineralogical Society of America, 1990; v. 23, pp 177-260.

(17) Schindler, P. W.; Stumm, W. In *Aquatic Surface Chemistry*; Stumm, W., Ed.; John Wiley and Sons: New York, 1987; pp 83-110.

(18) Daughney, C. J.; Fein, J. B.; Yee, N. *Chem. Geol. submitted.*

(19) Beveridge, T. J.; Murray, R. G. E. *J. Bacteriol.* **1980**, *141*, 876-887.

(20) Beveridge, T. J. *Annu. Rev. Microbiol.* **1989**, *43*, 147-171.

(21) Westall, J.; Leuenberger, C.; Schwartzenbach, R. P. *Environ. Sci. Technol.* **1985**, *19*, 193-198.

(22) Gunneruisson, L.; Lövgren, L.; Sjöberg, S. *Geochim. Cosmochim. Acta* **1994**, *58*, 4973-4983.

(23) Gunneruisson, L.; Sjöberg, S. *J. Colloid Interface Sci.* **1992**, *156*, 121-128.

(24) Müller, B.; Sigg, L. *J. Colloid Interface Sci.* **1991**, *148*, 517-532.

(25) Lövgren, L; Sjöberg, S.; Schindler, P. W. *Geochim. Cosmochim. Acta* **1990**, *54*, 1301-1306.

(26) Westall, J.; Hohl, H. *Adv. Colloid Interface Sci.* **1980**, *12*, 265-294.

(27) Westall, J. "FITEQL. A Computer Program for Determination of Chemical Equilibrium Constants from Experimental Data". Department of Chemistry, Oregon State University; Report 82-01.

(28) Westall, J. "FITEQL. A Computer Program for Determination of Chemical Equilibrium Constants from Experimental Data". Department of Chemistry, Oregon State University; Report 82-02.

(29) Herben, P. F. G.; Mozes, N. Rouxhet, P. G. *Biochem. Biophys. Acta* **1990**, *1033*, 184-188.

(30) Johnson, R. L.; Brillante, S. M.; Isabelle, L. M.; Houck, J. E.; Pankow, J. F. *Groundwater* **1985**, *23*, 652-665.

(31) Pankow, J. F.; Johnson, R. L.; Houck, J. E.; Brillante, S. M.; Bryan, W. J. *Groundwater*, **1984**, *22*, 593-601.

(32) Pollard, S. J. T.; Hoffman, R. E.; Hrudley, S. E. *Can. J. Civ. Eng.* **1993**, *20*, 787-800.

CHAPTER 6:

CONCLUSION

CONTRIBUTION TO KNOWLEDGE

The stability constants presented in this thesis are the first to quantify the extent of aqueous complexation and adsorption in a variety of chemical systems containing heavy metals, chlorophenols, mineral surfaces, and/or bacterial surfaces. The range of experimental chemical conditions applied here covers the effective limits expected in natural environments. The metal concentrations range from several ppm to ppb, the pH varies across the range common to most natural waters, the experiments were performed both well below and very close to the saturation of the metal hydroxides; the highest chlorinated phenol concentrations approached the limit of aqueous solubility, and a wide range of solid to solution ratios were investigated. As a result, these stability constants may be applied to model complexation and adsorption in virtually any natural system containing the heavy metals, chlorophenols, mineral surfaces and/or bacterial surfaces examined here. The quantification of such processes is pivotal to the prediction of the fate of these metals and chlorophenols in groundwaters.

This study is also one of the first to describe proton, metal and organic adsorption onto bacterial surfaces within the framework of equilibrium thermodynamics. Bacterial surfaces display several types of surface functional groups which can interact with chemical species in solution. The absolute concentrations of these surface functional groups varies slightly between the species examined here, and may be correlated to differences in cell wall structure. The deprotonation constant for each type of functional group also varies slightly

between species, suggesting that the pK_a values are affected by the structure of the surrounding cell wall. However, the deprotonation of each functional group is described by a single pK_a value, implying that the functional groups are electrochemically isolated on the cell wall, such that the deprotonation of one functional group is not affected by the deprotonation of its neighbouring functional groups. Metal adsorption onto bacterial surfaces involves more than one distinct type of surface functional group, depending upon the ratio of total bacterial surface sites to the total concentration of metal. A recognizable affinity series exists, with Cd (weak affinity) < Pb < Cu < Al (strong affinity). The adsorption of TCP onto the bacterial surfaces is better modeled by considering its interaction with discrete surface functional groups than by the non-specific, partitioning models that have been applied to describe organic adsorption in the past. Although this study has examined only two species of gram-positive bacteria, four metals and one organic compound, the data presented here illustrate that the equilibrium thermodynamic framework can provide an appropriate model for a variety of adsorption reactions involving bacterial surfaces. This suggests that this thermodynamic framework may be applied to many metal-organic-bacteria systems other than those examined in this thesis.

The thermodynamic approach used in this thesis has four advantages. First, the stability constants reported here are fixed in value, regardless of solution composition or solid to solution ratio, and so can be applied to virtually any chemical system. Second, the stability constants given here can be combined with other previously measured stability constants describing other reactions, to

develop speciation models for complex chemical systems, where a variety of reactions may be occurring simultaneously. Third, using a linear correlation technique, stability constants can be estimated from a small number of experimental measurements. This thesis shows that this approach can be applied to predict stability constants describing metal-chlorophenol complexation and metal adsorption onto bacterial surfaces. Fourth, a variety of chemical processes, such as complexation, adsorption, precipitation, oxidation and reduction, can be modeled with one governing theoretical framework. Due to these four advantages, the thermodynamic framework is much more flexible than an empirical approach which describes chemical reactions and processes with parameters that depend upon the conditions of measurement. Thermodynamic stability constants like those presented here are much more readily incorporated into reactive transport models to predict the mobility of contaminants in groundwaters.

This thesis also outlines novel experimental techniques for the measurement of thermodynamic stability constants. In studies of metal-chlorophenol complexation, the combined use of potentiometry and spectrophotometry is extremely useful. The potentiometric approach, because it measures changes in free metal activity resulting from metal-chlorophenol complexation, requires a chlorophenol-dominated system. By contrast, the spectrophotometric technique requires a metal-dominated system because it measures changes in chlorophenol concentration caused by complexation. The combination of the two methods allows for extensive variation in the total metal to ligand ratio, and corroboration of the

results by two independent techniques. In the studies of metal- and TCP-adsorption, the batch adsorption experiments, in combination with the kinetic and desorption experiments, allow for determination of the relative and absolute concentrations of surface functional groups present per unit weight of the solid, the deprotonation constant for each type of functional group present, and the metal- or TCP-binding constant for each important interaction. Although this thesis involves a limited number of reactants, the experimental techniques presented here can be applied to measure complexation and adsorption stability constants in virtually any metal-organic-solid system.

SUGGESTIONS FOR FUTURE RESEARCH

The information presented in this thesis represents a significant advance in the understanding of a variety of chemical processes, though additional research is warranted. In the binary metal-chlorphenol, metal-bacteria, and TCP-bacteria systems examined here, spectroscopic studies could confirm the structure of the complexes proposed. The thermodynamic framework is limited in that it attempts to predict microscopic interactions from macroscopic experimental data. While the existence and structure of the aqueous and surface complexes described here are probable, the rigour of the science would be improved by direct observation. This is particularly important in the metal- and TCP-bacteria systems, in order to confirm the association of the adsorbent with a particular type of surface functional group.

Additionally, the binary metal-bacteria systems examined in this thesis should be complimented by studies of other, similar systems. For example, a study of the bacterial adsorption of common rock forming cations, such as Na^+, K^+, Ca^{2+}, Mg^{2+}, Fe^{3+}, etc. would allow an evaluation of the role played by bacteria in mineral dissolution and the development of secondary porosity. Studies involving other species of bacteria are also required. For example, the mobility of metals, particularly Fe^{3+}, in oxidizing mine tailings is likely controlled, in part, by interactions with the bacteria *Thiobacillus ferrooxidans*, which catalyzes the pyrite oxidation reaction which liberates Fe^{3+} and H^+ (Davis, 1997; McIntosh et al., 1997). Studies of metal-*T. ferrooxidans* interactions would improve our ability to model the development and fate of acid mine drainage. Further, a variety of bacterial species are used in metallurgical processes to enhance the removal of Au^+ and Ag^+ from sulfide minerals (Hackl, 1997). A quantification of such processes may permit improvements in the design of the pre-treatment processes. An increased database of thermodynamic stability constants describing metal-bacteria interactions would also allow the elucidation of generalities relating to such processes.

Further studies of the interactions between organic molecules and bacteria are also suggested. Because bacteria are ubiquitous in natural environments, they have the potential to affect the migration of both anthropogenic and natural organics occurring in the subsurface. The bacteria present in oil field fluids may affect the transport and recovery of petroleum. Adsorption onto bacterial surfaces may also play an important role in the attenuation of the transport of compounds such as benzene, toluene and xylene, which are among the most common groundwater

contaminants (Domenico and Schwartz, 1990). As in the case of the metal-bacteria interactions, an increased number of organic-bacteria interaction studies will improve techniques for the prediction of organic-bacteria stability constants that have not yet been investigated in the laboratory.

Binary systems containing a mineral solid and a bacterial solid should also be investigated. It is possible that the two solids will coagulate to form colloids in a manner controlled by the electric charge of their surfaces. The data presented in this thesis indicate that bacterial surfaces carry an electric charge which varies with pH, and is best quantified through the use of the Constant Capacitance double layer model. The charge of a mineral surface can be predicted in the same manner (Stumm and Morgan, 1981; Langmuir, 1997). Thus it may be possible to develop a thermodynamic model which predicts the extent of coagulation (or bacteria-mineral adsorption) based on solution chemistry. Such a model has a wide range of potential applications. For example, because of its thermodynamic basis, stability constants describing bacteria-mineral interaction could be combined with a variety of other stability constants to model the transport of bacteria in groundwaters, or the mobility of contaminants in natural systems containing both bacterial and mineral surfaces.

Adsorption and complexation reactions must also be examined in ternary and quaternary systems containing a metal, an organic, a bacterial surface and/or a mineral surface. Such studies are required to determine the stability constants for the formation of any important ternary metal-organic-surface complexes. Systems containing the heavy metals, chlorophenols, bacteria and mineral surfaces examined

here provide a logical starting point, because the majority of the binary systems containing these components have already been examined.

Lastly, the chemical models developed to describe metal-organic-bacteria-mineral interactions should be applied to predict contaminant transport through natural materials. Such studies may be initiated by performing experiments in which solutions containing known concentrations of various metals and organics are passed through columns containing known mineral and bacterial solids. In this manner, the accuracy of the chemical model may be evaluated and verified before it is applied to a field situation.

REFERENCES

Davis, B. S. In *Biological-Mineral Interactions*; McIntosh, J. M., Groat, L. A., Eds.; Mineralogical Association of Canada Short Course, 1997, v. 25, pp. 93-112.

Domenico, P. A.; Schwartz, F. W. "Physical and Chemical Hydrogeology." John Wiley and Sons, N. Y., 1990.

Hackl, R. P. In *Biological-Mineral Interactions*; McIntosh, J. M., Groat, L. A., Eds.; Mineralogical Association of Canada Short Course, 1997, v. 25, pp. 143-168.

Langmuir, D. "Aqueous Environmental Geochemistry." Prentice-Hall, N. J., 1997.

McIntosh, J. M.; Silver, M; Groat, L. A. In *Biological-Mineral Interactions*; McIntosh, J. M., Groat, L. A., Eds.; Mineralogical Association of Canada Short Course, 1997, v. 25, pp. 63-92.

Stumm, W., and Morgan, J. J., "Aquatic Chemistry." John Wiley and Sons, N. Y., 1981.

IMAGE EVALUATION TEST TARGET (QA-3)

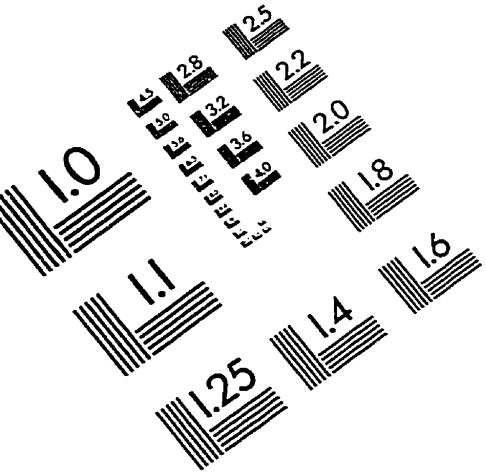

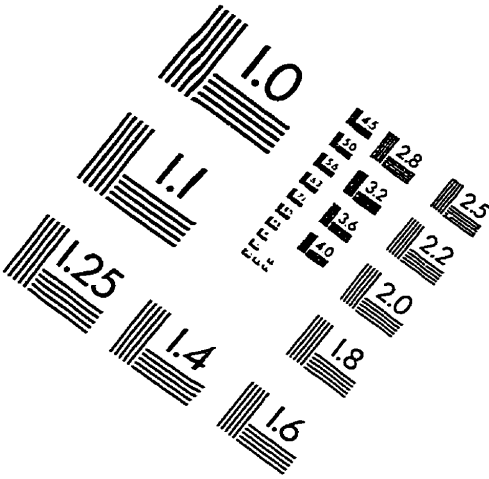

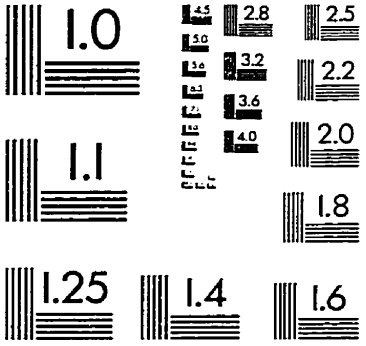

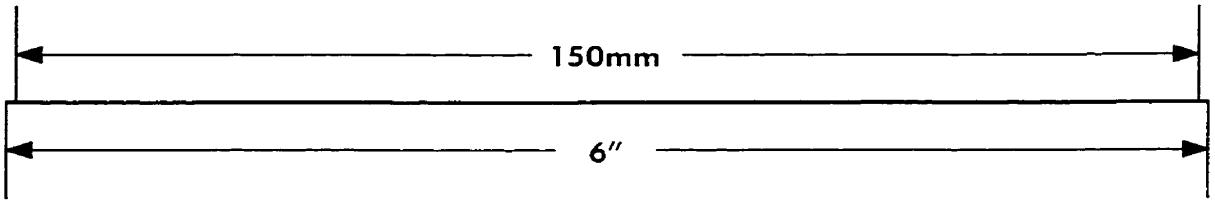

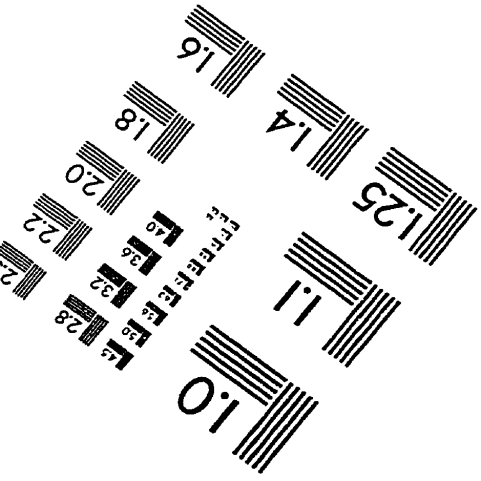

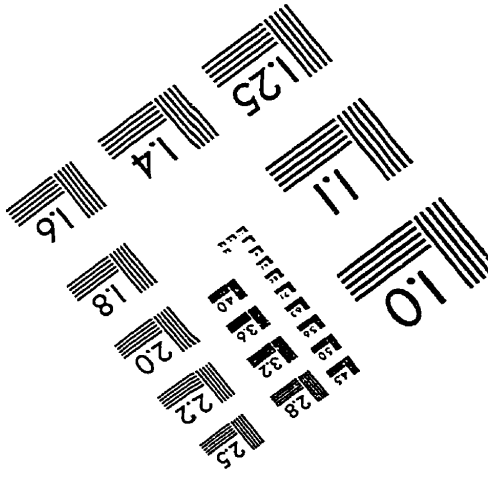

APPLIED IMAGE, Inc
1653 East Main Street
Rochester, NY 14609 USA
Phone: 716/482-0300
Fax: 716/288-5989